DESIGN AND DEVELOPMENT OF HIGH-PERFORMANCE TRIBOELECTRIC NANOGENERATORS (TENGS) USING POLYMER-CERAMIC AND POLYMER-METAL COMPOSITES

Thesis submitted to

University of Calicut

for the partial fulfillment of the requirements
for the award of the degree of

DOCTOR OF PHILOSOPHY IN PHYSICS
UNDER THE FACULTY OF SCIENCES

by

ANLIN LAZAR K

under the guidance of

Dr. SAJI K J

&

Co-guidance of

Dr. PRADEESH K

DEPARTMENT OF PHYSICS
GOVERNMENT VICTORIA COLLEGE
PALAKKAD-678001, KERALA, INDIA

JUNE 2022

DESIGN AND DEVELOPMENT OF HIGH-PERFORMANCE TRIBOELECTRIC NANOGENERATORS (TENGS) USING POLYMER-CERAMIC AND POLYMER-METAL COMPOSITES

PhD Thesis in Physics

Author: Anlin Lazar K

Department of Physics
Govt: Victoria College, Palakkad
Affiliated to University of Calicut
Kerala, India 678001
Email: aniline86@gmail.com

Under the guidance of

Dr. SAJI K. J.

Associate Professor
International School of Photonics, CUSAT, Kochi
Kerala, India
Email: saji@cusat.ac.in

&

Co-Guidance of

Dr Pradeesh K.

Assistant Professor in Physics
Department of Physics
Govt: Victoria College, Palakkad
Affiliated to University of Calicut
Kerala, India 678001
Email: pradphysics@gmail.com

Dedicated to.....

My beloved mother

DECLARATION

I hereby declare that the work presented in this thesis entitled **"**DESIGN AND DEVELOPMENT OF HIGH PERFORMANCE TRIBOELECTRIC NANOGENERATORS (TENGS) USING POLYMER-CERAMIC AND POLYMER-METAL COMPOSITES" is based on the original research work done by me under the guidance of Dr. Saji K. J., Associate Professor, International School of Photonics, Cochin University of Science and Technology, Kerala – 682022 and the co-guidance of Dr Pradeesh K., Assistant Professor, Department of Physics, Govt: Victoria College, Palakkad-678001. This work has not been included in any other thesis submitted previously for the award of any degree or diploma of the university or other institute of higher learning, except where due acknowledgment has been made in the text.

ANLIN LAZAR K
Research Scholar, Department of Physics
Govt: Victoria College, Palakkad

Govt: Victoria College
June 2022

CERTIFICATE

This is to certify that the work embodied in the thesis entitled **"**DESIGN AND DEVELOPMENT OF HIGH PERFORMANCE TRIBOELECTRIC NANOGENERATORS (TENGS) USING POLYMER-CERAMIC AND POLYMER-METAL COMPOSITES**"** is an authentic record of research work carried out by by **Ms. Anlin Lazar K** under my supervision and guidance at the Department of Physics, Govt: Victoria College, Palakkad in partial fulfilment of the requirement for the award of the degree of Doctor of Philosophy under the Faculty of Science. This thesis or any part thereof has not been submitted elsewhere for award of any other degree.

Dr. Saji K. J

Associate Professor

Kalamassery

June, 2022

CERTIFICATE

This is to certify that the work embodied in the thesis entitled **"**DESIGN AND DEVELOPMENT OF HIGH PERFORMANCE TRIBOELECTRIC NANOGENERATORS (TENGS) USING POLYMER-CERAMIC AND POLYMER-METAL COMPOSITES**"** is an authentic record of research work carried out by Ms. **Anlin Lazar K** under my co - guidance at the Department of Physics, Govt: Victoria College, Palakkad in partial fulfilment of the requirement for the award of the degree of Doctor of Philosophy under the Faculty of Science. This thesis or any part thereof has not been submitted elsewhere for award of any other degree.

Dr. Pradeesh K

Palakkad

June, 2022

ACKNOWLEDGEMENTS

To begin, I express my gratitude to GOD, the Almighty, for guiding me down the truthful path, ensuring my success, and bestowing upon me excellent health, courage, inspiration and enthusiasm. Neither my research tenure, nor myself, nor this thesis would be the same without the help and company of many people.

I would like to express my sincere gratitude and appreciation to my research supervisor, Dr Saji K J, Associate Professor, International School of Photonics, CUSAT, for his valuable guidance and scientific vision in conducting pioneering research. His encouragement and his constant, generous and unreserved support helped immensely during my research work and writing off this thesis. I have learnt a lot from Saji sir during research period, both professionally and personally. Whenever I feel depressed and frustrated, the inspiring encouragements from Saji sir always led me to the right direction with his unique foresight. I also sincerely thank Saji sir and his family for their care of me, not only in my academic research and study, but also in my personal life, which means a lot to me. Without these supports, guidance and care, I could not have gone thus far.

I would also like to extend my deepest gratitude to co-guide Dr. Pradeesh K,, for the precious time, patience and invaluable advices which he offered during different phases of my research.

I owe special thanks to Prof. (Dr.) Honey John, Professor, Department of Polymer Science and Rubber Technology, for the valuable directions and suggestions which helped a lot to move ahead in the research work.

I would like to express sincere thanks to the Principal, Dr. Maya C Nair, Govt: Victoria College, Palakkad for her kind support and motivation extended during the tenure of my research work.

I am highly thankful to the Principal, Dr. Sr. Gisala George (Principal, Mercy College, Palakkad) and the former principals Dr. Sr. Lilly P V, Dr. Sr. Alice Thomas, Dr. Sr. Kripa of Mercy College, Palakkad for their prayerful inspirations and support.

A special thanks to Dr Ambily Krishnan, Head of the department, Department of Physics, Govt: Victoria College, Palakkad for invaluable advice and moral support. I also place a heartfelt thanks to former Head, Mr: O. K. Ramesan for being so supportive during my research tenure.

I express my deep sense of gratitude and respectful regards to Ms. Mariyama John (Rtd: Associate Professor and Head of Physics Department, Mercy College, Palakkad) who gave me diligent support by extending substantial support, timely inspiration and official work moderations during the course of the entire study. I am happy to express my thanks to Dr. Lakshmi M, Head of Department, Department of Physics, Mercy College, Palakkad for the selfless support and precious discussions on research and various other aspects.

I am also very fortunate to receive help from a lot of people during my PhD endeavours. I also express my sincere gratitude to faculty of Department of Physics, Govt: Victoria College, Palakkad.

I am highly grateful to my colleague and mentor Dr. Sr. Jessy Mathew N for the inspiration, special care during my weak times, deep moral support and prayers throughout my career. The creative suggestions,

valuable advice and help given by my colleagues Ms Anu Kuruvilla, Ms Smiya John, Ms Melda Francis (Assistant Professors, Department of Physics, Mercy College, Palakkad) which equipped me to face all of the hurdles along the way.

I take this opportunity to thank my fellow lab mates at International School of Photonics: Cicily Rigi V. J., Praveen P., Hajara P., for making my research life and days at CUSAT very cheerful and memorable one in spite of all my worries. Special thanks to Vijoy K.V., for the untiring help, timely support and selfless favours rendered to me which helped me a lot during my Ph.D work.

I also cherish companionship with research scholars of IUCND and PSRT: Dhanu Treesa Mathew, Mathew Sunil Animasree V. P., Lakshmi Sreenivasan for their love and support. I am immensely indebted to Amrutha Thomas and Amruth Kumar N. T., for the favours rendered to me during my Ph.D tenure at IUCND, CUSAT. I thank both for the wonderful company and friendship they have provided. I also thank Amrutha's family for their kindly care and concern shown to me. Thanks for being such good friends and being there for me, when I need it.

I gratefully acknowledge for proving lab facilities at International School of Photonics and Inter University Centre for Nano materials and devices (IUCND), CUSAT. I also acknowledge IIT, Palakkad, SAIF-STIC, CUSAT, St Thomas College, Thrissur, IISER, Trivandrum for the services rendered for various analysis techniques.

Finally, and most importantly, I want to thank my family for always quietly watching out for me, patiently loving me, and sparing advice and support, when I need them most. I would like to especially thank my mother Mrs. Beena Lazar, who is no more with me, for the care and the love which she has given unconditionally with her persistence and aspiration. I would not be who I am if it wasn't for you. I would like to thank my father, Mr. K. T. Lazar from the bottom of my heart for all his love and encouragement. I would also express my gratefulness to my better half Tony Joseph, who goes through every tough moment with me together and always gives me his strongest supports no matter what. I am blessed to spend the rest of my life with him. I thank my beloved daughter, Emerin and son, Edwin for being so supportive, understanding and patient throughout my whole research tenure. I am also grateful to my younger brother, Cibin Mosses, for his constant love, motivation, criticism and affection. I feel a deep sense of gratitude for my father-in-law (Joseph Antony), mother-in-law (Philo Joseph) and all my siblings-in-law who has always been my strength. I am also very much grateful to all my family members and friends for their constant inspiration, prayers and encouragement.

As usual, it is hard to mention everyone who collaborated to this entire process. Therefore, I express my love and appreciation to everyone who contributed to the accomplishment of my work.

Thank you very much, everyone!

Anlin Lazar K

PREFACE

The pursuit for renewable and green energy supplies that could curtail carbon emissions is one of the most urgent concerns for sustainable development of human civilization. This is especially true in light of the threat posed by global warming and energy crises. Over the course of the last several decades, a significant number of research efforts have been dedicated to the pursuit for clean and renewable energy sources. Mechanical motion is a freely available energy present in the surroundings. In recent years, it has become an attractive option for energy harvesting as a promising research supplement to existing fuel sources and as an efficient energy source for gadgets that are powered by batteries. Energy sources based on piezoelectric effect, electromagnetic effect, electrostatic effect, and magnetostrictive effect were the only mechanical energy harvesting techniques available until recently. Possible drawbacks, such as complexity of geometry, low power output, manufacture of high-quality materials, dependency on external power sources, and lack of structural design adaptability for varied applications, may impede widespread adoption of these approaches. As a novel and renewable energy technology, triboelectric nanogenerator (TENG) was introduced in 2012 as an innovative technology for harvesting ambient mechanical energy based on the connection of triboelectric effect and electrostatic induction. This idea can significantly improve the development of TENG as renewable energy sources and self-powered active sensors. It will significantly aid in identifying TENG as a fundamentally new green energy technology that is simple, sustainable, reliable, cost-effective, and highly efficient.

This thesis reports on possibility of material modification techniques of triboelectric layers with in an aim to improve the surface charge density of the tribo electric materials under study.

Chapter 1 details about the overview of existing mechanical energy harvesting devices such as electromagnetic generators, solar energy harvesters, piezoelectric energy harvesters and thermal energy harvesters and their operating mechanisms. An introduction to triboelectric nanogenerators, review about the developments of TENG and details about materials chosen under study are included in this chapter. Main objective of the work is to develop high performance TENGs and special attention has been given to the material modification of the tribo-material chosen under study. Materials chosen under study includes polydimethylsiloxane (PDMS), polymer into which additives such as conducting ceramic namely lanthanum strontium cobaltite (LSCO) and metal nanoparticles are embedded.

Introduction of conducting ceramic and metal nanoparticles were done as a method of material modification. The properties of polymer ceramic composites and polymer metal composites are mentioned in detail in this chapter. Towards the end, challenges faced in the field of TENG has been addressed.

Chapter 2 discuss the concept and theory of TENGs by detailing the theoretical origin and fundamental working mechanism of triboelectric nanogenerators. Details of different working modes are included and ends by briefing about probable actions taken to improve the energy conversion of TENGs and boost their energy harnessing efficiency. The chapter explains the characteristics of the materials chosen for the research and the design of TENG structure. Material characterization, electrical characterization techniques and equipments for studying the properties of the fabricated devices are detailed in order to procure a vivid idea about the measurements results analyzed in the following chapters.

Energy harnessing gadgets which employ triboelectric effect have caught global attention due to excellent output performance compared to other nanogenerators for various applications. In c**hapter 3,** an attempt has been done to modify the properties of the tribo material by embedding it with metal nanoparticles of different conductivity (silver, copper, aluminium, zinc and tin) in different weight percentages. Metal /PDMS composites were prepared by embedding metal nanoparticles into PDMS matrix. PDMS is fabricated using room temperature curing method which act as bottom triboelectric material while copper act as top tribo material. Out of several metal/PDMS composites, silver/PDMS composite based TENG showed excellent properties. X-ray diffraction studies of metal /PDMS composites reveal the structural properties while Raman analysis suggests the enhancement of PDMS peaks due to the presence of metal nanoparticles. Silver/PDMS composite achieved an open circuit voltage of 33.6 V, short circuit current of 4.5 μA, an output power of 72.2 μW at 8 MΩ load and maximum energy storage of 1.8mJ at 220 nF capacitance at a working frequency of 10 Hz and force of 10 N. Variation of dielectric constant of the metal /PDMS composite materials onthe addition of various metal nanoparticles, and its dependence on the output performance of the TENG is studied. With the increase in the amount of metal nanoparticles, the properties got improved and 20 wt% Ag/PDMS composite manifested excellent properties. This work focuses on output performance of polymer based TENGs and tailoring the properties of polymers by introducing metal nanoparticles into polymer matrix.

Self-powered flexible and wearable electronic systems for developing human-integrated technologies require portable energy devices capable of efficiently scavenging the ubiquitous mechanical energy. Triboelectric nanogenerators (TENGs) made from soft polymers augmented with additives with good dielectric properties have been identified as suitable candidates for energy sources. In **chapter 4,** $La_{0.8}Sr_{0.2}CoO_3$ (LSCO) ceramic particles possessing high permittivity are introduced in to the PDMS polymer matrix with an aim to improve the dielectric property of tribo-layer. Improvements in the output performance of cost-effective TENG, based on PDMS/LSCO composites with varying amount of LSCO are studied in detail. X-ray diffraction studies indicate successful formation of polymer/composites while Raman analysis suggests uniform dispersion of LSCO particles into the polymer matrix. It is found that, in PDMS LSCO two-phase composites, dielectric constant of filler has an influence on the triboelectric output performance. Maximum short circuit current of 3.6 μA and an open circuit voltage of 23. 8 V was obtained when 20 wt% LSCO was added to PDMS. Highest power 29.4 μW was obtained at a load resistance of 10 MΩ. Capacitive model was utilized for exploring the energy storage ability of TENGs and the inherent capacitance of thePDMS/LSCO composite based TENG was found to be 300 nF. This work provides a feasible perception of improving output performance of polymer based TENGs by the incorporation ofceramic materials into polymer matrix and harvesting ubiquitous mechanical energy.

Chapter 5 briefs about the applications which has been extracted from the prepared samples by forming TENG structure. To enhance the power output, vertically stacked PDMS/LSCO composite TENG was fabricated by stacking four units of individual TENG, where each unit was separated using poly ethylene terephthalate sheet (PET). Device was further reinforced by acrylic sheets on top and bottom sides. Such vertically stacked device generated a current 43.2μA and an output voltage of 90 V. Driven by palm tapping, the stacked network could providea continuous AC supply which was converted to DC to act as a standard power source for driving small power electronic devices. Output of vertically stacked power unit was incorporated with a digital watch so as to convert it into self-powered electronic gadget This proves that mechanical energy source could empower the broad range of commercial mobile and wearable smart electronic devices which includes electronic displays, sensors etc. Even with irregular palm tapping (have irregular interval between the tapping), a wearable watch functions normally as long as the average power extracted through human motion exceeds its power consumption. Also output from vertically stacked device was connected to charge a capacitor through a bridge rectifier under periodic mechanical motion. For manifesting the

practical application of fabricated TENG as energy harnessing device, commercially available blue light emitting diodes (LED) were lit and capacitors were charged using LSCO /PDMS based TENG. A full wave bridge rectifier was connected between TENG and commercial LEDs or capacitors to examine the self-powering ability of developed device. TENG was connected to 25 LEDs to lit using the electrical output generated simply by human hand tapping. An impact sensor was developed using LSCO/PDMS composite TENG. It could be used as rain sensor in order to sense and harness mechanical energy from the rain drops. LSCO/PDMS composite based TENG used to fabricate single electrode mode based TENGs. This mode is adoptable for harnessing energy from moving parts of vehicles. The results of the PDMS/LSCO composite-based TENG suggest that these materials may be suitable candidates for inclusion into electrical devices, thereby changing them into self-powered devices.

Chapter 6 summarizes the work done so far and details about the work expected to be performed in future. Also, different possible applications of TENGs are explained. TENG has the potential to function as a very sensitive, self-powered sensor that can detect mechanical triggering and stimulations. The electric current and voltage signals that are produced by TENG reflect different types of information in relation to a mechanical action. The fact that such a sensor need not require a power supply to be driven will be a radical shift from the traditional sensors. Micromechanical systems, human-machine interfacing, touch-pad technology, security systems, and motion sensing are some of the sectors that find applications for this technology. Future work and recommendations provide work plan to support and sustain the research work with a sole aim to develop innovative and potentially efficient mechanical energy harvesting devices along with the commercialization of application of the fabricated devices in a large scale.

LIST OF TABLES

LIST OF FIGURES

LIST OF ABBREVIATIONS

NG	-	Nanogenerators
IoT	-	Internet of Things
WSN	-	Wireless Sensor Networks
MEMS	-	Micro electro mechanical systems
AI	-	Artificial intelligence
PV	-	Photovoltaic
TEG	-	Thermoelectric generators
PEG	-	Pyroelectric generators
SEH	-	Solar energy harvester
TEEH	-	Thermoelectric energy harvester
PEEH	-	Pyroelectric energy harvester
TEG	-	Thermoelectric generator
EMG	-	Electromagnetic generators
PENG	-	Piezoelectric nanogenerators
TENG	-	Triboelectric nanogenerators
PZT	-	Lead zirconium titanate
PTFE	-	Poly tetrafluoroethylene
FEP	-	Fluorinated Ethylene Propylene
PVDF	-	Polyvinylidene Fluoride
PDMS	-	Polydimethylsiloxane
TFT	-	Thin film transistors
CNT	-	Carbon nanotube
MWCNT	-	Multiwall carbon nanotube
CNF	-	Cellulose nanofibrils
LSCO	-	Lanthanum doped Strontium Cobalt Oxide
DBTDL	-	Dibutyl tin dilaurate
TOH	-	Tetraethyl orthosilicate
SEM	-	Scanning electron microscopy
SERS	-	Surface enhanced Raman scattering
ICT	-	Information and Communication Technology
PZT	-	Pb $(Zr,Ti)O_3$
BZTO	-	Ba $(Ti_{0.8}Zr_{0.2})$ O_3
LSP	-	Localized surface plasmons

LIST OF PUBLICATIONS

Journal Publications

1. **Anlin Lazar K**, K V Vijoy, Pradeesh K, Shibi Thomas, Honey John, K J Saji , "Effects of metal nanoparticles on the performance of PDMS based triboelectric nanogenerators" 639, 413952,2022, Journal **Physica B: Physics of Condensed Matter**.
2. **Anlin Lazar K**, K V Vijoy , Tony Joseph, Honey John, K J Saji, "Vertically integrated triboelectric nanogenerators using PDMS/LSCO composite" (Under review; **Materials Science and Engineering B**)

Conference Papers

1. **K Anlin Lazar**, V J Cicily Rigi, D Divya, and K J Saji, "Effect of annealing on structural and optical properties of SnS_2 thin films grown by thermal evaporation and post sulphur annealing technique" IOP Conf. Ser.: Mater. Sci. Eng. 1166 (2021) 012004, doi:10.1088/1757-899X/1166/1/012004.
2. Tony Joseph, **K Anlin Lazar**, D Divya. Preparation and structural, dielectric characterization of CaBSi2O6 (B = Mg, Co, Ni, Mn, Zn) ceramics" IOP Conf. Series: Materials Science and Engineering 1166 (2021), 012025, doi:10.1088/1757-899X/1166/1/012025.
3. **K. Anlin Lazar**, V. J. Cicily Rigi, P. Hajara, P. Praveen, and K. J. Saji, "Deposition of tin disulfide thin films by thermal evaporation and sulphurisation" AIP Conference Proceedings 2162, 020078 (2019); https://doi.org/10.1063/1.5130288
4. **Anlin Lazar K**, K V Vijoy, Shibi Thomas, Pradeesh K, Honey John, K J Saji, A Comparative Study on Impregnation of Silver and Aluminium Nanoparticles into PDMS Matrix: Dielectric Property Tailoring for Improving the Output Performance of Triboelectric Nanogenerators (AIP Conference Proceedings: accepted).
5. K V Vijoy , **Anlin Lazar K**, Honey John , K J Saji, Enhancing the triboelectricperformance of flexible PDMS/Boron nitride composite nanogenerators. (AIP ConferenceProceedings: accepted).
6. V J Cicily Rigi, **K Anlin Lazar**, P Hajara, P Praveen, K V Vijoy and K J Saji, Large Scale Deposition of Two-Dimensional Tungsten Disulfide Films Using Radio Frequency Magnetron Sputtering, (AIP Conference Proceedings: accepted).

.

Conferences Attended

1. **Anlin Lazar K,** K V Vijoy, Shibi Thomas, Pradeesh K, Honey John, K J Saji, "A Comparative Study on Impregnation of Silver and Aluminium Nanoparticles into PDMS Matrix: Dielectric Property Tailoring for Improving the Output Performance of Triboelectric Nanogenerators", International conference on **NANO icon 2022**, IUCND, CUSAT on January 11-15, 2022**.**
2. **Anlin Lazar K,** K V Vijoy, Honey John, K J Saji**, "**Metal Nanoparticle-PDMS: A Novel Polymer Composite for High Performance Triboelectric Nanogenerator", International conference on **Advances in Polymer Technology (APT-21)**, Department of Polymer Science and Rubber Technology, CUSAT on May 27-29,2021.
3. **K Anlin Lazar**, V J Cicily Rigi, D Divya, and K J Saji, "Effect of annealing on structural and optical properties of SnS2 thin films grown by thermal evaporation and post sulphur annealing technique", **Third International Conference on Materials Science and Manufacturing Technology (ICMSMT 2021)** during 08 - 09, April 2021, Coimbatore, Tamil Nadu, India.
4. **Anlin Lazar K,** Aparna Suresh, and K J Saji, "A dual step process for the fabrication of WS_2 thin films for optoelectronic applications", **National Photonics Symposium 2020 (NPS 2020)**, February 27-29 ,2020; International School of Photonics, Cochin University of Science and Technology, Kochi- 682 022, Kerala, India.
5. **Anlin Lazar K**, Cicily Rigi V J, Hajara P, Praveen P, K J Saji "Deposition of Tin Disulfide Thin Films by Thermal Evaporation and Sulphurisation", **International Conference on Advanced Materials (ICAM 2019)**, June 12 -14, 2019; Department of Physics, Nirmalagiri College, Kannur, Kerala, India.

TABLE OF CONTENTS

Chapter 1

An Introduction to Nanogenerators

Abstract

In the early decades, different energy harvesting techniques were employed to generate energy needed to drive the day today requirements. With the advent of flexible and wearable electronic gadgets, touch screen, smart phones, portable and rollup displays, the need for uninterrupted power sources became a necessity. Due to the limitations faced by these conventional energy harvesting sources, they became less suitable for empowering the future electronics industry. This chapter briefs about the different conventional energy harvesting sources and storage devices. This chapter also explains about the drawbacks faced by them and suggests a remedy to solve this energy crisis. The method is to incorporate energy storage devices along with energy harnessing gadgets among which triboelectric nanogenerators (TENGs) could form self-powered units. These nanogenerators opens an efficient way of converting mechanical energy into electrical energy and act as sustainable, uninterrupted power sources.

1.1 Energy demand for portable electronics

Energy is a basic resource in great demand because of its importance in defining the overall standard of living in modern civilization (1). Energy is utilized to power electronic

equipments such as computers, television, smart phones, house hold equipment, transportation system, telecommunication network security systems and so on. A major share of the energy we now use comes from the non-renewable sources of energy, especially the fossil fuels. But the conversion of energy into useful forms has become one of the most significant issues confronting humanity today, due to by environmental and fossil fuel scarcity concerns. As a result, there is a great need for new large-scale sustainable energy sources, such as solar, wind, and hydropower. Additionally, the near future is expected to see widespread distribution of a large number of mobile electronics, owing to recent advancements in the development of the internet of things (IoT), wireless sensor networks (WSN), microelectromechanical systems (MEMS), wearable electronics, implantable medical devices, robotics, and artificial intelligence (AI), all of which necessitate innovative compact and efficient energy sources. Precautionary measures must be taken to address the issues with the short lifetime and frequent replacement of conventional external power sources, such as batteries, in a large number of devices (2, 3).

Fortunately, the last decade has witnessed a steady decline in the size and power needs of most of the portable electronic devices to levels less than a few watts. Thus, the term "nano energy" was coined to refer to the use of nanomaterials and nanotechnology to the development of integrated power sources capable of harvesting many kinds of energy, including light, thermal, and mechanical motions (4) . With the initiation of Internet of Things, sensors, flexible, wearable and portable electronics, smart phones, national security monitoring system etc, the utilization of energy sources demands uninterrupted and maintenance free power sources. Modern electronic gadgets have been equipped with numerous functionalities in a small area which includes monitoring the heartbeat, stress level, oxygen level in the blood etc. There are devices incorporated with fabrics which could be easily used as portable devices in the form of dresses. Augmentation of these electronics

devices to human life offers secure as well as comfortable living situations (5, 6). Numerous nanogenerators (NG) have been investigated, including those for self-powered industrial and health monitoring systems, smart housing and clothing, artificial intelligence, self-powered mobile electronic devices, intelligent transportation systems, vibration dampers, and wireless power transmitters (7, 8). Thus, the current scenario of energy demands a novel and potential energy harvesting method so as to build up a self-powered energy system.

1.2 Background on mechanical energy harvesting

The prominent challenge faced by portable and wearable electronics is to get an uninterrupted and adaptable power source (9). Use of rechargeable Lithium-ion batteries and supercapacitors are the normal ways employed to power these electronic devices. But they need frequent maintenance and replacement which pose a lot of health hazards as well as environmental pollution (10). Also, these power sources are not enough to provide sufficient amount of energy to run the entire electronic industry. Excessive usage of rechargeable batteries and other power storage devices also pose serious threat to various ecological species because of the presence of harmful chemicals utilized for their fabrication (11). In this scenario, the remedy to overcome the energy scarcity is to upgrade the existing energy storage devices by increasing the energy output and also by the use of bio friendly and environmentally safe materials for fabricating these power sources (12, 13).

There have been numerous researches going on in order to connect the global energy consumption and energy storage to meet the energy requirements. Despite considerable efforts in this sector, the gap between energy demand and storage remains significant (14). Development of various energy harvesting devices are now a major concern to make up for the inadequacy faced by batteries and other energy storage devices. As one of the most commonly available forms of energy in day-to-day life, such as human movement, is mechanical energy which possesses a great number of benefits, including abundance,

persistence, and portability. Devices which could trap the ambient mechanical energy available from the surroundings such as from tides, wind, human motions etc. and convert these forms of energy to useful electrical energy has a wide range of applications as energy sources. These energy harvesting devices reduce the dependency on rechargeable batteries (15, 16). If the aforementioned energy harvesters are made out of materials which are very bendable, light weight, stretchable in nature, then they could be easily integrated onto any fabrics or act as self-powered wearable and portable gadgets (17). Sensors are much advantageous to become self-powered devices because they require no external energy sources to empower them thereby getting much adaptable and compact. Thus, we could expect portable self-charging as well as self-powered devices that utilize all types of energy in near future. Using these devices, energy could be harvested as well as stored for future to act as self-powered gadgets (18).

1.3 Energy harvesting devices

Earth receives energy mainly in the form of sun light and hence it can be harvested using photovoltaic cells. But the output performance of solar cells is influenced by factors like climate, location, season etc. (18). The low durability of the electrodes of the solar cells is also a major factor of concern and hence the output of the solar cells is lower than expected (19). Yet another abundant form of energy which can be utilized is thermal energy and is usually converted into electricity using thermoelectric generators (TEG), which works on the principle of Seebeck effect. The two main technologies which rely on thermal energy harvesting are thermoelectric energy harvesting and pyroelectric harvesting (20). Pyroelectric generators (PEG) also effectively convert thermal energy into electrical energy by the process of redirecting the dipoles which gets stimulated by temperature variations (21, 22). Even though these devices could trap the thermal energy due to body heat and convert it into useful form, the peculiar device geometry and low performance have limited their applications to

some extent (23). On the other hand, wind energy is trapped using wind turbines which is a practical energy harvesting device. But researchers are trying to improve the conversion rate of wind energy using modern technologies such as piezoelectric or hybrid technologies (24, 25).Thus, need for wearable and flexible energy harvesting devices with novel structures became a prominent demand (26, 27).

1.3.1 Solar energy harvesting technology

The prime source of energy is solar energy which is varying with time because of the periodic and seasonal climatic conditions. Photovoltaic (PV) cell is usually made out of semiconducting materials which converts solar light energy to electrical energy through the process of photovoltaic effect. Figure 1.1 represents the working principal of a conventional PV cell. When sunlight falls on the PN junction, free electrons and holes are created (28). Electrons and holes are then driven to the N and P layers, respectively, by the action of the built-in potential across the p-n junction. When the photovoltaic cell is connected to a load through an external circuit, there will be a flow of current. Even though solar cells find enormous applications, there are many factors which hinder their extensive utilization as a source of energy. The major issues that play a significant role in the outcome arise prominently from environmental effect, cell efficiency, average lifespan, fabrication costs, and maintenance costs. Nanomaterials and nanotechnology have emerged as the most promising and rising industries in the quest to considerably enhance the efficiency of solar energy harvesting. However, the use of solar energy harvester (SEH) is still embarrassed by factors like as terrain, climate, solar panel area, expense, and durability.

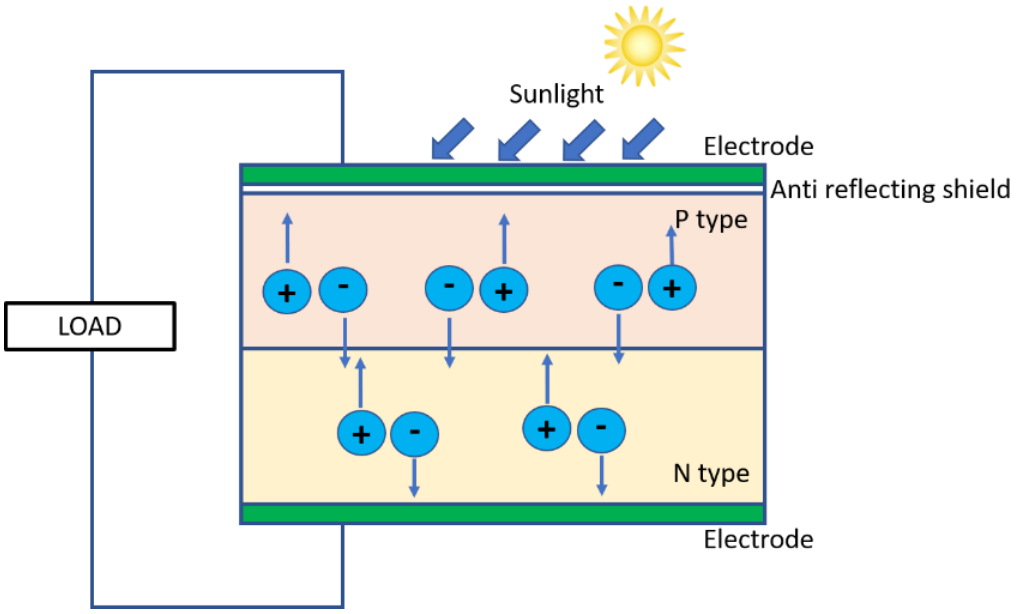

Figure 1. 1. Schematic representation of working principal a photovoltaic cell.

1.3.2 Thermal energy harvesting technology

Thermal conversion techniques are commonly used to convert heat energy, which arises from temperature variations in the surrounding environment, into electrical energy. Thermoelectric energy harvester (TEEH) and pyroelectric energy harvester (PEEH) are two of the most extensively utilized techniques. They are based on two separate operating principles: temperature changing over distance and time.

1.3.2.1 Thermoelectric energy harvesting (TEEH)

The Seebeck effect is used in the conversion of thermal energy into electrical power, which is known as thermal energy conversion (figure 1.2 (a)). When there is a temperature difference between the hot and cold ends of a thermoelectric generator (TEG), an electrical voltage is developed between p-type and n-type semiconductors as a result of the temperature gradient. Figure 1.2 (b) depicts the schematic diagram of an energy scavenging device known as a TEG where many p-type and n-type semiconductors are linked in series in order to maximize the efficiency of the device. In order to increase the efficiency of energy harvesters,

researchers are investigating potential nanomaterials as well as the optimization of structure and circuits (29, 30). TEEH has been commonly used in a variety of industrial applications (31). Despite the fact that the temperature difference is steady, persistent and readily available, the poor conversion efficiency of TEEH is the primary drawback of this technology.

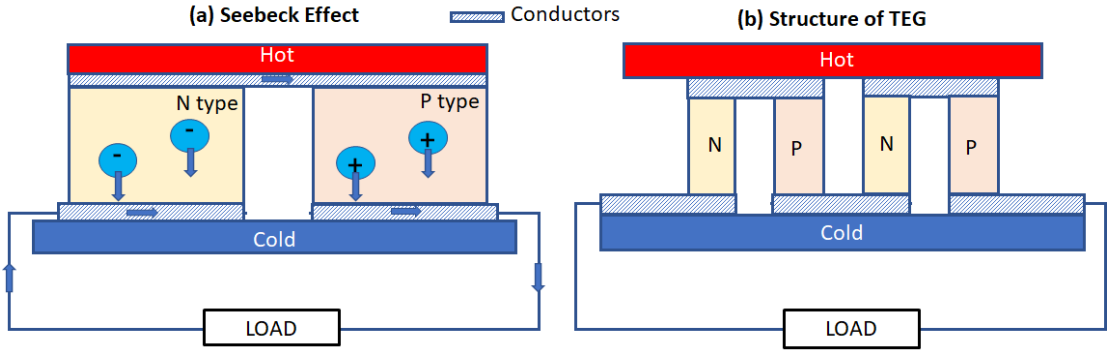

Figure 1. 2. The schematic structure of thermoelectric generator (a) describes the mechanism of Seebeck effect (b) Structure of thermoelectric generator (TEG) which consists of N type and P type semiconductors with connecting pads.

1.3.2.2 Pyroelectric energy harvesting (PEEH)

Pyroelectric materials contain internal spontaneous polarization (P_s) in the absence of an electric field, and the pyroelectric effect is the momentary alteration of P_s caused by the temperature variation of pyroelectric materials. Whenever the temperature rises, there occurs a reduction in Ps followed by thermal agitation which decreases the surface charges bonded to the surface. If the pyroelectric substance is in the short circuit condition, current flows through the external circuit and if it is in open circuit condition, voltage difference is developed across the material. The polarization of the crystal occurs because of the temperature difference and a voltage is generated on the crystal's surface. Ayesha et al. (32) revealed that the commercial Dura Act Patch Transducer can harvest energy at a rate of 0.034 W/cm^3 under temperature fluctuations ranging from 310 K to 340 K, which may be utilized to create a self-powered temperature sensor using a temperature variation (33). Thus, in a nutshell, energy harnessed by the pyroelectric effect employing innovative temperature cycling techniques (such as the Olsen

cycle) has a greater efficiency than energy scavenged by the thermoelectric effect. However, the low-frequency temperature variations and poor efficiency of energy harnessing cycles that contribute to the PEEH are incompetent when used in conjunction with other energy harvesting methods. Establishing excellent thermal conductivity on both the heat and cold ends is the primary goal of pyroelectric energy harvester. This means that a substantial heat flow over the converter or the induction of high-frequency temperature variations is fundamentally important and necessary for an efficient power generator to function properly and effectively (33).

1.3.3 Mechanical energy harvesting

Mechanical energy, which is another renewable and safe energy source, may be properly harnessed to provide clean and substantially usable electric power for self-powered devices. Mechanical energy in industrial applications is primarily comprised of various forms of kinetic energy stimulated by the motion of objects, elastic potential energy induced by the deformation of objects and electric potential energy resulting from conservative Coulomb forces. Kinetic energy is the most common type of mechanical energy in industrial applications. The main source of mechanical energy includes wind (34), ocean waves (35), human (36) and animal body movements and sound (37). This ubiquitous mechanical energy can be efficiently converted into electricity using different devices. They include conventional electromagnetic generators (EMG) (38), piezoelectric nanogenerators (PENG) (39) and triboelectric nanogenerators (TENG) (40).

Maxwell's equation rules the output of EMG since it involves time varying magnetic field. In the case of TENG and PENG, it is the displacement current that determines the output performance (41). Flexible as well as lightweight materials are exploited in the fabrication of PENG and TENG. Piezoelectric effect is exhibited by materials which have no inversion symmetry and they get electrically polarized when exposed to mechanical stress. As a result of polarization, changes in the surface charge density occurs. The commonly used materials for

piezoelectric devices includes lead zirconium titanate (PZT) (42), ZnO, $BaTiO_3$ and polyvinyl fluoride (PVDF). Studies point out that traditional piezoelectric devices possess power densities of around 0.416 W/m^3 (43) . The modern piezoelectric nanogenerators forms a class of mechanical harvesting modules made out of piezoelectric nanostructures and an output power density of 0.78 W/cm^3 has been achieved through manual pressing. The disadvantages of piezomaterials include expensiveness, less adaptable nature and comparatively lower output performances. As far as choices in the case of device structure, materials opted for fabrication and the output performance are concerned, TENG is found to more beneficial than PENG. Triboelectric nanogenerators (TENGs) was initially proposed by Wang et.al in the year 2012 (42). They caught much attention due to the ability of the materials to harness the ubiquitous mechanical energy available from the environment. In nut shell, TENG will take up a superior hierarchy in the realm of smart world (44, 45). Figure 1.3 represents different types of nanogenerators and their applications in the era of the IOT.

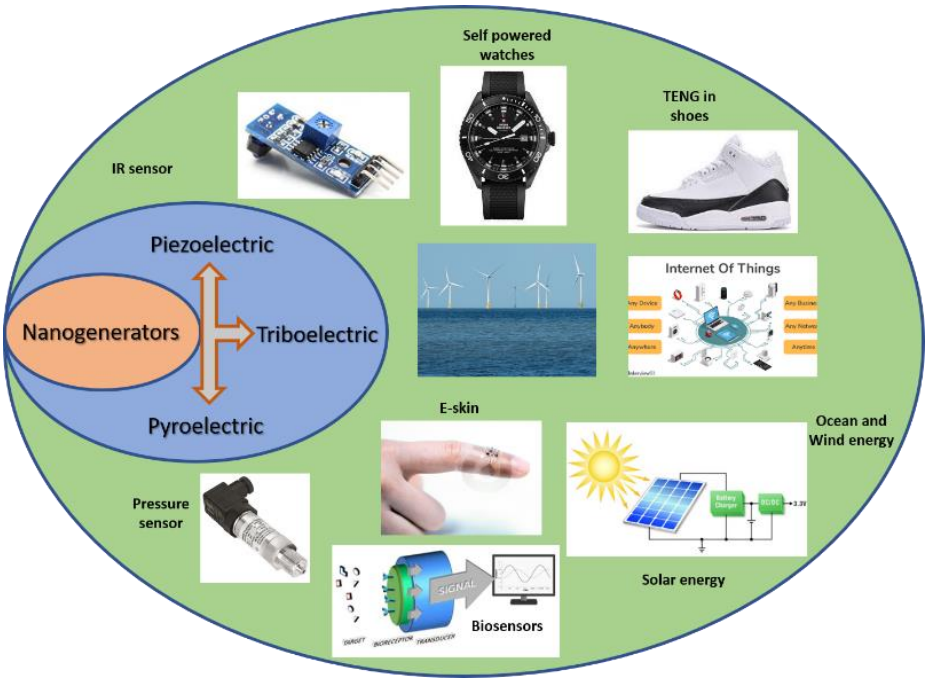

Figure 1. 3. Different types of nanogenerators and their applications in the era of the Internet of Things.

There are different types of energy harvesters which can be widely grouped depending upon the type of energy source utilized (46). They include (i) electromagnetic energy harvesting technique (ii) piezoelectric energy harvesting technique (iii) triboelectric energy harvesting technique.

1.3.3.1 Electromagnetic energy harvesting

Electromagnetic generators are the most familiar type of energy harvesting device which are usually employed for large scale production of electricity (47). Electromagnetic induction is the phenomenon whereby a segment of a closed circuit cuts a magnetic field in a direction that is not parallel to the field lines and hence produce current in the circuit. It is possible to transform kinetic energy into electricity with the help of a magnetic field. When combined with magnetic fields, kinetic energy that would otherwise be dissipated may be gathered and used to power self-powered sensors. Electromagnetic energy harvesting systems have the potential to gather a large amount of other mechanical energy. Several researchers have developed a vibration-based electromagnetic generator to substitute the battery in sensor nodes used for continuous monitoring of pump motors or other production and commercial gadgets back in 2013 (48). Three years later, rotational kinetic energy was successfully harvested and used to power wireless sensor nodes that were used to monitor the conditions of milling operations and cutters (49). This was accomplished through the use of an attachable electromagnetic harvester.

In the case of thermal power plants, fossil fuels are being continuously burnt and is transformed into mechanical energy and then to electrical energy. Using electromagnetic induction process, the mechanical energy is being harnessed and electricity is generated. Tidal power plants are also incorporated with electromagnetic generators to convert wave energy to electricity. In the case of electromagnetic generators, the output is obtained by relative

movement of the electric coils placed inside the field of permanent magnets which causes change in the magnetic flux. Since the EMG employs magnets which are usually huge and stout ones, they cannot fulfil the conditions for wearable and flexible electronic devices (50). When using present technology, the limitation of electromagnetic generators is the difficulty of achieving low dimension manufacture of gadgets.

1.3.3.2 Piezoelectric energy harvesting

Piezoelectricity, commonly known as the piezoelectric effect, is a process that causes when mechanical energy is converted into electrical energy by a mechanical force. According to the direct piezoelectric effect, when dielectrics composed of certain materials are deformed by a force operating in a specific direction, charges with opposing polarity can be created as a result of internal polarization on the surfaces of the dielectrics (figure 1.4). Using a piezoelectric-based electrical model, the researchers were able to power an automated wireless sensor in heating, ventilation, and air conditioning systems (51). As a result of the advancement of materials science, together with the increasing need for high efficiency in energy harvesters, nano piezoelectric materials have been studied in depth and are now being employed extensively in a variety of applications. For example, a new MEMS-based energy harvester was created and manufactured using the combination of strain sensitive nanocomposite materials with MEMS (52). Moreover, one of the most significant obstacles towards the widespread use of nano-piezoelectric materials in commercial production is the limitation on the types of alternative materials available and the intricacy of the manufacturing procedures used to create them. As a result, the design of the energy harvester is another challenge, in which the resonant frequency of the device should be selected in the frequency band with energy concentrated to achieve the efficient energy harvesting.

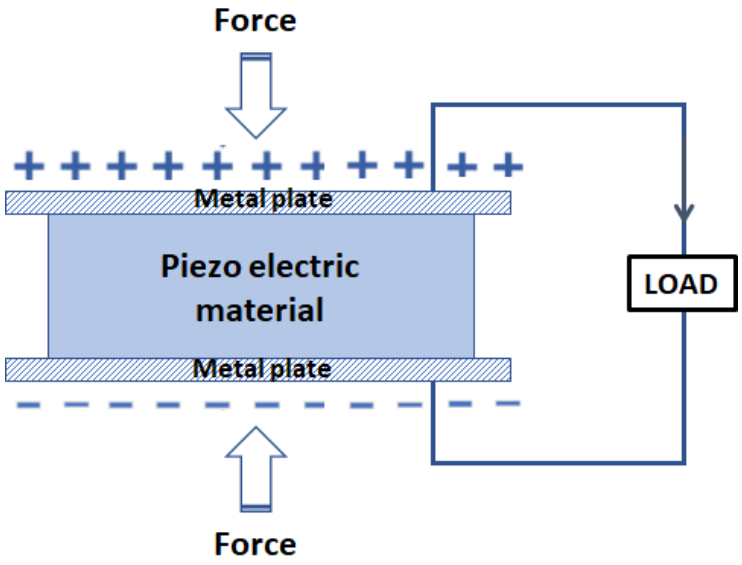

Figure 1. 4. The mechanism of generation of electrical energy using piezoelectric effect

1.3.3.3 Triboelectric energy harvesting

Triboelectric effect is the process of contact electrification when two dissimilar materials come into physical contact. As a result of external stimuli, the electrons in the two objects gather enough energy to migrate in a given direction as illustrated in figure 1.5 (53). Due to the fact that different materials have varying abilities to reject or receive electrons, friction between the materials also play a crucial role in the effectiveness of contact electrification systems. Because of their features of low cost and endurance, triboelectric nanogenerators (TENG) made from materials in the triboelectric series have attracted the attention of academia and industry that are interested in energy harvesting technologies throughout the world. A paper-based TENG that was ultra-soft and flexible was constructed from inexpensive commercial materials in order to scavenge the energy associated with the human body's mobility, sound energy, and wind energy (54). A self-powered air cleaning system for eliminating SO_2 and particle matters with the aid of rotating TENG was initially introduced in 2014 by Chen et al (55).

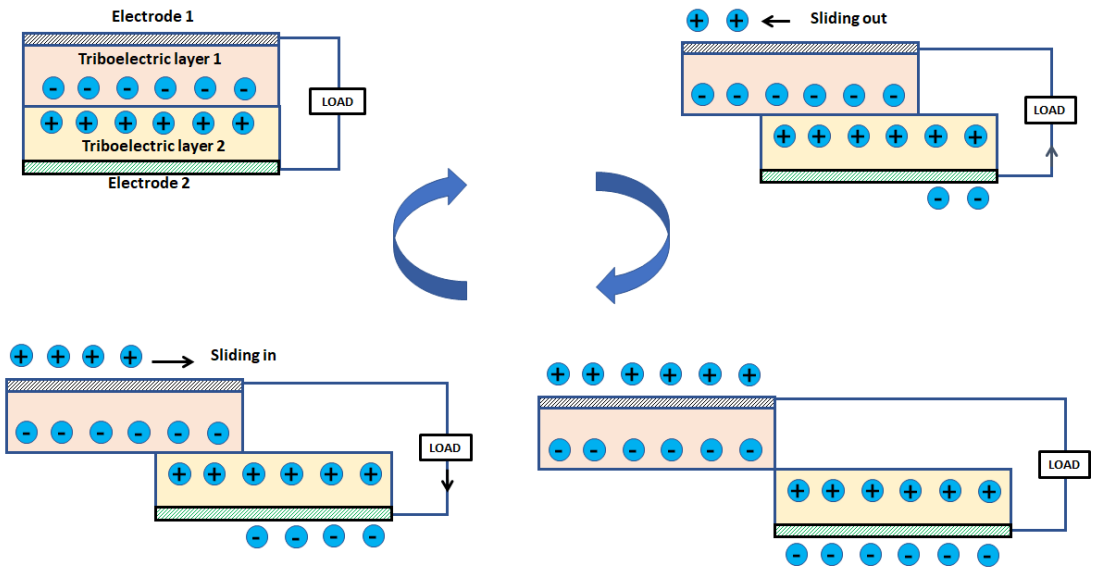

Figure 1. 5. Mechanism of a standard parallel sliding mode based triboelectric nanogenerator.

1.4 Triboelectric Nanogenerators

1.4.1 History and development of nanogenerators

Devices which can generate electrical energy from ubiquitous mechanical energy are usually designated as nanogenerators. By the end of 17th century, researchers tried practical ways to extract electricity from friction. It was in 1663, the oldest form of friction machine which could generate electricity from friction was fabricated and many researches were carried out on this machine to improve the performance (56). In 1831, discovery of electromagnetic motor led to the utilization of generator widely in thermal power plants. In 1878, popular static electricity generator named Wilmshurst machine was invented. Van de Graaff generator was invented in the year 1929 which could produce high voltage direct current. Output potential of about 25 megavolts is obtainable from modern Van de Graaff generators. Figure 1.6 depicts the history of energy generators. With the advent of nanotechnology, new technologies namely piezoelectric, pyroelectric and triboelectric were developed which could generate electricity. The availability of high surface area, adaptable physical and chemical properties etc. have

placed nanoscale structures potentially efficient technology which extract, convert and save for future use from different forms of energy namely thermal, electrical, chemical and mechanical (57).

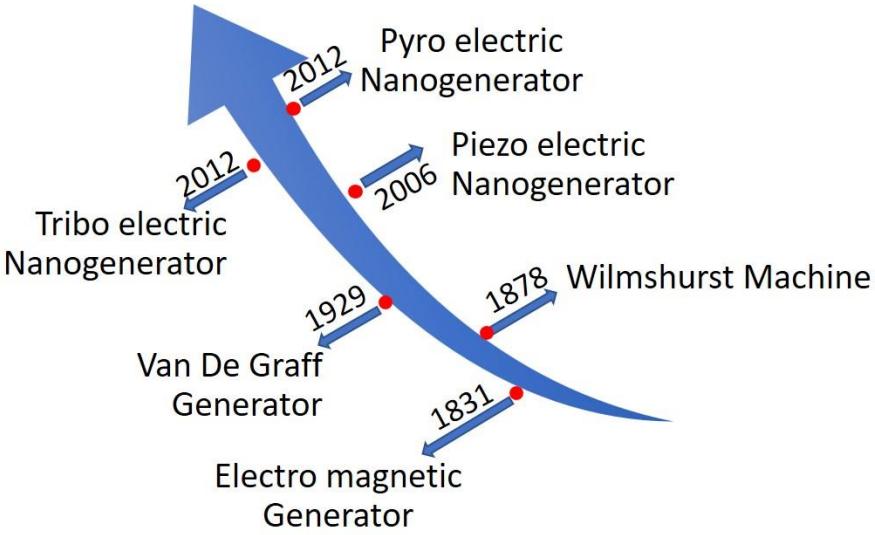

Figure 1. 6. The major inventions in the history of mechanical energy-harvesting technology

There are numerous energy-harvesting methods which works on the basis of piezoelectric effect, triboelectric effect, pyroelectric effect and electromagnetic induction. These devices convert freely available mechanical energy into electrical energy. New energy harvesting devices, nanogenerators are capable of harvesting different mechanical motions (such as walking, breathing, running, heartbeat), vibration, ocean waves, raindrops, wind and heat energy. First fabricated nanogenerator worked on the principle of piezoelectric effect and was developed by Wang et.al in the year 2006 (58). The main advantage of nanogenerators which are usually made at nanoscale regime was its ability to harness could harness low-frequency mechanical vibrations.

The concept of triboelectric nanogenerator (TENG) was introduced in 2012 by the research group led by Prof. Zhong Lin Wang at Georgia Tech (59). Triboelectrification effect

has been observed for thousands of years and during olden days this phenomenon was considered as a hazardous one than a useful technique. The triboelectric effect is commonly observed in daily life, for example a rubbed cloth piece attracts small particles such as dust, paper bits etc. As triboelectric effect causes creation of noises which get mixed with electric signals, it affects the equipment's performance. As a result of triboelectric effect, high voltage is generated and discharge of electrostatic charges often hampers electronic devices. Also, occurrence of sparks between electrically charged surfaces results in fire threats (60)**.** However, TENGs which basically works on the principle of contact electrification and electrostatic induction, could be employed for harvesting energy from mechanical motions (40).

1.4.2 Fundamentals of TENG

Triboelectric nanogenerators (TENGs) are the devices that generate electricity by a combination of triboelectrification and electrostatic induction. During the fabrication of a piezoelectric nanogenerator with a small gap, Prof. Zhong Lin Wang and his team found that the device exhibit high voltage due to triboelectric effect (61). The term "triboelectrification" refers to the creation of charge due to the interaction between the surfaces of two different materials when they come into physical contact. Electrostatic induction is the process where electricity is generated in which electrons travel from one electrode to another electrode, causing a current flow in order to nullify their potential differences (59, 62). Usually in TENGs, a couple of different dielectric surfaces are present. As electron affinities of the two surfaces are different, the time-varying triboelectric charges are produced on their surfaces and when they are separated, the triboelectric charges are dissipated.

The mechanism that results in the production of charges on a surface of the triboelectric material has not been properly characterized and continues to be a source of intense discussion

(1). Only in the year 2017, a fundamental physical model was developed, in which the triboelectrification process was explained. The origin of a mechanism that has been known for thousands of years may be traced back to Maxwell's Displacement current. Materials that exhibit the triboelectrification phenomena are typically insulators with low conductivity and hence they have capacity to hold the transferred charges over an extended period of time. Due to this nature, there are several negative effects that occur in industrial manufacturing, transportation, aviation, and other fields.

Polyester and Kapton thin films were kept together to form the TENG structure which generated an open-circuit voltage (V_{OC}) of 3.3 V and a short circuit current (I_{sc}) of 0.6 μA with a power density of 10.4 mW/cm^3 (59). Wang et.al also designed an arc shaped triboelectric nanogenerator by using one of the tribo material as polymer layer and another one as metal layer (63). By incorporating the electrostatic induction effect, production of electric energy using TENG turned out to be a remarkable achievement. It was through the attachment of conductive electrodes; the induction procedure was accomplished. The process of energy generation involves creation of potential difference when two pieces of opposite tribo-polar materials make a relative movement. This results in the flow of induced charges producing electric current through the external circuit. In this process, easily available mechanical energy is utilized for the production of electrical energy. Thus even a small vibration act as the source of energy which could be harvested using TENG (64).

1.4.3 Contact electrification in TENGs

Though the concept of contact electrification is a vivid one, it is difficult to refer to the same picture in terms of the theory that reinforces it. Contact electrification process is noticed in everyday life, industrial applications, natural phenomena etc. The study of triboelectric charge creation has been a topic of interest for decades in a wide range of fields in which physicists, chemists, engineers, and meteorologists have attempted to comprehend the theory

underlying it (65). However, no definitive conclusion has yet been reached. There have previously been three distinct processes believed to explain triboelectric charge creation, which have been primarily described as follows: The transfer of electrons, the transfer of ions, and the transfer of materials.

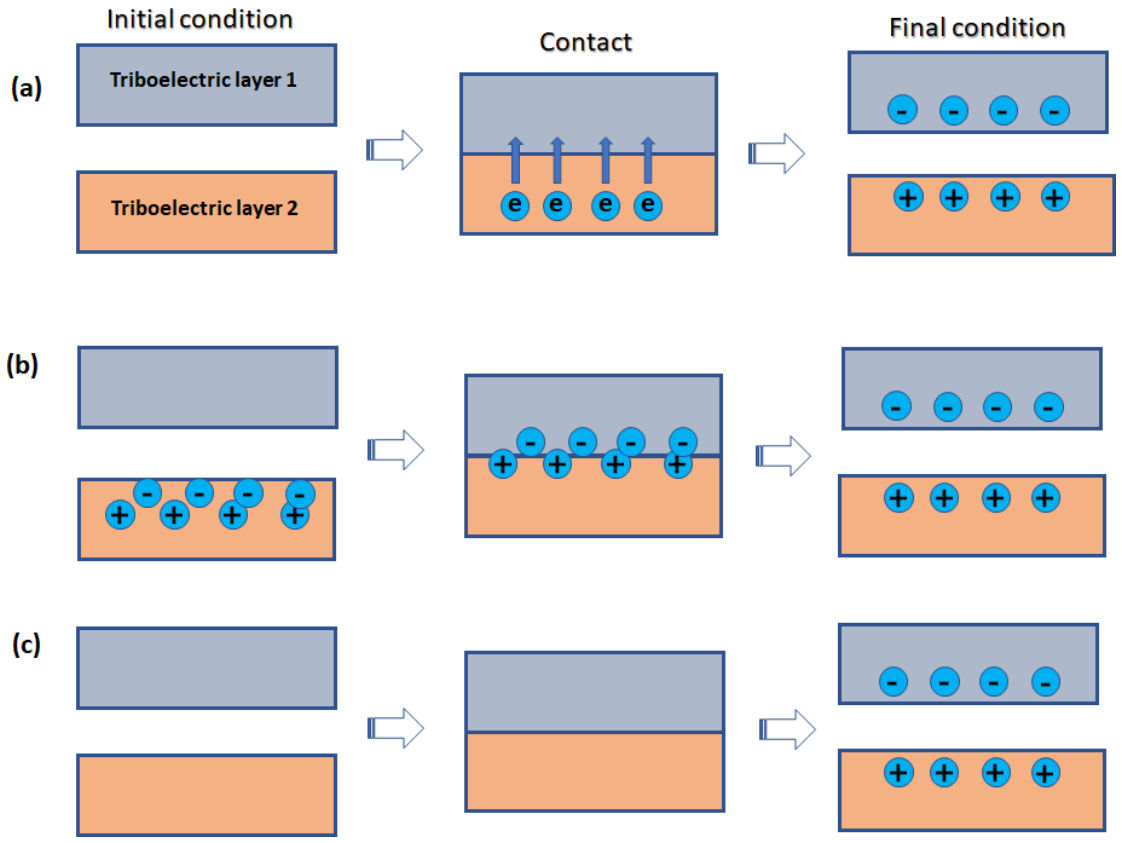

Figure 1. 7. Triboelectrification mechanisms (a) Electron transfer mechanism (b) Ion transfer mechanism and (c) Material transfer mechanism.

1.4.3.1 Electron transfer mechanism

The electron transfer mechanism is depicted in figure 1.7 (a). The electron transfer process has been mostly concentrated on conductor triboelectrification, where it is assumed that electron exchange occurs as a result of conductor work function differences (66). The work function φ of a conductor is an inherent property defined as the least amount of thermodynamic work required to remove an electron from the surface of a solid. When metals with dissimilar

work functions come into contact, the contact potential difference V_0 between their surfaces results in electron tunnelling in order to preserve thermodynamic equilibrium (Figure 1.8). φ_1 and φ_2 denotes the work functions of metal 1 and metal 2 respectively. From the equation (1.1), it is evident that contact potential difference is directly proportional to the difference in the work functions of two metals.

$$V_0 = \frac{\varphi_2 - \varphi_1}{e} \tag{1.1}$$

Harper demonstrated how the parallel plate capacitor technique could be employed to estimate the total amount of charge transported (67). In terms of the contact area and metal to metal separation distance dependent capacitance *Cs* of the system, the entire amount of charge transferred (*Q*) may be computed as follows:

$$Q = C_s \times V_0 \tag{1.2}$$

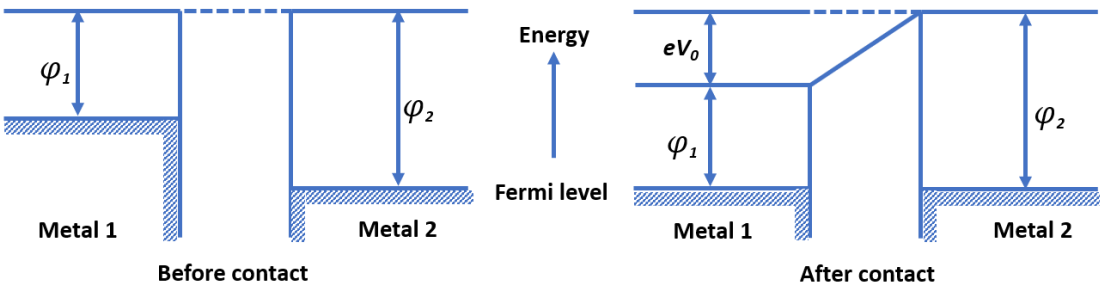

Figure 1. 8. Electron transfer between metal-metal contact.

As previously stated, triboelectrification involves both contact and separation processes; the contact process initiate charge transfer, while the separation process regulates charge transfer by terminating tunnelling of electrons over a certain separation distance (67). Until now, experts suggest that metal-metal contact electrification is the sole process for which there is a consistent explanation exists and hence electron transfer is the primary cause for triboelectrification.

However, as insulators have a large bandgap between their valance and conduction bands, electrons cannot flow between them directly (68). Thus, electron transfer process which is based on the work function differences cannot be applied to metal-insulator and insulator-insulator contacts directly. In other words, when two distinct insulators I_1 and I_2 are in close contact, electrons in the valance band of I_1 cannot be transferred to the valance or conduction bands of I_2, as all valance states in I_2 are completely occupied and electrons lack the energy required to occupy the conduction band. In this scenario, researchers proposed work function difference-based electron transfer model with surface state theory for metal-insulator and insulator-insulator interfaces (69). According to this theory, insulator surfaces have distinct surface state levels and associated effective work functions by which electrons in various materials migrate among these states. Subsequently, Fabish and Duke developed a novel electron transfer model for insulator contacts which describe about acceptor and donor states for insulator surfaces (70). Unfortunately, due to theoretical inadequacies and a lack of research observations, both electron transport models for insulator-metal and insulator-insulator interactions continue to be debated (65).

1.4.3.2 Ion transfer process

Electrophotography advancements in the 1960s revealed that polymeric toners including ionomers or molecular salts include mobile ions on particle surfaces of polymers. Usually, tightly bonded immobile ions and loosely bound mobile counter ions occur with opposing polarity (71, 72). Thus, when different insulators come into contact, mobile ions can be transported between them, resulting in oppositely charged triboelectric insulators as shown in figure 1.7 (b). Similar to this theory, various investigations prove that there is a transfer of ion concentrations between polymer-polymer and polymer-metal contacts (73, 74). However, because non-ionic polymers do not contain mobile ions, ion exchange mechanism cannot be considered as the reason for contact electrifications. The reports suggest that the presence of

hydroxide ions on polymer surfaces (74, 75) can supply the mobile ion required for the ion exchange process. Recently an experiment was conducted by Baytekin and colleagues which established that although water is not required for triboelectrification, it does assist to balance the surface charges (76), which contradicts the idea that contact electrification is solely due to ion exchange.

1.4.3.3 Material transfer process

According to the material transfer theory, friction causes sub-micron-scale fragments of materials to get exchanged among the surfaces of rubbed materials (Figure 1.7 (c)). These particles are charged and transferred as a result of the bond breaking process or contamination of surfaces (77). However, contact electrification is a repeatable process and material transfer cannot be a prominent cause for triboelectrification, as its magnitude may get reduced during repeated process (78). In 2011, Baytekin and colleagues conducted extensive studies and characterizations of contact electrification, challenging the long-held belief that surfaces are charged uniformly with opposite polarities upon physical contact with materials(79). On the other hand, "mosaics" with both positive and negative charges scattered in varying amounts over each surface result in positive or negative net charge distributions (79). Additionally, a comprehensive x-ray photoelectron spectroscopy analysis were conducted by the same group established the existence of charge and material transfer during contact electrification (80).

1.5 Triboelectric series

The performance of TENG is also affected by the nature of the materials used. In general, organic materials may be arranged in a table according to the amount of positive charge that can be transferred, which is known as the triboelectric series which is shown in figure 1.9 (81). Materials chosen for the current study includes copper as both electrode as well as positive tribo layer while PDMS serves as polymer matrix for negative tribo layer and are highlighted in the figure 1.9. It is usually analogous to the electrochemical series of materials that describes

the tendency of a material to gain or loss electrons. The series lists materials towards the bottom of the series in an order of decreasing tendency to charge positively (lose electrons), and increasing tendency to charge negatively (gain electrons). Further away two materials are separated apart from each other in the series, the greater the charge transferred.

When two different materials come into close contact, one of the materials has a greater affinity to attract electrons than the other. It is always better to choose materials which has high charge density since the prominent approach to enhance the output performance of TENG is to improve the charge generation. It was John Carl Wickle in 1757 published the first triboelectric series based on the static charges. Later, out of numerous researches done by Bill W. Lee, a series has been developed which accounted that the amount of charge exchanged between the surfaces of materials in contact depended on the electron affinity of the materials involved (40). There is wide collection of materials which is mentioned in the table which can be used for the generation of TENG. According to Lee, a positive charge affinity intends that the particular material has a tendency to give up electrons while negative charge affinity implies a tendency to accept electrons.

As the materials comes in contact with each other either through rubbing or touching, they gain or lose electrons there by acquiring a polarity. So, if two materials are chosen from the series, one from the positive part and another from the negative part and as they come in contact with each other, transfer of charges occurs.

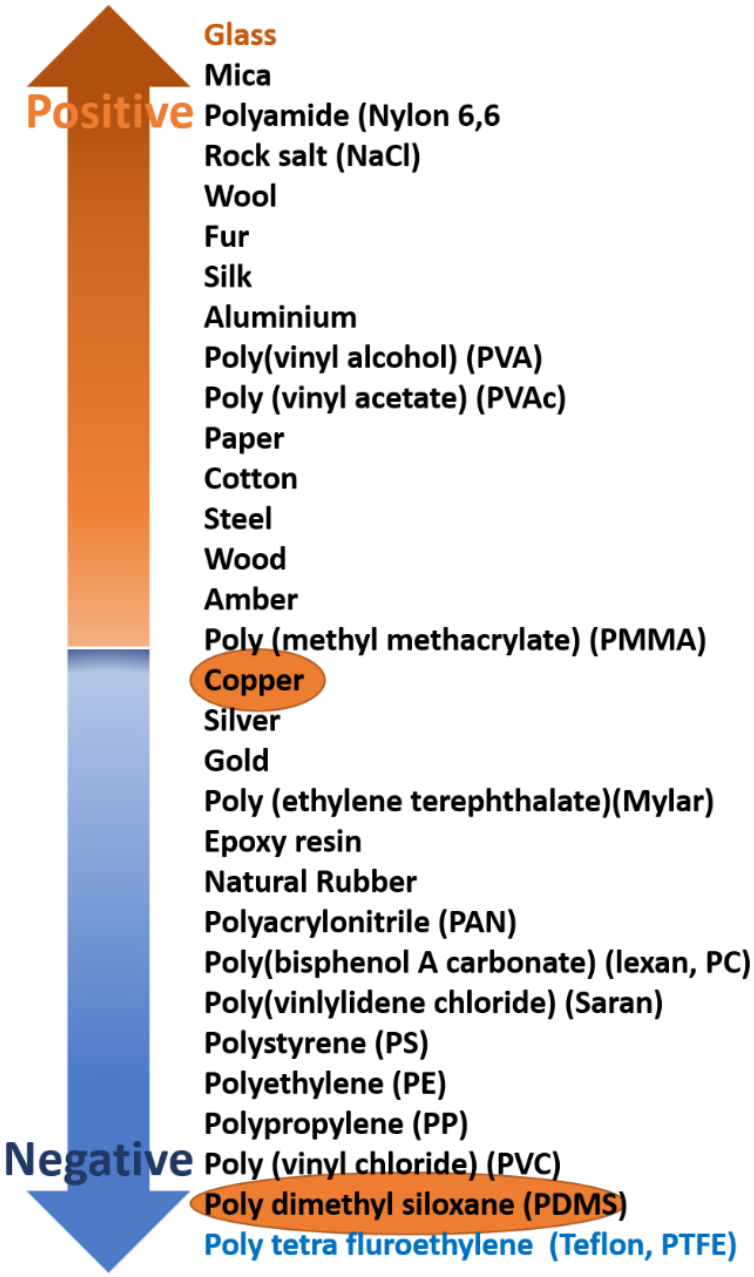

Figure 1. 9. The triboelectric material series (1)

Usually, insulators exhibit low conductivity which could produce triboelectric charge. Electron affinity, surface functional groups, and work function are important factors affecting TENG's output performance from a material perspective (82). It is noteworthy that materials which contain elements of group 17 such as Cl, F or O of the periodic table, are found to have higher affinity and hence such materials become electron acceptors (83). They include Poly tetrafluoroethylene (PTFE), Fluorinated Ethylene Propylene (FEP) and Polyvinylidene

Fluoride (PVDF). Positive materials of triboelectric series are those which contains amino group (NH_3) since this group have tendency to donate electrons (84). Hence the choice of two materials which are far apart in the series is always favorable for the maximum transfer of charges. If the materials selected are nearer to one another in the series, then there is a less possibility of charge transfer between them. Zhong et al. proposed a new triboelectric series based on observed triboelectric charge density (40).

1.6 Four working models of TENG

Triboelectric nanogenerators basically traps physically applied periodic vibration motions which is utilized for electricity generation. Based on the configuration of electrodes and positioning of triboelectric layers that helps for process of induction, there are four fundamental modes of TENG (85, 86). The working modes includes vertical contact – separation mode (CS), in-plane lateral-sliding (LS) mode, single-electrode (SE) mode, and freestanding triboelectric-layer (FT) mode, as shown in figure 1.10. The contact separation mode employs polarization in the vertical mode while lateral sliding mode uses polarization in the lateral direction due to the relative sliding between two dielectrics (87). The single electrode mode harnesses energy from a free movable body without having any contact (88). The free standing triboelectric layer mode is used for the production of power by utilizing electrostatic induction between a couple of electrode layers (63).

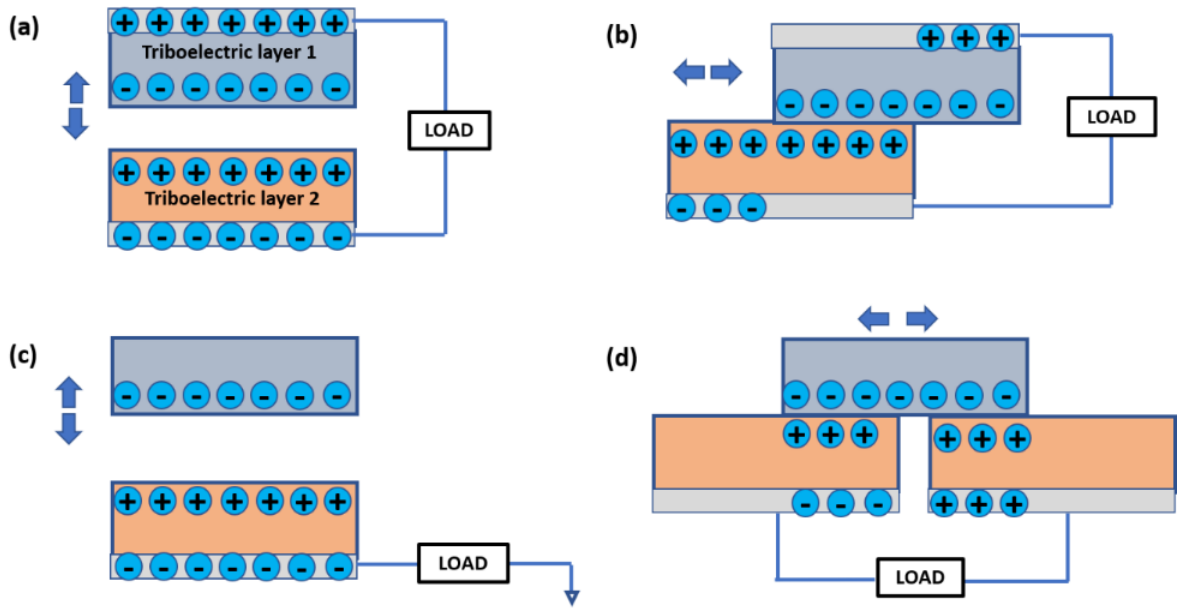

Figure 1. 10. The four working modes of TENG (a) vertical contact – separation mode (b) in-plane lateral-sliding mode (c) single-electrode mode, and (d) freestanding triboelectric-layer mode.

1.6.1 Vertical contact separation mode

The vertical contact separation mode becomes the first and fundamental mode of TENG which possess a very simple design. The working mechanism is exhibited in figure 1.11. Here, the two triboelectric layers with distinctively different triboelectric polarities are arranged in such way that they face each other. Electrodes are positioned on top and bottom layers of the layered structure with at least one of the tribo-layer is dielectric in nature. Electrode for the dielectric layer can be positioned on the outer surface and if the second tribo-layer is a conductor, then it can act as electrode as well.

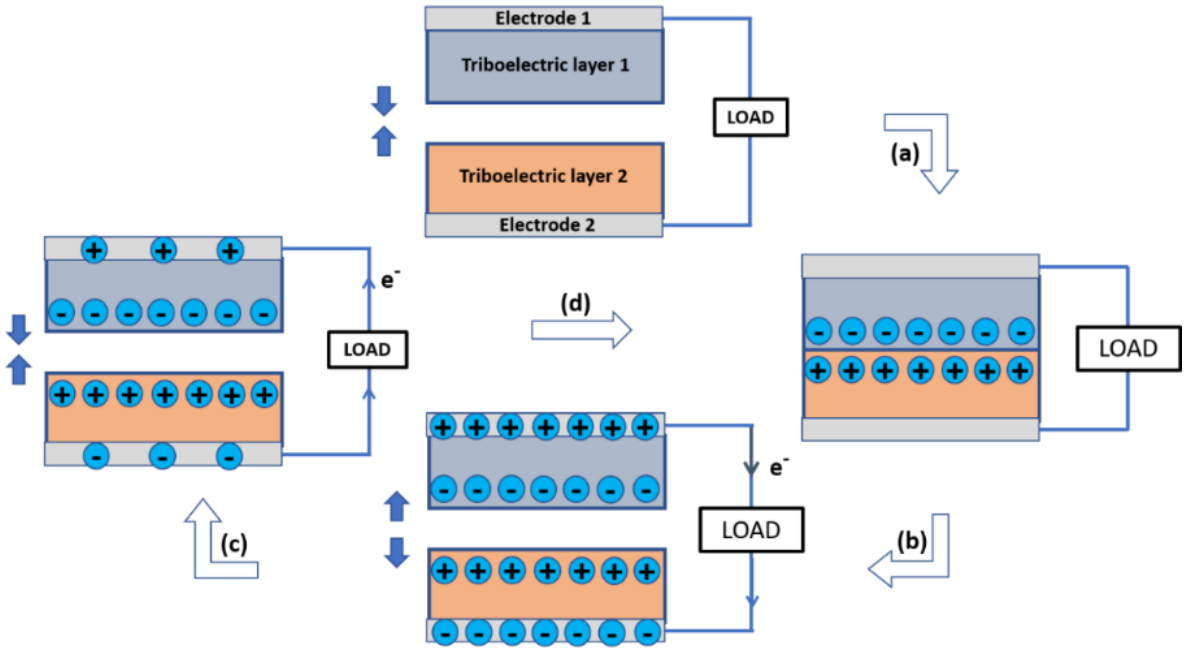

Figure 1. 11. Working mechanism of contact-separation mode (a) pressing step in which external force brings the two insulators into contact, resulting in triboelectric charge generation on surfaces (b) releasing step leads induced electron flow between electrodes (c) re-pressing by external force leads electron backflow due to potential difference variation (d) intimate contact step is established again in which electron flow reaches equilibrium.

When the two tribo layers get contacted, their surface becomes oppositely charged. While releasing, an external mechanical force creates a space between the two surfaces, resulting a potential drop between the electrodes. This potential drop is a result of the work done to overcome the electrostatic attraction and elasticity which arose due to the application of external mechanical force. When the two electrodes are connected to external circuit, the charge carriers move from one electrode to another so as to compensate the potential drop developed. As the two tribo electric layers comes back into contact, the electrons start flowing and the potential drop due to triboelectric charges ceases. As a result, AC power is produced. The production of electricity in this mode is achieved through toggling between two states viz; close contact condition and completely detached condition. There are different ways in which

the gap between the triboelectric layers is introduced for accomplishing the above-mentioned states. They include spacer structure (63), arch shaped structure (89), spring-assisted structure (90) etc. The advantage of this mode is that TENG could efficiently extract energy from even tiny recurrent movements such as human motions, small impacts etc (91). The other peculiarities of this mode include effortless structural schemes, enormous instantaneous power density etc.

1.6.2 Lateral sliding mode

Lateral sliding mode is based on the relative gliding of two materials in the direction parallel to the surface (92). Device configuration of lateral sliding mode is much more similar to that of vertical contact-separation mode as shown in figure 1.12. Electricity is generated by means of repeated contact and not getting separated, but move in plane to create different effective contact area of two tribo-electric layers having dissimilar tribo-polarity (93). The initial step for electricity generation is contact process followed by the separation process which happens in-plane direction by means of the gliding of tribo-layers.

When two surfaces are in contact, the positive charges developed on one side gets fully nullified by the negative charges created on the opposite layer. The external mechanical force results in the relative movement in the direction parallel to the interface and due to the mismatched areas, the complete cancellation of the tribo-charges does not occur. This results in the creation of effective dipole polarization in the sliding direction. During horizontal sliding, both triboelectric charges and polarization oriented in the sliding direction are generated. As a result of charge creation, to keep the electrostatic neutrality, electrons will move between top and bottom electrodes due to the induced potential. Sliding process is continued and alternating current is extracted from this mode. There are different ways to achieve lateral sliding process namely planar motions (94), disc rotation (95), cylindrical rotation etc. (96). Lateral sliding mode is more beneficial than contact- separation mode since

the production of triboelectric charges due to sliding of tribo layers are more. The sliding surfaces can be made rough through gratings which allows effective transfer of surface charges and hence improved output performance. But mechanical abrasion can pose problem for this mode of operation.

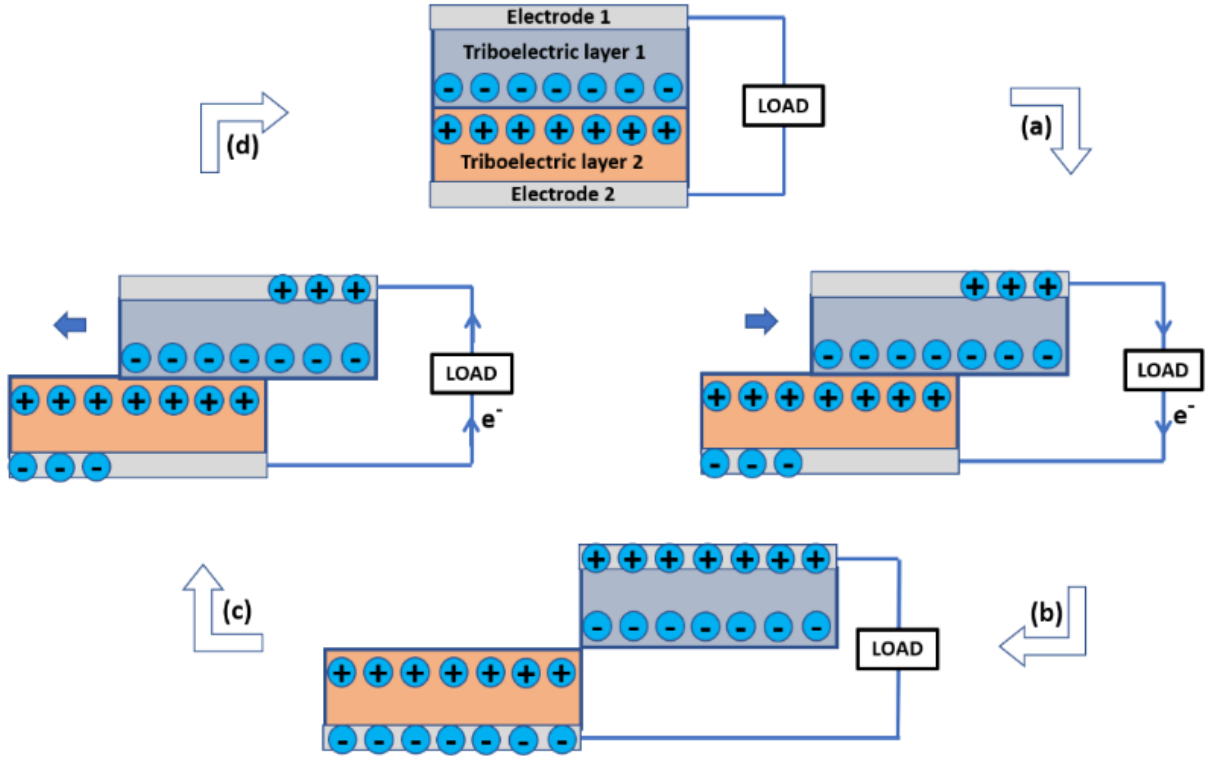

Figure 1. 12. Working mechanism of sliding mode (a) lateral sliding via external force initiates induced electron flow (b) full separation of insulators results in electron flow saturation (c) backward sliding yields electron backflow to balance electrostatic potential drop (d) complete contact step in which electrostatic potential difference vanishes to zero.

1.6.3 Single electrode mode

The first two modes required a pair of electrodes connected to the portable tribo-layers. Usually, all the moving objects come in contact with air or any other surfaces which automatically gets charged through the process of contact electrification phenomenon. Hence those objects which move could act as a tribo-electric layer for the production of electricity.

Practically for such tribo-layers, the presence of electrodes becomes inappropriate and hence Yang et.al (97) proposed a single electrode TENG (figure 1.13).

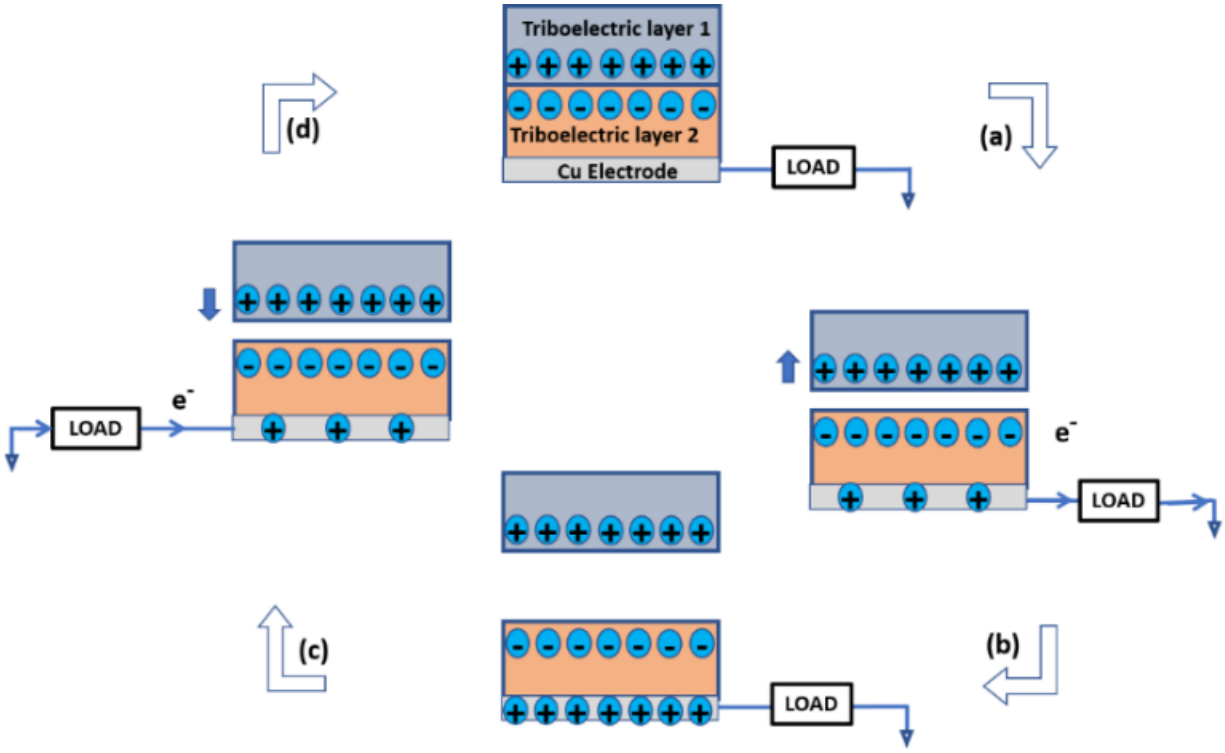

Figure 1. 13. Working mechanism of single electrode mode (a) contact and separation of human skin generate electrostatic potential difference which yields electron flow through external load (b) when critical separation is reached, system comes into equilibrium (c) while human skin coming close to the tribo layer, electrostatic potential drop is emerged which results in backflow of electrons (d) complete contact condition is established again in which electron flow reaches equilibrium.

This system has just one electrode, which communicates with the movable triboelectric layer. Usually, ground is considered as the other electrode which supply enough electrons. Because the triboelectric layer is moveable, contact with both the top and reference electrodes will preserve the equilibrium between them. The effect of electrostatic screening is very prominent in this mode and hence transfer of electrons through the process of electrostatic induction is not an effective method (98). The only advantage of this mode is the free

movement of tribo-electric layer without any constraints. Any mode can be utilized for the movement of layers such as vertical contact mode (97) or lateral sliding mode (99) or combination of both modes. Adaptability of the single electrode mode to choose any mode of movement ensures its potentiality as a self-powered active sensor. This mode can be utilized for generation of energy from direct human touch such as finger/hand/skin touch or body vibrations.

1.6.4 Freestanding triboelectric layer mode

This is a mode in which, a pair of electrodes are fixed to particular positions while the tribo layer is free to move as shown in figure 1.10 (d). There is a natural friction between the freely portable triboelectric layer and the surrounding layer. Because of the tribo layer's mobile nature, it can come into contact with any of the electrodes, resulting in a cyclic fluctuation in the induced potential difference, which produces alternating current via the output circuit. Figure 1.10(d) describes the working of freestanding-triboelectric mode of TENG (100). Because the screening effect that existed in single electrode mode is minimized in this manner, induced electron transport is efficient. This helps to collect equal number of triboelectric charges on the freestanding tribo layer and thereby this mode is better than the single electrode mode. Furthermore, because the electric charges produced on the tribo-layer persist for an extended period of time, this mode does not necessitate recurrent electrification via external mechanical stimulation. An asymmetric electric field is produced at the two substances due to the irregular movement of the moving triboelectric layer, which varies with the distance between the electrode and the charged material.

There are basically two types of configurations for freestanding triboelectric layer mode. In the first type, pair of immovable electrodes are fixed on one plane, while the triboelectric layer slithers on the overlying positions of two electrodes (101). Even though the tribo-electric layer slides on the stationary electrodes, contact between them is not necessary.

Hence this offers a new mode in which the sliding operation is done without contacting the electrodes. The main merit of this mode is that it improves the durability of the layers since the friction is eliminated. In the second configuration, the electrodes are positioned in such way that the triboelectric layer wobbles between the oppositely placed electrodes similar to vertical contact separation mode (102). This structure has found applications in extracting energy from human walking as well as automobile transportation and thereby it is possible to harness energy from a freely moving object without electric contact.

1.7 Review on TENG

For TENG applications, polydimethylsiloxane (PDMS) is regarded one of the most ideal materials because of its unique qualities such as flexibility, transparency, high negative polarity, and ease of production. Zhu et.al in the year 2013, fabricated TENG in which gold nanoparticles were mixed with PDMS and possessed an open circuit voltage of 1200 V with a power density of 313 W/m^2 (103) . When PDMS was exposed to ultraviolet-ozone together with spraying of NaOH solution into PDMS matrix, an open circuit voltage of 49.3 V and short circuit current of 1.16 μA was obtained (104). There was an enhancement of electrical properties when PDMS was exposed to UV – ozone compared to pure PDMS. Hu et.al in 2013 worked on 3D spiral structure which was based on vertical contact separation mode and output properties were well appreciated (105).

A nanogenerator typically produces high output voltage but low output power. In an attempt to optimize the instantaneous power output of the TENG, Cheng and colleagues (2013) developed a nanogenerator that used off–on–off contact switching during the mechanical triggering process, which significantly reduced the duration of the charging and discharging processes. As a result, the pulse of the instantaneous power output strengthens while the output voltage remains unchanged. With a 500 Ω load, the output current and voltage reached as high as 0.53 A and 142 W, respectively (106). The current density and power density was as high

as 1325 A/m^2 and 3.6×10^5 W/m^2, respectively, depending on the application. Yang et al. developed 3D integrated multi-layered TENGs later in 2014 as a solution to the problem of minimal power output in TENGs. When using this form of TENG, the output of separate TENGs was synchronized in order to produce the highest possible instantaneous power output (107). It featured a multi-layered construction with acrylic supporting substrates, which made it a 3D TENG. Nanowires of PTFE were employed as triboelectric materials, while electrodes and contact surfaces were made of aluminium and copper. In addition to a short circuit current of 1.14 mA and an open circuit voltage of 303 V, the synchronized 3D TENG generated a power density of 104.6 Wm^{-2} and was able to illuminate 20 spotlights (0.6 W each) and a white G 16 globe light in synchronized 3D TENG mode.

Lin et al. investigated the link between a single water drop's motion on a water TENG, and a sequential contact-electrification and electrostatic-induction process was developed in order to better understand the working mechanism of the water TENG (108). Single electrode mode TENG was constructed from a nanostructured PTFE thin film and a PMMA substrate layer coated with a copper electrode. When a 30 μL water drop struck the TENG, it produced a maximum voltage of 9.3 V and a peak current of 17 μA. In this case, when the generator was linked to a resistor with a resistance of 5 MΩ, it produced the highest power output of 145 W. The results of the investigation further showed that the superhydrophobic character of the PTFE film was responsible for the high output.

In a recent study, Yong and colleagues (109) showed that energy could be produced from wind by rotating a lightweight triboelectric sphere over a vortex whistle substrate. A single unit of this TENG generated an open-circuit voltage of 11.2 V and a short-circuit current of 1.86 μA. The output power of the nanogenerator was improved by using different electrode designs and increasing the number of triboelectric spheres contained within the nanogenerator. In 2017, Chen et al. developed an ultra-flexible 3D TENG that was made using a novel hybrid

UV 3D printing technique (110). As an electrification layer and an electrode, the TENG used printed composite resin components, as well as ionic hydrogel as a conductive substance. At a low frequency of 1.3 Hz, a satisfactory output of 10.98 W/m^3 was produced. In 2018, Mallineni et al. successfully gathered mechanical energy using a 3D printed wireless triboelectric nanogenerator that used graphene polylactic acid nanocomposite and teflon as triboelectric surfaces to harvest mechanical energy (111). With only a few hand gestures, this TENG was able to create unprecedented performance of output voltage of 2 kV and instantaneous peak power of up to 70 MW. It was possible to transmit electric field across a distance of 3 m using this constant voltage output which could charge a capacitor using wireless transmission.

The concept of TENG expanded to different working modes (88, 93) and possess many merits which includes wide availability of materials for fabrication, ease of fabrication, cost effectiveness, high performance and efficiency even at low working frequencies. The materials which possess different charge affinity can be implemented for the construction of TENG devices. Materials from the opposite end of the triboelectric series when paired up exhibit high performance for potential applications. Most commonly used materials which forms the tribo-negative materials includes poly tetrafluoroethylene (PTFE) and silicone and most of the metals act as tribo-positive materials (112). Recent researches use TENGs based on polymers which are easily bendable, portable and wearable. High temperature devices were made of ceramics which were deployed at extreme working conditions (113). The power density of a TENG mainly dependents on the structure of device and the materials used. The harvested energy from TENG devices was utilized for driving many electronic gadgets and also these devices acted as self-powered sensors. In this era of internet of things (IoT) , TENG has a great prevalence to pacify the energy needs and to act as a better choice for energy source (35).

Xion et.al developed a wearable and washable textile TENG in which the trapping layer of black phosphorus were mixed with cellulose derived hydrophobic nanoparticles (114). A

real time monitoring of human physiological signals was trapped using a self-powered sensor which was fabricated from wearable and portable, potentially efficient fish gelation based TENG (115). Yet another important, all in one self-powered integrated system was developed based on strain sensors which were highly sensitive, translucent and distinct. It can also be chosen as electrodes for both TENG and SC (super capacitor). Many researchers try to improve the performance of TENG through material modification, embedding novel micro/nano structures into tribo layers, development of different device structures etc. (116-118). With the introduction of high permittivity ceramics such as $CaCu_3Ti_4O_{12}$, high performance TENG can be obtained (119) .

1.8 Challenges faced by TENG devices

TENGs have emerged as a most prominent technology for harnessing the abundant mechanical energies into electrical energy, due to the benefits such as simple fabrication techniques, vast variety of materials for the choice as tribo material etc. Merits of TENG includes novel and unique device structure, durability, toughness, authencity, and eco-friendly nature. The output from a TENG is a pulsating ac, which poses a real challenge for running majority of electronic equipment (120, 121). Another challenge faced by TENG devices are their high internal resistance, which is of the order of several mega ohms. This causes impedance mismatch with the electronic appliances and energy storage devices. Hence due to the alternating pulsating output, possessing non uniform amplitudes and frequency along with high input impedance makes it tough for incorporating TENG for efficient transfer of energy to a load as well as to energy storing devices (122). For powering electronic devices, power needed has to be controlled through fixed input voltage as well as power. Due to temporal dependent and fluctuating output of TENG, it has been always a difficult task to incorporate TENG with the electronic devices. However, this issue can be resolved with the introduction of energy storage devices which could store the energy extracted from TENG and supply to

any electronic device as a stable and sustainable energy source. These advantages always support to incorporate TENGs with energy storage devices so that it will act as power sources for majority of the mobile electronics and sensors (123).

TENG has also been utilized for some other applications along with energy harvesting devices. This includes sensor technology in portable electronic industry and play a very remarkable position since they could measure the human vibrations as well as other important signals (123). These sensors which were derived from triboelectric nanogenerators are designated as triboelectric sensors. When these sensors are arranged in the sliding mode, they could trap the human hand vibration and couple it with a robotic hand (124). The fabricated sensors procure movements from human fingers and produces stimuli from it. Thus, with the aid of these sensors, it was possible to identify the movements of human fingers especially the speed and direction of motion of fingers just by noting the number of positive and negative voltage pulses. The incorporation of magnetic array into the sensors could convert sliding movement into vertical contact separation movement, thereby enhancing the life span as well as the amplitude of the low frequency vibrations. These portable sensors based on triboelectric materials opens a new area for research which couples human hand motions with that of robotic gestures (125).

1.9 Role of TENG in human health care

Wang's team first proposed the notion of combining TENG with health care in 2013, citing a demand for self-powered electronic devices that might play a significant role in improving the overall quality of human health care industries [11]. The biological characteristics of a human being are influenced by elements such as the temperature of the body, blood pressure, heart rate, degree of oxygen consumption, and glucose concentration in the blood. Consequently, the differences that occurred in the body were determined by variations in these characteristics. [12]

Health tracking systems have always necessitated the use of highly sensitive sensors that can detect even the smallest of signals. These signals must be sent to signal processing modules for further processing. In order for these types of gadgets to function properly, they must be connected to a power source. Because TENG can function as self-powering units, they have the potential to power these delicate devices while also making them transportable. This function provided an additional benefit in terms of lowering the cost of gadgets, which was a welcome addition. Support, benefit, and cost effectiveness are all important considerations when it comes to portable and wearable technologies. Many studies report that the significant technologies such as piezoelectric effect or chemical batteries were utilized in medical devices and found to be effective. [5,16,17]. However, these devices were constantly at risk of running out of power if they were to be used for an extended period of time. With the invention of TENG [7], a whole new method of fabricating not only wearable devices, but also self-powered charging units, was introduced into the world of technology.

Yang and colleagues developed a sensor that links the motion of humans with that of mechanical devices [31]. This gadget was capable of gathering signals from human motions and transmitted them to a computer for further analysis, making it useful as a health monitoring device. One of the devices that has been created was based on fluorinated ethylene propylene (FEP), which acted as a triboelectric material and was used as a sensor to measure the blood pressure of humans. This sensor had an arch form that contains flexible latex in order to produce the process of contact-separation with a FEP layer on top. In addition to heart beat, this sensor could measure breathing rate. The drawback of this sensor was the inconvenience in fitting it to the body due to its design. To overcome this difficulty, novel design structures were proposed. The fiber-like wearable electronic medical device proposed by Zhong and colleagues in April 2014 was one of the earliest representative results [37]. PTFE and carbon nanotube coated cotton thread were used as contact materials in this application. When worn

on body parts, it was possible to detect their motion/vibration, which could then transform into energy with an average output power density of 0.1 W/cm^2.

While the application of TENG for health monitoring has been increasingly standardized, the wearable patch device has emerged as the clear leader in the category of TENG-based health monitoring devices. Yang et.al showed a self-powered biomedical monitoring device using Kapton as a triboelectric material [39]. During tests, its highest output voltage was 700 V and maximum short-circuit current reached 75 μA, both of which were impressive results. A self-powered sensor for cardiovascular system characterization and throat-attached anti-interference voice recognition were also disclosed at the same time by Yang and colleagues [40], who drew inspiration from the human eardrum membrane. The recognition function of the sensor was achieved through the use of a contact and separation TENG made of PTFE and Nylon materials. It has been proven in the experiments that, despite a relatively low output signal intensity, the signal change has an adequate resolution to complete tasks such as cardiovascular system characterization measurement and throat voice recognition successfully. In particular, the suggested speech recognition capability opened up a new field of application for TENG; human-computer interaction.

TENGs must have a basic device design, cost effectiveness, and be lightweight in order to capture the omnipresent mechanical energy from their surroundings. A crucial ability of TENGs has also been demonstrated to be the conversion of low-frequency mechanical energy from walking, waving, and blinking the eyes into electricity. TENGs, have demonstrated promising and significant characteristics that have been applied to power units at the micro and nanoscale [39-44], high-voltage sources [45], self-powered systems [46-50], and blue energy harvesting devices [51-56] among other applications.

A little more than 2000 years ago, Chinese scientists invented paper, which is by far one of the most affordable and flexible materials available for use in everyday life. These materials are also available in a variety of compositions, thicknesses, and surface roughness. First and foremost, paper is biocompatible, biodegradable, and environmentally friendly, and it offers significant advantages which includes lightweight, renewable, and air-permeable nature. Furthermore, because paper is flexible, it may be easily folded or bent into 3D structures without causing structural harm to the paper itself. Paper-based electronic devices, such as microfluidic paper-based analytical devices [57-60] and PDMS) [61-65], have received a significant attention in recent years [57-60]. A number of energy-related technologies have also benefited from their use recently [66-68]. Despite the fact that paper is implicitly insulating, conductive materials (e.g., metal nanowires, conducting polymers, carbon nanotube (CNT) inks, multiwall carbon nanotube (MWCNT) inks, and reduced graphene oxide) can be easily absorbed or used as a coating layer on the surface of the paper due to its wettability and moisture-retention capacity [69-82). This method of preparing paper electrodes for TENGs is quick and easy to use. TENG friction layers made of paper have also been shown to be effective at reducing slipping. This results in it having a tendency to lose electrons (i.e., becoming electropositive) when it comes into touch with a material that can easily receive electrons (such as a semiconductor i.e., electronegative). The high roughness and porous nanofiber structure of the material can also contribute to higher TENG output performances as a result of improved charge-trapping abilities.

Chapter 2

Triboelectric Nanogenerators: Concept and Theory

Abstract

For a comprehensive understanding of TENGs, knowledge of their theoretical origins is crucial. In this chapter, theoretical analysis of TENG is explained in detail. Both conductor-to-conductor mode and conductor-to-dielectric mode V-Q-x (voltage-charge -interlayer distance) relations are studied independently. The current investigation uses conductor-to-dielectric mode. A brief idea about electrical characterization of TENGs and the parameters that influence their performance is discussed. In addition, the chapter enumerates potential measures made to increase the output of TENGs as well as measures done to improve the energy conversion of TENGs. The chapter describes the peculiarities of materials chosen for the research work, designing of TENG structure and concludes by explaining different characterization techniques employed in the current study.

2.1 Introduction

With the implementation of techniques which could harvest ambient mechanical energy into electricity, smart portable electronic devices are losing their dependency on conventional power supplies such as rechargeable batteries (42). Energy harvesting devices for electronic gadgets possess some inherent advantages, such as great endurance, low maintenance and eco-friendly nature. These features distinguish energy harvesting techniques from traditional battery and hardwire power. In spite of these advantages, better performance, smaller size and lower prices are still needed if energy harvesting technology is to be prominent. A novel and simple generator can be fabricated which is incredibly inexpensive for efficiently harvesting mechanical energy present in the form of vibrations and random displacements/deformation. Electric generation was made possible by a cycled process of contact and separation between two polymer films, which works on the basis of combination of contact charging and electrostatic induction (126).

2.2 Theoretical origin of TENG: Displacement Current Analysis

The basic phenomena which govern the working of TENG are contact electrification and electrostatic induction. As the tribo layers comes in contact and get separated, charges of opposite signs are developed on the dielectric surfaces due to the triboelectric effect. As the electrodes are attached to the other surfaces of the tribo-layers, electrostatically induced charges are developed on these electrodes. When the electrodes are connected to external circuit, the induced charges on the electrodes begins to flow in order to balance the electric potential. This current flowing through the external circuit forms the output of the TENG which is basically Maxwell's displacement current. Theoretical models were developed to detail the generation mechanism of displacement current of TENG output (127). Parallel plate capacitor model is one of the models which could explain electrical output performance of TENG when

the device fabricated has planar geometry. The theory of nanogenerators were developed from Maxwell's equations which was initially proposed by Maxwell in 1861. The displacement current is the partial derivative of the electrical displacement flux with respect to time rather than the current which arises due to the charges moving in a directional motion.

The maxwell's displacement field D is given by,

$$D = \varepsilon_0 E + P \tag{2.1}$$

Where E is the applied electric field, P is the polarization and ε_0 denotes the relative permittivity of free space.

This polarization in a dielectric material is due to the effect of an electric field, which results in separation of bound charges and give rise to bound charge density,

$$-\rho_b = -\nabla . P \tag{2.2}$$

and surface charge density

$$|\sigma| = -P . n \tag{2.3}$$

Maxwell's displacement current is defined as follows:

$$J_D = \frac{\partial D}{\partial t} = \varepsilon_0 \frac{\partial E}{\partial t} + \frac{\partial P}{\partial t} \tag{2.4}$$

where D is the displacement field; ε_0 is the permittivity in vacuum; E is electric field; P is the polarization field. The above expression contains two components of displacement current, first one is the time dependent electric field which contributes for electromagnetic waves and second part mentions the time dependent polarization vector.

The corresponding displacement current density of a TENG is as follows:

$$J_D = \frac{\partial D_Z}{\partial t} = \frac{\partial \sigma(z,t)}{\partial t} \quad (2.5)$$

The reason for current flow in the material is prominently due to the time varying polarization field of surface charges. Surface charges in triboelectric nanogenerators are generated by simple physical contact between two distinct materials caused by any mechanical force. In some materials, because of a mechanical stimulation surface charges develop which can behave as a source of polarization field. In 2017, Wang introduced displacement current in addition to the surface polarization vector P_s with an aim to explain piezoelectric nanogenerators and triboelectric nanogenerators. As in triboelectric nanogenerators, the formation of surface charge through the process of electrostatic induction, the equation connecting displacement field and surface polarization P_s is given by,

$$D = \varepsilon_0 E + P + P_s \quad (2.6)$$

where P_s is due to the existence of the surface charges that are independent of the presence of an applied electric field. For an isotropic media, the polarization field takes the form of:

$$P = (\varepsilon - \varepsilon_0)E \quad (2.7)$$

Hence, $D = \varepsilon E + P_s$ (2.8)

Hence without an external electric field, triboelectric nanogenerator could work since the polarization vectors produced by the surface charges are merely due to the contact or friction between two surfaces.

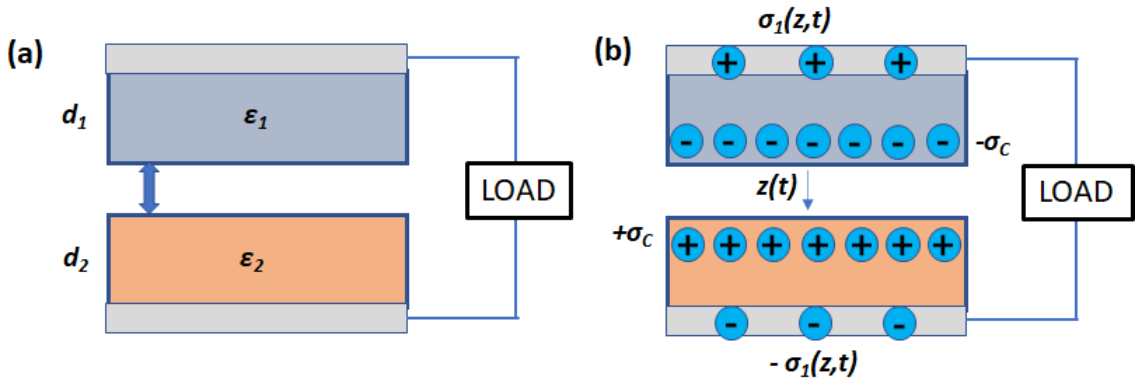

Figure 2. 1. Illustrations of the working mechanisms of TENG (a) Original state, and (b) after contact and separation.

Figure 2.1 depicts the classic four-layer contact-separation TENG and the displacement current corresponds to the TENG model is given by (128).

$$J_D = \frac{\partial D_z}{\partial t} = \frac{\partial \sigma_1(z,t)}{\partial t} = \sigma_c \frac{\partial z}{\partial t} \frac{d_1 \frac{\varepsilon_0}{\varepsilon_1} + d_2 \frac{\varepsilon_0}{\varepsilon_2}}{[d_1 \frac{\varepsilon_0}{\varepsilon_1} + d_2 \frac{\varepsilon_0}{\varepsilon_2} + z]^2} \quad (2.9)$$

where σ_c denotes the surface charge density on the dielectric surface. $\sigma_1(z,t)$ is the charge density on the top electrode and it is a function of inter layer gap distance $z(t)$. From the above equation, it is possible to relate that displacement current density is proportional to the charge density on dielectric surface and also to the speed with which the interlayer distance is varying.

2.3 V-Q-x relationship

The real mechanism of triboelectric phenomenon and working of triboelectric nanogenerators was explained by Niu et.al who developed a theoretical model based on a V-Q-x relationship (129).

2.3.1 Dielectric to dielectric mode

The basic TENG working mode is designated as attached electrode contact mode TENG and it works on the vertical charge separation mechanism. This mode is the primitive mode of TENG and depending on the materials chosen for triboelectric pairs, this mode of TENG is classified into two, which are dielectric-to-dielectric mode and conductor-to-dielectric mode. Figure 2.2 (a) shows the model chosen for dielectric-to-dielectric contact mode TENG. There are two dielectric sheets which possess thickness of d_1 and d_2, relative dielectric constants of these two triboelectric layers are designated as ε_{r1} and ε_{r2} and they are placed in such a way that they face each other. At the other end of the two dielectrics, metal layers are attached which act as two electrodes. The inter layer distance between the tribo sheets is *x* and it is variable under the influence of external mechanical force. As the layers are brought into physical contact, the two dielectric layers will gain opposite charges. These are called tribo charges and both tribo-layers have equal surface charge density σ which is due to the process of contact electrification. The surface charge generated on the tribo layers are determined by the ability of the dielectric materials to donate or accept electrons/ions or molecules. When the surfaces get into contact, the triboelectric surface charge density increases and reaches saturation. Due to the external mechanical force, the dielectrics go apart and a potential difference (*V*) is created. This difference allows transfer of charges between metal electrode 1 and metal electrode 2 which is a function of distance between the dielectric layers and time.

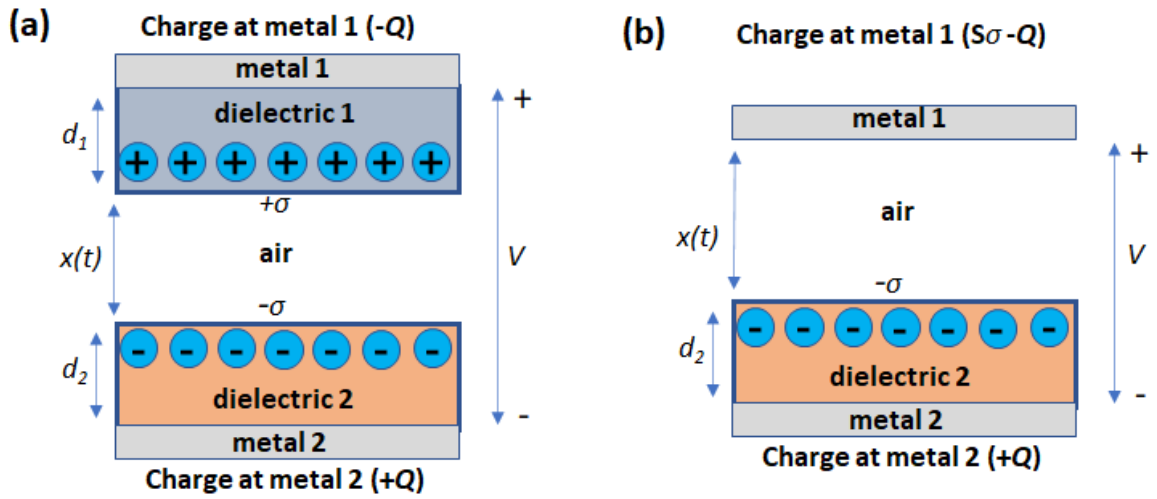

Figure 2. 2. Theoretical models for **(a)** dielectric-to-dielectric attached-electrode parallel plate contact-mode TENG and **(b)** conductor-to-dielectric attached-electrode parallel plate contact-mode TENG.

To construct the V-Q-x relationship, this model is used together with the principles of electrodynamics. Theory assumes that the charged electrodes are infinitely large because area of the metal electrodes comes to several order of magnitude when compared to separations between them as well as thickness of metal electrodes. Also, the bound charges on the dielectric materials result in the uniform distribution of the electrostatic potential on the inner surface of metals. Since the electrodes possess a planar geometry, charge distribution confines the electric field in the direction perpendicular to surface. Let area of the two dielectric layers is assumed to be same and equal to S. The direction of field pointing to metal 2 is assumed as positive, then using Gauss theorem, electric field intensity inside dielectric 1 (E_1), dielectric 2 (E_2) and inside the air gap (E_{air}) will take the forms

$$E_1 = \frac{-Q}{S\varepsilon_0\varepsilon_{r1}} \tag{2.10}$$

$$E_2 = \frac{-Q}{S\varepsilon_0\varepsilon_{r2}} \tag{2.11}$$

$$E_{air} = \frac{-\frac{Q}{S}+\sigma(t)}{\varepsilon_0} \quad (2.12)$$

The potential difference between two metal electrodes is given by

$$V = E_1 d_1 + E_2 d_2 + E_{air} x \quad (2.13)$$

Therefore, the V-Q-x relationship for dielectric-to-dielectric TENG is given by

$$V = \frac{-Q}{S\varepsilon_0\varepsilon_{r1}} d_1 + \frac{-Q}{S\varepsilon_0\varepsilon_{r2}} d_2 + \frac{-\frac{Q}{S}+\sigma(t)}{S\varepsilon_0} x = \frac{-Q}{S\varepsilon_0}\left(\frac{d_1}{\varepsilon_{r1}} + \frac{d_2}{\varepsilon_{r2}} + x(t)\right) + \frac{\sigma x(t)}{\varepsilon_0} \quad (2.14)$$

2.3.2 Metal to dielectric mode

The presence of dielectric layer makes a notable difference in the quantification of charges when compared to above model. From figure 2.2 (b), metal 1 act as top electrode as well as triboelectric material. Thus, total charge on the metal 1 will be sum of the triboelectric charges $S.\sigma$ and transferred charges between the metals ($-Q$). Instantaneous number of charges in metal 1 will be ($S\sigma$-Q).

V-Q-x relationship for the conductor-to dielectric TENG is given by

$$V = E_2 d_2 + E_{air}\, x \quad (2.15)$$

The potential difference between two electrodes takes the form

$$V = \frac{-Q}{S\varepsilon_0\varepsilon_{r2}} d_2 + \frac{-\frac{Q}{S}+\sigma(t)}{\varepsilon_0\varepsilon_{r2}} x = \frac{-Q}{S\varepsilon_0}\left(\frac{d_2}{\varepsilon_{r2}} + x(t)\right) + \frac{\sigma x(t)}{\varepsilon_0} \quad (2.16)$$

The equation (2.15) and equation (2.13) have same form, in which former doesn't contain d_1 and ε_{r1} (which is included in dielectric-to-dielectric mode). General V-Q-x relation for contact separation mode is given by

$$V = \frac{-Q}{S\varepsilon_0}(d_0 + x(t)) + \frac{\sigma x(t)}{\varepsilon_0} \quad (2.17)$$

Where d_0 is the effective thickness constant. In equation (2.17) d_0 takes the values $\frac{d_1}{\varepsilon_{r1}} + \frac{d_2}{\varepsilon_{r2}}$ while in equation (2.16), d_0 takes the form $\frac{d_2}{\varepsilon_{r2}}$. A great part of TENG mechanism roots from the open circuit and short circuit studies. In open circuit condition, no charge transfer occurs between the conductors, then $Q = 0$. So that

$$V_0 = \frac{\sigma x(t)}{\varepsilon_0} \quad (2.18)$$

This is applicable to both metal-to-metal mode and metal to dielectric mode. In short circuit condition, no potential drop across circuit, that is $V = 0$. So that,

$$Q_{sc} = \frac{S\sigma x(t)}{d_0 + x(t)}. \quad (2.19)$$

$$I_{sc} = \frac{dQ_{SC}}{dt} = \frac{S\sigma d_0}{(d_0 + x(t))^2}\frac{dx}{dt} + \frac{x(t)}{(d_0 + x(t)}\frac{d\sigma}{dt} = \frac{S\sigma d_0\, v(t)}{(d_0 + x(t))^2} + \frac{x(t)}{(d_0 + x(t)}\frac{d\sigma}{dt} \quad (2.20)$$

The results reveal two important features of triboelectric nanogenerator, one is regarding the surface charge density and other regarding the speed with which contact-separation occurs. The first term of equation (2.20) tells that short circuit current is directly proportional to both the surface charge density as well as speed of contact-separation process. The second term of equation (2.20) shows the influence of rate at which surface charge density develops. As the σ attains saturation, the latter part of the equation vanishes. This equation shows the ability of triboelectric nanogenerators in generating electrical energy even from low frequency vibrations. Thus, short circuit current depends on surface charge density, dielectric constant of triboelectric material and thickness of the material. Hence a detailed examination as well as optimization of all these parameters are necessary for the improvement of the output performance of the TENG.

2.4 Open circuit voltage

In the metal-to-dielectric mode, surface charges are created due to contact electrification. When they are far apart, there are no charges generated or induced on the tribo-layers. Thus, there is no electric potential difference. Under the influence of external mechanical force, the two surfaces come into contact and transfer of charges or molecules/ions takes place due to triboelectric effect. From triboelectric series, metal layer has tendency to lose electrons and dielectric layer have a tendency to gain electrons. Consequently, upper tribo layer accomplishes positive surface charge density and lower tribo layer surface attains negative surface charge density. As the frictional surfaces are in contact, created charges are confined on the surface itself. Since the opposite charges coincide at same plane, there is no electric potential difference between the two electrodes. When the external mechanical force is removed, the two tribo layers return back to original position. With the separation of tribo layers, electric potential is developed at the two electrodes. Since separation between two electrodes is relatively small when compared to their surface area, these electrodes are considered to be frictional surfaces with charges placed at infinite planes.

Consider different working stages of TENG in open circuit voltage which is shown in figure 2.3. Let the relative permittivity of the air is equal to 1. If we define electric potential difference of bottom electrode (V_{BE}) to be zero, electric potential difference of the top electrode (V_{TE}) can be calculated as follow

$$V_{TE} = \left(\frac{|-\sigma|x(t)}{2\varepsilon_0} - \frac{|-\sigma|d_1}{2\varepsilon_0\varepsilon_{r1}}\right) + \left(\frac{|+\sigma|x(t)}{2\varepsilon_0} + \frac{|+\sigma|d_1}{2\varepsilon_0\varepsilon_{r1}}\right)$$

$$= \frac{|-\sigma|x(t)}{\varepsilon_0} > 0 = V_{BE} \qquad (2.21)$$

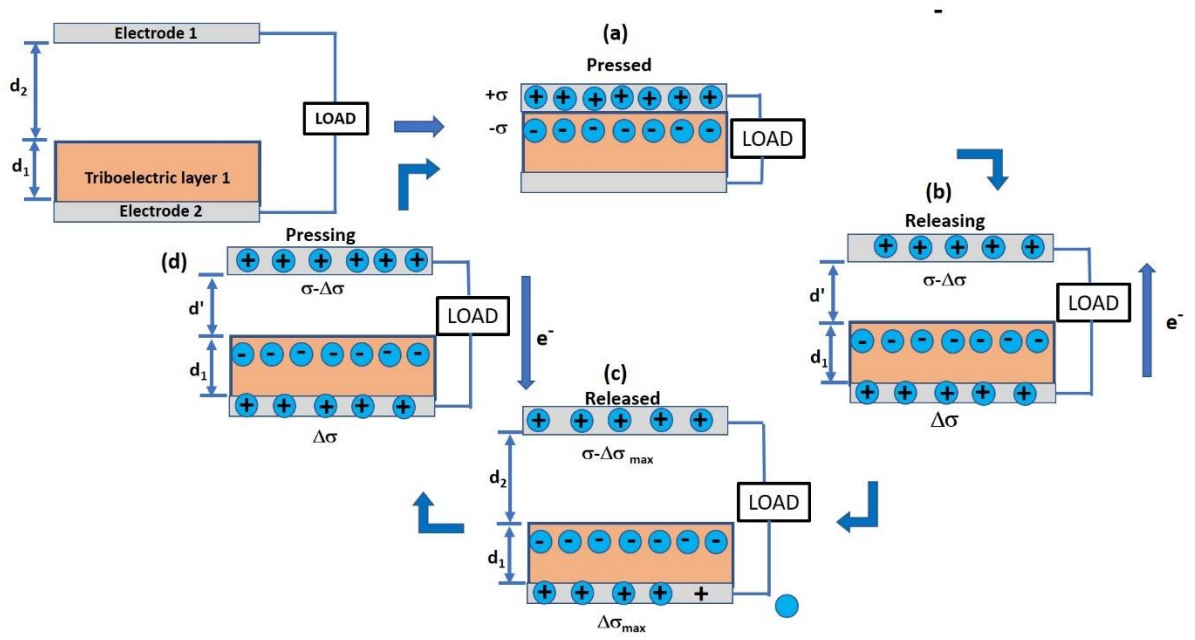

Figure 2.3. Working stages of TENG. (a) Pressed condition - electrode layer and tribo layer comes in contact state (b) Releasing condition – electrode layer moves *d'* distance away from tribo layer (c) Released condition – electrode layer moves d_2 (maximum distance) from tribo layer (d) Pressing condition - electrode layer moves *d'* distance towards tribo layer.

Where σ is the surface charge density, ε_0 is the permittivity of the free space, $\varepsilon_{r1}$is the relative permittivity of the material, d_1 is the thickness of the material, $x(t)$ is the interlayer distance at a given state. The terms in the first and second parentheses are the potential on top electrode due to negative triboelectric charges and positive triboelectric charges. The above equation indicates a higher potential development at the top electrode during the releasing process compared to bottom electrode. Thus V_{oc} keeps on increasing until top electrode reaches maximum height.

$$V_{max} = \frac{\sigma d_2}{\varepsilon_0} \tag{2.22}$$

V_{max} is the open circuit voltage designated as V_{oc}.

For the electric measurement, an oscilloscope is connected such that positive terminal is connected top electrode and negative terminal is connected to the bottom electrode. V_{oc} goes on increasing when the top electrode moves away from the tribolayer after the frictional surfaces come in contact. Electric potential difference decreases to zero from saturation value when the two tribo layers come into contact again.

2.5 Short circuit current

Short circuit current is the external current flow when the electrodes are electrically shorted. Let two electrodes are shorted initially and under an applied external mechanical force, the two tribo electric layers are allowed to separate. Electric potential difference is developed between the two tribo layers which can be calculated using equation (2.22) and this will cause instantaneous positive current flow through the load. Hence accumulation of positive charges on the top electrode reduces and same number of positive charges will be developed on the bottom electrode due to the current flow. This current flow persists till a balancing is accomplished between the electric potential difference created due to the triboelectric charges and induced charges on the electrodes due to electrostatic induction. At the equilibrium state, potential difference between top electrode and bottom electrode equalizes. If $\Delta\sigma$ is the amount of charge density reduced from top electrode and gained by bottom electrode, the transferred charge density can be calculated as follows.

$$\mathrm{V_{TE}} = \left(\frac{|-\sigma|x(t)}{2\varepsilon_0} - \frac{|-\sigma|d_1}{2\varepsilon_0\varepsilon_{r1}}\right) + \left(\frac{(\sigma-\Delta\sigma)x(t)}{2\varepsilon_0} + \frac{|-\sigma|d_1}{2\varepsilon_0\varepsilon_{r1}}\right) + \left(\frac{(-\Delta\sigma)d_1}{2\varepsilon_0\varepsilon_{r1}} - \frac{\Delta\sigma x(t)}{2\varepsilon_0}\right) \qquad (2.23)$$

Since at equilibrium, electric potential difference (EPD) at top electrode (TE) and bottom electrode (BE) should be equal and considering the EPD at BE to be zero, V_{TE} also turns to zero.

$$\mathrm{V_{TE}} = \left(\frac{|-\sigma|x(t)}{2\varepsilon_0} - \frac{|-\sigma|d_1}{2\varepsilon_0\varepsilon_{r1}}\right) + \left(\frac{(\sigma-\Delta\sigma)x(t)}{2\varepsilon_0} + \frac{(\sigma-\Delta\sigma)d_1}{2\varepsilon_0\varepsilon_{r1}}\right) + \left(\frac{(-\Delta\sigma)d_1}{2\varepsilon_0\varepsilon_{r1}} - \frac{\Delta\sigma x(t)}{2\varepsilon_0}\right) \qquad (2.24)$$

$=0 \ = V_{BE}$

The terms within second and third parenthesis of equation (2.24) corresponds to potential contribution of charges accumulated on TE and BE to V_{TE} . After simplification,

$$V_{TE} = \frac{\sigma x(t)}{\varepsilon_0} + \left(\frac{-\Delta\sigma d_1}{\varepsilon_0 \varepsilon_{r1}}\right) + \left(-\frac{\Delta\sigma x(t)}{\varepsilon_0}\right)$$

$$= \sigma x(t) - \Delta\sigma \left(\frac{d_1}{\varepsilon_{r1}} + x(t)\right) = 0 \qquad (2.25)$$

This gives $\Delta\sigma$ which is the amount of charge density transferred between the electrodes,

$$\Delta\sigma = \sigma \left(\frac{\varepsilon_{r1} x(t)}{d_1 + \varepsilon_{r1} x(t)}\right) \qquad (2.26)$$

Where $x(t)$ is the interlayer distance at a given state, ε_{r1} is the relative permittivity and d_1 is the thickness of the tribo-material. This equation states that $\Delta\sigma < \sigma$

When the TENG reaches maximum separation, $\Delta\sigma$ attains maximum value,

$$\Delta\sigma_{max} = \sigma \left(\frac{\varepsilon_{r1} x'}{d_1 + \varepsilon_{r1} x(t)}\right) \qquad (2.27)$$

Where x's the maximum interlayer distance.

$$Q_{sc} = \Delta\sigma_{max} S \ = S \sigma \left(\frac{\varepsilon_{r1} x'}{d_1 + \varepsilon_{r1} x'}\right) \qquad (2.28)$$

Dividing by ε_{r1} on both numerator and denominator;

The short circuit charge is Q_{sc} which is given by,

$$Q_{sc} = S\sigma \left(\frac{x'}{\frac{d_1}{\varepsilon_{r1}} + x'}\right) \text{ and replace } d_0 = \frac{d_1}{\varepsilon_{r1}} \qquad (2.29)$$

$$I_{sc} = \frac{dQsc}{dt} = \frac{d}{dt}\left(S\sigma\left(\frac{x'}{d_0+x'}\right)\right) \quad (2.30)$$

On taking the derivative of the above equation and replacing $v = \frac{dx'}{dt}$

$$I_{sc} = \frac{S\sigma d_0 v(t)}{(d_0+x')^2} \quad (2.31)$$

The expression for short circuit current is given by the equation (2.31). Once the external mechanical force is applied again, the reduction in separation Δx Δx will make will make,

$$\left(V_{TE} = \frac{|-\sigma|(x'-\Delta x)}{2\varepsilon_0} - \frac{|-\sigma|d_1}{2\varepsilon_0\varepsilon_{r1}}\right) + \left(\frac{(\sigma-\Delta\sigma)(x'-\Delta x)}{2\varepsilon_0} + \frac{(\sigma-\Delta\sigma)d_1}{2\varepsilon_0\varepsilon_{r1}}\right) + \left(-\frac{\Delta\sigma d_1}{2\varepsilon_0\varepsilon_{r1}} - \frac{\Delta\sigma(x'-\Delta x)}{2\varepsilon_0}\right)$$

$$= \frac{\Delta x}{\varepsilon_0}(\Delta\sigma - \sigma)$$

Since $\Delta\sigma < \sigma$, $V_{TE} < 0 = V_{BE}$. The above results point out that the higher potential at BE would allow electrons to flow from BE to TE till the two frictional surfaces are back into contact. This creates an instantaneous negative current signal.

2.6 Capacitive model

There are charged surfaces on every triboelectric generator. When external mechanical force act on them, the distance between them changes. This is akin to the process of charging and discharging of a capacitor. From equation (2.17), open-circuit voltage ($V_{OC}(x)$) shows an explicit dependence on both distance between the tribo-layers and the quantity of transferred charges (Q). The short-circuit current depends on both Q which denotes the number of charges transferred and the rate at which the distance between the tribo-layers changes. So TENG can

be assumed similar to a typical capacitor. Total voltage difference between the two electrodes is given by the equation (130)

$$V = -\frac{1}{C(x)}Q + V_{OC}(x) \tag{2.32}$$

Where *x* and *C* represents the distance and capacitance between the electrodes respectively. At short circuit condition, the equation becomes,

$$0 = -\frac{1}{C(x)}Q_{SC} + V_{OC}(x) \tag{2.33}$$

This gives the fundamental relationship between Q_{sc} , C and V_{oc}

$$Q_{SC}(x) = C(x)V_{OC}(x) \tag{2.34}$$

Thus it is possible to model TENG as an ideal voltage source and a capacitor connected in series as shown in the figure 2.4 (98).

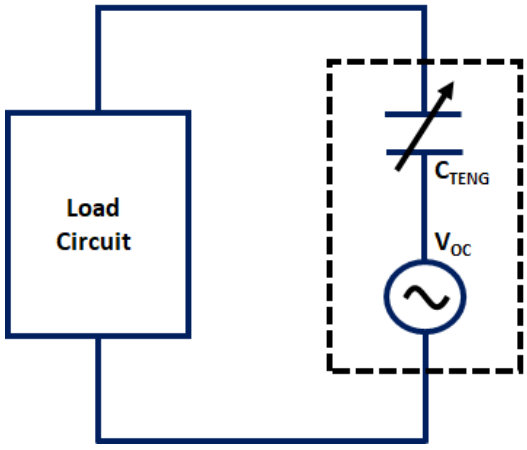

Figure 2.4. Equivalent circuit model of a triboelectric nanogenerator.

2.7 Factors affecting TENG performance

In the early stages when the TENG was introduced, the output power obtained was very low. It was not enough to meet the required demands due to the inadequate output from TENG. Hence the priority was to improve the efficiency of TENGs. There are many factors which influence the output performance of TENGs. The most prominent one is quantity of tribo

charges on dielectric layers which determines the current flowing through the external circuit. The charge density solely resides on the surface chemical properties of both triboelectric materials involved in forming the TENG structure. Main methods to modify the chemical property of a triboelectric material includes surface functionalization and tailoring of morphologies. These modifications could greatly enhance the charge transfer and thereby the output of TENG (131). The efficiency of energy harvesting of TENG depends on the ratio of input mechanical energy and output electrical energy (132) . The input of TENG includes different kinds of vibratory motions which act as the fuel for the operation of TENG while output extracted from the TENG device is electrical energy. It is in the form of alternating current since the involuntary motions are the source of vibrations. Researchers are still carrying out the studies in order to enhance the output performance of TENG.

2.8 Methods adopted to enhance the output performance of TENGs

In order to improve the efficiency of TENG, several methods were tried since the time of invention as indicated in figure 2.5. The two major factors that effects the output electrical energy are electrostatic attractive force between the oppositely charged tribo layers and relative displacement of charges which moves against the force of attraction. The output of TENG increases when either one of these factors or both factors get increased (133). Many methods have been introduced to improve the output performance of TENGs and prominent methods are explained under this section.

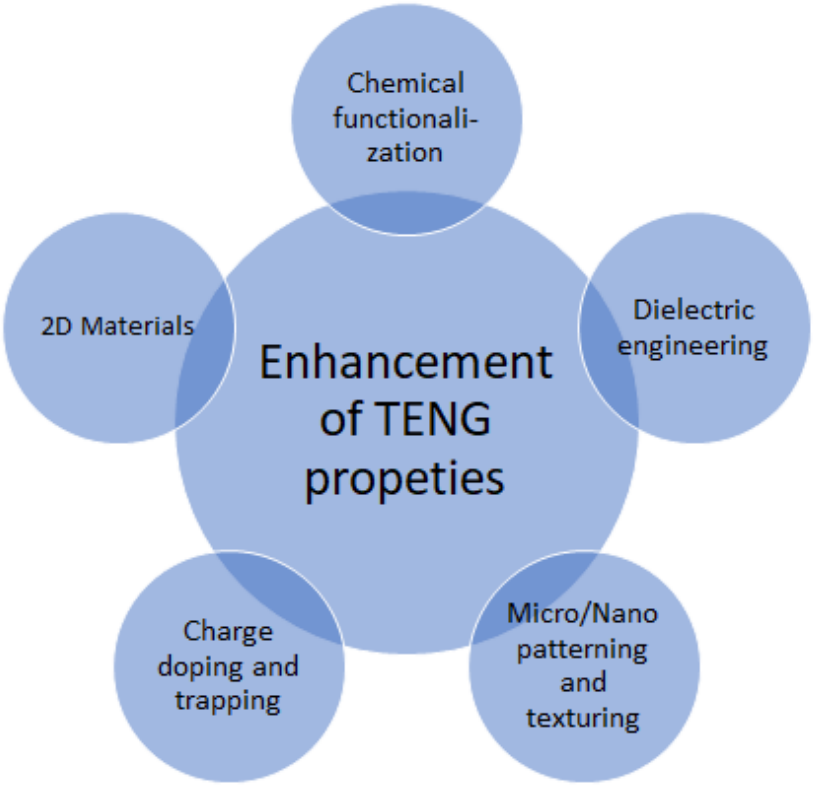

Figure 2. 5. Various methods adopted to improve the output performance of TENG devices.

2.8.1 Micro/nano-patterning and texturing

Physical surface modification is one method to improve the performance of TENG and through this method, an increase in the surface charge density as well as the effective charges on the tribo electric layers can be accomplished (134). The surface of the tribo layers has a large influence on the output power of TENGs (135). It is proposed that, rather than a planar polymer surface, a patterned surface enhance contact area between the tribo-layers and thereby improving triboelectrification (136). Flat surfaces are altered by introducing nano or micro patterns of various forms, such as rectangular, linear, cylindrical, conical, pyramidal or hemispherical structures (137). Rectangular structures have larger surface area than other structures, therefore this form enhances the contact area between the triboelectric layers (138, 139). Strength of contact forces also influences the efficiency of the TENG devices. Lesser the contact forces between the electrodes or tribo layers, smaller will be the contact area as well as

the tribo electric charge density. Studies indicates that when the contact force gets increased, the charge density also increases sharply and saturates, which indicates the tensile nature of contact force feedback in TENGs (140). Pressure and strain also influence the physicochemical properties of materials which affects the charge transfer among the tribo layers in TENG. When a small amount of pressure is applied between the triboelectric materials, due to less contact area, the charge induced is less. But when the tribo layers are subjected to high pressure, contact surface increases thereby charge production enhances (140). Strain is created when the tribo layers have an elastic nature. When forces applied is very large, the charge transfer occurs in the reverse direction due to the strain developed between the tribo-layers (141).

2.8.2 Chemical functionalization

The surface potential of contact materials used in triboelectric energy harvesters is found to boost the output performance (142, 143). Thus, several attempts have been made to modify the surface chemical characteristics of triboelectric energy harvesters in order to maximise the difference in triboelectric polarity between two contact areas. For example, polar Si-O bonds of PDMS surface were replaced for non-polar Si-CH_3 bonds by using ultraviolet-ozone (UVO) and sodium hydroxide treatments. The chemical modification of the PDMS surface enabled the device to produce adequate triboelectric charges (104), and the modified surface-based TENG demonstrated almost 15-fold larger current density than the pure TENG.

Numerous researchers have demonstrated that fluorinated polymers are one of the best tribo-negative contact materials for triboelectric energy harvesters owing to the fluorine element's strong electronegativity. Through a simple and modified physical vapour deposition approach, one research group generated the fluoropolymer-coated polypropylene nanowires (144). The surface composition with functional groups exhibits outstanding triboelectric properties and enhanced the effectiveness of generating triboelectric charges, resulting in high output performance. Chemical functionalization not only alters the surface of the contact

material but it also optimizes the changes in electronegativity and electro positivity between the electrodes. This helps to improve the surface charge density of the triboelectric layers. Cheon et al., used nylon nanofibers combined with PVDF-silver nanocomposites to increase the output performance of triboelectric nanogenerators (145). Studies report that the triboelectric properties of nitro and methyl groups linked to cellulose nanofibrils (CNFs) got improved through chemical reaction (146). Cellulose exhibits neutral polarity, but the nitro and methyl groups exhibit strong electron-accepting and electron-donating characteristics, respectively. When nitro- and methyl-CNF-based TENGs were compared to CNF-based TENGs, former one demonstrated an increase in output power. Additionally, the chemical functionalization of surface contact materials can be considered as a realistic solution to the friction related to the structural problem of sliding mode TENGs. Reports points that the positively charged nylon film partially transformed to negatively charged surface using the reactive ion etching (RIE) with a metal mask.

Surface functionalization can be achieved through introduction of nano molecules in the form of nanoparticles, nanowires or nanotubes into the matrix of triboelectric layer. Reports point out that this technique has a significant influence on TENG output performance (147-149). With the introduction of nanoparticles, there is an increase in the contact surface roughness as well as the permittivity of the triboelectric layers (150, 151). Since the choice of materials are numerous, this type of modification suggests many options in order to improve the output performance of TENG devices. The selection of materials with outstanding chemical characteristics is a currently active field of research and scientists concentrate to meet the demand through the appropriate selection of materials and polymer composites.

2.8.3 Charge doping and trapping

Method to introduce charges on or within the contact materials also can be regarded as an efficient method to improve the output performance of triboelectric energy harvesters. The

presence of large number of triboelectric charges which got accumulated on the surface of the tribo materials through the process of charge doping or trapping results in a strong driving force to produce high output voltage and current. It is found that surface charge density pile up through the introduction of single polarity charged particles and ions onto the contact layers (152). Wang et.al suggested that trapping charges inside the triboelectric materials is a facile and efficient method in which maximum power density improved up to 25 times and sustained performance was extracted for a prolonged period (153). The process of trapping charges inside the tribo materials causes enhancement in the output performance of TENGs. This is mainly due to the shielding of triboelectric charges near the trapping sites. Out of different ways for producing trapping sites, fabrication of groove structure on the Au layer through the plasma treatment is a method adopted where triboelectric charges are trapped in these grooves (153). Another work reported method of embedding graphene oxide into PVDF nanofibers which served the same role of charge trapping sites (154). As a result of charges trapped in the graphene oxide, the surface potential of the PVDF nanofibers improved and also noticed a delay for the distribution of surface charges. Polymer mixture of poly (3,4-ethylene dioxythiophene) with poly (styrene sulfonate) (PEDOT: PSS), as the charge trapping layer was employed to increase the number of triboelectric charges (155).

2.8.4 Surface modification by introducing 2D materials

The class of ultra-thin nanomaterials which are made up of a few atomic layer dimensions are designated as 2D materials e.g., graphene, MXenes etc. The main peculiarity of these class of materials includes large interfaces and surfaces which helps them to possess entirely different physical and chemical properties when compared to the original bulk material. Kim et.al reported an enhancement in the output performance of TENG by introducing graphene of monolayer to quad layers on copper foils, was observed. They found that the output of graphene based TENG has an explicit dependence on the number of graphene

layers (156). This was due to the reason that as the number of graphene layers varies, there was a deviation in the work function and friction.

TENG devices based on a novel and developing family of 2D layered transition metal carbides and nitrides, generally called as MXenes, were tried by Dong et.al (157). The striking nature of MXenes is that their compositions and functional groups can be tailored. Also, they exhibit high electron negativity similar to that exhibited by fluorinated groups. MoS_2, another member of 2D family, possess electron accepting property similar to graphene sheets and MoS_2 based TENG device was introduced by Wu et.al. (158, 159). Since the 2D materials possess large bandgap energy, interface trap states are available within the band gap. Thus, power density of 2D MoS_2 based TENG was 120 times higher than that of pure TENGs (160). These examples illustrate that 2D materials can be considered as efficient way to tune the surfaces of tribo layers for improving the output performances of triboelectric devices.

2.8.5 Dielectric engineering

Gold (Au), aluminium (Al), and copper (Cu) are commonly used for the metallic friction layers, whereas polydimethylsiloxane (PDMS, [Si $(CH_3)_2O$] n) has proven to be an excellent dielectric material for the fabrication of TENGs (161) due to its appealing characteristics such as plasticity, transparency, tractability, excellent electronegativity, and biocompatibility (162). Pure PDMS is a non- conducting polymer with low dielectric constant. Hence, pure PDMS is ineffective as a triboelectric material for high-performance TENG manufacturing. Several research works show that expanding the contact surface area of TENGs based on PDMS by nano-structure formation (163) and fluorocarbon plasma operation can improve energy conversion efficiency (164). TENGs with composite-based friction layers are currently attracting a lot of attention from academics who want to improve the output performance of nanogenerators. For example, multiple studies have been conducted on composite-based TENG containing various nanoparticles such as $BaTiO_3$ (165), ZnO (166),

$CaCu_3Ti_4O_{12}$ (166), Na_2CO_3 (167), and $ZnSnO_3$ (168). Also it is reported that Pb-free ferroelectric material $ZnSnO_3$, which is from the nonsymmetric group, possess a strong piezoelectric response and a large spontaneous polarization value (169). This high polarization value is due to the considerable displacement of the Zn atom from the centre of gravity compared to other oxides such as $KNbO_3$, ZnO, and $BaTiO_3$ (170) and hence $ZnSnO_3$ has lately found a place in the fabrication of composite-based TENGs in order to improve the TENG's output performance (168).

Although composite-based TENGs have a high output performance, the degree of nanoparticle distribution in the polymer matrix is critical for the nanogenerator to work well (165). When nanoparticles are added to a polymeric matrix, they have a tendency to settle on the bottom surface of the polymeric film. The surface charge density does not vary as the nanoparticles settle near the bottom surface, resulting in no appreciable change in the TENG's output performance. As a result, raising the nanoparticle concentration in the composite can lowers the TENG's output performance.

Incorporating multiwalled carbon nanotubes (MWCNTs) or graphite nanoparticles into the PDMS matrix is one of the successful methods for accomplishing enhanced output of TENGs (171). The primary role of MWCNTs is to improve surface charge density by lowering internal resistance along with significant reduction in the thickness of the PDMS, hence improving the TENG's output performance. Karumuthil et al. used an approach of incorporating conducting nanoparticles reduced Graphene Oxide and MWCNT into the PDMS matrix to distribute the ZnO nanoparticles and fabricate a high-performance piezo-/tribo nanogenerator (172). Park et al. used MWCNT as a functionalizing agent to disperse $BaTiO_3$ in the PDMS homogeneously in the composite, preventing the nanoparticles from aggregating (173). MWCNT also aids in the improvement of piezo potential by solidifying stress scattering to nanoparticles. Internal and surface microstructure, on the other hand, are crucial for

improving the nanogenerator's output performance (174, 175). So, for a uniform distribution of the nano-filler in the condensed polymer matrix, the nano-filler desires to be surface treated or a foreign element needs to be mixed (176). For instance, Alam et al. used MWCNT as dispersant for the $ZnSnO_3$ nanoparticles along with conducting filler (177). In many cases, a mixture of solvents also performs a chief part in the distribution of the filler in the polymeric matrix. For example, Han et al. added ethanol in PVDF matrix for distributing the PLZT (Perovskite Lead Lanthanum Zirconate Titanate) nanoparticles (178).

2.9 Remedies to enhance the energy conversion of TENGs

The output of TENG is usually extracted using self-charging power units by coupling a full wave bridge rectifier between TENG and capacitors. The main properties of TENG includes high open circuit voltage, low short circuit current and huge internal resistance. As a result of large internal resistance, there is a substantial mismatch of impedance between TENG and capacitors which act as energy storing devices. This causes wastage of energy along with reduction in competence of energy conversion. Steps taken to improve the energy conversion productivity include framing of suitable power controlling devices which could efficiently lessen impedance mismatch of TENG. There have been many works carried out which suggests that basically two techniques namely (a) charge boosting and (b) buck converting is most suitable for tackling this issue (179, 180). The idea of charge boosting is to harness more charge from TENG with an aim to achieve higher output performance and in the case of buck converter, it converts high voltage and low current obtained from TENG output to low voltage and high current. However, for its irregular and random high voltage and low-current pulse output characteristics, the TENGs usually exhibit low-energy supply efficiency when directly coupled to powering conventional electronics or charging energy storage devices (181). These factors have always been a blockage for TENGs toward practical application in self-powered microsystems to some extent. Hence, effective power management is highly desired for

increasing the energy supply efficiency of TENGs. Over the past few years, several strategies of power management have been proposed, such as rectification (182), electromagnetic transformation (183), capacitive transformation, (184) and direct current (DC) conversion (185), which could be used for voltage regulation, impedance matching, and efficiency improvement.

2.10 Materials chosen for current study

The materials which possess different charge affinity can be implemented for the construction of TENG devices. It is already understood that materials placed at the opposite end of the triboelectric series when paired up exhibits' high performance for potential applications. Most commonly used materials which forms the tribo-negative materials includes Polydimethylsiloxane (PDMS) and all metals usually act as tribo-positive materials. For this work, Polydimethylsiloxane (PDMS) mixed with fillers was chosen to act as tribo-negative layer while copper metal was chosen as both tribo-positive layer and electrodes. This section details about the peculiarities of polymer under study as well as prominent features of fillers which are introduced to polymer matrix with an aim to achieve desired properties for the tribo negative layer.

2.10.1 Polydimethylsiloxane (PDMS)

Polydimethylsiloxane (PDMS) belongs to a group of silicones which is basically a polymeric organosilicon compound. The formula of PDMS is $CH_3[Si(CH_3)_2O]_n\ Si(CH_3)_3$, where n represents the monomer $Si\ O(CH_3)_2]$ units as shown in the figure 2.6 (186).

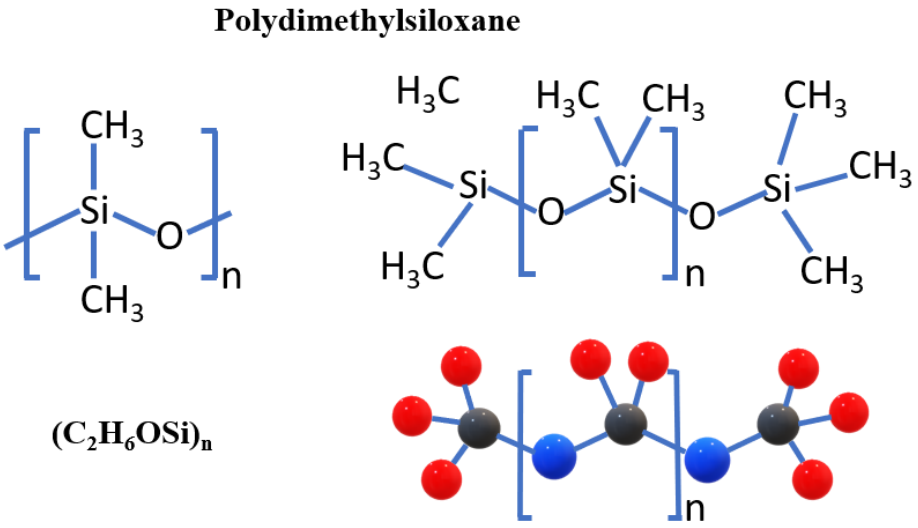

Figure 2. 6. A schematic of the chemical structure of Polydimethylsiloxane.

PDMS is silicon-based organic polymer which finds numerous applications because of its viscoelastic properties. It is a hydrophobic elastomer after the cross-linking process and could be molded into any structures even to nanoscale regime (187). PDMS is a translucent and optically vivid polymer (188), non-toxic (189), and inflammable. Due to its peculiar features, this polymer has found extensive applications which include PDMS as stamp resin in soft lithography (190), used as common material for flow delivery in microfluids (191) and also utilized for fabrication of lab-on-chip devices (192). By regulating the degree of cross-linking, PDMS can be made very soft and its dimensions can be adjusted to accommodate mechanical modifications to its physical surroundings. This mechanical flexibility makes it suitable for use in tissue engineering and as some flexible parts in medical equipment (193). The important property of PDMS, which is utilized for electronic applications, is its stretchable nature (194). The translucent nature of PDMS are employed in suspended particle devices which is an important component for smart window applications (195).

Other applications of PDMS includes deformers (196), contact lenses (197), water repellent coatings (198) cosmetics (199), lubricants (200) etc. PDMS possess good adhesion which is used for fabrication of polymer brushes (artificial adhesives) and Gecko-inspired structures (201). Studies show that PDMS possess high adhesion and this property has been exploited for fabrication of patterns by lithographic methods (202). This property is also used in the field of microfluids where adhesion of PDMS is crucial for ensuring appropriate and tight contact between the PDMS and the glass substrate in order to prevent any leakage (203). It is this adhesive property of PDMS which makes it suitable for triboelectric nanogenerators, and has been extensively employed as contacting layers for mechanical energy harvesting (204). Adhesion plays a vital role in producing larger surface charge, which is one of the important parameters for high performance as far as TENGs are concerned (205). Exfoliation, dry transfer, and stamp printing of monolayers of 2D materials such as graphene, transitional metal dichalcogenides (MoS_2, WS_2, etc), h-BN, and other layered van-der-Waals materials are all made possible by the use of polydimethylsiloxane (PDMS) (206). Furthermore, PDMS stamp printing may be employed for the production of 2D heterostructures as well as the construction of functional devices (207).

In addition to adhesion, the mechanical properties of PDMS are important and play a critical role in different applications (208). Recent research in microfluidics and micro electromechanical systems (MEMS) has revealed that high elasticity of PDMS provides supreme benefits over more rigid substrate materials such as glass, silicon, and harder polymers (208). However, the poor hardness of PDMS restricts many possible uses, such as in certain chemical and high pressure domains (209). It is reported that PDMS possess low surface roughness and has a larger surface charge compared to polymers with a rougher surface. During contact electrification process, at each contacting-separation event, material transfer happens in both directions (80). Researchers suggest that to get a high net surface charge density on the

polymer, it must have strong surface adhesion and a low cohesion energy in the bulk. As a result, energy of the adhesive bonds existing between contacting surfaces is greater than the energy of the chemical and physical bonds in bulk. This may facilitate covalent bond breakage and subsequent material transfer (210). It has been reported that the intermolecular force among the molecules at the surfaces of PDMS is the van der Waals forces (210). During mechanical modification of the surface of PDMS through contact electrification, splitting of bonds from the polymeric chains ($-Si(CH_3)_2O-$) of PDMS creates the formation of anions ($-(CH_3)_2SiO-$) on the surface of PDMS which occurs due to the heterolytic cleavage of the chains. This phenomenon vividly explains that both charge and material get transferred simultaneously during contact electrification (211, 212).

Mechanical properties of PDMS can be tailored by introducing different fillers (207). When fillers are added to silicone elastomers, it improves the service life and performance of insulators and decrease the difficulty in fabrication procedures. In order to improve the mechanical properties of PDMS, various reinforcing materials are incorporated into PDMS matrix. In the current study, incorporation of conducting fillers and ceramic has been done with an aim to tailor the properties of PDMS for TENGs applications.

2.10.2 Polymer composites

A composite is said to be a system which contain at least two or more immiscible materials forming a new material with characteristics that are different from that of its constituent components. Polymer, metal, glass or ceramic act as host or matrix and particles such as fibres, ribbons, flakes, sheets, platelets or tubes act as fillers or reinforcement materials ,(213). Generally, polymers are used as matrix which are often low-cost materials that are adaptable and can be easily processed into any shape, especially thin films and they are also easy to work with. In spite of the large amount of research that has been done in the field of structural polymer-based nanocomposites (214), only a small amount of study has been done

on polymer nanocomposites for functional purposes (215, 216). Nanocomposites, which are made up of metal nanoparticles distributed in a dielectric matrix, are of special interest among functional nanomaterials because of their innovative features that open the door to a plethora of new application possibilities (215, 217). Polymer composite materials finds applications in diverse fields such as transportation, aerospace, energy, sporting goods, automotive, defence and infrastructure owing to their peculiar characteristics such as light weight, good mechanical strength, excellent durability, ease of fabrication and flexible nature (218).

Polymer materials, in general, have a low dielectric permittivity and a limited percentage of dielectric loss. Conductive fillers such as carbon black, carbon nanotubes, graphene, and reduced graphene oxide (219-221) may be used to improve dielectric properties. They are also extended for energy storage and electronic applications. Previous studies have concentrated on the investigation of electrical characteristics such as capacitance, impedance, permittivity, and conductivity (222). The kind of material, volume fraction, shape, size of the filler particle, and other aspects such as bonding and interaction, processing, all have an impact on these qualities(223).

High energy storage systems have always demanded the development of polymer composite systems which consists of polymers incorporated with high dielectric constant fillers. The presence of fillers always improved the total dielectric constant of the composite without impairing the tensile strength of the polymers. Research works are being done to fabricate polymer composite materials with better properties by gaining a knowledge about the physical phenomena ruling the composite dielectric permittivity. Most of the recent works focus on the dielectric polymer composites and metal polymer composites with an aim to improve the dielectric permittivity of the composites.

2.10.3 Metal nano-particles - polymer composite

For decades, nanoparticles (NPs) have sparked the interest of scientists and research of NPs is promising due to their potential usage in nanotechnology. In recent years, academics and industry have promoted noble metal NPs for both basic research and practical purposes. A significant aspect that draws researchers to these materials is their optical, magnetic, electrical, and catalytic capabilities, which are finding commercial uses. Despite their increased beneficial qualities at the nanoscale, these NPs display extraordinary physical properties when implanted in a matrix such as a polymer due to quantum size effects (224). The synergistic capabilities of their constituents make nanocomposite materials made of metal NPs embedded in a polymeric matrix extremely attractive for a number of technological applications (225). When activated by electromagnetic radiation, these NPs in a dielectric matrix exhibit remarkable SPR absorption, which is often detected in the visible range (226). For instance, it has been discovered that incorporating noble Ag NPs in the active layer boosts the solar cell's optical absorption (227). Studies (228) reported that thin composite films containing NPs had excellent mechanical characteristics (225). Metallic nanoparticles embedded in a dielectric matrix exhibit a variety of functional properties. Their peculiar features studied include plasmonic property (229), magnetic properties governed by ferromagnetic single domain behavior or super-paramagnetism (230), granular giant magnetoresistance (231), and enhancement of catalytic activity due to large surface area and contribution of surface energy towards chemical potential (231).

Many methods have been employed to embed metal NPs in polymer substrates, including vacuum deposition on viscous polymers; plasma polymerization combined with metal evaporation (232), chemical synthesis in organic solvent (233), co-sputtering of metal and polymer (234), vapor-phase co-evaporation (235, 236) etc. Heating of polymer substrates with supported metal NPs on the surface (237) , metal ion implantation in polymer films (225),

laser or ion beam irradiation of metal NPs on polymer surfaces (238) are some of the other ways. An extensive selection of production techniques for metal nanoparticle-encapsulated nanocomposites have been published in recent reviews (239). The majority of the literature, including review papers, discusses the manufacturing techniques for embedded NPs and their increased characteristics in nanocomposites materials when inserted into a polymer matrix.

Polymer nanocomposite thin films serve as model systems for interpreting key material features, physical/chemical processes underlying the embedding process, and fundamental principles governing the embedding of NPs into polymer surfaces (237). Polymer/metal composites exhibit excellent dielectric behaviour when the metal loading percentage is low. Hence the current study focusses on introducing metal nanoparticles into PDMS polymer matrix and investigating the properties of resulting metal/ polymer composite for TENGs applications (240, 241). The metals used for the present study includes silver, copper, aluminium, tin and zinc. The properties of metals are tabulated in the table 2.1.

Table 2. 1.Properties of various filler nanoparticles used in this study

Filler	**Conductivity (S/m)**	**Density (g/cm^3)**	**Dielectric constant**
Silver	6.3×10^7 (242)	10.5 (243)	Theoretically ∞
Copper	5.98×10^7 (244)	8.96 (243)	Theoretically ∞
Aluminium	3.5×10^7 (244)	2.7 (245)	Theoretically ∞
Zinc	1.68×10^7 (246)	7.13 (247)	Theoretically ∞
Tin	8.7×10^6 (246)	7.31 (247)	Theoretically ∞
LSCO	1.15×10^6 (248)	7.11 (247)	
PDMS	2.53×10^{-5} (249)	970	~3

2.10.4 Polymer - ceramic Composites

The desired characteristics of different materials such as the flexibility of polymers and the electrical/mechanical properties of ceramics are combined in a composite material, which can meet the restrictive demands of different devices or applications more efficiently than the individual materials combined. The majority of composites designs achieve strength and flexibility by reinforcing a relatively flexible but weaker polymer with a considerably tougher and more durable ceramic fibres. Filling a polymeric matrix with fine fillers results in the alteration of both the polymer network and the characteristics of composite materials as a result of the development of an interface at the boundary between the matrix and the filler particles (250). By improving the interaction at the interface between the matrix and the filler, the introduction of sub-micro and nanosized fillers to polymeric matrices may result in the enhancement or stability of electrical, mechanical, and thermal characteristics of polymeric dielectrics (251, 252). Triboelectric nanogenerators (TENGs), which are made of soft polymers with incorporated materials and tailored dielectric properties, appear to be the most promising candidate which possess enhanced output properties.

Ferroelectric metal oxides such as Pb (Zr,Ti)O_3(PZT), $Pb(Mg_{0.33}\ Nb_{0.77}\ )O_3$-$PbTiO_3$ (PMNT) and $BaTiO_3$(BT) are introduced to polymer matrices in order to enhance the dielectric permittivity of the polymer ceramic composites. Usually, polymers possess dielectric constant less than 10 and hence inorganic fillers possessing dielectric constant of the order of hundreds or thousands are introduced into the polymers for increasing the composite's effective dielectric constant. Even though the fillers possess high dielectric constant, the effective dielectric constant of the composite generally does not improve to very high value as expected. The improvement of effective dielectric constant of the polymer matrix is due to the increase in the average field in the polymer matrix. Since there is a large contrast between the permittivity of the two phases, inhomogeneous electric fields occur in the matrix. The present

design process for TENGs is confronted with an investigational attempt in which the strontium doped lanthanum cobalt oxide (LSCO) ceramic is introduced into PDMS matrix with an aim to tailor the properties of polymer matrix and also to study the performance of TENG based on LSCO/PDMS polymer composites.

2.10.5 Lanthanum doped Strontium Cobalt Oxide ($La_{0.8}Sr_{0.2}CoO_3$, LSCO)

Perovskites are a kind of ceramic having a chemical composition of ABO_3. As a material, they exhibit a diverse range of intriguing features. Certain perovskites show piezoelectric properties, while others exhibit low-temperature superconductivity (253). They also exhibit good catalytic properties and are utilised as cathodic materials. Improvements in the properties of $LaCoO_3$ was noted with introduction of strontium. With the increase in the strontium content, the structure of $LaCoO_3$ becomes non-stochiometric. A great deal of interest has been dedicated to the perovskite-type oxide $La_{1-x}Sr_xCoO_3$ for its potential use as oxidation catalysts, sensor materials, electrode materials for solid oxide fuel cells (SOFC), and other applications (254). There have been several reports on the electrical transport features of the mixed-valent perovskite type oxides La_{1-x} Sr_xCoO_3 (255). With a rhombohedral perovskite structure, the parent chemical $LaCoO_3$ is an excellent insulator at room temperature and lower temperatures (256). The bulk conductivity and dielectric characteristics of materials below 350 ^oK are favourable for polaronic charge transfer (257). The transport characteristics of $LaCoO_3$ vary gradually from those of a thermally activated semiconductor to those of a metal in the temperature range $350 < T < 650$ ^oK, with the metallic temperature dependency becoming stable above 650 K (258). Mineshige et.al (256) investigated the metal-insulator transition behavior and found that the conductivity of $La_{1-x}Sr_xCoO_3$ with $x < 0.25$ exhibited semiconducting nature and that the conductivity of the material in the range $0.25 < x < 0.7$ exhibited metallic behavior when temperature was close to room temperature. At room temperature, the change from a metal to an insulator in $La_{1-x}Sr_xCoO_3$ was at $x = 0.25$. When

the x value was 0.25, the Co-O distance and the Co-O-Co angle of this system displayed a sudden reduction. As the x value increased beyond 0.25, the Co-O distance and the Co-O-Co angle also increased which resulted in an insulator to metal transition. Afterwards, Kozuka et al. found out that, in the bulk LSCO, the metal-insulator transition (MIT) arises at x=0.2 and that the maximum conductivity is attained at x = 0.5. Figure 2.7 depicts the crystallographic structure of $La_{1-x}Sr_xCoO_3$ (259) .

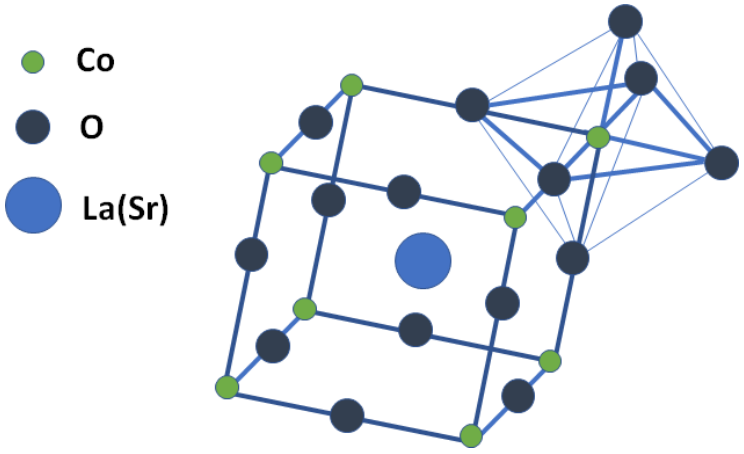

Figure 2. 7. The crystallographic structure of $La_{1-x}Sr_xCoO_3$.

2.11 Structure and fabrication

Pure PDMS films were fabricated by room temperature curing method. Curing agent used was tetraethyl orthosilicate (TOH) while the accelerator used was dibutyl tin dilaurate (DBTDL). PDMS, TOH and DBDTL were taken in a ratio of 100:10:1 and stirred in the room temperature. The mixture was transferred to a petri dish and kept in a desiccator under vacuum for 12 hours to form a self-standing film. Ceramic LSCO ($La_{0.8}Sr_{0.2}CoO_3$) and metals namely silver, copper, aluminium, zinc and tin nano particles (30-50 nm, Platonic Nanotech, India) were added in different weight percentage to the PDMS solution. The mixture of PDMS solution fillers were probe sonicated for 2.5 hours. After thorough mixing, the curing agent and catalyst were added to the stock solution in the aforementioned ratio. This mixture was

transferred to a mold and kept undisturbed for 12 hours. Finally, the polymer composite films were peeled off for further characterization studies. The weight percent of filler introduced into PDMS were 0.5, 1, 5, 10, 15 and 20 wt%. Figure 2.8 depicts the fabrication process of polymer-nanocomposite samples.

In this study, dielectric to metal model is used to form the TENG structure. PDMS mixed with different weight percentage of fillers act as negative tribo material and was attached to a copper electrode. Another copper plate (2 cm × 2 cm) acts as both positive tribo material as well as top electrode so as to form the dielectric-metal model TENG. Output for electrical measurement was taken from the copper electrodes.

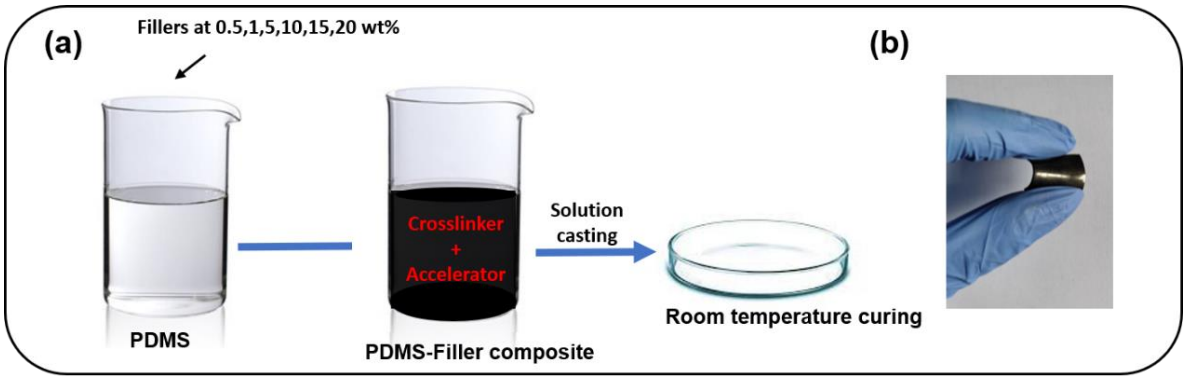

Figure 2. 8. Fabrication steps of polymer-nanocomposite samples.

2.12 Characterization Techniques

This section provides an overview of the primary techniques employed during this work for material/electrical characterization. The basic knowledge of methodologies and equipment is intended to aid in the knowledge of the subsequent chapters' characterization and measurement outcomes. Material characterization methods used throughout this research can be classified into the following categories:

(i) Phase analysis (using X-ray diffraction technique)

(ii) Material characterization (using Raman spectroscopic technique),

(iii) Surface analysis (using Scanning electron microscopy),

(iv) Dielectric measurements (using HIOKI LCR meter),

(v) Electrical measurements (using oscilloscope and source meter).

(vi) Mechanical excitation system (using triboelectric measurement system).

2.12.1 X-Ray diffraction

The structural characterization of the samples was accomplished by capturing their x-ray diffraction (XRD) patterns. PANalytical, AERIS x-ray diffractometer with Cu-K radiation (λ = 1.540598 A^o) was used to get the XRD patterns. This technique is a non-destructive method for the phase identification of crystalline materials. The fundamental idea is based on Laué diffraction, where crystalline materials diffract incident x-rays in the same way as a diffraction grating. Crystals placed in the lattice planes act as diffraction grating and diffraction patterns are obtained. A given material always creates a specific diffraction pattern, regardless of whether it is present in its pure form or as a constituent of a mixture. This is the fundamental concept behind the diffraction technique of chemical analysis. The benefit of x-ray diffraction analysis is that it reveals the existence of a material in the sample in the form in which it exists, rather than in terms of its individual chemical constituents. Diffraction analysis is advantageous because it provides the chemical state of the constituent components or their present phase. Apart from the non-destructive nature of this analysis, the technique is a quick method and only small amount of sample is needed (260).

Bragg's law is the fundamental law underlying the diffraction technique of structural investigation. When monochromatic x-rays strike the atoms placed in a crystal lattice, each atom serves as a scattering source. The lattice structure of the crystal functions as a series of

parallel reflecting surfaces. At certain angles, the greatest intensity of the reflected beam occurs when the path difference between two reflected waves from two separate planes is an integral multiple of wavelength. This is referred to as Bragg's law, and it is defined by the relation

$$2d \sin\theta = n\lambda \qquad (2.35)$$

where n is the order of diffraction, λ is the wavelength of the x-rays, d is the spacing between consecutive parallel planes and θ is the glancing angle (or the complement of the angle of incidence) (261). The schematic of Bragg's diffraction is given in figure 2.9.

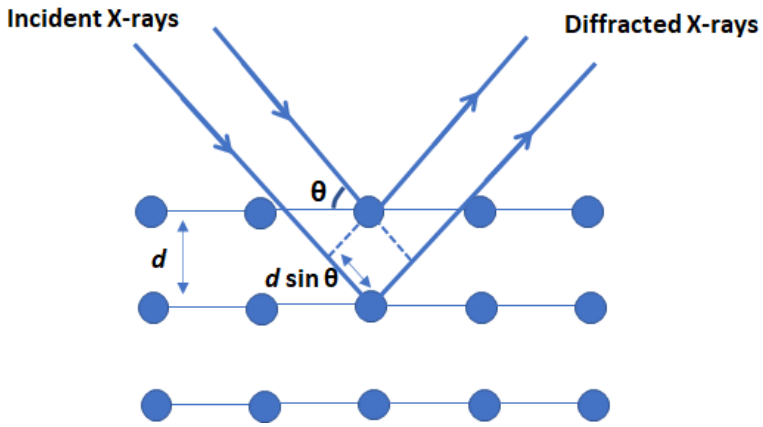

Figure 2. 9. X-ray diffraction by crystallographic planes according to Bragg's law.

2.12.2 Raman Spectroscopy

Raman spectroscopy is a powerful technique for determining the structure of molecules. Its objective is to gather information about molecular vibration and rotational change by evaluating the difference between the incident and scattered light spectra. Raman spectroscopy is performed by irradiating the sample with a laser, causing energy transfer, followed by recording the Raman spectrum with a grating spectrometer. The energy shift and the resulting spectrum offer information about the molecules' vibrational states.

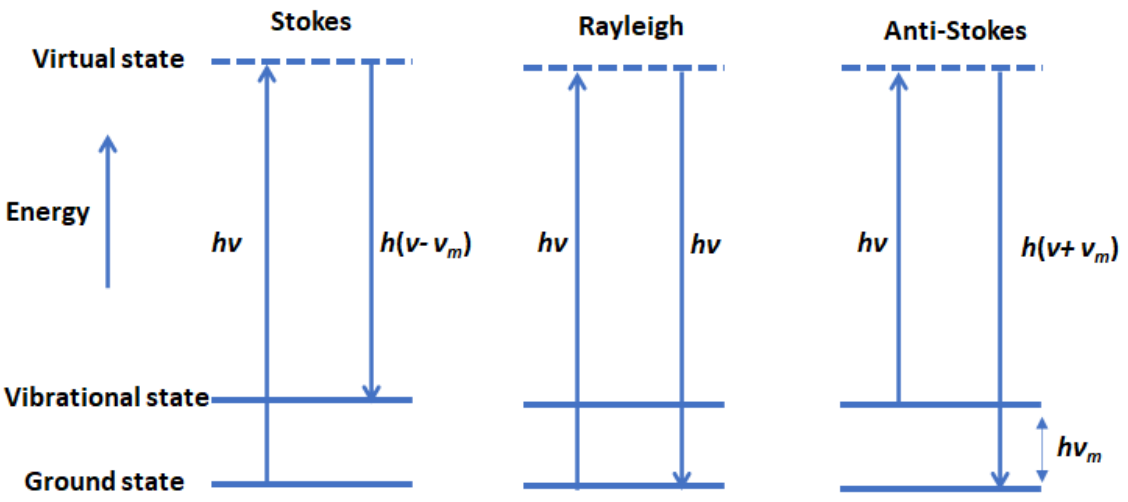

Figure 2.10. A simplified diagram of Stokes process, anti-Stokes process and Rayleigh process.

Raman scattering is caused by the inelastic scattering of light impinging on the specimen. The energy of scattered light either decreases when an elementary excitation of the solid material is stimulated by donating a phonon or enhances when a phonon is absorbed. The Raman spectrum describes the intensity of scattered light as a function of the energy difference between it and the incoming light. This phenomenon is referred to as Raman shift. The primary advantage of Raman analysis is its measurement precision, which is typically on the range of 1 cm^{-1} (0.1 meV).

When the light interacts with sample's electron cloud and electric field of incident monochromatic light which generate a dipole moment within the molecule due to its polarizability. Incident light does not excite the molecule and hence there will be no transition between energy levels. Thus, Raman effect is not a photoluminescence emission, but rather a vibrationally excited state on the ground electronic state potential energy surface in many circumstances. When a photon collides with molecules, both elastic and inelastic collisions may occur. Some of these collisions are elastic where no energy exchange occurs, while some are inelastic and frequency of the scattered photon fluctuates, causing a shift in the emission

spectrum of the stimulated light. This type of scattering is referred to as Raman scattering. Stokes Raman scattering occurs as the frequency of the scattered photon is high when compared to the incident ones. When the associated frequency rises, the scattering is referred to as anti-Stokes Raman scattering. Additionally, the molecules acquired a new state in proportion to the degree of the energy shift. Thus, by observing the shift in the direction of this energy change, typical value of the molecules' vibrational energy may be determined. In the present work, the samples with metal nanoparticles are present and hence Surface enhanced Raman scattering (SERS) was also observed. A simplified version of Raman scattering is depicted in figure 2.10.

Surface enhanced Raman scattering (SERS) has developed as a remarkable vibrational spectroscopic method by eliminating the most major limitation of conventional Raman spectroscopy for analytical applications (262). SERS improves the cross section of Raman scattering by stimulating the sample with an appropriate laser line in contact with a 'plasmonic' surface. As a result, the Raman signal strength is dramatically increased, lowering the detection limit to a single molecule (263). Thus, success in SERS detection is inextricably linked to advancements in the synthesis and optical characterization of novel plasmonic nanostructured materials. Raman studies were carried out with Lab RAM HR spectrophotometer (HORIBA JOBIN YVON) with 532 nm as the excitation source with laser energy 5mW and 1.8 s integration time.

2.12.3 Scanning electron microscopy

Scanning electron microscopy (SEM) is a well-established technique for examining the morphology of a material. It targets a high-energy electron beam onto the sample in order to collect data about surface topography and composition. Electron guns (also known as field emission guns or thermionic guns) generate electron beams when an extremely high voltage is applied; the generated electrons are then accelerated and is focused towards the sample by an

anode grid. Prior to making contact with the sample, the electron beam will travel through a series of condensing lenses to focus and guide the beam. As the high-energy electrons collide with the sample, multiple signals are created as a result of the electron-sample interaction.

The signals, which comprise of secondary electrons, backscattered electrons, characteristic X-rays and photons, will be recognized by the appropriate detectors to provide a vivid picture and information about the sample. For example, the secondary electron formed by these incident electron beams offers information about the sample's morphology, while backscattered electrons generated by deeper penetration of these incoming electron beams provide information on the sample's chemical composition. The sample's atomic composition may be determined using X-ray characteristic emission caused by inner shell electron bombardment of canned samples.

SEM analysis of nonconductive materials is often problematic due to the fact that SEM analysis is based on electron interaction with the sample. However, a thin coating of conducting material with a thickness of 10 to 20 nm can be deposited on top of these non-conducting materials to improve the secondary electron emission and to eliminate the surface charging effect caused by the incident electron beam bombarding the non-conducting surface. This results in obtaining more stable and refined image of surface morphology.

2.12.4 Radio frequency dielectric measurements

Generally, LCR meters are used to determine the capacitance, conductance, impedance, and dissipation factor of dielectric ceramics in the radio frequency region using the well-known parallel plate capacitor technique (Figure 2.11). Parallel plate capacitors are formed by inserting a thin sheet of the sample between two electrodes. This is accomplished by evenly covering both sides of cylindrical specimens of diameter 10 mm and thickness 1 mm with

copper electrodes of same dimension. The capacitance in vacuum is compared to that of a

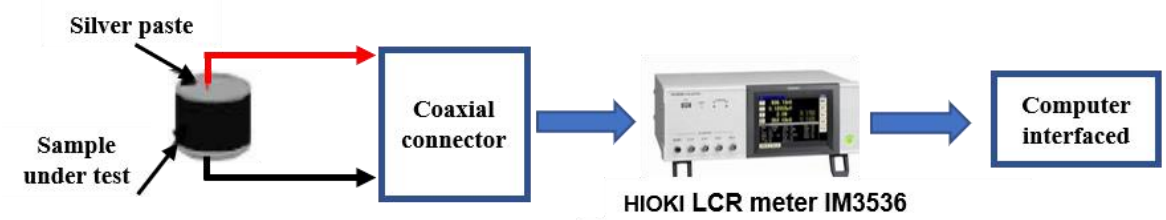

Figure 2. 11. Dielectric constant measurements using an LCR meter.

parallel-plate capacitor in the presence of the substance whose dielectric characteristics are to be determined. Then relative permittivity is calculated using the equation

$$\varepsilon_r = \frac{Cd}{\varepsilon_o A} \tag{2.36}$$

where C is the capacitance of material, ε_r and ε_0 is the relative permittivity of material and relative permittivity of free space respectively. In the present study, the dielectric properties were measured using LCR meter (HIOKI IM 3536) (parallel plate capacitor method). When time varying electric field is applied to a dielectric material, its relative permittivity changes with frequency and become a complex number given by

$$\varepsilon^*(\omega) = \varepsilon'(\omega) - j\varepsilon^{"}(\omega) \tag{2.37}$$

$$\omega = 2\pi f \tag{2.38}$$

Where ω and f represents the angular and linear frequencies, j is the imaginary unit, ε' and $\varepsilon^{"}$ denotes the real and imaginary parts of relative permittivity respectively. The real and imaginary parts of permittivity can be obtained as

$$\varepsilon' = \frac{-Z^{"}}{\omega C_0 (Z'^2 + Z^{"2})} \tag{2.39}$$

$$\varepsilon^{"} = \frac{-Z'}{\omega C_0 (Z'^2 + Z^{"2})} \tag{2.40}$$

Where Z' and $Z"$ are the real and imaginary parts of impedence. For a real dielectric material, imaginary part $\varepsilon_{eff}^{"}$ is defined by the imaginary part of the dielectric constant $\varepsilon^{"}$ and conductivity σ as

$$\varepsilon_{eff}^{"} = \frac{\sigma}{\varepsilon_0 \omega} + \varepsilon^{"} \tag{2.41}$$

Similarly, AC conductivity can also be evaluated from the relation

$$\sigma = \omega \varepsilon_0 \varepsilon_r \frac{\varepsilon^{"}}{\varepsilon'}, \tag{2.42}$$

where, $\varepsilon_r = \frac{C}{C_0}$ is the relative permittivity, C_0 is the capacitance in vacuum.

2.12.5 TENG design and fabrication

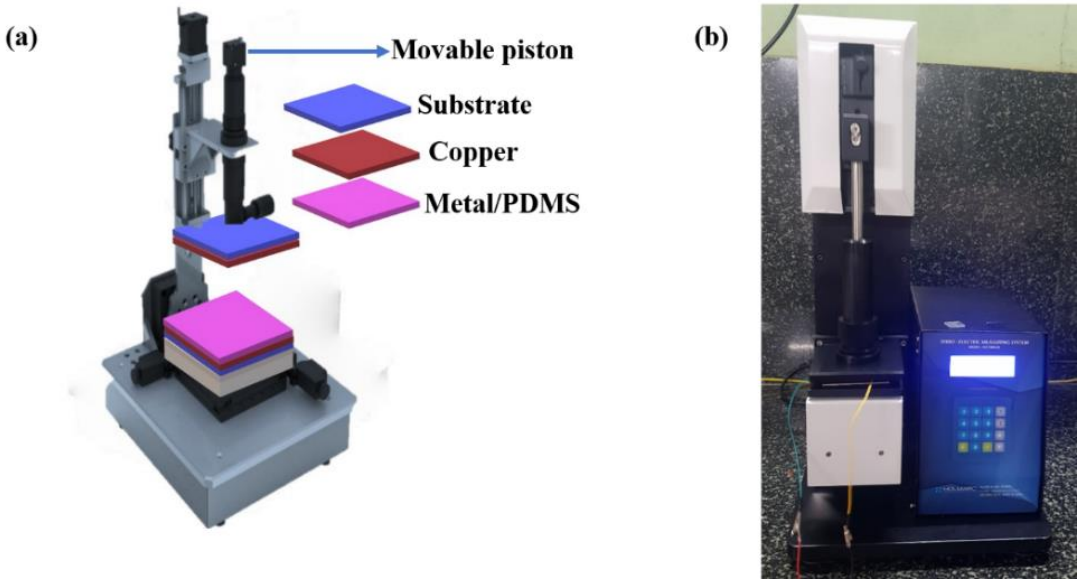

Figure 2.12. **(a)** Schematic diagram of TENG mechanical excitation system **(b)** Photograph of Triboelectric nanogenerator measurement system which produces mechanical excitation with force up to 10 N and frequency up to 10 Hz.

Contact-separation vertical mode TENG was developed and manufactured for hand-driven real-world application testing. Schematic design of TENG characterization system is shown in figure 2.12. Electrodes used were copper sheets and negative tribo layer was

PDMS/filler sheet. A pair of acrylic sheets are used to reinforce copper sheets. In order to produce contact separation movement, the triboelectric measurement system was equipped with a motor assisted movable piston which could produce mechanical excitation with force up to 10 N and frequency up to 10 Hz.

2.12.6 Electrical Characterization

The electrical measurements of the assembled TENGs were initially carried out using a triboelectric measurement system in conjunction with a KEYSIGHT DSOX3054T oscilloscope and KEITHLEY 2450 source measure unit (SMU). The equipment can produce mechanical excitation with force up to 10 N and frequency up to 10 Hz. Thus, TENG output measurements were carried out by using this machine with impact load setting maximum up to 10 N.

To increase the accuracy of the electric test results and to measure their systematic response to input mechanical force, the outputs of the produced TENGs were further tested/measured by a combination of an oscilloscope KEYSIGHT DSOX3054T, and a KEITHLEY 2450 source meter. The triboelectric measurement system interfaced with a personal computer, performs accurately controlled and repeated pressing/releasing in the 1-10 N load range at a fixed frequency of the range 1-10 Hz. In the case of vertical contact-separation mode TENG devices, this measurement equipment was found to be appropriate setup for the electrical characterizations. Figure 2.13 shows the triboelectric measurement system used in the laboratory and red double-sided arrow indicates piston which up and down to produce vertical contact – separation movements.

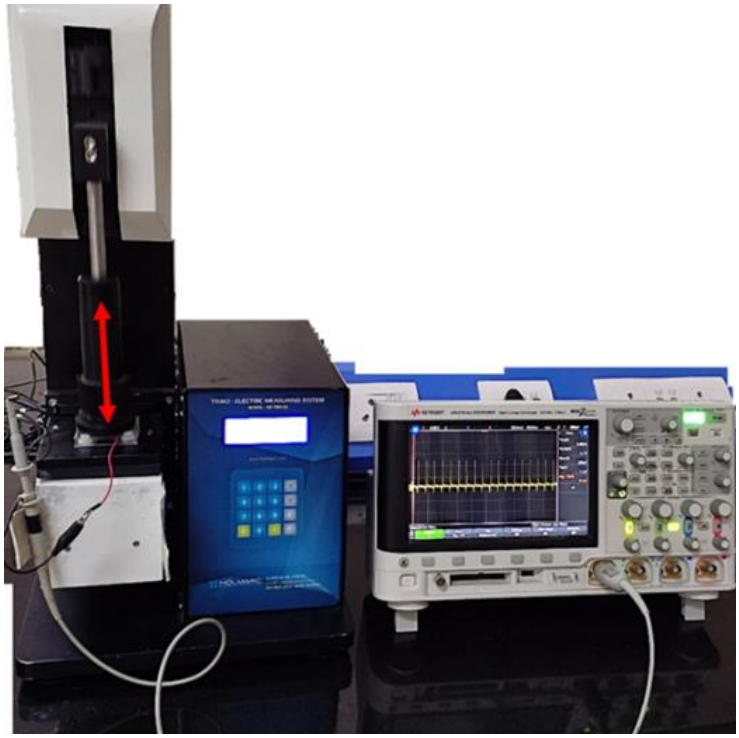

Figure 2.13. Triboelectric measurement system used for testing TENG devices. Contact- separation movements are performed by the periodic up – down movement of piston which is shown by red double-sided arrow.

2.6 Conclusions

In this chapter, theory of TENG was discussed in detail by explaining displacement current analysis and capacitive model. Depending on the materials selected, two different modes were explained. Several strategies for the improvement of performance of TENGs were explained and also remedies for overcoming the challenges faced by devices based on TENGs were detailed. For the present study, polymer PDMS was chosen and its properties were tailored by adding metal nanoparticles and inorganic ceramic LSCO. The peculiarities of materials along with fabrication technique carries an important impact on the output performance of TENG device. Finally, various characterization techniques used in the present study were described.

Chapter 3

Preparation and characterization of metal/PDMS composite TENGs with different metals nanoparticles

Abstract

Due to their superior output performance in comparison to that of other nanogenerators for a variety of applications, energy harvesting devices that make use of the triboelectric effect have attracted the attention of people all over the world. In this chapter, an attempt was made to tailor the characteristics of tribo material by embedding it with metal nanoparticles of varying conductivity in varying percentages by weight. The fabrication and electrical properties of TENG based on metal nanoparticle-PDMS composite films are investigated. The results demonstrate that the filler with the highest conductivity possesses exceptional qualities. At 1kHz, the presence of silver nanoparticles raised the permittivity of the tribolayer from 5.3 to 16.9 in a Silver-PDMS composite containing 20% silver nanoparticles. Electrical investigations of a silver /PDMS composite film yielded commendable results, including 5.1 A (Isc), 33.6V (Voc), and 72.2 W power at 8MΩ with 10N force and 10Hz excitation frequency. This work analyses the role of metal nanoparticles of different conductivity on the triboelectric characteristics of poly dimethyl siloxane (PDMS)

3.1 Introduction

Progress in personal and portable electronic gadgets along with the growth of Information and Communication Technology (ICT) caught much attention in modern era (264). Recent changes in the electronic industry can be considered as a revolution because of the intrusion of technologies into day today life, which predominantly includes Internet of Things (IoT) (265), Artificial Intelligence (AI), data analysis and augmented reality. Use of smart platforms has found an immense role in every realm of life which needs sustainable and maintenance free power sources.

Since triboelectric nanogenerators (TENGs) have proved to be an excellent option for generating electric energy even from low frequency mechanical vibrations, researchers are trying various options to improve the output performance of TENG devices. Out of different physical modifications, the simplest option is the introduction of high dielectric ceramic materials such as $BaTiO_3$ (266), $SrTiO_3$ (267), $CaCu_3Ti_4O_{12}$ (CCTO) (268), $Pb(Zr,Ti)O_3$ (PZT) (269), $Ba(Ti_{0.8}Zr_{0.2})O_3$ (BZTO) (270) etc. into the polymer matrix which inherently possess low dielectric constant. As the dielectric property of the tribo material improves, the surface charge accumulation as well as the charge transfer phenomenon enhance. Another prominent and easiest method to enhance the surface charges is to introduce conducting nanoparticles into the polymer matrix (271). This helps to alleviate the dielectric constant of the nanoparticle/polymer composite. Several attempts have been reported to incorporate conducting fillers such as carbon nanotubes (272) and metals such as gold (103) silver (273) and nickel (274) to improve the dielectric constant of the host polymer matrix. But a systematic study on the effect of incorporating metal nanoparticles having different conductivities has not been done earlier.

In this study, metal nanoparticles of various conductivity were mixed in different weight percent (wt%) into PDMS polymer matrix to form metal/PDMS composite based

triboelectric nanogenerators. The effect of these metal nanoparticles on the dielectric property of the composite as well as on the output characteristics of TENG were examined. The results point to the influence of surface charges on the dielectric properties of triboelectric layers of fabricated TENG devices (275).

3.2 Experimental section

Pure PDMS films were fabricated by room temperature curing method. This synthesis process is a very simple and facile method. Fabrication process does not need high temperature, and there are no complicated reactions involved. It is very cost-effective technique because costly equipments are not employed for synthesis process. Curing agent used was tetraethyl orthosilicate (TOH) while the accelerator used was dibutyl tin dilaurate (DBTDL). PDMS, TOH and DBDTL were taken in a ratio of 100:10:1 and stirred in the room temperature. The mixture was transferred to a petri dish and kept in a desiccator under vacuum for 12 hours to form a self-standing film. Metals having various conductivity such as silver, copper, aluminium, zinc and tin nano particles (30-50 nm, Platonic Nanotech, India) were added in different weight percent to the PDMS solution for the preparation of metal/PDMS composite films. The mixture of PDMS solution and metal nanoparticles were probe sonicated for 2.5 hours. After thorough mixing, the curing agent and catalyst were added to the stock solution in the above-mentioned ratio. This mixture was transferred to a mold and kept undisturbed for 12 hours. Finally, the metal nanoparticles/polymer composite films of ~1 mm thickness were peeled off for further characterization studies. The weight percent of metal nanoparticles introduced into PDMS were 0.5, 1.0, 5, 10, 15 and 20 wt%. Figure 3.1 explains the various steps involved in the preparation of metal nanoparticle/PDMS composite

This study employs dielectric to metal model to form the TENG structure. PDMS mixed with different weight percent of metal nanoparticles act as negative tribo material and was attached to a copper electrode. Another copper plate (2 cm × 2 cm) acts as both positive

tribo material as well as top electrode so as to form the dielectric-metal model TENG. Output for electrical measurement was taken from the copper electrodes. Studies report (276) that the output performance of TENG show a gradual increase as the applied force increases. Since better properties were obtained for force of magnitude 10 N at a frequency of 10Hz, electrical properties were done at a force of 10N. N.

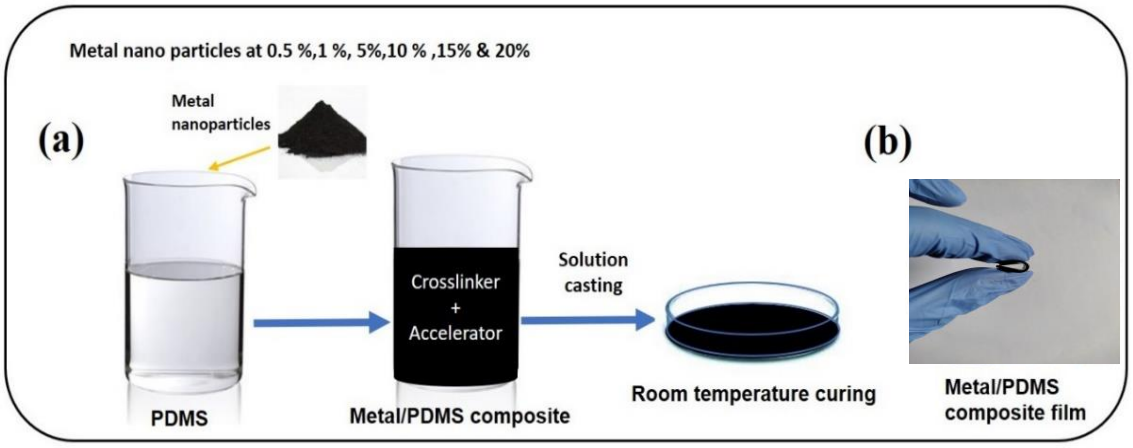

Figure 3. 1. Steps involved in the preparation of metal nanoparticle/PDMS composite.

3.3 Results and discussions

3.3.1 Structural analysis

XRD patterns of metal/PDMS composites prepared by varying weight percent of metals (silver, copper, aluminium, zinc and tin) nanoparticles from 0 wt% to 20 wt% are shown in figure 3.2. All peaks were indexed with corresponding ICDD files as mentioned in table 1. Absence of extra peaks points to the phase purity of the composite films. When the weight percent of the filler content increases, the intensity of the diffraction peaks corresponding to the filler increases.

Table 3. 1. XRD peaks of different metal/PDMS composites and ICDD file number

Filler	**ICDD File Number**	**Standard Peak position (degrees)**	**Observed peak positions (degrees)**
Silver	004-0783	38.12	38.10
		44.30	44.39
		64.44	64.53
		77.40	77.43
Copper	004-0836	43.29	43.37
		50.42	50.57
		74.08	74.33
Aluminium	004-0787	38.71	38.56
		44.85	44.82
		65.29	65.25
		78.38	78.43
Zinc	42-1014	36.89	36.50
		39.01	39.16
		43.24	43.27
		54.33	54.35
		70.10	70.16
		70.66	70.77
Tin	004-0673	30.63	30.62
		32.01	31.99
		43.87	43.98
		44.89	44.99
		55.32	55.47
		62.50	62.71
		63.77	63.83

Diffraction peak at 11.84^{o} corresponds to tetragonal phase of PDMS and with the increase in the filler content, intensity of this peak decreases (277). The monotonous increase of the diffraction peaks of metal with increasing weight percent of metal nanoparticles suggests a continuous increase in the content of metal nano particles in the polymer matrix.

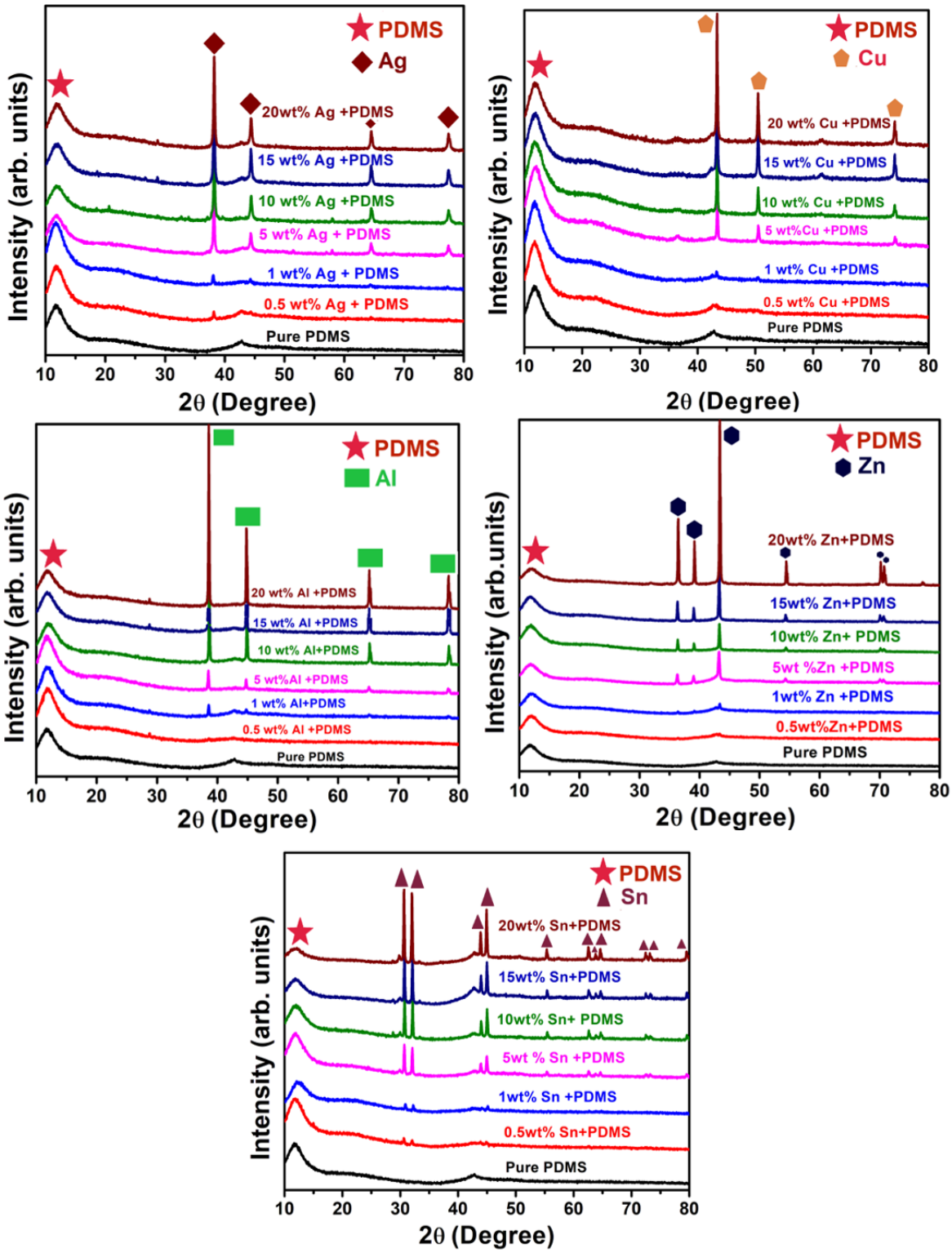

Figure 3. 2. X-ray Diffraction patterns of metal (Ag, Cu, Al, Zn Sn) /PDMS composites.

3.3.2 Raman spectra analysis

Figure 3.3 depicts the Raman spectra of metal/PDMS polymer composites. Raman spectroscopy was done to verify the incorporation of metal nanoparticles in the PDMS matrix. Presence of metal nano-particles produces SERS (surface enhanced Raman scattering) effect and the prominent contribution to the SERS effect is the electromagnetic enhancement phenomenon. Enhancement of electromagnetic field intensities occurs around sub wavelength-size metal particles as a result of coupling between incident photons and collective oscillation of free electrons at the metal surface (278).

Raman scattering occurring from molecules interacting with the metal nano particles experience an enhancement of peaks due to the strong electromagnetic fields which are generated by the excitation of localized surface plasmons (LSP) at resonant condition (279). Raman spectrum of PDMS elastomer shows the peaks which corresponds to different chemical bonds namely : 488 cm^{-1} (Si O Si symmetric stretching); 709 cm^{-1} (Si C symmetric stretching); 787 cm^{-1} (CH_3 asymmetric rocking and Si C asymmetric stretching); 859 cm^{-1} (CH_3 symmetric rocking); 1262 cm^{-1} (CH_3 symmetric bending); 1411 cm^{-1} (CH_3 asymmetric bending); 2909 cm^{-1} (CH_3 symmetric stretching); and 2970 cm^{-1} (CH_3 asymmetric stretching) (280) .

Raman spectra of silver/PDMS composite shows the presence of extra peaks namely one at 1128cm^{-1} which is associated to the C-H mode in plane bending and another at 1599 cm^{-1} which is due to the C-C stretching mode (281). In the case of zinc/PDMS composite, a peak at 550cm^{-1} is observed which is associated to E_1(LO) vibration mode of ZnO (282).

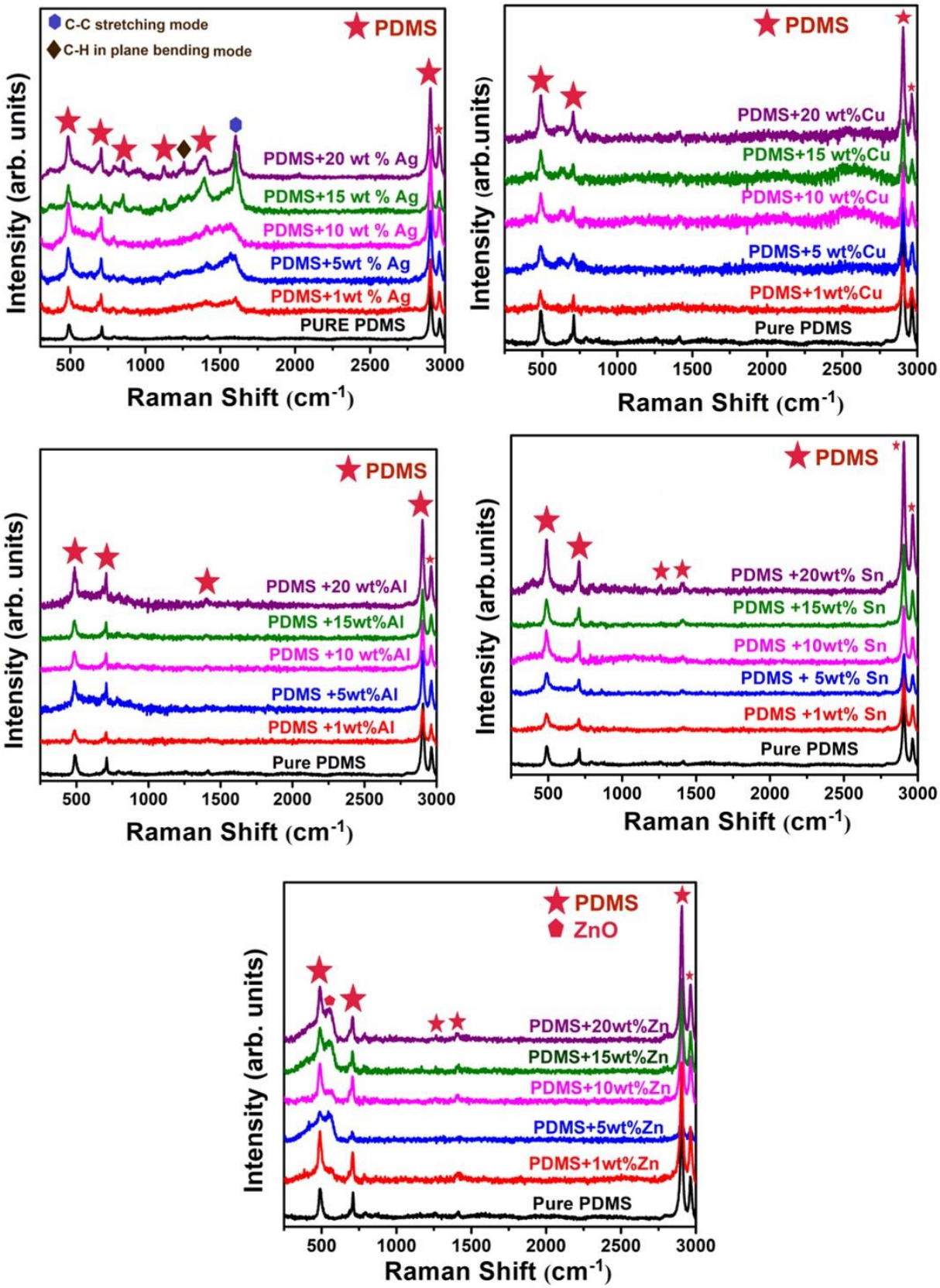

Figure 3. 3. Raman spectrum of metal (Ag, Cu, Al, Zn Sn) /PDMS polymer composites.

3.3.3 Microstructure

Figure 3.4 shows the SEM images of 20 wt% of silver/PDMS composite film and 20 wt% of aluminum/PDMS composite film respectively. Small clusters of metal nanoparticles are visible, which indicates that further dispersion of higher weight percent of fillers is difficult. It will result in the non-uniform mixing and ultimately causes agglomeration of metal nano particles. Agglomeration is a serious concern as far as polymer composites are concerned. It may cause deterioration of many properties of the samples. Some of the important issues are porosity entrapment leading to low density of the samples, deterioration of mechanical properties of the samples, moisture absorption etc. Composites with low filler loading do not have these issues since low filler loading always results in uniform distribution of filler particles. Hence in this study the filler loading was limited to 20 wt% for all metal nano particles/PDMS composites.

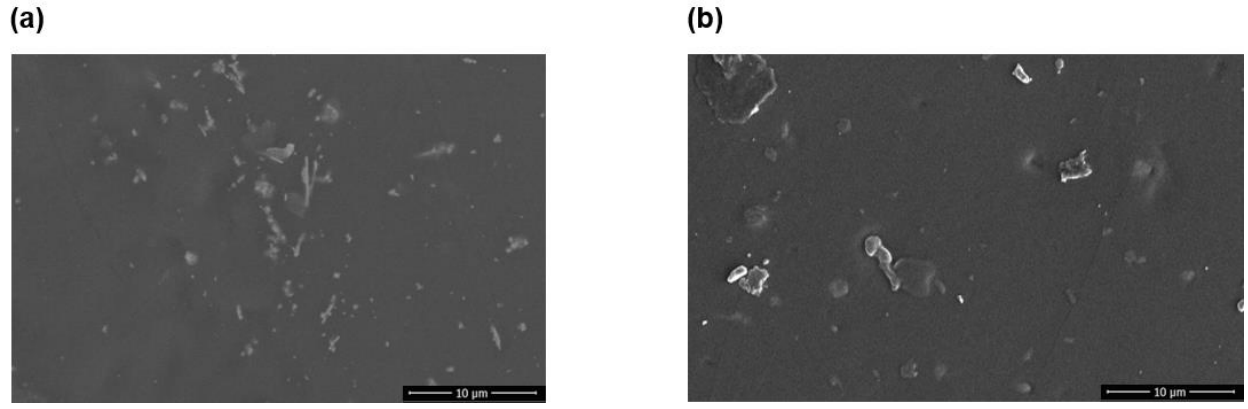

Figure 3. 4. The SEM images of **(a)** 20 wt% of silver/PDMS composite film **(b)** 20 wt% of aluminium/PDMS composite film.

3.3.4 Dielectric constant and conductivity

Metal/polymer composites are called two-phase systems which consists of polymer matrix as insulator phase and metals as the conductor. In the presence of electric field, charges are induced on the filler surfaces and dielectric properties of the composites are influenced by

interactions of local electric field present around each metal nanoparticle. It is reported that PDMS has low dielectric constant and with the introduction of metal nanoparticles, dielectric constant of the composite enhances because of Maxwell Wagner mechanism (283).

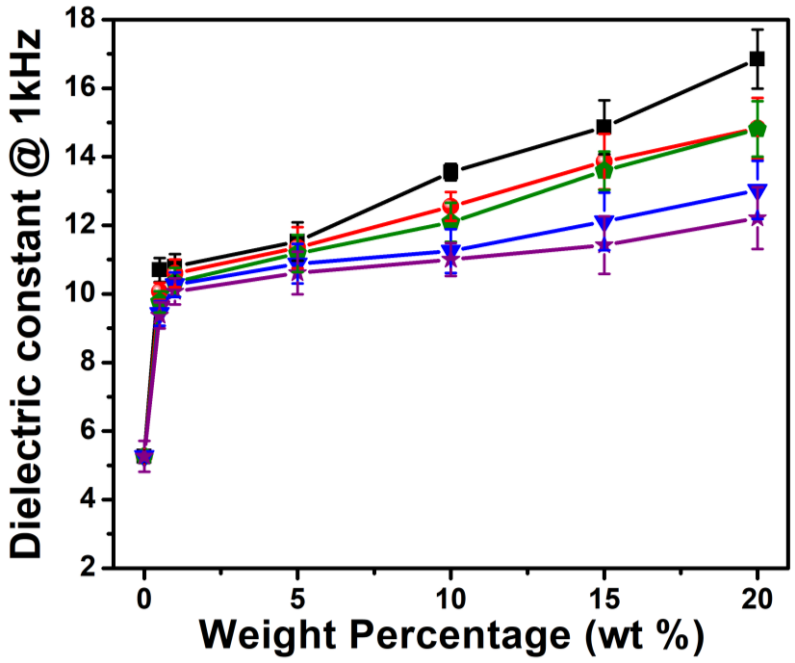

Figure 3. 5. Dielectric constant of metal/PDMS composite films with various weight percent, measured at 1 kHz.

The improved dielectric constant shown by the conductor-dielectric composites attributes to the inclusions of the metal nanoparticles. Studies show that if the fillers are having dimensions scaled downward to tens of nanometers in diameter, there is an increase in interface-to-volume ratios (284). Also, this enhances space charge accumulation and short-range dipole-dipole interactions. Thus, it is predicted that with the introduction of conducting nanoparticles, it is possible to enhance the dielectric constant of PDMS composite. Higher weight percent of fillers increases the polarization of the triboelectric layer which is due to the increase in the electrical charge trapping capacity of the tribolayer (156).

With the improved dielectric constant, polymer composites are employed in microelectronic devices (285) such as capacitors, dielectric filters, dielectric resonators and transducers applications (286). Metal nanoparticles dispersed into polymer matrix forms a random heterogeneous system (287). Two main factors upon which the electrical properties of the composite depends are permittivity and conductivity of the constituent phase (288). The introduction of metal nano particles into PDMS matrix were executed with an aim to increase the dielectric constant of the tribo layer. It can be seen that the relative permittivity of the polymer composites increases from 5.3 to 16.85 with the increase in the weight percent of metal nanoparticles from 0% to 20%. Maximum relative permittivity value was obtained for 20 wt% silver/PDMS composite because silver possess highest conductivity. Since V_{oc} is proportional to ε_r, there was corresponding increase in the V_{oc} value with increase in the filler contents. It is reported that with the increase in the dielectric constant, the capacitance of the metal/PDMS based TENG also increases and this would enhance the surface charge density on the PDMS polymer due to the repeated friction (289). Figure 3.5 depicts the variation of dielectric constant of different metal/PDMS composite films, which provides ample evidence to the fact that as the electrical conductivity of the metal nanoparticles increases, dielectric constant also increases.

Figure 3.6 shows the variation of electrical conductivity of the metal/PDMS composites at 1 kHz. Electrical conductivity of all metal/PDMS composites increases with filler concentration. The addition of metallic nanoparticles increases the dielectric constant and causes interfacial charging between filler and polymer matrix. This in turn magnifies the electric field arising from surface charge and results in stronger electrostatic induction. The electrical conductivity of silver/PDMS composites were found to be higher than other metal/PDMS composites.

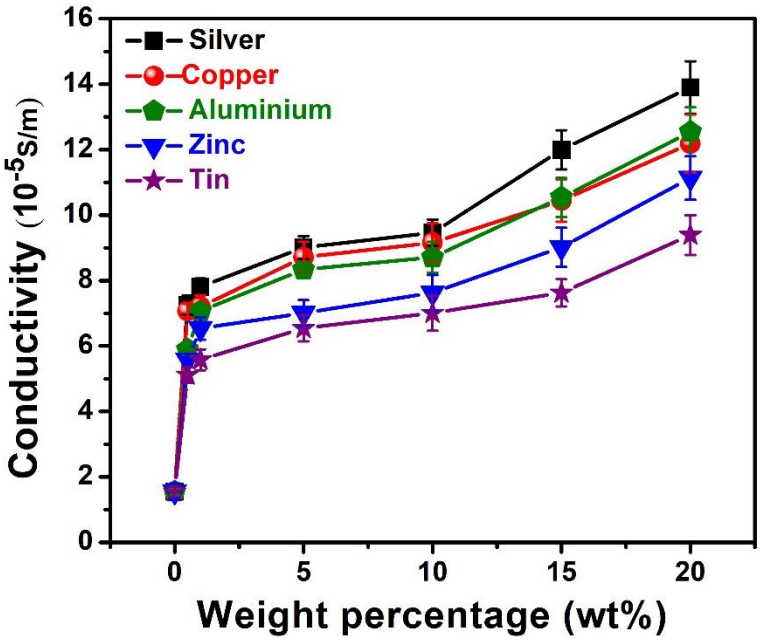

Figure 3. 6. Electrical conductivity of metal/PDMS composite films at 1 kHz with various weight percent.

Even though, the conductivity of aluminium is low when compared to copper, the dielectric constant of aluminium/PDMS composites was found to be in the range of that of copper, for the same amount of filler weight percent. This is due to the fact that, the density of aluminium [37] is low, compared to copper and silver. This means that for same amount of filler weight percent in the composite, aluminium metal particles occupy a larger share of the volume relative to the volume occupied by copper and silver in the respective composites. Thus, though the conductivity of aluminium is low compared to copper and silver, the composites involving aluminium shows dielectric constant values which are comparable to those of silver and copper. A comparison of figure 3.5 and figure 3.6 suggests that the increases of dielectric constant with filler content is a direct consequence of the increase in the electrical conductivity of the composites.

Table 3. 2. Conductivity of various metal nanoparticles used in this study.

Filler	**Conductivity (S/m)**
Silver	6.3×10^7 (242)
Copper	5.98×10^7 (244)
Aluminium	3.5×10^7 (244)
Zinc	1.68×10^7 (246)
Tin	8.7×10^6 (246)

3.3.5 Electrical characterizations

All the measurements were done at a fixed force of 10 N and frequency of 10 Hz. Electrical characterization of TENG comprises of open circuit voltage and short circuit current measurements. Figure 3.7 show the TENG design fabricated with top and bottom electrodes as copper sheet and negative tribolayer is metal/ PDMS composite.

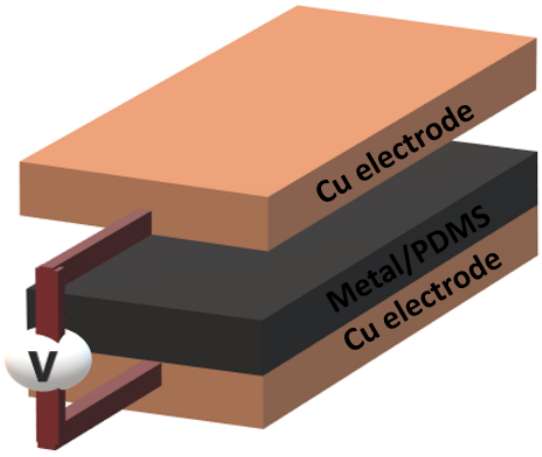

Figure 3. 7. TENG design fabricated for the current study. Top and bottom denotes the copper electrode and middle layer represents the metal/ PDMS composite.

3.3.5.1 Open circuit voltage

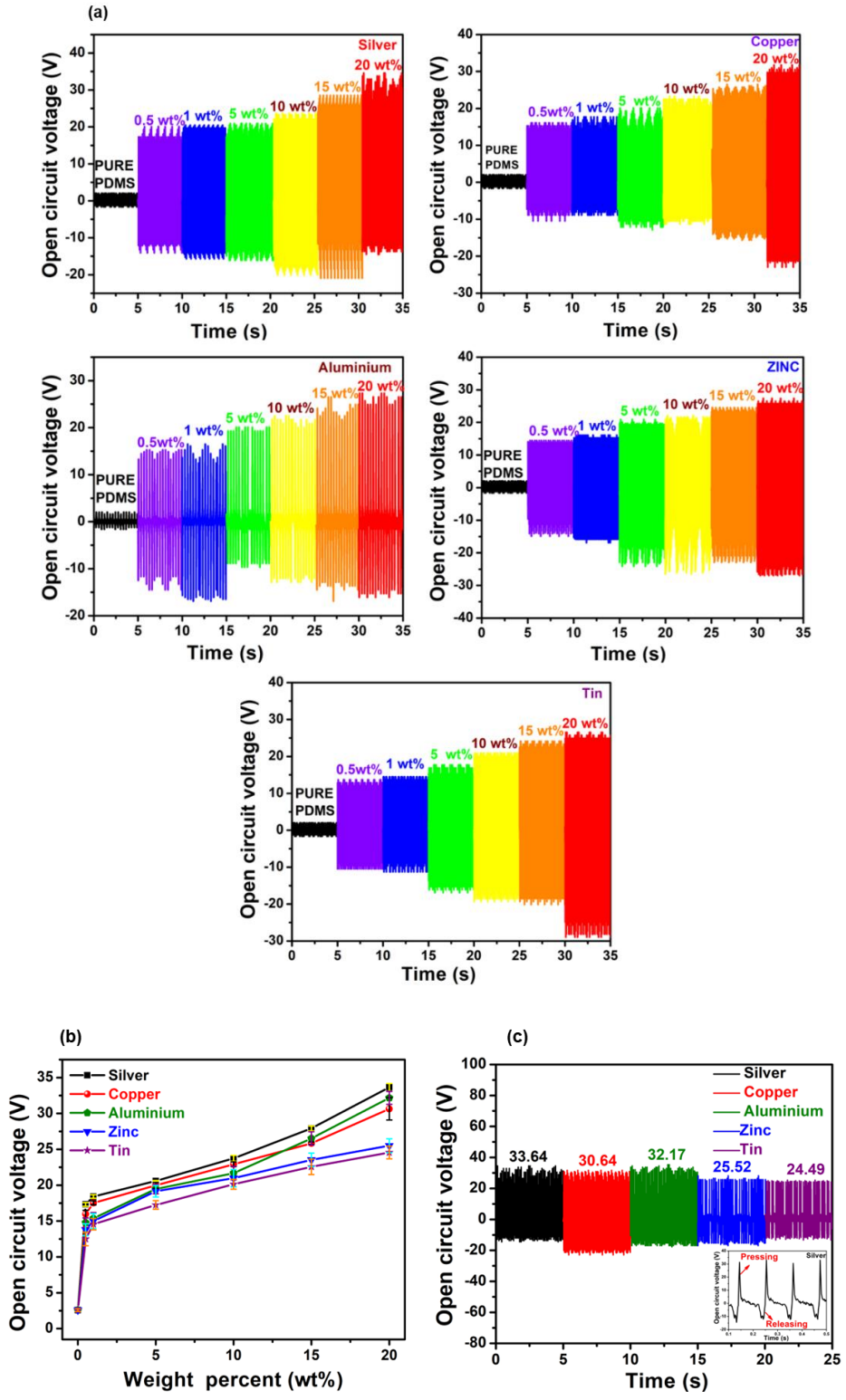

Figure 3. 8. Open circuit voltage with different metal nanoparticles in PDMS matrix (a) shows the open circuit voltage versus time interval (5 s) plotted for different weight percent of individual metal nanoparticles (b**)** variation of V_{oc} plotted against weight percent of metal nanoparticles (c) graph depicts V_{oc} values versus time interval (5 s) for 20 wt% of different metal/PDMS composites.

Figure 3.8 depicts the graph where open circuit voltage of metal/PDMS composite is plotted for different metal fillers. The weight percent of metal nanoparticles varied from 0 wt% to 20 wt%. All graphs show similar trend of increase in the V_{oc} as the filler contents increases in the PDMS polymer matrix. Highest obtained V_{oc} was 33.64 V which was for 20 wt% silver/PDMS composite while for pure PDMS, V_{oc} was 2.59 V. This proves that the introduction of conducting fillers enhanced the open circuit voltage to around 13 times compared to pure PDMS. Result supports the fact that enhancement of relative permittivity improves the output performance of metal/PDMS based TENG.

Output voltage of TENG is given by the expression (181)

$$V_{output} = \frac{(\sigma - \Delta\sigma).d_{gap}}{\varepsilon_0} - \frac{\Delta\sigma.d_{\text{metal/PDMS}}}{\varepsilon_0\varepsilon_r} \quad (3.1)$$

where σ is the triboelectric charge density on metal/PDMS, $\Delta\sigma$ is the charge density transferred between the copper electrode, ε_0 is the vacuum permittivity and ε_r is the relative permittivity of the metal/PDMS composite. d_{gap} denotes the inter layer spacing, and $d_{\text{metal/PDMS}}$ is the thickness of metal/PDMS film. In the open circuit condition, there is no charge transfer ($\Delta\sigma$=0) and hence the open circuit voltage (V_{oc}) is then given by

$$V_{OC} = \frac{\sigma.d_{gap}}{\varepsilon_0} \quad (3.2)$$

Surface charge density (σ) is a function of dielectric constant of the triboelectric material (290). Maximum charge density (σ) can be related to the dielectric constant of the triboelectric material through the expression (267)

$$\sigma = \frac{\sigma_0 d_{gap}}{d_{gap} + \frac{d_{\text{metal/PDMS}}}{\varepsilon_{\text{metal/PDMS}}}} \quad (3.3)$$

where σ_0, d_{gap} , $d_{\text{metal/PDMS}}$, and $\varepsilon_{\text{metal/LSCO}}$ are the triboelectric charge density at equilibrium state, the interlayer spacing, the thickness of metal/PDMS film and dielectric constant of metal/PDMS film respectively. Dependency of V_{oc} on dielectric constant and

thickness of the tribolayer is established through the equation (3.3) which implies that as the dielectric constant increases, σ also increases. But, V_{oc} shows a decreasing trend with the thickness of the tribolayer. Hence the effect of thickness is eliminated by preparing all samples with a constant thickness of around 1 mm.

During contact electrification process, the two tribo layers come into contact and transfer of material or electron happens in both directions (80). Previous reports point out that in order to obtain a high net surface charge density on the polymer, the cohesive energy in the bulk must be lower than that of surface adhesion. This increases the energy of the adhesive bonds which prevails among the contacting surfaces and decreases the energy of the chemical and physical bonds present in bulk. As a result, cleavage of covalent bond followed by the transfer of materials occurs (80).

It has been reported that van der Waals force bonds the molecules at the surfaces of PDMS (210) and during contact electrification, mechanical modification of the surface of PDMS occurs through splitting of bonds from the polymeric chains (−Si $(CH_3)_2$O−) of PDMS. This splitting creates anions (−$(CH_3)_2$SiO−) on the surface of PDMS which proves that both charge and material get transferred simultaneously during contact electrification (211, 212). Figure 3.9 gives the enlarged output signals of open circuit voltage measurements of different metal/PDMS composites where metal nanoparticles are fixed to 20 wt%.

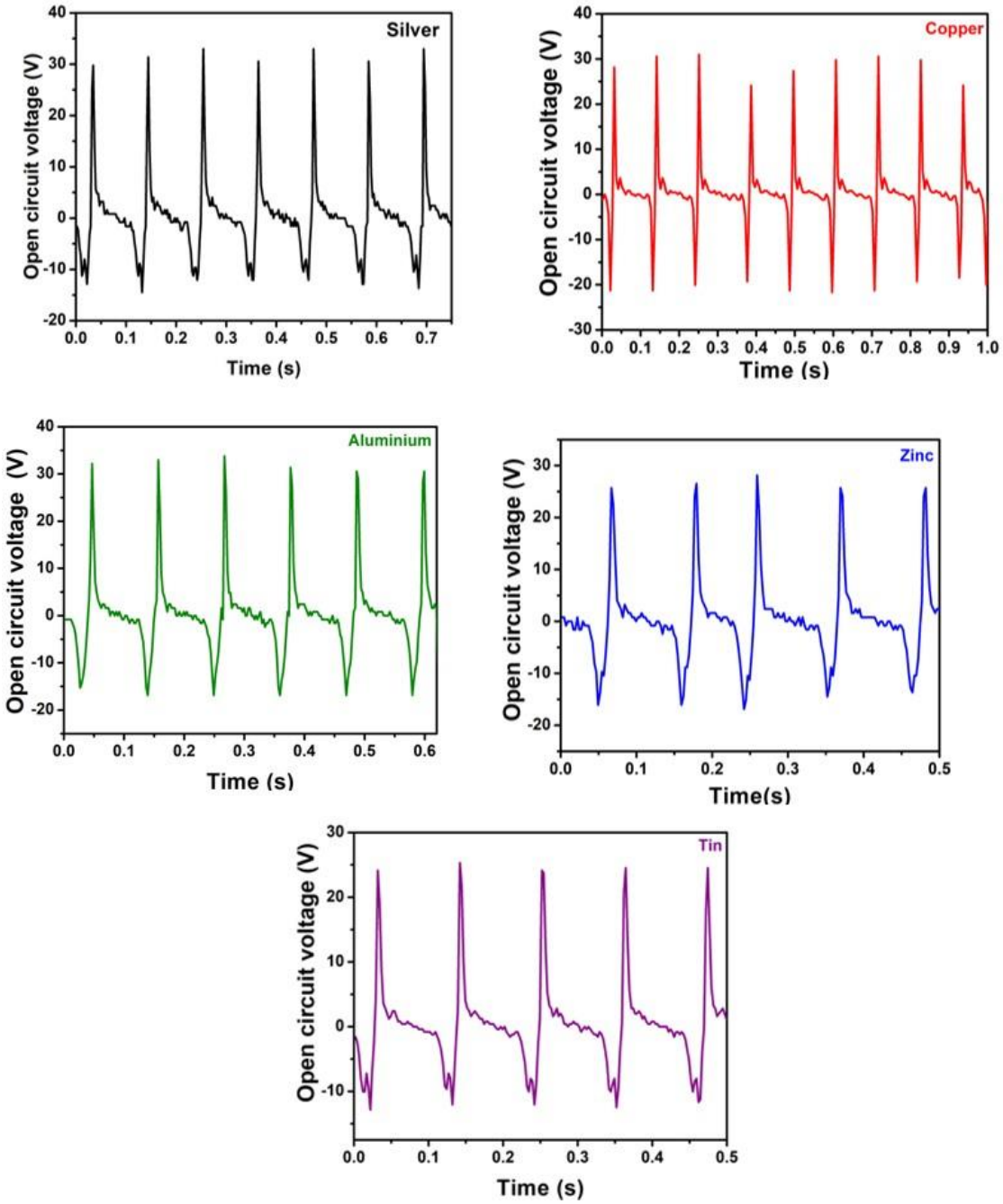

Figure 3. 9. Enlarged output signals of open circuit voltage measurements versus time of metal/PDMS composite with 20 wt% filler concentration.

3.3.5.2 Short circuit current (Isc)

Figure 3.10 shows the dependence of short circuit current with time of 5 wt% PDMS/Copper composite based TENG as the external force changes from 5 Hz to 10 Hz. As expected, the output current increases as the applied force increases and maximum is obtained for a force of 10 N.

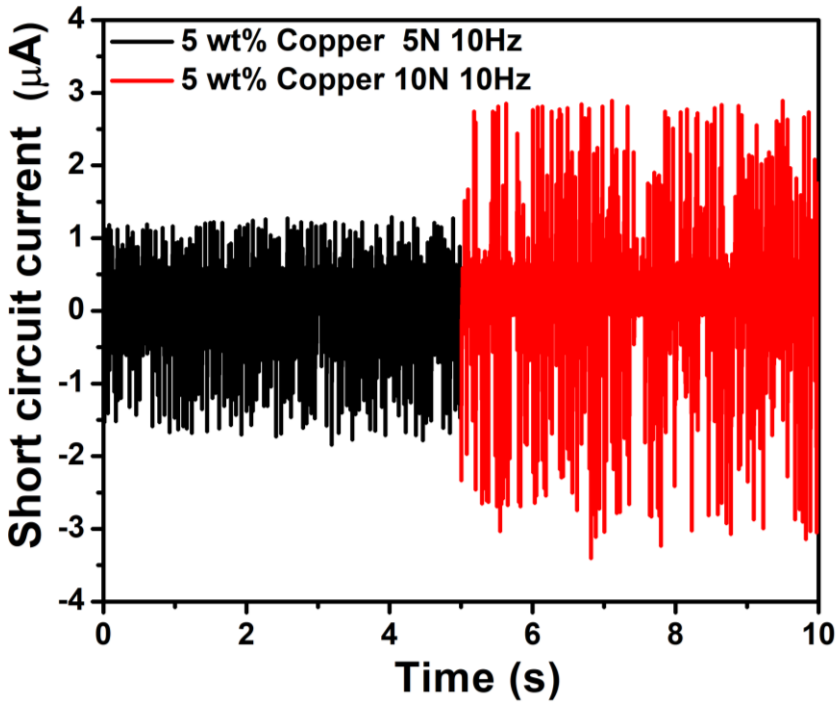

Figure 3. 10. Dependence of short circuit current versus time interval (2 s) of 5 wt% PDMS/Copper composite based TENG with applied force.

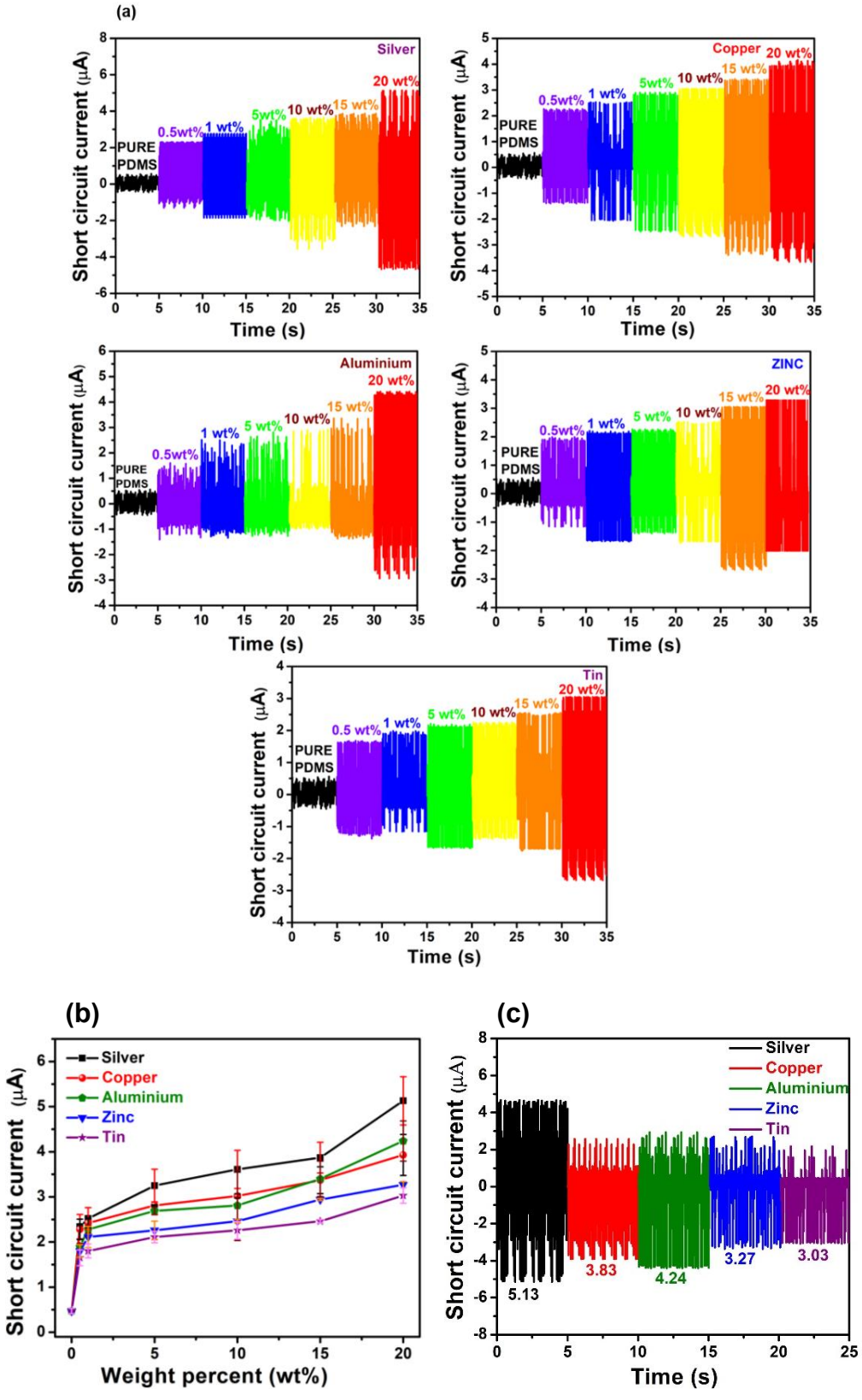

Figure 3. 11. **(a)** the short circuit current versus time interval (5 s) plotted for different weight percent of individual metal nanoparticles **(b)** variation of I_{sc} plotted against weight percent of metal nanoparticles **(c)** I_{sc} of 20 wt% metal/PDMS composite TENG versus time interval (5 s).

Figure 3.11 depicts the variation of short circuit current for different weight percentage of metal/PDMS composite films. When silver nanoparticles were mixed with PDMS, short circuit current of 5.1 μA was achieved at a working frequency of 10 Hz at 10 N force. As the filler weight percent increases, all properties showed an increasing tendency and excellent results were exhibited by 20 wt% Ag/PDMS composite. As the short circuit current also explicitly depends on the surface charge density, with increase in the dielectric constant, Isc also increased in the same trend as in the case of Voc. Figure 3.12 gives the enlarged output signals of short circuit current measurements of different metal/PDMS composites with 20 wt% metal nanoparticles.

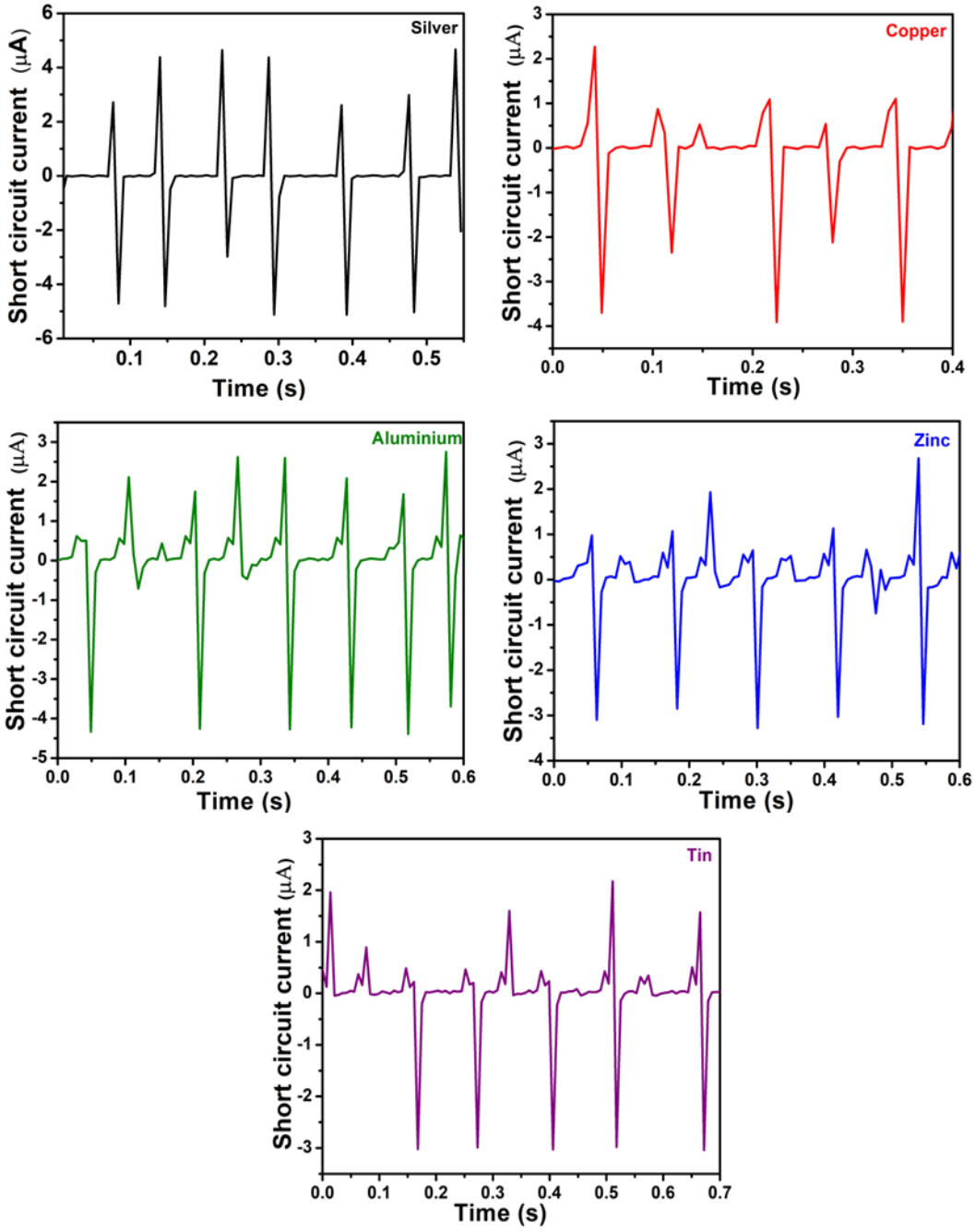

Figure 3. 12. shows the enlarged output signals of short circuit current measurements of metal/PDMS composite with 20 wt% filler concentration.

3.3.5.3 Resistive load characteristics of triboelectric nanogenerators

The simplest load for TENG is resistive load. The equivalent circuit diagram of TENG when connected with a resistive load R is shown in the figure 3.13 (a). By utilizing the Kirchhoff's law, the voltage equation can be written as

$$V_{output} = R\frac{dQ}{dt} = -\frac{1}{C}Q + V_{oc} \qquad (3.4)$$

This equation is a first order differential equation which is solved by applying the intimal boundary condition $Q_{(t=0)}$. Two boundary conditions are applied to solve the equation (3.4). First condition is x(t) = 0 which is the equilibrium position mentioned in figure 3.13(c). When x(t) = 0, both tribo- layers are in contact condition and system is said to be in electrostatic equilibrium.

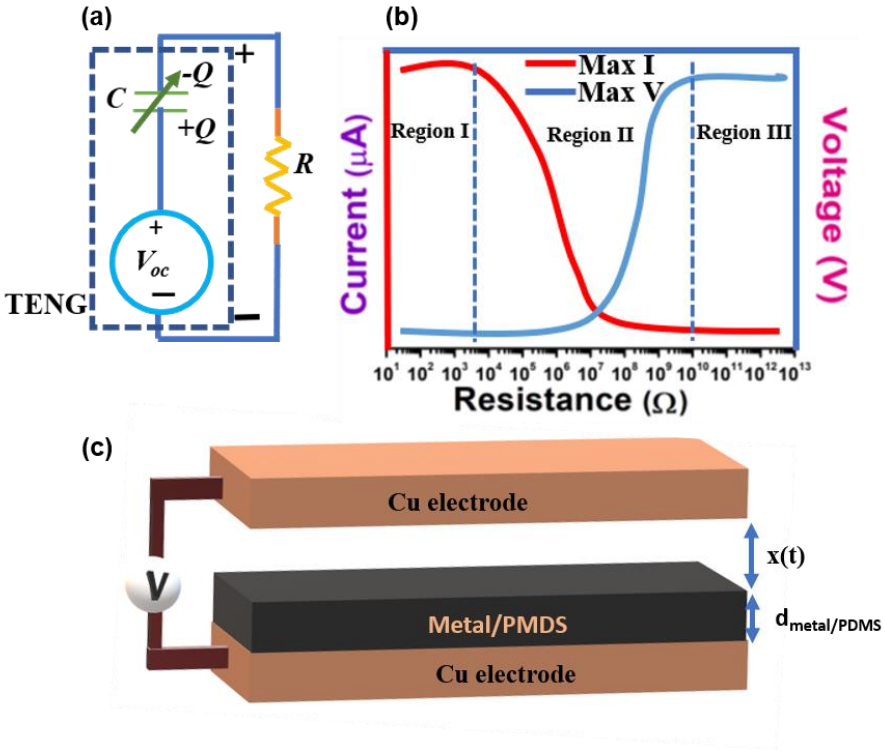

Figure 3.13.shows the TENG resistive-load output characteristics under fixed velocity separation. At time = 10ms**,** the top electrode reaches maximum separation distance. (a) depicts the equivalent circuit model of TENG (b) shows the effect of load resistance on the values of output current and voltage (c) Structure of metal/PDMS composite based TENG when top electrode is at maximum distance of x(t).

During contact state, $Q_{(t=0)} = 0$. Other state is when the tribo-layers are in motion with a constant frequency. In this condition, output comprises of repeated pulses and after few cyclic processes, a steady state is achieved. Hence to solve this steady state solution, boundary conditions utilized must be periodic in nature ie; $Q_{(t=0)} = Q_{(t=T)}$. Where T is the time period of the cyclic motion. Applying the boundary condition to equation (3.4), the solution is given as (291)

$$Q(t) = \frac{1}{R}\, e^{\left[-\frac{1}{R}\int_0^t \frac{dt}{C(x(t))}\right]} \int_0^t V_{OC}(x(t)) e^{\left[\frac{1}{R}\int_0^t \frac{dt}{C(x(t))}\right]}\, dt \tag{3.5}$$

$$I(t) = \frac{V_{OC}}{R} - \frac{1}{R^2 C} e^{\left[-\frac{1}{R}\int_0^t \frac{dt}{C(x(t))}\right]} \int_0^t V_{OC}(x(t)) e^{\left[\frac{1}{R}\int_0^t \frac{dt}{C(x(t))}\right]}\, dt \tag{3.6}$$

$$V_{output}(t) = V_{OC} - \frac{1}{R^2 C} e^{\left[-\frac{1}{R}\int_0^t \frac{dt}{C(x(t))}\right]} \int_0^t V_{OC}(x(t)) e^{\left[\frac{1}{R}\int_0^t \frac{dt}{C(x(t))}\right]}\, dt \tag{3.7}$$

The charge transfer occurs at faster rate when system is in the short circuit condition. As the top electrode stops its movement at t =10 ms and when *R* takes comparatively small value, *Q* value remains in the saturation value. At t =10 ms, when *R* is greater than 100 MΩ, there is a transfer of charge through the resistor between the two electrodes and hence charge does not remain in the saturation condition. Thus, initially the current was high and resistance in the load was small. As the tribo-layers start to move and also when load resistance is increased to higher value, current through the external circuit begins to decrease. Voltage also shows similar variation as that of current but in the opposite trend shown in figure 3.13(b). Initially, voltage showed a very low value when *R* is low, but with the increase in the load resistance value, voltage also increased and reached saturation.

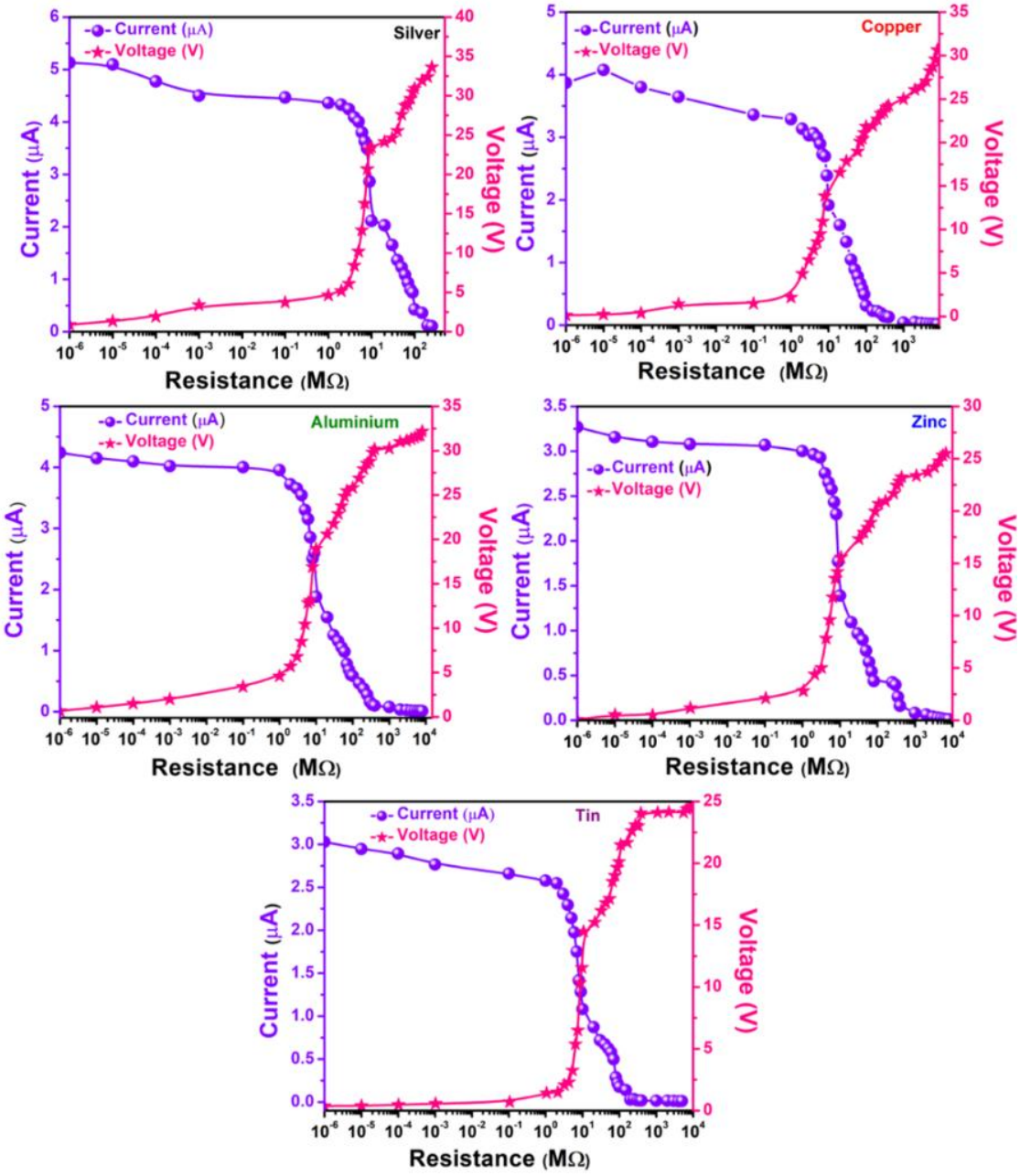

Figure 3. 14. Variation of current and voltage of metal/PDMS composite TENG with load resistances.

From the figure 3.14, working of TENG can be classified into three working regions. First region is where the resistance ranges from 0.1-1000 Ω, the current is in the saturated condition. The variation of current in this resistance range is appreciably low and system is in the short circuit condition. The voltage is found proportional to external resistance and since initially resistance is having low value, voltage also is low in the first region. In the third region, the resistance takes values larger than 1 GΩ, output of TENG is in the open circuit condition

when output voltage reaches it saturation value V_{oc}. In this region as already the value of resistance is high, the output current decreases to very low value. In the second region of the graph, resistance is in the medium range, current reduces from its maximum value while voltage shows an increasing trend. It is found that there is an optimum resistance in the medium range where the maximum instantaneous output power is extractable from the TENG. The output performance of the device across different load resistances were studied and variation of output current as well as voltage for different load resistances were examined. Figure 3.14 shows current and voltage outputs when TENG output is connected to different load resistances.

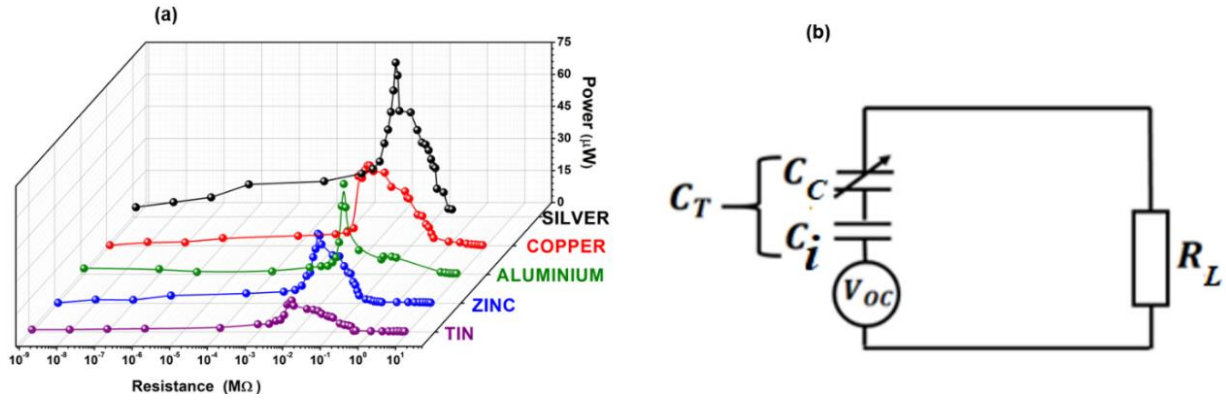

Figure 3. 15. **(a)** Variation of power of different metal/PDMS composite at 20 wt% with load resistance **(b)** Equivalent circuit model of TENG to study load resistance characteristics.

From the equivalent circuit diagram shown in figure 3.15 (b), voltage division rule is applied to find the voltage drop across the load resistances R_L. The output voltage is given by

$$V_{output} = \frac{V_{OC}R_L}{X_T+R_L}, \tag{3.8}$$

where X_T is the capacitive reactance.

$$C_c = \frac{S\varepsilon_0}{d_{gap}}, \tag{3.9}$$

where, S is the area of contact between the metal/PDMS composite and electrode, and

$$X_T = \frac{1}{j\,\omega\,C_T}, \tag{3.10}$$

The output power is obtained using the formula

$$P = \frac{V_{output}^2}{R_L}, \tag{3.11}$$

where V_{output} is the output voltage in the external load per cycle and R_L is resistance across external load. When R_L is low, compared to the capacitive impedance of TENG, majority of V_{OC} drops across C_T and minimum V_{output} is obtained. This condition is regarded as short circuit condition. If the load resistance R_L is much higher than capacitive impedance of TENG, V_{OC} will drop mostly across the load resistance R_L obtaining maximum V_{output}. This condition of TENG can be designated as open circuit condition. From the aforementioned equations, maximum power transfer takes place when $R_L = X_T$.

Variation of output power with load resistance of all metal nanoparticles are examined and is tabulated in table 3.3. Maximum output power obtained was 72.2 μW for Ag/PDMS composite at a load of 8 MΩ, which is evident from figure 3.11 (a). It can be inferred that intrinsic capacitive impedance of fabricated TENG is at 8 MΩ. It is always advantageous to obtain the peak power of the developed TENG at lower external load resistances for practical applications.

Table 3. 3. Variation of output power with load resistance 8 MΩ of all metal nanoparticles.

Filler	**Power (μW)**
Silver	72.2
Copper	37.6
Aluminium	42.3
Zinc	32.5
Tin	14.7

3.3.6 Capacitive load characteristics and charging behaviors

TENG operating in contact separation mode can be well explained using capacitive model where the dielectric property of the triboelectric material influences the energy storage capacity of the TENG device. With the increase in the dielectric permittivity, the displacement current in the tribo material increases and hence the surface charge density. These factors help to enhance the output of TENGs (292). Capacitance of TENGs were measured by coupling voltage source in series with capacitors. The output of TENG is connected to capacitance and hence this load condition is called capacitive load condition. By examining the charging characteristics of metal/PDMS composite TENG, maximum energy stored in TENG for an optimum load capacitance was found out. Figure 3.16 depicts the charging behavior capacitors for 60s cycle at a force of 10N.

For utilizing the energy produced from the TENG, output was connected to a bridge rectifier to convert alternating current into direct current. Repeated movement was created by connecting the device to a triboelectric measuring system that could generate the contact-separation movement with 10 N force at 10 Hz frequency The energy harnessed from the TENG was used to charge capacitors, as a continuous regulated supply of electrical energy is needed to power electronic equipments. Capacitors act as a storage for the energy extracted from the TENG devices [51]. Hence capacitors with different capacitances were charged utilizing the output of TENG.

Capacitance of TENG is considered as equivalent to C_i and variable capacitance be C_c in the vertical-contact separation mode and TENG connected to load capacitance is considered as a combination of voltage source in series with capacitor. Figure 3.17 (b) shows two capacitors C_i and C_c which are connected in series. The dimension of copper electrodes is considered to be larger as in a parallel plate capacitor.

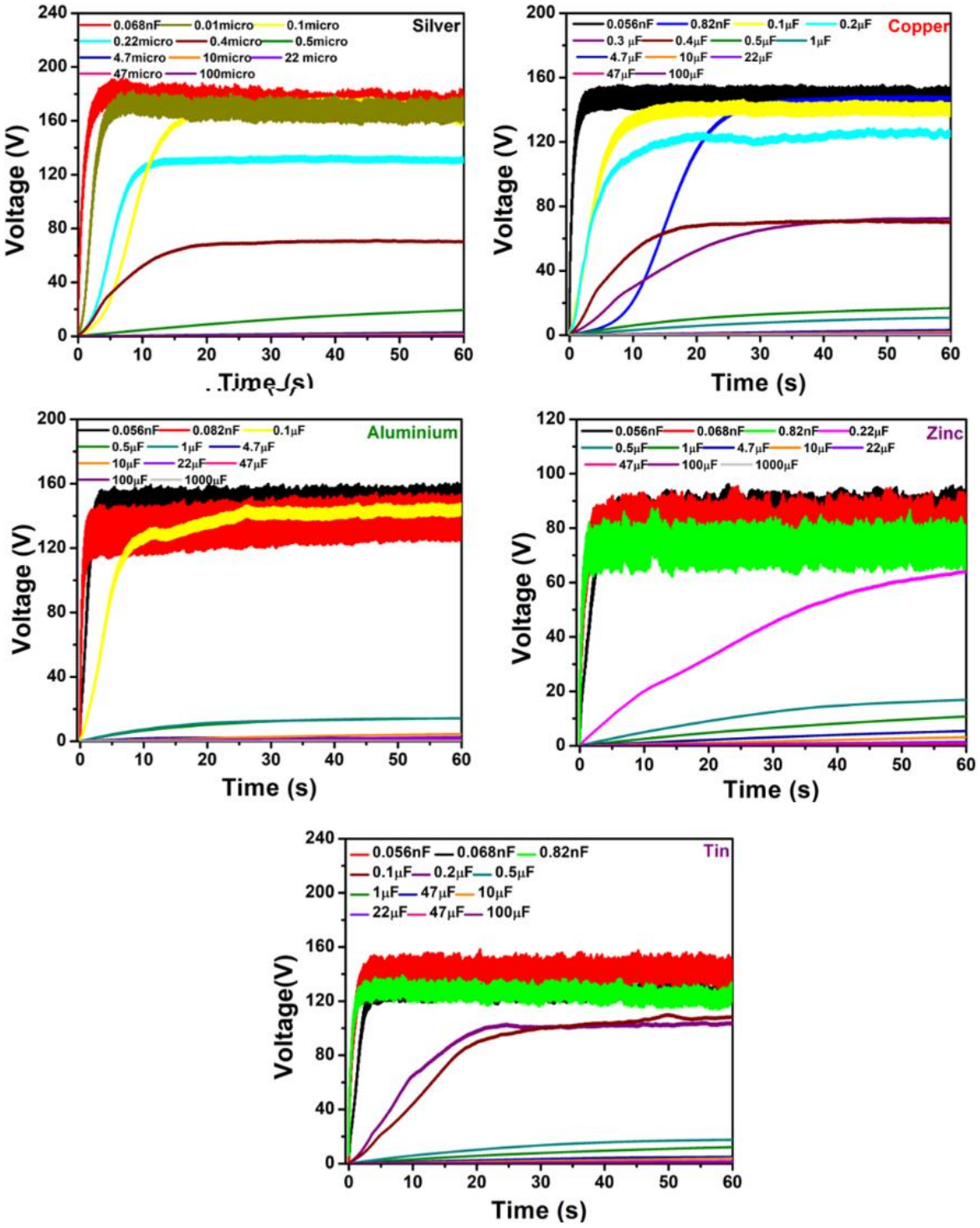

Figure 3. 16.Capacitor voltage versus time for different capacitance values for 60 s working cycle at a frequency of 10 Hz and force of 10N, (charging cycle).

The thickness of metal/PDMS film is $d_{\text{metal/PDMS}}$ and inter layer distance is $x(t)$, then inbuilt capacitance and variable capacitance are given by the formulae,

$$\mathrm{C_i} = \frac{\mathrm{S}\,\varepsilon_0\varepsilon_\mathrm{r}}{d_{\text{metal/PDMS}}} \tag{3.12}$$

$$\text{and } \mathrm{C_c} = \frac{\mathrm{S}\,\varepsilon_0}{x(t)} \tag{3.13}$$

where, S is the area of contact between the metal/PDMS composite and electrode. Equivalent capacitance C_T is given by

$$\mathrm{C_T} = \frac{\mathrm{S}\,\varepsilon_0}{\frac{d_{\text{metal/PDMS}}}{\varepsilon_\mathrm{r}} + x(t)} \tag{3.14}$$

In order to find the voltage and charge across load capacitor, Kirchhoff's law is applied in circuit shown in figure 3.17 (b),

$$\mathrm{V_{output}} = \frac{-\mathrm{Q_T}}{\mathrm{C_T}} + \mathrm{V_{oc}} = \frac{\mathrm{Q_L}}{\mathrm{C_L}} \tag{3.15}$$

$$\mathrm{Q_T(t)} - \mathrm{Q_L(t)} = 0 \tag{3.16}$$

From these equations, voltage output can be derived as,

$$\mathrm{V_{output}} = \frac{\mathrm{V_{oc}C_T}}{\mathrm{C_T + C_L}} \tag{3.17}$$

The energy stored is given by

$$\mathrm{E_{stored}} = \frac{1}{2}\mathrm{C_L V_{output}^2} \tag{3.18}$$

The condition of maximum energy stored is given by

$$\frac{\mathrm{dE_{stored}}}{\mathrm{dC_L}} = 0 \tag{3.19}$$

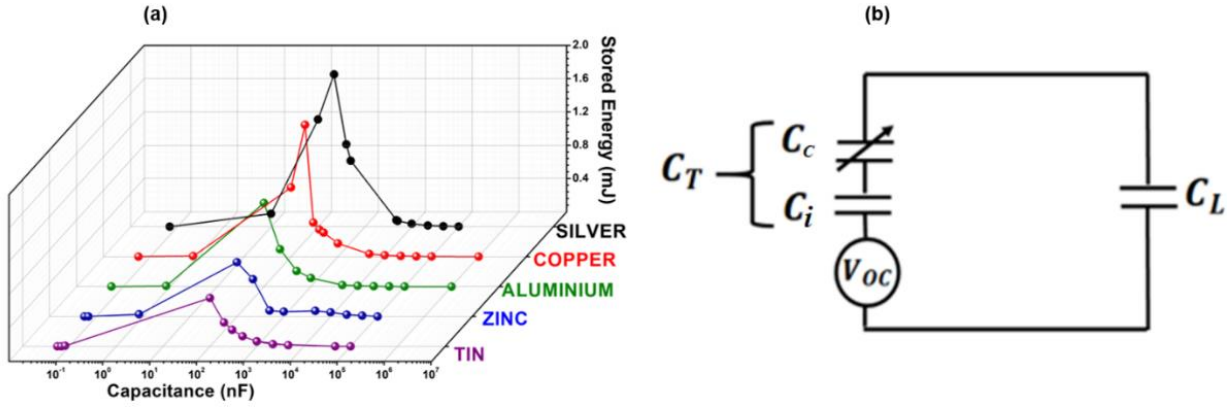

Figure 3. 17 **(a)** stored energy of different metal/PDMS composite at 20 wt% with load capacitances **(b)** Equivalent circuit model of TENG to study load capacitance characteristics.

When C_L is having very low value, its capacitive impedance is higher than the impedance of C_T. The voltage on the load capacitor is equivalent to the saturation voltage V_{oc}. This condition of TENG is quasi -open circuit condition. This phenomenon is manifested in the figure 3.16 where the voltage charging curves of small C_L are found to closer to the V_{oc} curve. The charge stored in the capacitor is close to zero due to the very low value of C_L. When the C_L is very large, its capacitive impedance is very small compared to the impedance of C_T. This working condition of TENG is called quasi-short circuit condition. At this condition, output voltage is near to zero and inversely related to load capacitance C_L. By taking the first derivative of equation (3.18) with respect to C_L and equating to zero, the threshold load capacitance is calculated. This threshold load capacitance is found to be equal to total capacitance C_T when the energy stored reaches maximum value. The impedence matching between TENG and the load capacitance is achieved when energy stored reaches a maximum value.

Periodic excitation was done by connecting the device to a triboelectric measuring system that can produce the contact – separation movement with the applied force of 10 N at 10 Hz frequency. A full wave rectifier was used to convert alternating charging current to store

in a capacitor. For all capacitors, the output graph bears a resemblance to that of normal resistor- capacitor charging curve. There is a sudden hike to saturation voltage with low capacitors values. But in the case of high valued capacitors, charging performance slows down and exhibits smaller slopes.

Figure 3.17 (a) depicts the maximum voltage and energy stored in capacitors after 60 s of operation. Maximum value for stored energy obtained was 1.8 mJ for silver/PDMS composite TENG at a capacitance of 220 nF. Capacitive studies of metal/PDMS composites vividly manifest the energy storage capacity of the fabricated TENG devices. From the current study, capacitance of the TENG device made out of silver/PDMS composite exhibits higher value, indicating better storage ability compared to others. Theoretical analysis vividly explains that when the load capacitance become equal to inherent capacitance, energy stored will be maximum. Hence the inherent capacitance of the Silver/PDMS composite based TENG can be approximated as 220 nF.

Table 3. 4. Electrical properties of metal/PDMS composite based TENG

(20 wt%)	**Silver**	**Copper**	**Aluminium**	**Zinc**	**Tin**
Current (µA)	5.1	3.9	4.2	3.3	3.03
Voltage (V)	33.6	30.6	32.2	25.5	24.6
Power (µW)	72.2	37.6	42.3	32.5	14.7
Stored Energy (mJ)	1.8	1.6	1	0.7	0.6
Capacitance (nF)	220	200	100	100	100

Capacitive studies of metal/PDMS composites manifest the energy storage capacity of the fabricate TENG devices. From the current study, capacitance of the TENG device made out of silver/PDMS composite exhibits higher value, indicating better storage ability compared to others. These results sum up that the output performance of polymer based triboelectric

nanogenerators could be enhanced by adding metal nanoparticles with maximum conductivity. The properties of metal/PDMS composite films are examined tabulated in table 3.4 and could act as power source as well as smart sensors.

3.4 Conclusions

Metal/PDMS composites based TENGs were prepared by introducing metal nanoparticles into PDMS matrix and copper sheets served as electrodes. Out of different metal/PDMS composites, silver/PDMS composite based TENG showed good properties. X-ray diffraction studies of metal/PDMS composites revealed the structural characteristics. Raman analysis was also done to identify the vibrations modes of composite. SEM images indicate agglomeration of metals in the polymer matrix at higher filler concentration (20 wt%). Variation of dielectric constant of the metal/PDMS composites on the addition of various metal nanoparticles shows a similar trend to the variation of electrical conductivity of the respective samples. With the increase in the amount of metal nanoparticles, the electrical properties got improved and 20 wt% Ag/PDMS composite manifested good properties. 20 wt% Ag/PDMS composites achieved an open circuit voltage of 33.64 V, short circuit current of 4.5 μA, an output power of 72.2 μW at 8 MΩ load and maximum energy storage of 1.8 mJ at 220 nF capacitance at a working frequency of 10 Hz and force of 10 N. This work focusses on output performance of polymer based TENGs and tailoring the properties of polymers by introducing metal nanoparticles into polymer matrix.

Chapter 4

Preparation and characterization of LSCO/PDMS composite TENGs

Abstract

The development of human-integrated technologies necessitates the use of portable energy devices which have to be self-powered, adaptable, and wearable. Triboelectric nanogenerators, also known as TENGs, are potential candidates used as energy sources. TENGs are typically fabricated from flexible polymers that are augmented with chemicals that have favorable dielectric properties. This chapter introduces an effective method in which $La_{0.8}Sr_{0.2}CoO_3$ (LSCO) ceramic particles which possess high permittivity are embedded into the PDMS polymer matrix. The technique allows to increase the charge trapping ability of the tribo-materials by a significant amount. The systematic study demonstrates that surface charge density is closely associated with the relative permittivity of the tribo-layers as well as the effect of dielectric materials on the output performance is explored. Optimizing the dielectric characteristics of the triboelectric materials allows to tune the output performance of TENGs. Pure PDMS film was compared to an optimised film that contained 20 weight percent of LSCO and was found to have superior electrical characteristics. At a working frequency of 10Hz, the maximum short circuit current and open circuit voltage obtained were 6.5 and 13 times higher than those of TENG based on pure PDMS film, respectively. This study definitely emphasizes the significance of dielectric engineering by demonstrating the incorporation of additives into polymer matrices. Thus, flexible and lightweight TENGs have greater promise as multifunctional power sources for next-generation wearable electronic equipment.

4.1 Introduction

Possibility of electronic gadgets to harness the mechanical energy from the surroundings through feasible ways have envisaged immense interesting opportunities in the field of mobile power generators. The key factors that are necessary for improving the electrical performance of TENG mainly includes suitable choice of triboelectric layers and surface morphology of the tribo layers. Numerous reports suggests that surface morphology or structural alteration of PDMS films could substantially enhance the performance of TENG devices (136), (104).

Recent studies point out that polymers incorporated with high k dielectric materials are preferred for TENG applications instead of pure ceramic materials due to its excellent physical and chemical properties such as low density, mechanical flexibility and ease of fabrication. However, polymers possess low dielectric constant in their pure form resulting poor relative capacitance and limited output performance of TENG. Studies reveals that a fine way to overcome this problem is to fabricate inorganic/polymer dielectric composites which possess combined nature of high dielectric constant, ultra-low dielectric loss, light weight, easy processing and flexible nature (293). In previous attempts, ceramic materials like $BaTiO_3$ (266), CCTO (268), Pb(Zr, Ti)O_3 (PZT) (269) as well as conducting/semiconducting materials like carbon nanotubes (CNT) (294), zinc Oxide (ZnO) (295), cadmium sulphides (CdS) (296), silver (273) and nickel (274) have been used as additives to increase the dielectric properties of polymer composites. As the additive content increases, the dielectric constant of polymer-ceramic composites increases (297). There have been many studies that were based on the effects of dielectric properties of inorganic/polymer composite materials on the output performance of TENG (298). One of the approaches is the introduction of high dielectric constant inorganic materials or conducting materials into polymer matrices (299).

Oxides with perovskite structures are employed in numerous applications such as in functional magneto-electronics, solid oxide fuel cells, radiation detectors, luminescent materials etc. (300, 301). The peculiar properties of the class of compounds include electronic and ionic conductivity, dielectric constant, magnetic and electric moments which can be tuned by varying the stoichiometry of composition as well as by varying the structure of ABO_3 (302). Among the perovskite structured oxides, Lanthanum cobaltite oxides are found to be promising materials for cathodes of solid oxide fuel cell, oxygen membranes, CO_2 laser etc. (303) . Undoped lanthanum cobaltite, $LaCoO_3$ is a semiconductor with p-type nature and possess rhombohedral structure. Alkaline earth (AE) – doped $LaCoO_3$ is found to be a very interesting material since these materials possess highest electrical and ionic conductivities among the oxides (304). Carrier doping is done to parent compound $LaCoO_3$ by introducing strontium into La site so that the resulting compound takes up general formula $Ln_{1-x}\,Sr_x\,CoO_3$ (LSCO) where Ln denotes lanthanide ion (305). The compound found attention of many researchers due to two factors: structural stability and the capacity to adjust the oxygen composition across a large range, and the ability to substitute cations in both the lanthanum and cobaltite sublattice without much deviation in structure (306).

The amount and position of different cobalt oxidation states depend on the distribution of oxygen vacancies which has a prominent influence on different properties such as chemical stability and ionic conductivity exhibited by LSCO. Contribution of oxygen ions towards ionic conductivity of compound depends on the arrangement of oxygen vacancy and related structural relaxation (307). Variation of the structure of $La_{1-x}\,Sr_x\,CoO_3$ is found to be a function of strontium doping which is the reason for many interesting properties namely high conductivity, fairly high magnetoresistance and also a good cathode material (307). $La_{1-x}\,Sr_x\,CoO_3$ phase possess rhombohedrally distorted cubic perovskite when $x \leq 0.5$ and highest ionic conductivity is exhibited by $La_{1-x}\,Sr_x\,CoO_3$ for $x = 0.5$ (308). Structural studies reveals

that when there is no strontium content ($LaCoO_3$), the structure is rhombohedral. With the introduction of strontium, structure gradually varied to rhombohedrally distorted cubic perovskite structure and to cubic (309). They have high dielectric constant (ε_r) and been found applications in non-volatile memory (310), thermoelectric conversion material (311) oxygen-permeable membranes (312) and cathode for solid oxide fuel cells (313). A co-existence of ferromagnetic ordering and glassy behavior is noticed in LSCO. As a result of structural and chemical inhomogeneity prevailing in $La_{1-x}\ Sr_x\ CoO_3$ due to strontium doping, it can be interpreted as hole-rich short-range ordered metallic ferromagnetic (FM) clusters immersed in non-FM insulating background. As the doping amount increases, non-magnetic behavior of parent compound is reduced. Magnetic phase diagram of $La_{1-x}\ Sr_x\ CoO_3$ suggest that at low temperatures when $x < 0.18$, spin-glass behavior is noticed while when $x \geq 0.18$, ferromagnetic nature is observed (314). Studies suggests (305) that the system undergoes an insulator-metal (I-M) transition at $x \approx 0.2$. $La_{0.8}Sr_{0.2}CoO_3$ act as an oxidation catalyst with high activity (315). Strontium doped lanthanum cobalt oxide (LSCO) ceramics when associated with other kind of materials, such as polymers can produce composites with interesting electric and dielectric properties (316). Even though LSCO possess excellent properties, triboelectric properties of LSCO have not been reported earlier. Aforementioned features prove LSCO to be a novel material as an additive which could improve the charge transfer between PDMS/LSCO and copper electrodes, thus, enhancing the output performance of TENGs fabricated based on PDMS/LSCO composites.

The dielectric to metal contact mode TENG was fabricated using PDMS/LSCO composite and dependency of dielectric constant on output performance was examined in detail. LSCO in the matrix of PDMS forms micro capacitors and hence helps to attain high dielectric constant composite. To improve the performance of triboelectric nanogenerators, PDMS/LSCO composite films were prepared with different LSCO content (expressed in

weight percentages). The effect of dielectric constant on the output performance was conferred experimentally which showed that surface charge density has a significant correlation with the relative permittivity of the tribo-material used. The effect of filler in the polymer composite films and the triboelectric property of TENG was systematically examined by measuring the permittivity of the prepared composite as well as the output performance of the TENG device. With the introduction of LSCO, permittivity of the tribo-material got improved and revealed better properties against TENG based on pure PDMS film. This ceramic blended polymer composites ensure an excellent motif for wearable and flexible self-powered gadgets.

4.2 Experimental section

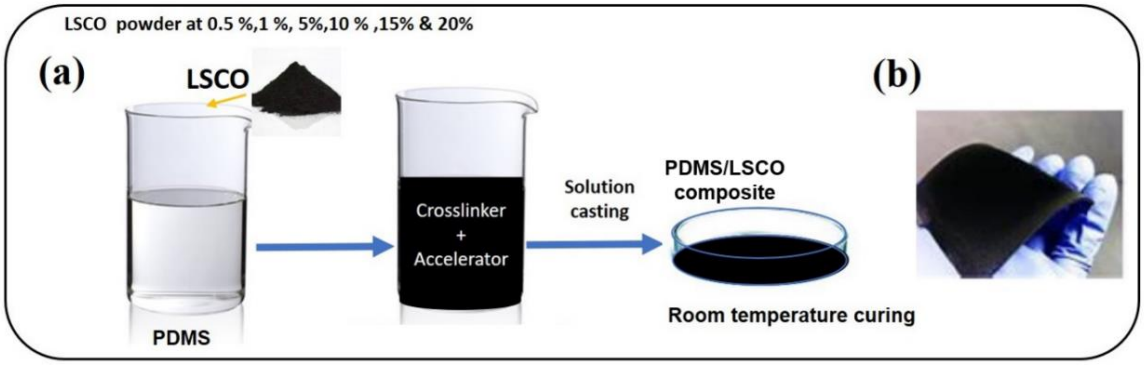

Figure 4.1. **(a)** Schematic representation of the steps involved in the preparation of PDMS/LSCO composites and **(b)** PDMS/LSCO composite film.

The room temperature curing procedure was utilized to make pure PDMS films, with tetraethyl orthosilicate (TOH) as the curing agent and dibutyl tin dilaurate as the accelerator (DBTDL). There were 100:10:1 ratio of PDMS, TOH, and DBDTL. In a desiccator under vacuum, the mixture was transferred to a petri dish and allowed to dry for 12 hours. The LSCO powder was added to the PDMS solution in varying weight percentages to get PDMS/LSCO ceramic composite films. 2.5 hours of probe sonication was done to disperse LSCO ceramic in

to PDMS matrix. Once the stock solution was thoroughly mixed, the curing agent and catalyst were added to it in the aforementioned ratio. After transferring the mixture to a petridish, it was allowed to set for 12 hours at room temperature. Finally, the polymer-ceramic composite films were subsequently taken for further characterization. The weight percent of LSCO introduced into PDMS were 0.5, 1, 5, 10, 15 and 20. Figure 4.1 (a) gives the steps involved in the fabrication of PDMS/LSCO ceramic composites and figure 4.1 (b) represents the photograph of the sample prepared.

In this study, as mentioned in the previous chapter, dielectric to metal model is used to form the TENG structure. PDMS mixed with different weight percentage of LSCO act as negative tribo material and was attached to a copper electrode. Another copper plate (2 cm × 2 cm) acts as both positive tribo material as well as top electrode so as to form the dielectric-metal model TENG. Output for electrical measurement was taken from the top and bottom copper electrodes.

4.3 Results and discussions

4.3.1 Structural studies

Figure 4.2 shows the XRD patterns of PDMS/LSCO composites prepared by varying weight percent of LSCO from 0 wt % to 20 wt %. Diffraction peaks were indexed using ICDD card no:87-1079 of LSCO ($La_{0.8}$ $Sr_{0.2}$ CoO_3) which possess rhombohedrally distorted perovskite structure with a space group $R\bar{3}c$ (307) which is a distinct class of space groups denoted by hexagonal and rhombohedral lattice systems. As the weight percent of LSCO increases, the intensity of peak at $2\theta = 33.42^0$ also increases which corresponds to the (104) plane. The peak at $2\theta = 11.84^0$ corresponds to that of PDMS and shows a slight shift when LSCO is added to it and as the weight percent of LSCO increases, the intensity of this peak decreases. This shows a gradual reduction of amount of PDMS in the PDMS/LSCO composite

as the LSCO weight percent increases. Composite films show the peaks of LSCO and PDMS, indicating successful formation of the composites. Table 4.1 shows the 2θ values and (*hkl*) planes of $La_{0.8}Sr_{0.2}CoO_3$ (317).

Table 4. 1. 2θ values and (hkl) planes of $La_{0.8}Sr_{0.2}CoO_3$ (ICDD card no.87-1079)

2θ (degree)	hkl
23.16	012
33.12	104
40.56	202
47.33	024
58.83	214
69.55	208

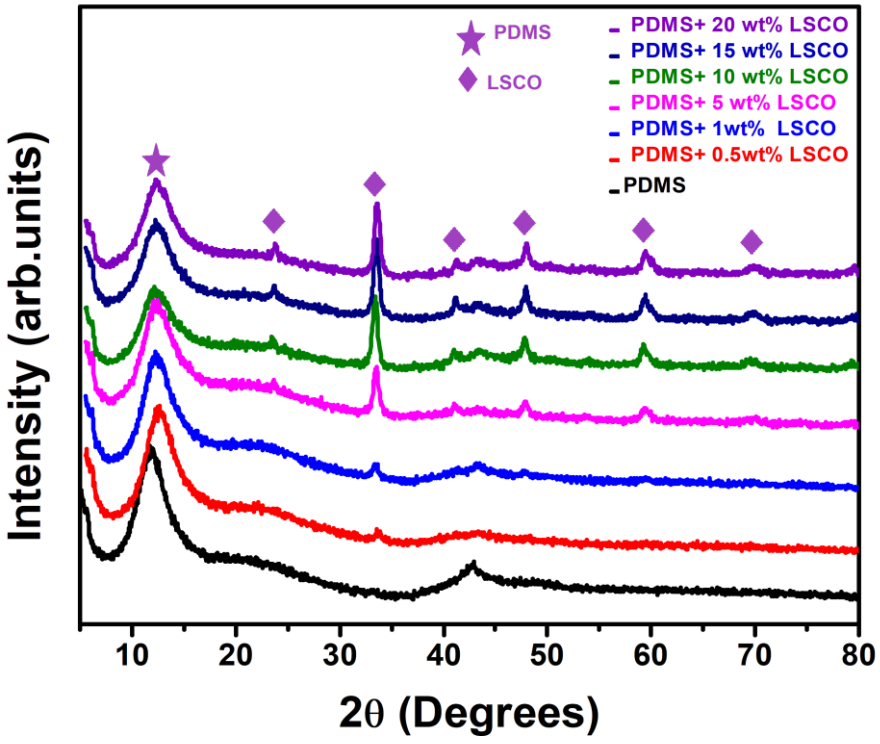

Figure 4. 2. XRD patterns of PDMS/LSCO polymer ceramic composites with different filler concentration.

4.3.2 Raman spectra analysis

Raman spectra of composite films contain the superimposed spectra of both PDMS and LSCO with no additional peaks. The presence of LSCO in the matrix is identified using the peak corresponding to E_g mode (150 cm^{-1}) of LSCO. This mode is associated with pure La internal vibration in the hexagonal (001) plane (318). As the LSCO weight percent increased, all peaks corresponding to PDMS showed a gradual increase in the intensity. Raman spectrum of PDMS elastomer show the peaks which corresponds to different chemical bonds namely: 488 cm^{-1} denotes Si-O-Si symmetric stretching, 709 cm^{-1} indicates Si-C symmetric stretching, 787 cm^{-1} (318) corresponds to CH_3 asymmetric rocking + Si C asymmetric stretching, 859 cm^{-1} corresponds to CH_3 symmetric rocking and 1411 cm^{-1} denotes CH_3 asymmetric bending. Figure 4.3 details about the Raman spectra recorded from the PDMS/LSCO polymer ceramic composites.

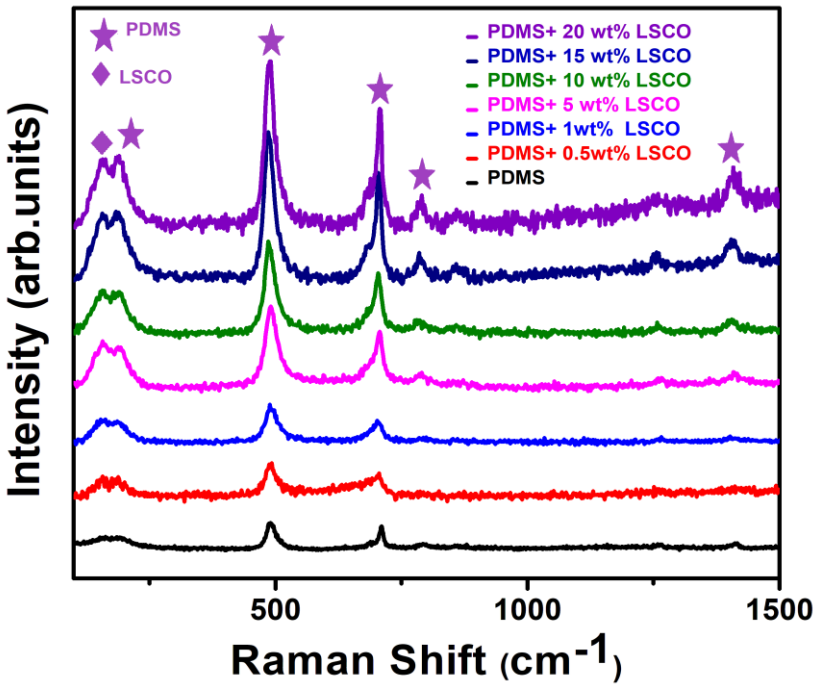

Figure 4. 3. Raman spectra of PDMS with different LSCO weight percentages.

4.3.3 Microstructure

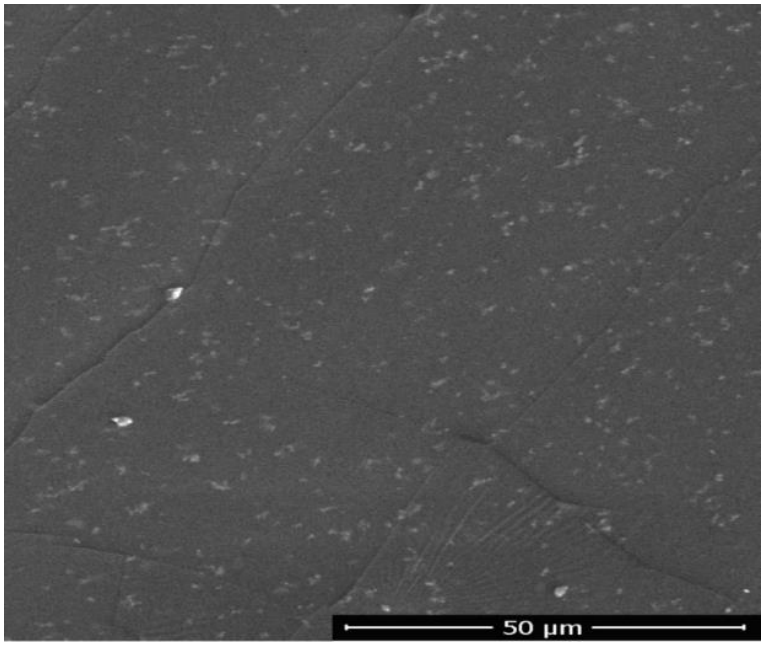

Figure 4. 4. SEM image of 20 wt% of PDMS/LSCO composite film.

Figure 4.4 shows the SEM image of 20 wt% of PDMS/LSCO composite film. Even though small clusters of LSCO particles were visible, dispersion of LSCO in PDMS matrix was more or less uniform. Uniform distribution of the filler particles is crucial for good dielectric, electrical and mechanical properties. In this study we have limited the content of filler in PDMS matrix to 20 wt%, since non-uniform mixing occurs at higher weight percent which ultimately causes agglomeration of fillers leading to poor microstructure and deterioration of dielectric and mechanical properties.

4.3.4 Dielectric studies

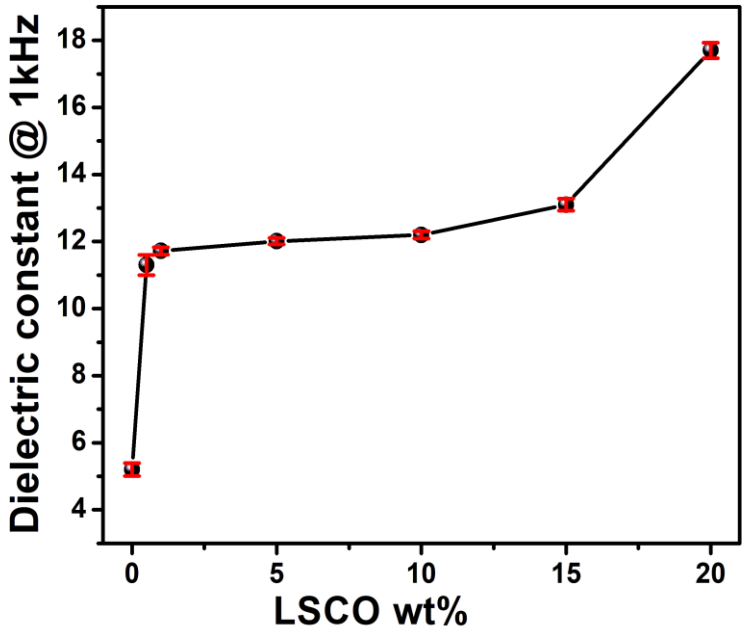

Figure 4. 5. Dielectric constant measured at 1kHz of PDMS/LSCO composite films for various weight percent of LSCO.

Figure 4.5 gives the variation of dielectric constant of the PDMS/LSCO composite film as a function of LSCO content (in weight percent). The dielectric constant of composite films exhibited a higher value compared to pure PDMS film. The dielectric constant of pure PDMS was found to be 5.3 at 1kHz which decreased to 3.7 as frequency increased beyond 10 kHz (Figure 4.6). This is due to the fact that interfacial polarization becomes prominent at low frequencies and vanishes as frequency increases (319). It is found that the dielectric constant of the composite film increased from 5.2 to 17.7 as the weight fraction of LSCO is increased from 0 to 20. The improved dielectric constant of the PDMS/LSCO composites could enhance the transferred charge density which is the prime factor that affect the output performance of TENG. This increase in the dielectric behavior of the composites with increase in the weight percent is mainly due to (i) polarization produced by movement and entrapment of charge

carriers at the interface between LSCO and PDMS which results in interfacial polarization (320) and (ii) when uniform distribution of LSCO into PDMS matrix occurs, as the LSCO particles comes closer to each other, there is a formation of large number of Internal Boundary Layer Capacitor (IBLC) structures connected in series and parallel (321).

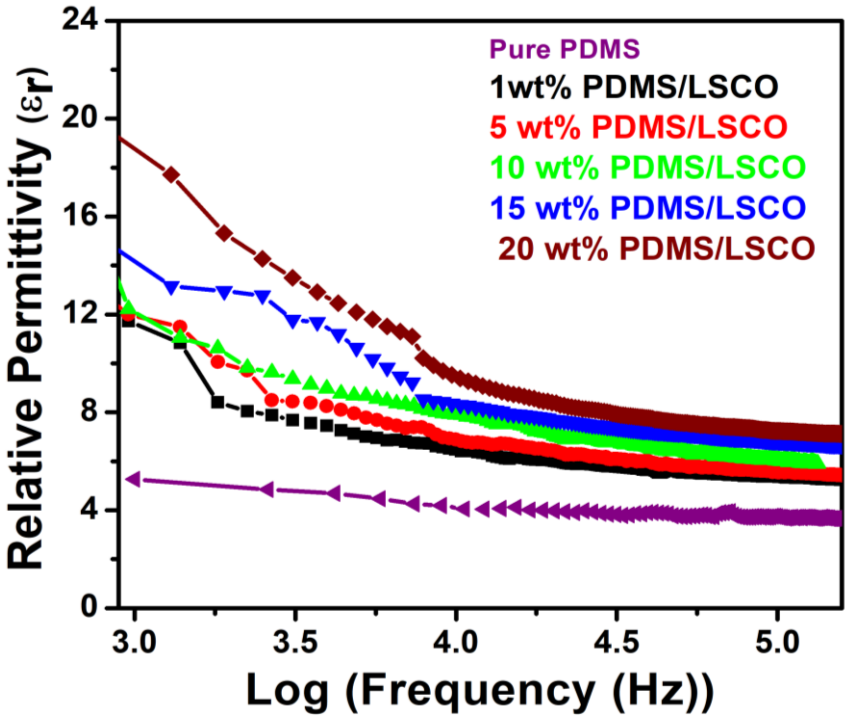

Figure 4. 6. Dielectric constant of PDMS/LSCO composite films with various weight percent of LSCO plotted as a function of log frequency.

These structures are formed since LSCO particles are surrounded by thin barriers of PDMS dielectric matrix. The effective dielectric behavior of the composites can be attributed to the total capacitance of all these individual capacitors. When LSCO particles are introduced into the PDMS matrix, it perturbs the interacting force between the molecules of PDMS creating an interface with the matrix. The region surrounding the each LSCO particle is considered as an interface where there is a co-existence of LSCO as well as PDMS. Hence

interface can be considered as a localized space around LSCO particle where the intensity of any chosen property varies from LSCO to that of PDMS. The interfacial region for an insulator-conductor composites is determined by the charge carriers at the boundaries between the two phases. These charge carriers produce an electric field which polarizes the enclosing polymer matrix and create an internal field forming charge clouds (322). When the weight fraction is low, the fillers (LSCO) are well separated and hence there is no interaction with filler particles. As the filler content increases, the concentration of LSCO particles as well as the interfacial area with PDMS increases. This elevates the average polarization linked with the filler particles and eventually helps to improve the permittivity of the composites.

4.3.5 Electrical characterization

Electrical measurements of PDMS/LSCO composites were done using triboelectric measurement system at a force of 10 N and frequency of 10 Hz.

4.3.5.1 Open circuit voltage (Voc)

As the weight percent of LSCO ceramic is varied from 0 wt% to 20 wt%, an increase in the V_{oc} was noticed in the PDMS/LSCO composites. Highest obtained V_{oc} was 23.8 V which was for 20 wt% PDMS/LSCO composite while for pure PDMS, V_{oc} was just 2.6 V. This proves that with the introduction of conducting fillers, the open circuit voltage has been enhanced to approximately 8 times compared to pure PDMS. These results support the fact that enhancement of relative permittivity improves the output performance of PDMS/LSCO composite based TENG. Figure 4.7 gives the variations in V_{oc} when different weight percent of LSCO was added to PDMS matrix and individual signals of V_{oc} of all weight percent of LSCO is plotted in figure 4.8.

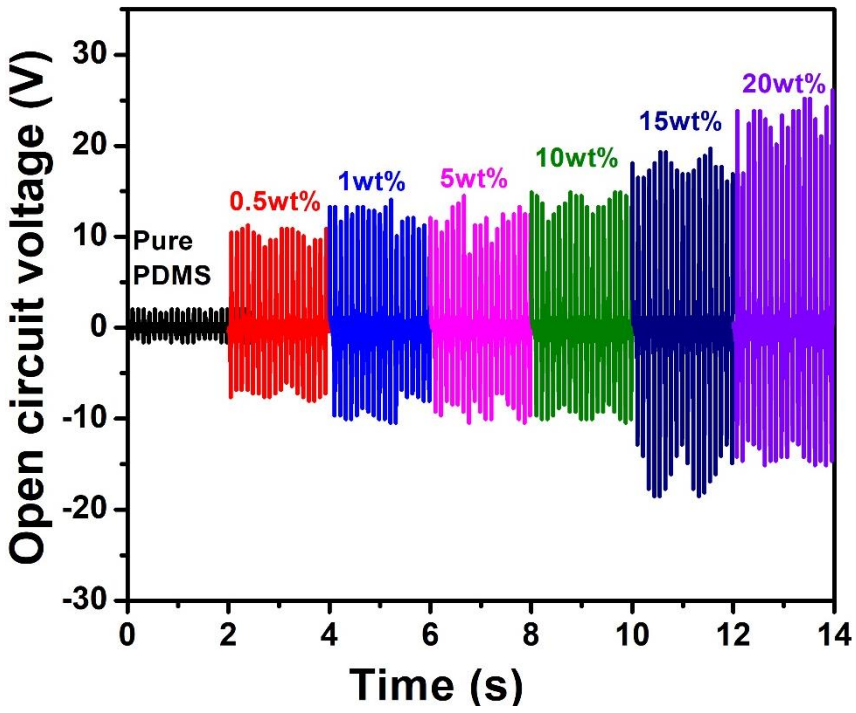

Figure 4. 7. Open circuit voltage versus time interval (2 s) of PDMS/LSCO composites for different weight percent of LSCO

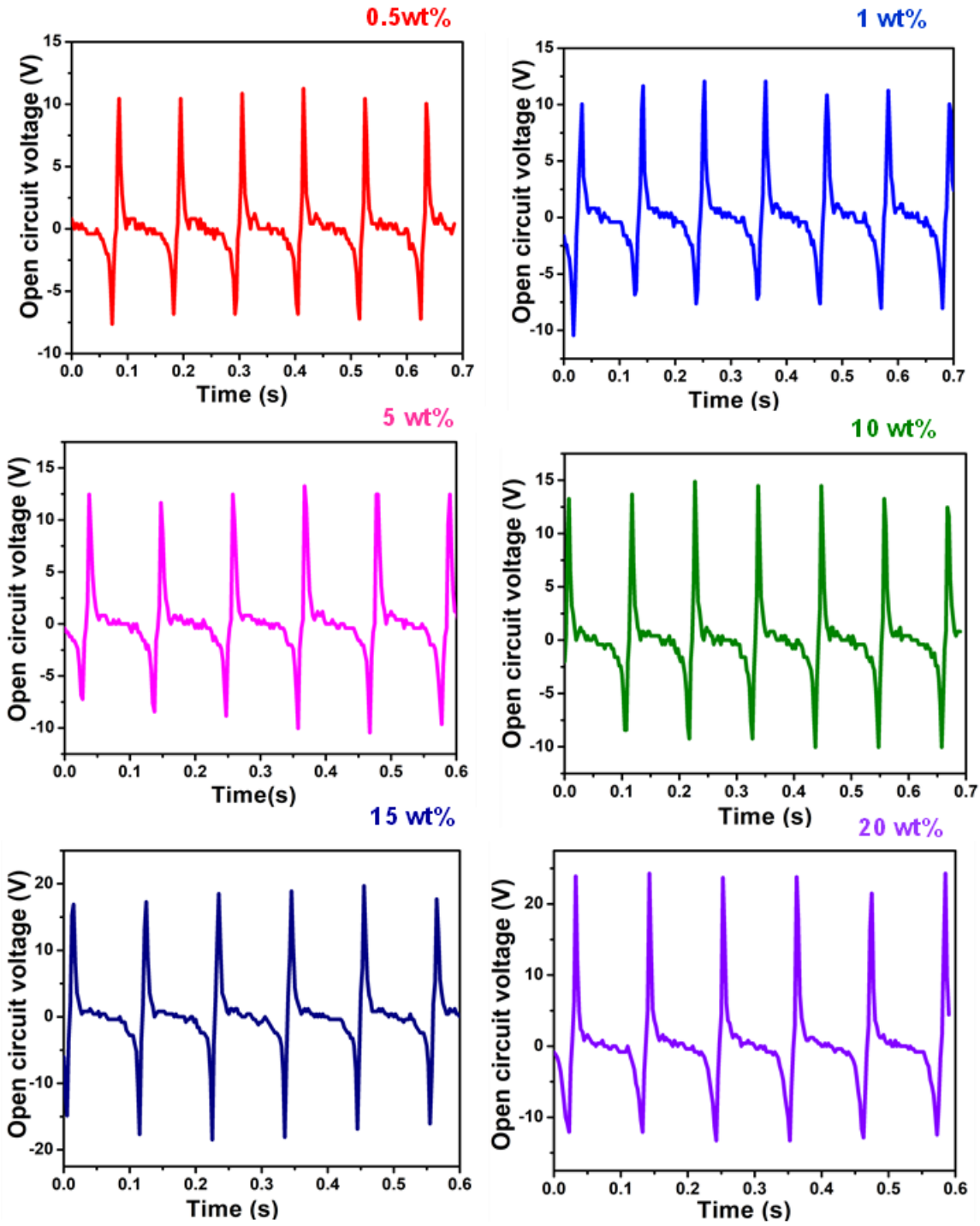

Figure 4. 8. Individual peaks of open circuit voltage versus time of all weight percent of PDMS/LSCO composites.

4.3.5.2 Short circuit current (Isc)

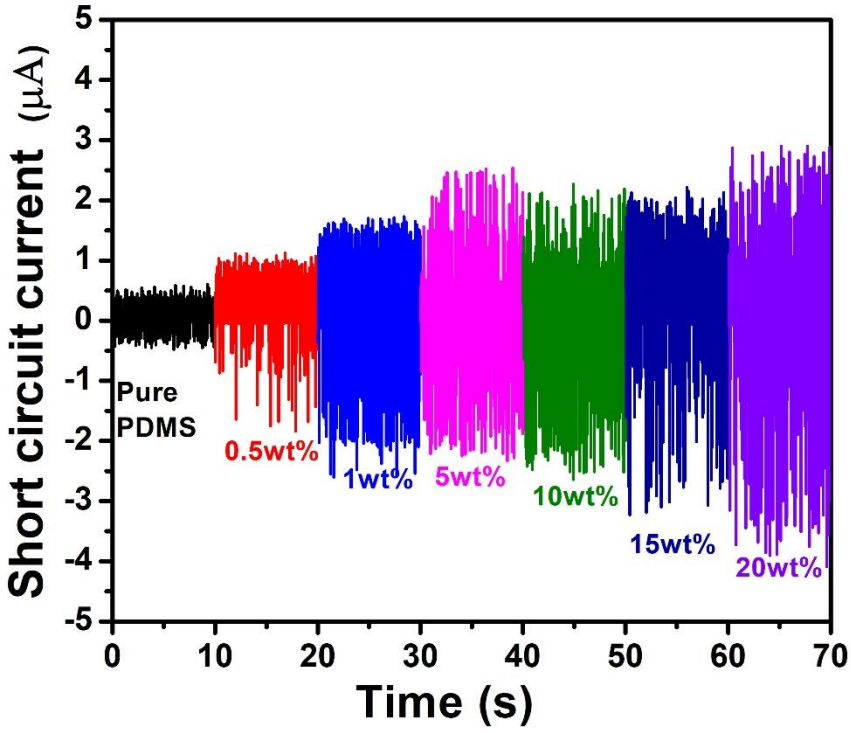

Figure 4. 9. Short circuit current versus time (10 s) of PDMS/LSCO composites for different weight percent of LSCO.

Variation of short circuit current with weight percent of LSCO ceramic from 0 wt% to 20 wt% is depicted in the figure 4.9. An increase in the I_{sc} was observed when filler contents were added to the PDMS polymer matrix. Highest obtained I_{sc} was 3.57 μA, for 20 wt% PDMS/LSCO composite while for pure PDMS, I_{sc} was 0.5 μA only. With the introduction of LSCO ceramic particles into PDMS polymer matrix, the short circuit current improved approximately 6 times compared to pure PDMS. The improvement in electrical properties were found in agreement with the results of relative permittivity and conductivity of PDMS/LSCO composite based TENG. Figure 4.10 depicts the graph where individual peaks of short circuit current of PDMS/LSCO composites is plotted for all weight percent of LSCO.

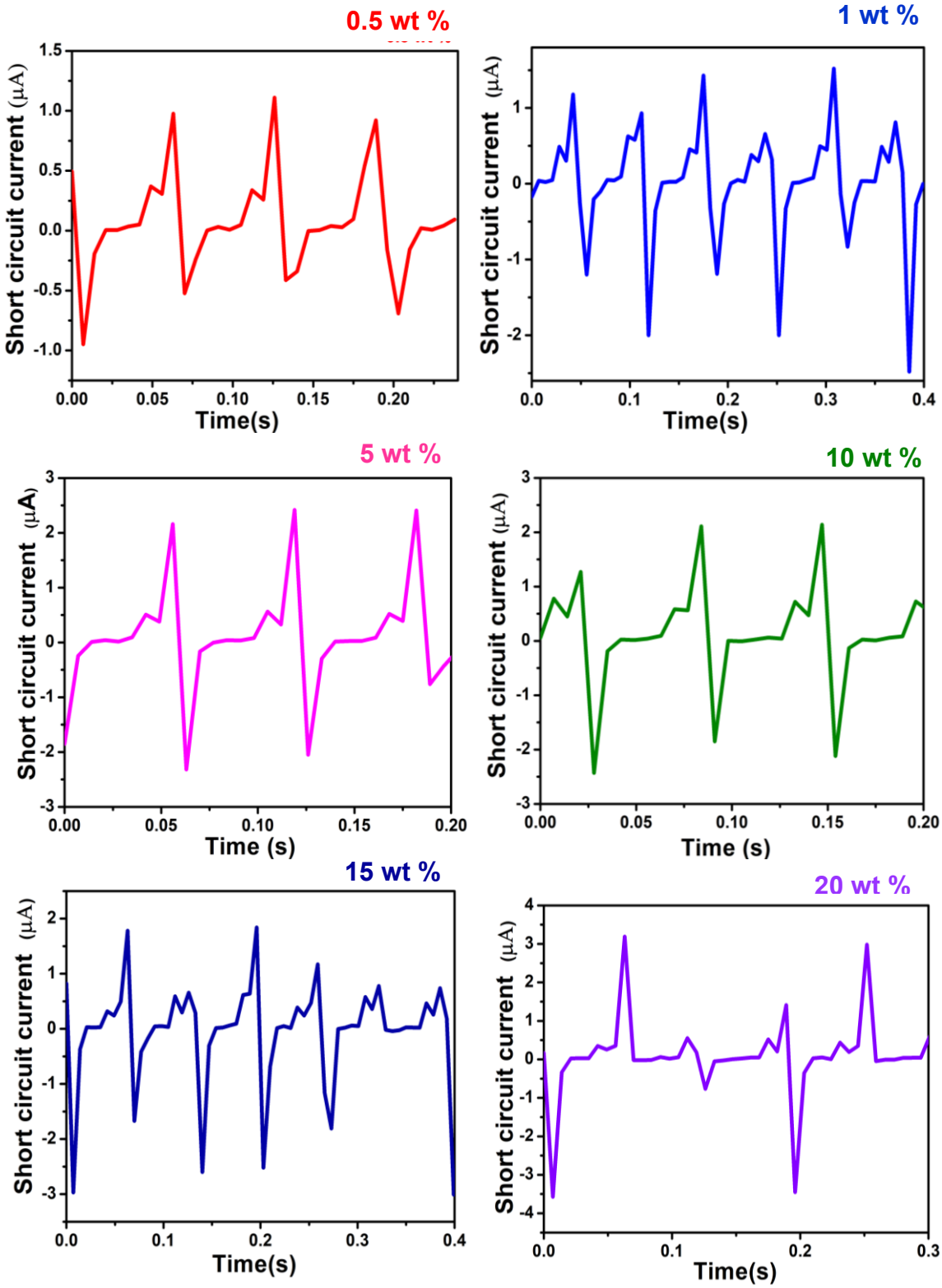

Figure 4. 10. Individual plots of short circuit current versus time of PDMS/LSCO composites for different weight percent of LSCO.

The peak values of both open circuit voltage and short circuit current of all weight percentages of PDMS/LSCO composites, for different weight percent of LSCO, is shown in figure 4.11. It is evident from the graph, that both parameters V_{oc} and I_{sc} show an increasing trend when the filler content in the polymer increases. The measurement of electrical parameters illustrates the influence of dielectric property of tribo-layers on the output performance of TENG.

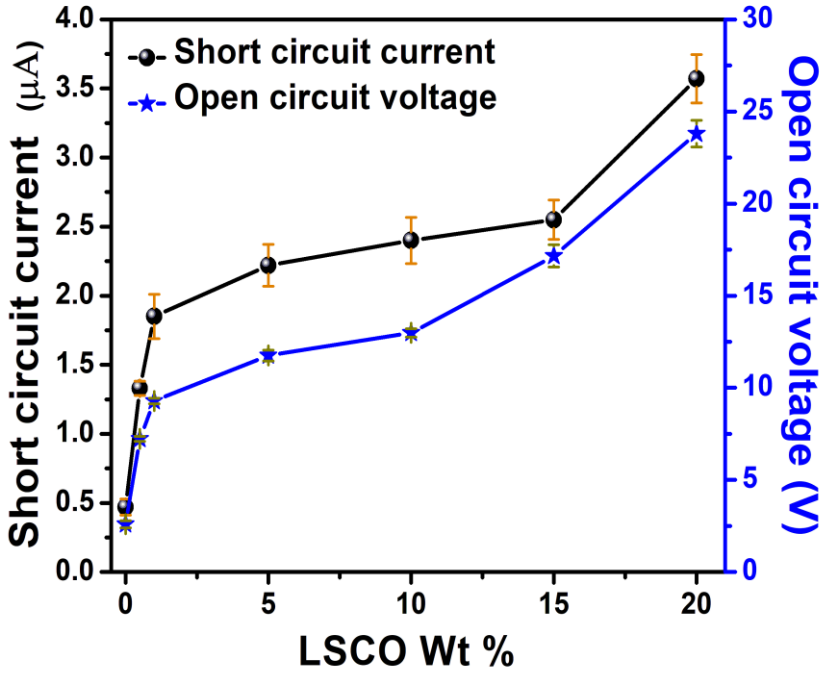

Figure 4. 11. Variations in the peak values of short circuit current and open circuit voltage for various LSCO content in PDMS/LSCO composite TENGs.

4.3.6 Resistive load characteristics of triboelectric nanogenerators

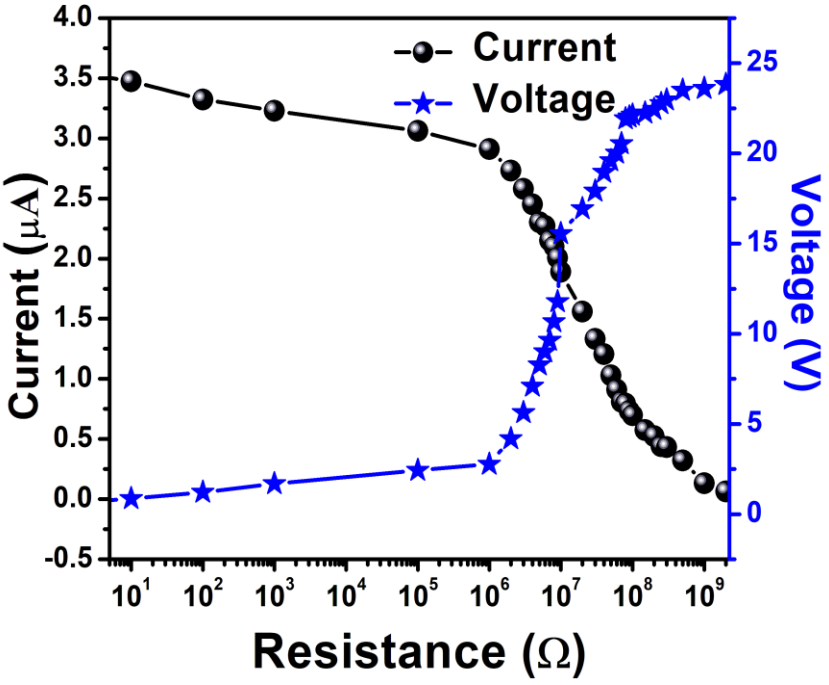

Figure 4. 12.Variation of current and voltage of PDMS/LSCO composite-TENG with varying load resistances.

Output properties for a contact-mode PDMS/LSCO composite TENG for different load resistances are plotted in figure 4.12. The graph can be divided into three regions and region I range from 1 to about 100 kΩ. Current in this case corresponds to that of short circuit condition I_{sc} =3.57 μA. At this condition, the voltage is proportional to output resistance and TENG act as an ideal current source. For load resistance beyond 10^8 Ω (region III), open circuit condition is observed in which the maximum voltage saturates at V_{oc} = 23.8 V. At this condition, TENG functions as a constant -voltage source. For intermediate load resistances (region II), current begins to decrease while voltage increases in the opposite trend. Around 10 MΩ inside this region, highest instantaneous output power was extracted from the TENG. This shows that the intrinsic impedance of this TENG is around 10 MΩ.

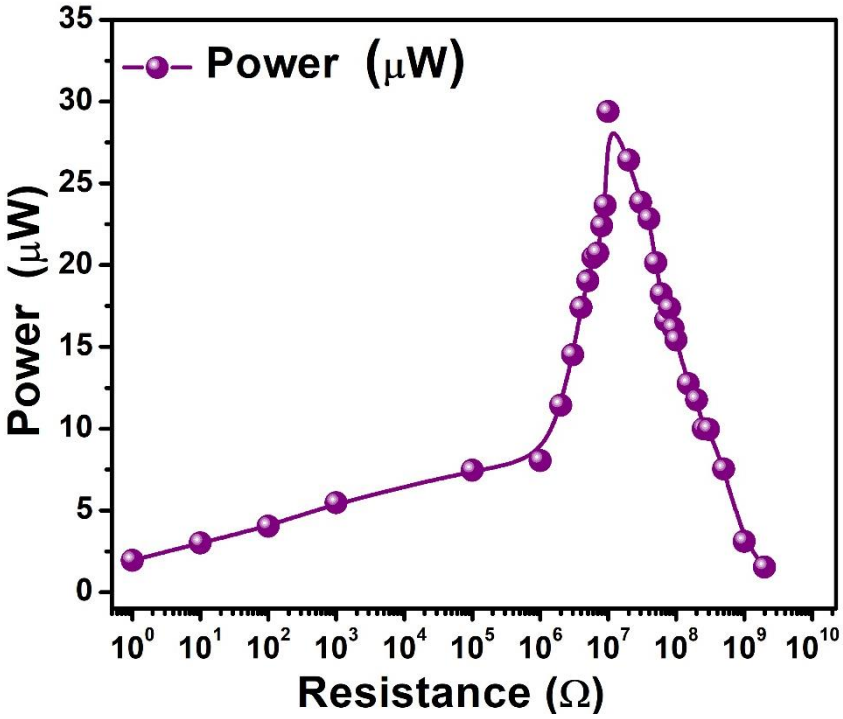

Figure 4. 13. Variation of output power of PDMS/LSCO composite-TENG with load resistances.

Variation of output power with load resistance of PDMS/LSCO composite based TENG was studied. Output power of TENG is the product of output current and output voltage. From the graph 4.13, the maximum output power is 29.4 μW at 10 MΩ. When the load resistance was increased further, the output power exhibited a decreasing trend. It can be inferred that intrinsic impedance of fabricated TENG is around 10 MΩ. It is always advantageous to obtain the peak power of the developed TENG at lower external load resistances for practical applications.

4.3.7 Capacitive load characteristics and charging behaviors

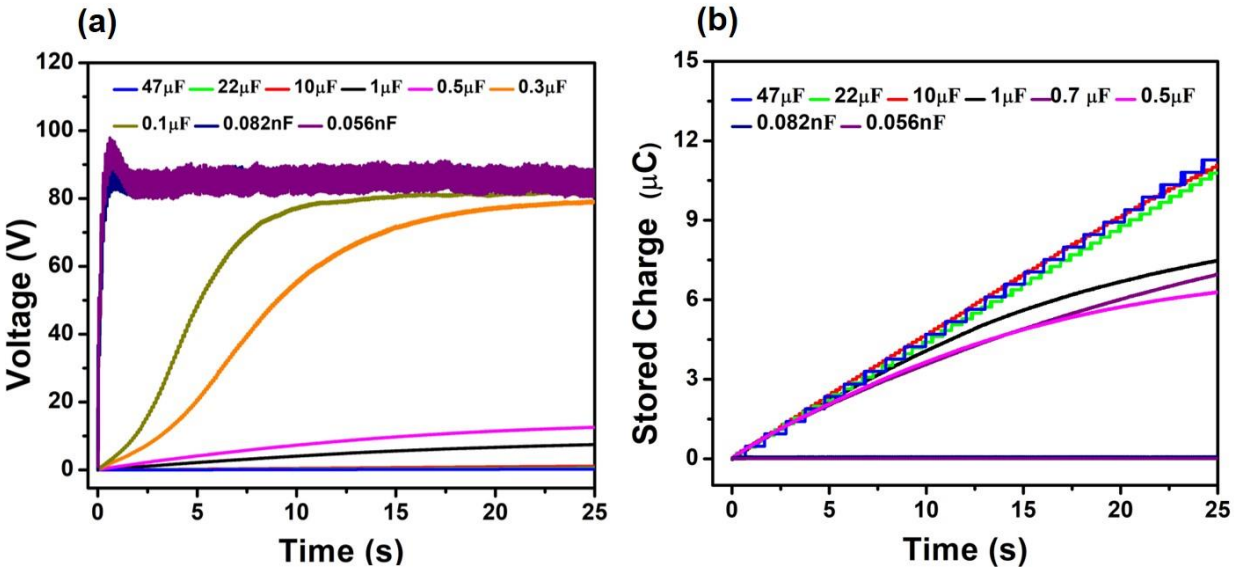

Figure 4. 14. (a) Charging voltage – time relationship at different load capacitance for 25 s charging cycle. (b) Stored charge –time relationship at different load capacitance for 25 s charging cycle.

A detailed study of TENG as an energy storage device was carried out by connecting different capacitors across the fabricated PDMS/LSCO composite TENG. Capacitor voltage versus time for different capacitors for 25 s working cycle at a frequency of 10 Hz and force of 10 N, (charging cycle) is shown in Figure 4.14 (a). Figure 4.14 (b) depicts the variation of charge stored with time in various capacitors. In the case of high valued capacitors, charging performance slows down and exhibits smaller slopes, as the time constant increases with capacitance values. The charging trend changes for capacitors nearest to 300 nF and reaches a saturation state. Periodic excitation was done by connecting the device to a triboelectric measuring system that can produce the contact – separation movement with the applied force of 10 N at 10 Hz frequency. A full wave rectifier was used to convert alternating charging current to store in a capacitor. For all capacitors, the output graph bears a resemblance to that of normal resistor- capacitor charging curve. There is a sudden hike to saturation voltage with low capacitors values.

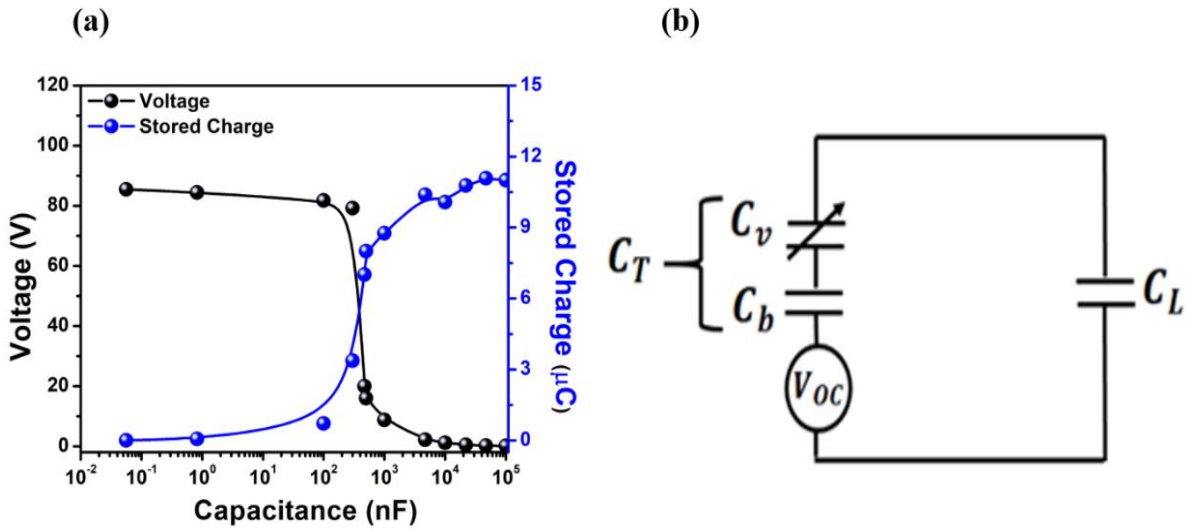

Figure 4. 15. **(a)** Variation of output voltage and stored charge with respect to different load capacitance **(b)** Equivalent circuit model of TENG to study load capacitance characteristics.

Figure 4.15 (a) gives the variation of voltage and charge stored with varying load capacitance. Figure 4.15 (b) represents the equivalent circuit of TENG, where C_T denotes the TENG capacitance and C_L denotes the load capacitance. Initially there are no charges stored on the load capacitor and hence initial charges on both C_T and C_L are equal to zero. When C_L takes smaller values, capacitive impedance of C_L is very large compared to the impedance of C_T. This working condition of TENG is called quasi-open circuit condition and majority of V_{OC} is dropped across C_L. So voltage across the capacitors quickly saturates to V_{OC} values. However, since the C_L is so small, the stored charge remains close to zero, resulting in a low stored energy. In contrast, when C_L takes larger values, its impedance is significantly less than impedance of C_T, therefore the voltage across C_L is close to zero. The TENG is now operating in a quasi-short circuit mode, and the stored-charge curves for large C_L are all quite near to the Q_{SC} curve. However, the low voltage across C_L limits the overall amount of stored energy. From the aforementioned studies, it is understood that stored energy can only achieve its greatest potential in the transition zone.

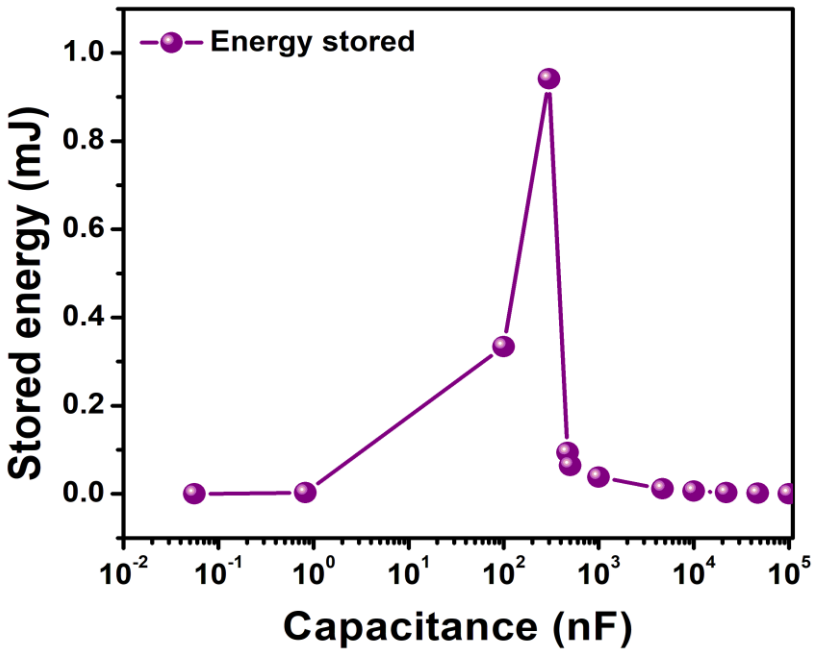

Figure 4. 16. Variation of stored energy measured at different load capacitance.

The stored energy has got a maximum value of 0.94 mJ at load capacitance of 300 nF. Figure 4.16 shows the variation of the values of stored energy for different load capacitance. Theoretical analysis vividly explains that as the load capacitance become equal to TENG's intrinsic capacitance, energy stored will be maximum. Hence the intrinsic capacitance of the PDMS/LSCO composite based TENG can be approximated as 300 nF. The capacitive study of PDMS/LSCO -composite TENG ensures the characteristic of energy storage of developed TENG device. This proves that mechanical energy source could empower the broad range of commercial mobile and wearable smart electronic device which includes electronic displays, sensors etc.

4.4 Conclusions

Improvements in the output performance of cost-effective TENG, based on PDMS/LSCO composites with varying amount of LSCO is investigated. The effect of dielectric constant of the composite materials on the output performance is discussed through

systematic analysis which reveals that the surface charge density is closely related to the relative permittivity of the tribo-layers. X-ray diffraction studies indicate successful formation of polymer/composites while Raman analysis gave different vibration modes possessed by LSCO and PDMS compounds. Contact separation mode TENG is fabricated by optimizing the dielectric properties of the PDMS/LSCO composite film. SEM image also helps to reveal the microstructure of PDMS/LSCO composite. It is found that in PDMS/LSCO two-phase composite system, dielectric constant of filler directly influences the triboelectric output performance. Maximum short circuit current of 3.57 μA and open circuit voltage of 23.78 V was obtained when 20 wt% LSCO was added to PDMS. Highest power obtained is 29.4 μW for a load resistance of 10 MΩ. Capacitive model was utilized for exploring the energy storage ability of TENGs and the intrinsic capacitance of the PDMS/LSCO composite based TENG was found to be 300 nF. This chapter provides a feasible perception of augmenting output performance of polymer based TENGs by enhancing the dielectric constant of the tribo-layer by the incorporation of ceramic materials into polymer matrix.

Chapter 5

Application of PDMS/LSCO composite TENGs

Abstract

This chapter details various applications of PDMS/LSCO composite based TENG. A module was fabricated which consists of four layers of PDMS/LSCO composite TENG and the output was extracted by mechanical excitations. Human hand tapping was the mechanical stimulus provided to the module as an input which gave an output current of around 45 μA and output voltage of 90 V. The output of the module was utilised to charge different capacitors which demonstrates the capability of energy harvesting from TENG for practical applications. This module was integrated into a circuit meant to operate a digital watch which converted the electronic circuit incorporated with watch a self-powered automated system. Also, the output of PDMS/LSCO composite based TENG was used to lit light emitting diodes which is another application, even pulsed nature of output could be employed to light up a system. An impact sensor was fabricated to demonstrate self-powered sensor operations using TENG. It could be employed as rain sensor to sense the impact of rain drops and extract energy from rain drop. An attempt was done to fabricate single electrode mode of PDMS/LSCO composite in order to utilize its output for powering portable electronic gadgets. The results of the PDMS/LSCO composite-based TENG imply that these materials have the potential to be appropriate candidates for incorporation into electronic devices, thereby transforming such devices into self-powered gadgets.

5.1 Introduction

The triboelectric nanogenerator (TENG) is a promising and unique energy conversion device that converts mechanical energy to electricity using triboelectric friction. To enhance the output of TENGs, increment in the contact friction area is one of the methods adopted recently. In order to minimize the size of the device, a better approach is to extend the device from a 2D planar device to a 3D device. By coupling the outputs of all individual layers, it is possible to extract maximum power from a minimized area. Multilayer integrated structure can be designated as module which consist of three to four TENGs coupled together and has been fabricated with an aim to reduce the area of the device without compromising the output. The area can be controlled to desired dimensions and by synchronizing the output of individual TENG in a proper way. It is a promising approach for harvesting electrical energy from freely available low frequency mechanical energy. The output of module was used to study the charging behavior of capacitors and also to power a digital watch. This application successfully demonstrated that output of TENGs could be incorporated as a self-powering unit in electronic gadgets. Single electrode mode of PDMS/LSCO composite TENG was also fabricated with an aim to incorporate them to extract energy from human motions, especially human footsteps. Single electron mode is always a better option as far as moving objects are concerned. Hence by investigating the output of single electrode mode PDMS/LSCO composite TENG, it is concluded that human motions can be harnessed, which can be used to generate electricity for driving portable electronic gadgets.

5.2 Vertically stacked PDMS/LSCO composite based TENG

Enormous amount of mechanical energy is prevalent in the surroundings and majority of these vibrations are generally of low frequency. Selection of proper device geometry has an important part in improving the performance and stability of TENGs. Researchers have suggested TENGs based on a multilayer wavy-structure (323), elastic bellows (324), case-

encapsulated cylinder (325), rotating-cylinder (96), inter-locking kirigami patterns (326), and origami structures (327). There studies illustrated that right choice of device structure of TENGs could enhance the ability to harness green energy effectively. It can trap mechanical vibrations of low as well as high frequencies from various external forces.

Even though freely available mechanical energy can be synergistically harnessed and convert into useful electrical energy, a challenge faced by TENG is its low output current and high output voltage. A method to address this issue is to develop multiple unit cells which are connected parallel to each other. By fabricating the vertically integrated three-dimensional (3D) TENG, the above-mentioned problem can be solved. 3D TENGs have two main advantages (328). One is the enhancement in frictional area and second one is that they can be treated as numerous individual planar TENGs which are connected parallel to each other in a small area so as to enhance the output performance of device. Under applied external force, stacked-layer of TENG structure traps and convert mechanical energy into electrical energy.

Studies show that power obtained from 3D TENGs is large compared to single layer and can be stored in an energy storage device for future usage (328). The 3D design is basically having a sandwich stack geometry where architectural symmetry is preserved. Phan and colleagues demonstrated improved output performance when multi-layered TENGs were constructed by stacking single units (329). They designed a simple method for producing airflow-driven TENGs which utilize a fluttering-membrane energy harvester placed between parallel counter plate electrodes to produce triboelectricity impulsively by harnessing dynamic mechanical interactions caused by airflow across the flexible membrane. Jiahui Wang et.al reported fabrication of stacked-layer TENG which has a dimension of 10 cm × 10 cm , a square shaped PET sheet arranged in a zigzag pattern (330). This structure was integrated with human body movements which provides mechanical distortion to stacked structure of TENGs. For

instance, the TENGs may be activated by the user's feet while walking or by tapping them with their hands, allowing the regulation of TENG activation time. By connecting the output of the TENG to several intramuscular electrodes, it was possible to collect mechanical energy from body movements in order to electrically stimulate muscles for therapeutic or rehabilitative purposes.

Tang et.al investigated the power generation using stacked triboelectric nanogenerator and they had chosen PDMS and PET as the tribo layers **(331)**. Micro-pyramidal structure was patterned on the surface of PDMS layer while flat PET layer was made into arch shape and counter arch shape to maintain the distance between the two tribo-layers. They found out that TENGs act as electron pumps which when connected in parallel gave maximum output current and charge. When they are connected in series, no significant enhancement was noticed. They also reported that as the stacking number grows, the endurance of the cell's signal increases, resulting in higher continuous non-zero output even at a lower frequency. The stacked 3D TENG turns out to be a continuous and uninterrupted green power source which could be employed in our day today life. This approach takes the advantage of designing triboelectric generators, which permits the production of a sustainable, economic energy-harvesting system with a stable device configuration. Thus 3D-TENGs possess advantage of improving the area of friction without compromising the device dimension so that they could be incorporated to miniature electronic devices.

5.2.1 Design and analysis

Vertically stacked PDMS/LSCO composite based TENG uses vertical contact separation mode to generate electrical signals. 3D structure was fabricated by stacking four units of individual TENG, where each unit was separated using poly ethylene terephthalate sheet (PET). Negative tribo layer is PDMS/LSCO composite while the copper electrode forms the tribo-positive layer. Device was further reinforced by acrylic sheets on top and bottom

sides. Acrylic sheet was chosen as reinforcing layer due to its light wight, economic and excellent machinability. Spacers were used to sustain the gap between the tribo-layers of each unit as it works in vertical contact-separation mode. They have an elongated cylindrical structure made of soft and flexible rubber. Thickness of spacers gives the air gap between the tribo-layers. As far as device dimension, total contact area and mechanical sturdiness is concerned, a thin air gap between the tribo-layers are preferable. But if the distance between the tribo-layers become very small, due to the coupling between the electrodes, a reduction in the induced current is observed (332). To prevent this loss of induced current, spacers of thickness ~0.5 mm are used. The advantage of spacers is that they act as elastic potential repositories which help to maximize the temporal mechanical vibrations (333).

The Vertically stacked PDMS/LSCO composite based TENG had a dimension of 5 cm × 5 cm. The 3D multi-stacked device has an increased frictional area in the same space which improves the number of transferred charges in the circuit. Such vertically stacked device generated an impressive current of 43.2 μA and an output voltage of 90 V. Schematic diagram of the vertically stacked PDMS/LSCO composite TENG is shown in figure 5.1. Figure 5.1 (a) shows the fabricated stack configuration and (b) shows the 3D model where each layer has been indicated in detail. Electrical characteristics of vertically stacked PDMS/LSCO composite TENG is shown in figure 5.2 where 5.2(a) denotes the short circuit current and 5.2(b) denotes the open circuit voltage. The specific design of the TENG resulted in increased output performance and quick operation.

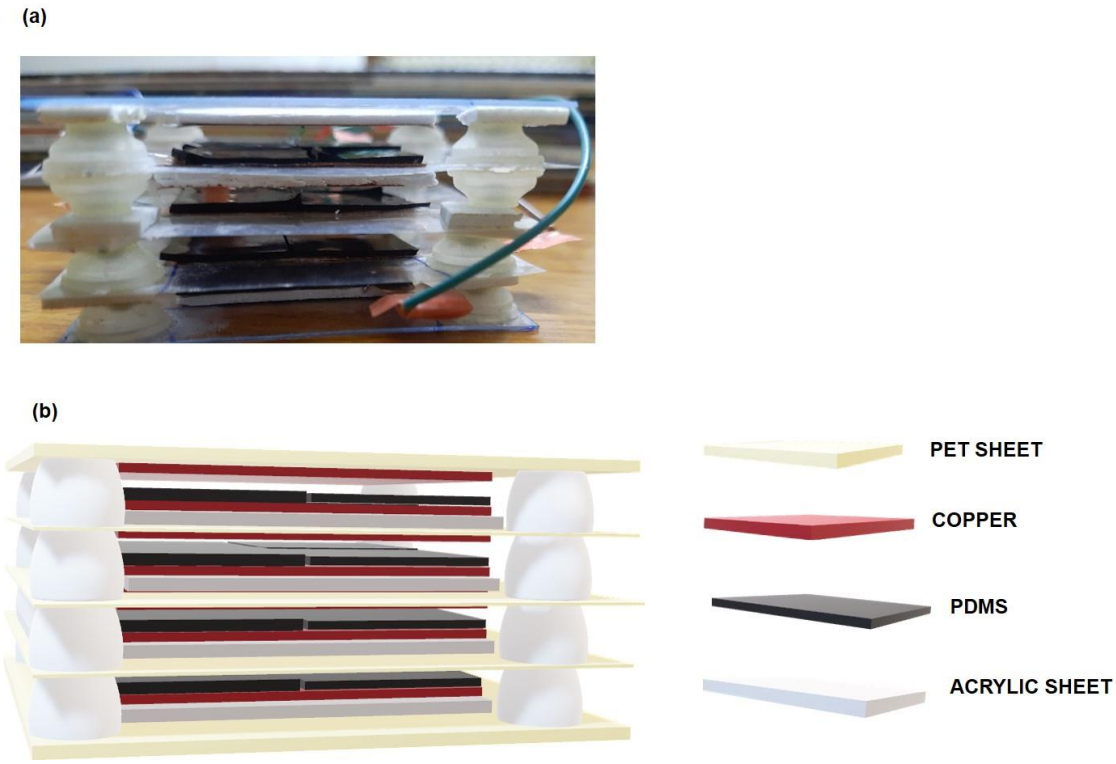

Figure 5. 1. Vertically stacked PDMS/LSCO composite based TENG. (a) Fabricated stack configuration and (b) 3D model of vertically stacked PDMS/LSCO composite based TENG.

Driven by palm tapping, the stacked unit (module) could provide a continuous ac supply which was converted to dc to act as a standard power source to drive small power electronic devices. The number of layers within the stack can be varied according to the need and requirement of the user. The drawbacks of the vertical stacked geometry include variations in the structure with time and asynchronous vibrations of inner electrode layers. But performance enhancement of the device and adaptive engineering machinability suits vertical stacking method an attractive one. Also, these structures find difficulty in coupling the outputs of individual units to obtain synchronized output. Figure 5.2 shows the electrical characteristics of vertically stacked PDMS/LSCO composite based TENG.

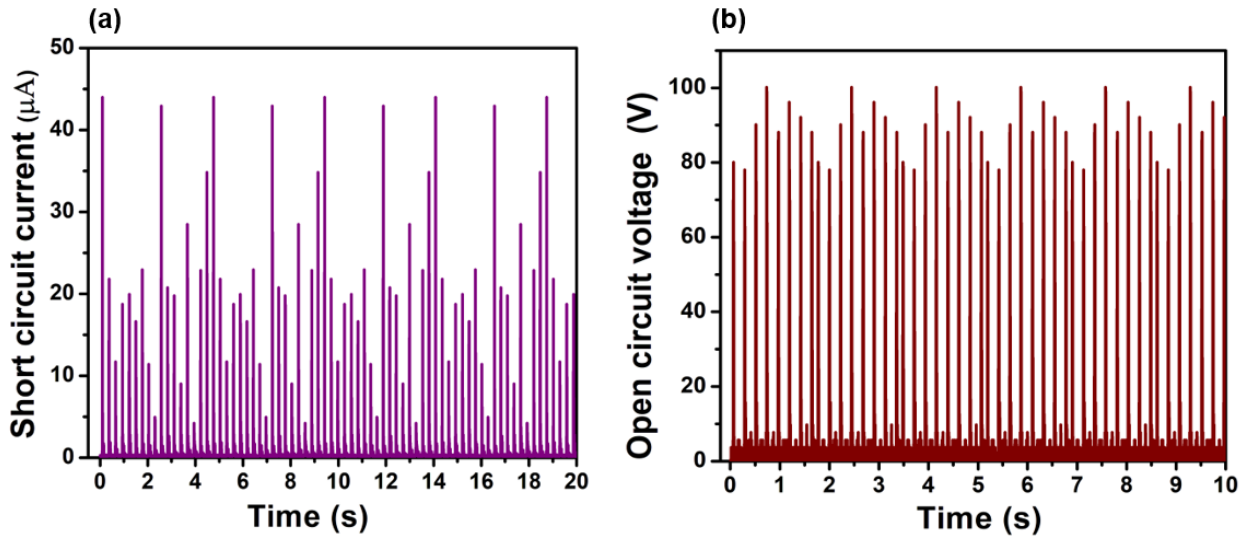

Figure 5. 2. Electrical characteristics of vertically stacked PDMS/LSCO composite based TENG. (a) Short circuit current versus time and (b) open circuit voltage versus time.

To ensure the energy conversion capability of the developed vertically stacked PDMS/LSCO composite based TENG device, real time charging of capacitor is carried out. The output from vertically stacked TENG was rectified into one direction with the help of a bridge rectifier circuit. Rectified output current was used to charge capacitors which were connected to an external load. As the capacitor was charged by the rectified current, the load volage increased. The charges accumulated in the load capacitor can act as an uninterrupted direct current supply to electronic gadgets. In the case of commercial applications, it is better to recharge a battery rather than charging a capacitor so that it can be stored for future purposes. Even with irregular palm tapping (have irregular interval between the tapping), capacitors of different capacities were charged. Figure 5.3 shows the charging behavior of capacitors using vertically stacked PDMS/LSCO composite based TENG.

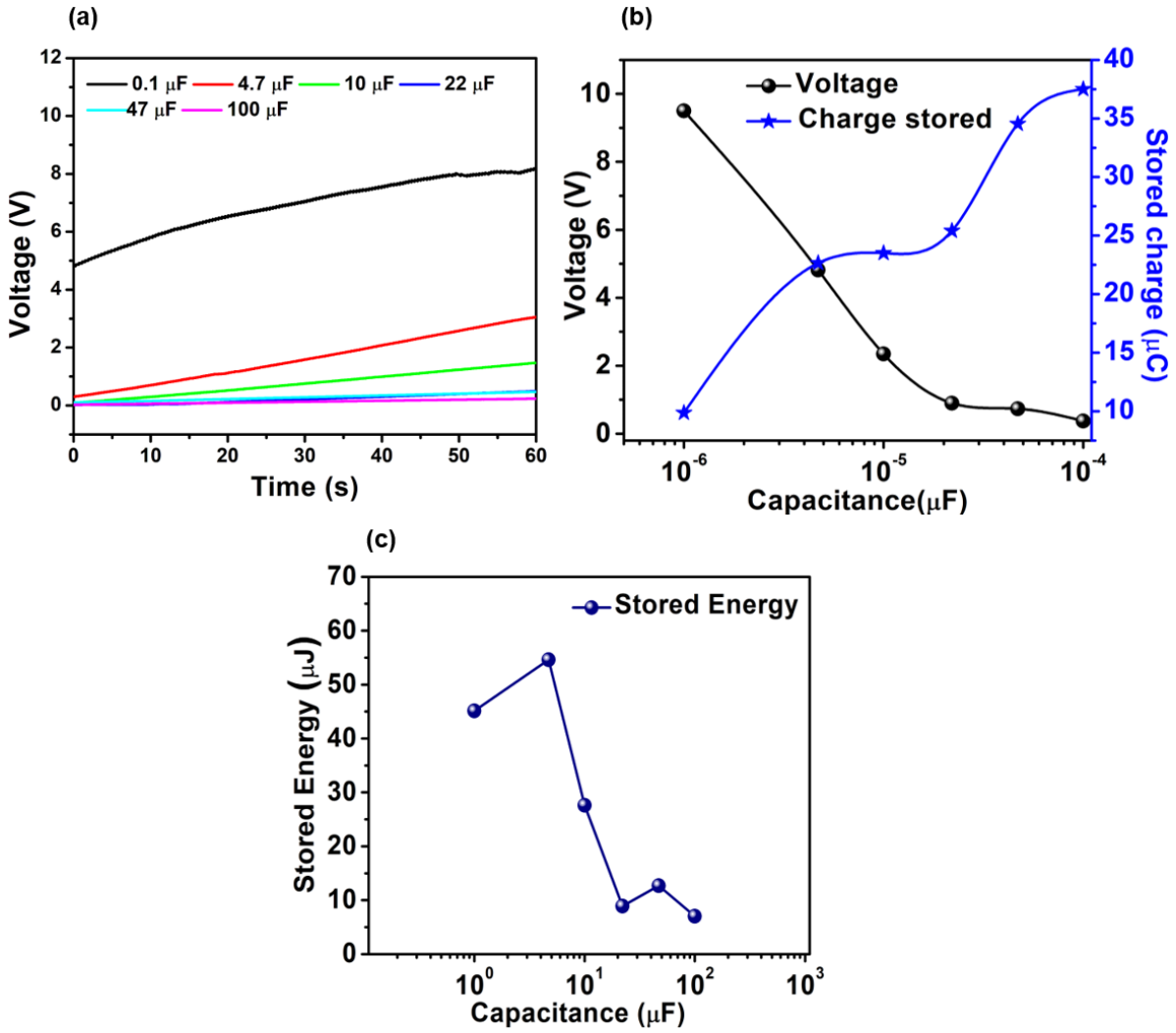

Figure 5. 3. Load capacitor charging behavior. (a) Charging behavior of capacitors using vertically stacked PDMS/LSCO composite based TENG, (b) stored charge and voltage for varying load capacitances, and (c) stored energy for various load capacitances.

Variation of load capacitances were done to examine the charging behaviour of fabricated vertically stacked PDMS/LSCO composite based TENG. Figure 5.3 (b) depicts the relation between stored charge and voltage for varying load capacitances. Using slight hand tapping process, it could store a maximum charge of 38 μ C and maximum energy of 55 μ J. From this graph, the intrinsic capacitance of vertically stacked PDMS/LSCO composite based TENG could be calculated and was found to be 4.7 μ F.

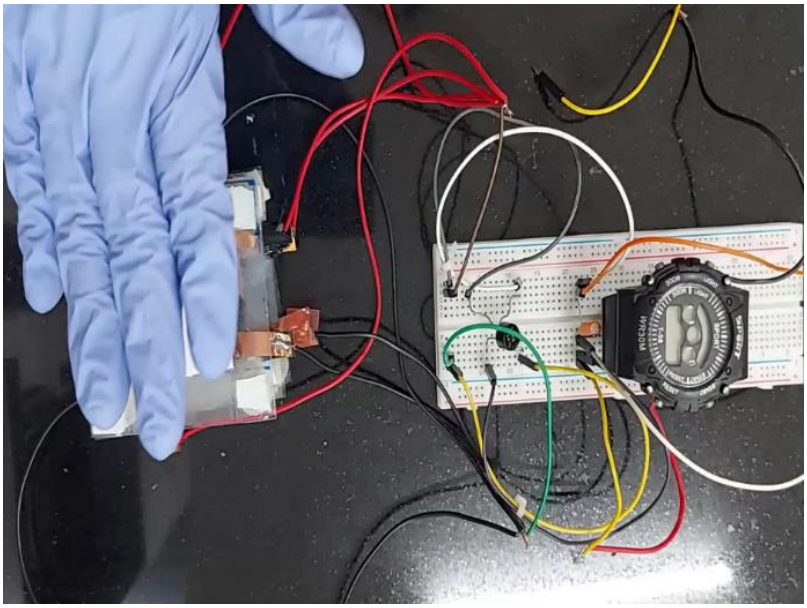

Figure 5. 4. Circuit incorporating vertically stacked PDMS/LSCO composite based TENG for driving a digital smart watch.

To realize self-powering of smart electronics using vertically stacked PDMS/LSCO composite based TENG, a circuit was designed to power a digital watch. This was equipped with a primary circuit which consist of a capacitor of 1 μ F and a secondary circuit having a digital watch which is a representative of wearable electronics. When alternating current was generated from the fabricated TENG device, rectifying circuit converted it into direct current and the output from rectifying circuit charged the capacitor. Multimeter was connected parallel to capacitor and as the multimeter read an output voltage of around 1.5 V, the secondary circuit was closed and the digital watch begins to work. Thus, using the output of the stack of PDMS/LSCO composite TENG was used to charge capacitor and also using this energy, a commercial smart watch was made working without the aid of any external power source. Hence the charging circuit system coupled with improved output performance of the stack of PDMS/LSCO composite TENG has proved to be a promising self-powered unit which could be employed for integrating in wearable electronic devices. Figure 5.4 shows the circuit which

incorporated the output of vertically stacked PDMS/LSCO composite based TENG to drive the smart watch. The PDMS/LSCO composite based TENGs on a vertically integrated 3D stack have aided in the exploration of architectural expertise. When PDMS/LSCO composite TENGs are stacked vertically, their production is improved because this shape makes better use of the limited space available.

For manifesting the practical application of fabricated PDMS/LSCO TENG as energy harnessing device, output of PDMS/LSCO composite based TENG was incorporated for powering a unit of light emitting diodes. Dimension of the TENG was 4 cm × 4 cm and PDMS/LSCO composite (negative tribo-layer) was placed on copper sheet (positive tribo-layer). A full wave bridge rectifier was connected between TENG and commercial LEDs to examine the self-powering ability of developed device. When TENG was connected to LEDs (Figure 5.5), around 25 LEDs were lit using the electrical output generated simply by human hand tapping.

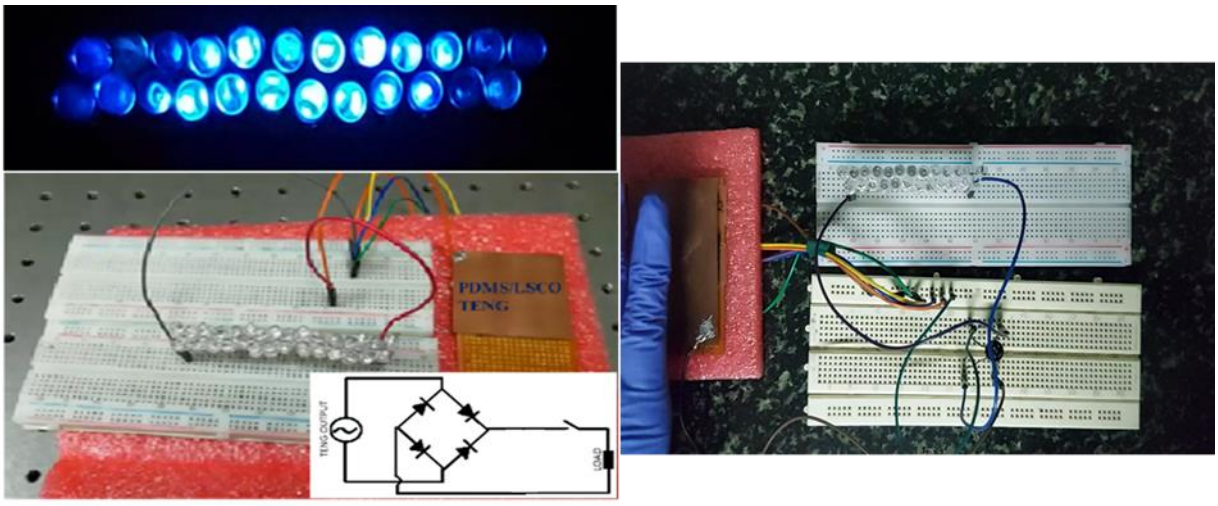

Figure 5. 5. PDMS/LSCO TENG used for lighting 25 light emitting diodes. Inset shows the circuit which consist of a bridge rectifier and capacitor connected in parallel.

5.3 Self powered impact sensor

The phrase "self-powered sensor" has dual meanings. First, it is a sensor that, when mechanically actuated without an external power source, emits an electric signal automatically. The majority of sensors used today are passive, implying they do not emit a signal in the absence of an external power source. Secondly, the sensor's operational power source is self-generated. This is achievable when the active and sleeping modes of a sensor are considered. In many instances, a sensor does not need to provide a signal in every second; in environmental monitoring, for example, a signal at a predetermined period is sufficient. In such instances, the energy captured during the sensor's "sleep" state can be used to power it once it becomes active. This is a strategy for continued functioning of self-powered sensors. Recent advancements of self-powered sensors based on TENGs find a variety of applications, including physical sensors, wearable devices, biomedical and health care devices, human–machine interface, chemical and environmental monitoring, smart traffic, digital cities, robotics, and fabric sensors.

The emergence of factory automation is boosting the demand for motion sensors, particularly mechanical motion sensors (334). Current mechanical motion sensors are primarily constrained by their complicated device designs, high prices, and fabrication and assembly difficulties. Due to their simple and flexible constructions, high degree of integration and cost effectiveness, the TENG-based mechanical motion sensors are frequently studied by researchers (1) (335). They are capable of monitoring the motion characteristics of moving objects and may be utilised in several industrial domains. There are three types of triboelectric sensors for different types of motion: location sensors, speed sensors, and acceleration sensors. Monitoring motion and position is crucial for mechanical equipment. The TENG-based linear position sensors have been focussed and studied in detail. A micro-grated triboelectrification-based motion sensor with a displacement resolution of 173 nm and a linearity error of 0.02

percent has been reported (336). Due to the restrictions of their test motion, however, the development of single-dimensional motion sensors is limited, hence multi-dimensional motion sensors have been rapidly devised.

Han et al. (337) created a triboelectric trajectory tracking sensor with a resolution of 250 m. Planar multidimensional positioning sensors such as a multidimensional displacement vector sensor system (338) and a two-dimensional sensor (339) have been researched and multidimensional sensors with distinct functionalities (340) were developed. Multidimensional sensors have strengthened the mechanical motion detecting capabilities of TENGs.

Impact sensor is a very common and useful type of sensor which utilises the disturbance between the tribo-layers as input and convert it into electrical signals. The dominance of impact sensors is increasing day by day and have become an important component in automotive industry, aviation industry, building sectors, health monitors, fault detection in equipments etc.

Since the impact forces sustain for a very short period of time, detection of impact forces is found to be a difficult one. Recently, detection of impact forces was done with the help of TENG technology since the impact forces act as external stimulus for the functioning of TENGs (341). Vijoy et.al demonstrated a self - powered ultra- sensitive impact sensor with a sensitivity of 4.1 V/mJ using PDMS based triboelectric nanogenerator (342). He et.al reported a TENG based impact force monitor which is basically a 3D printed square grid which is filled with aluminium balls (343). Heo et.al studied about the direction of impact pulses by keeping the sensing material intact. This method has been implemented in detecting the car crashes (344). Sports industry demands the need for impact sensors since the detection of impact is important in order to identify the judgement of boundary, ball impact sensing, indication of foul movements etc (342). Since the impact forces last only for ultra-short time, sports industry utilises piezoelectric sensors (345), MEMS (346), accelerometric sensors (347), optical fibre

sensors (345) to record data and to monitor the movements. The intensity of impact force may be evaluated using TENG's output response. Monitoring the intensity of vibration is one of the most essential sensory aspects that may help us avoid calamities like as accidents, tsunamis, and earthquakes, among others. Several complex, expensive, and bulky devices for measuring impact force with better precision have been documented (348). The compact and lightweight TENG could offer a more effective method for measuring impact forces.

Using the ball drop approach, a PDMS/LSCO composite based impact sensor was designed for monitoring small energy impacts especially for sensing rain drops. The impact force derived from the output of the fabricated sensor found matching with the theoretical findings derived from the work energy theorem.

PDMS/LSCO based TENG which was developed as an impact sensor was made to work in dielectric-to-metal mode. The PDMS/LSCO layer was employed as an active triboelectric layer to create triboelectric charges. Top electrode was aluminium (Al) sheet and bottom electrode employed was copper. There is a wide difference between the work function of Al and the electron affinity of PDMS, which leads in the formation of a significant number of static charges when the two materials come into physical contact (349). The transport of electrons from Al to the PDMS/LSCO surface of the as-fabricated TENG is consistent with the electron-cloud-potential-well concept, which defines the charge transfer mechanism between metal and polymer occurs as a result of contact electrification (350). The impact sensitivity of developed TENG was assessed using the bead-drop experiment. In this procedure, a 0.1 g weighing bead with a 1.2 cm diameter was dropped into the device from heights of 5 cm to 40 cm in steps of 5 cm. The free-falling impact of a bead from various heights has promising results which influence energy in the increasing trend. Figure 5.6 depicts a schematic depiction of the experimental setup. The TENG-based impact sensor offers an output voltage as its

response. Due of the repeated bouncing and collisions of the bead, the output of TENG consist of a multitude of voltage peaks with each impact. The initial peak with greater amplitude corresponds to the direct hit from a specific height, while successive peaks indicate the subsequent bouncing of the bead. When the bead is dropped from a height of 40 cm onto TENG, output voltage peaked around 20 V and followed by rebounding as a result of maximum energy transfer. When the experiment was repeated by dropping the bead at a height of 5 cm onto the developed TENG sensor, the output obtained was ~4 V with subsequent rebounding of peaks. It is concluded that height is a prominent factor which influenced the output voltage of the PDMS/LSCO composite based impact sensors.

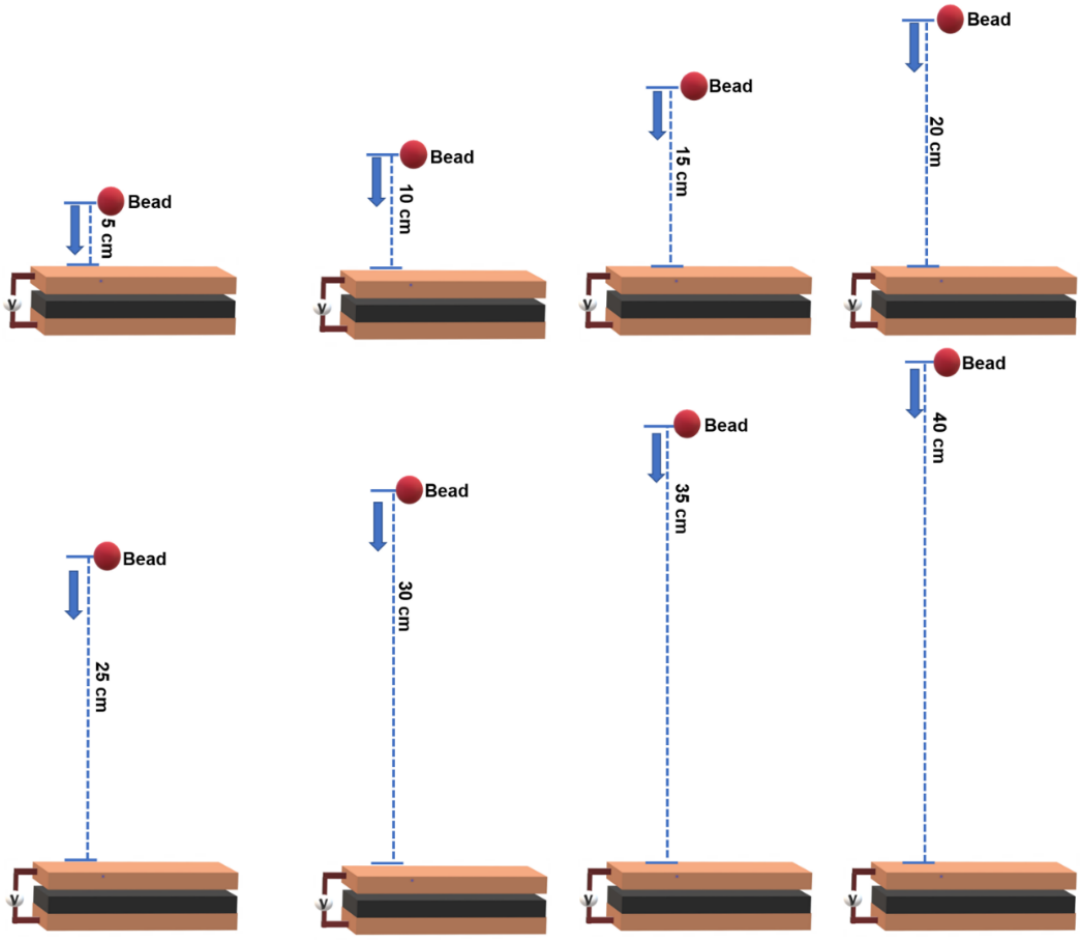

Figure 5. 6. Schematic diagram of free-falling bead onto PDMS/LSCO based TENG impact sensor from different heights.

Freely falling bead experiment is an illustration of law of conservation of energy. Potential energy before dropping of bead is found to be equal to kinetic energy just before the impact. Also, the kinetic energy possessed by the freely falling body result in inelastic collision from the top electrode of TENGs. A part of this energy is used up for the deformation of the target body and remaining part will be utilised for the recoiling of the object. Equation for energy conservation can be written as,

$$mgh = \frac{1}{2}mv^2 \qquad (5.1)$$

where *m* is the mass of the bead, *g* is the acceleration due to gravity, *h* represents the height level from where the bead is dropped and *v* denotes the impact velocity.

Thus, impact velocity can be calculated using the equation

$$v_{imp} = \sqrt{2gh} \qquad (5.2)$$

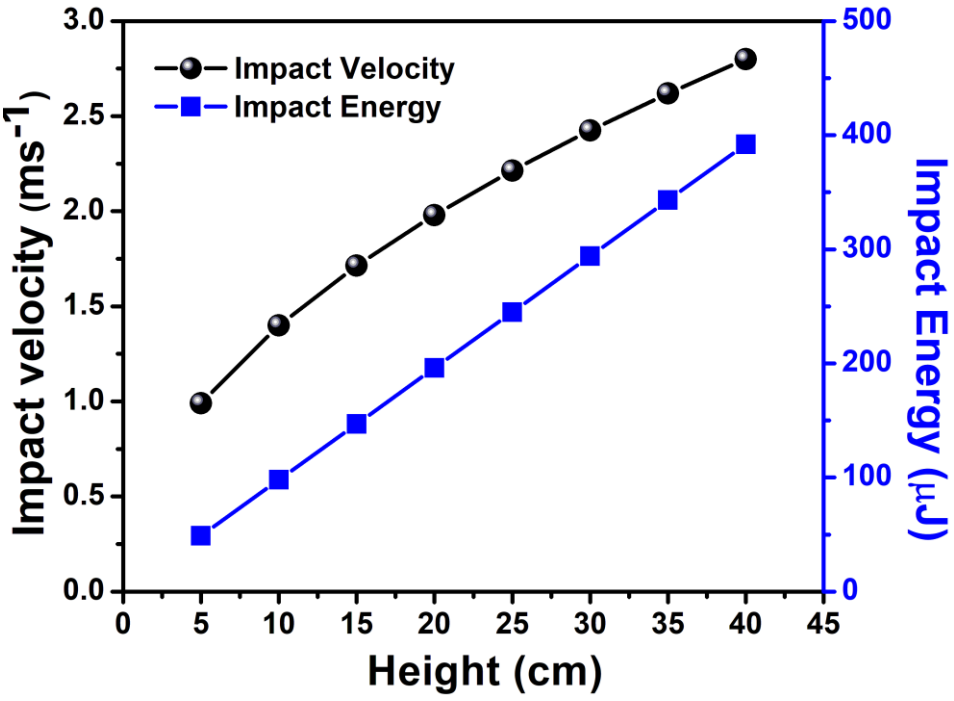

Figure 5. 7. Variation of impact energy and velocity of 0.1 g bead as function of height.

By utilising equations (5.1) and (5.2), the impact velocity and the energy of the bead are calculated from heights 5 cm to 40 cm as shown in the figure 5.7. These empirical results demonstrate that by increasing dropping height, the associated impact velocity and energy also rise. Typically, the impact force varies with the free-falling body's mass, the surface it strikes, and the impact energy. Using the work-energy theorem, the impact force could be determined.

$$\text{Work done} = (\text{K.E})_{\text{final}} - (\text{K.E})_{\text{initial}} \quad (5.3)$$

$$\text{Work done} = \frac{1}{2}mv_{final}^2 - \frac{1}{2}mv_{inital}^2 \quad (5.4)$$

$\boldsymbol{v_{initial}}$ denotes the initial velocity which is taken as zero and hence the net work done is given by $\boldsymbol{\frac{1}{2}mv_{final}^2}$

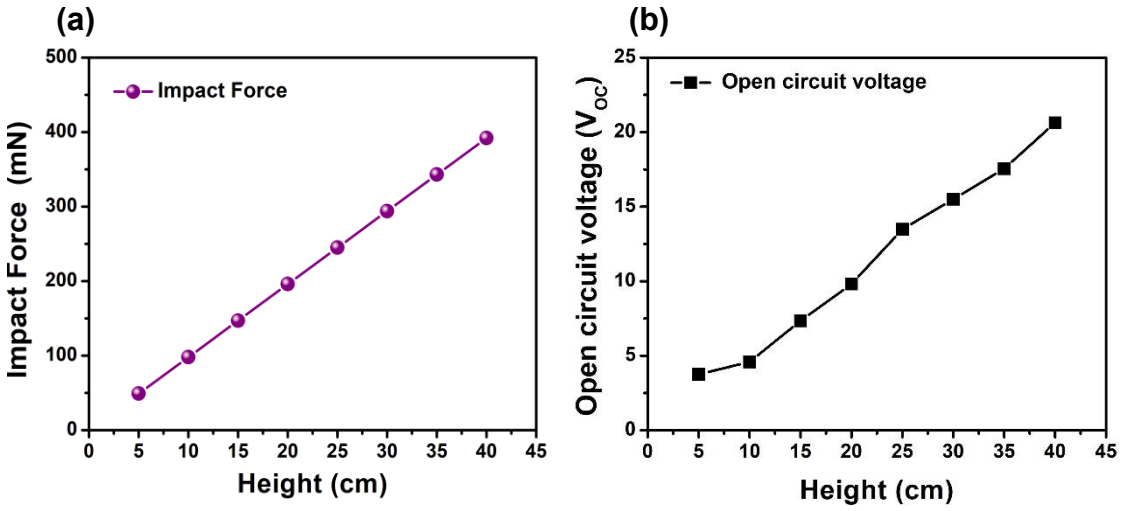

Figure 5. 8. (a) Calculated impact force as a function of height, and (b) the open circuit voltage of TENG impact sensor as a function of height.

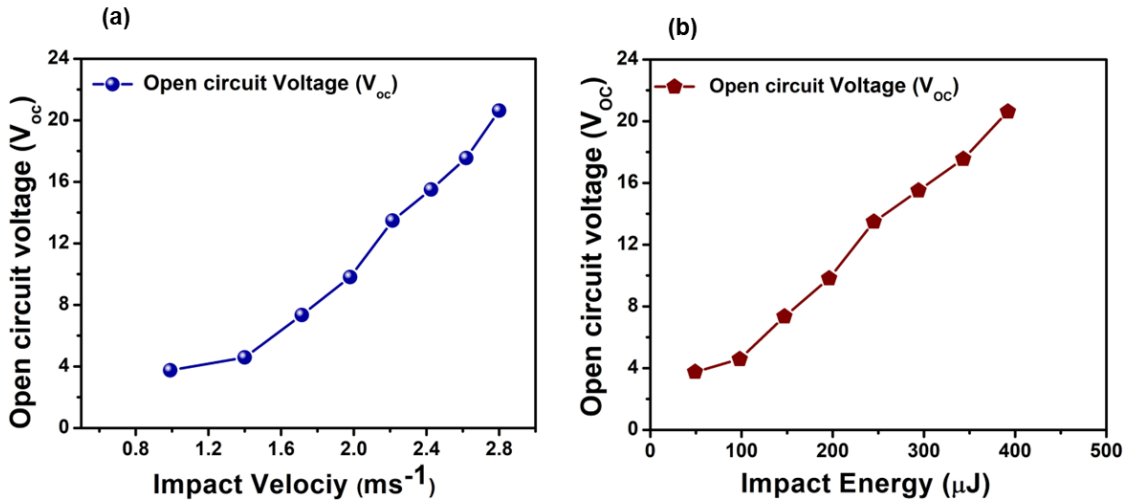

Figure 5. 9. (a) Calculated impact velocity and (b) the impact energy as function of open circuit voltage of TENG impact sensor.

Thus, the impact force is determined by the relation

$$F_{impact} = \frac{Work\ done}{d} = \frac{\frac{1}{2}mv_{final}^2}{d} = \frac{mgh}{d} \qquad (5.5)$$

Where *d* denotes the distance covered following an impact, which is inversely proportional to the impact force. For instance, the value of *d* in our TENG-based impact sensor is almost same and equals 1 mm, which is the thickness of the spacer between the surface of PDMS/LSCO composite and the top Al electrode. Using equation (5.5), the impact force was computed, and it was determined, as seen in Figure 5.8 (a), that the impact force increases with height. Figure 5.8 (b) depicts the open circuit voltage behavior of our manufactured TENG as a function of height.

Figure 5.9 shows the variation of impact velocity and impact energy with open circuit voltage. It is found that the output voltage increases linearly with height. From the experiment results, it is concluded that the impact force and output voltage of TENG has a direct dependence on dropping height. These studies ensure that the developed impact sensor using

PDMS/LSCO composite based TENG could measure impact force and can be made as rain sensor.

Rainfall is a highly frequently occurring process in nature and is an essential part of the water cycle of Earth. In addition, the energy contained in a single raindrop may be split into two distinct forms, making it a type of renewable energy source. The first is the kinetic energy, which is derived from the potential energy, and the second is the electrostatic energy, which is produced by the contact friction with the air and other dielectric substance. Both of these energies come from the potential energy (351). However, due of the limitations imposed by technology, their energy is not extracted properly. Numerous efforts based on TENG have made to harness raindrop energy by using triboelectric nanogenerators (TENGs), which are devices that use both the kinetic and electrostatic energy that raindrops create as they fall (352). Due to its fragmented nature, it is difficult to maximise the usage of this energy to its full potential. As the terminal velocity of rain drop is of the order of 10 ms^{-1} (353), the fabricated impact sensor could act as rain sensor.

5.4 Single electrode mode of LSCO/PDMS based TENG

Sustainable and flexible energy supply/storage technologies have been desperately needed in recent years to match improvements in flexible electronics (354, 355). The triboelectric nanogenerator (TENG) has evolved not only as an energy conversion technology (62), but also as a versatile framework for self-powered sensor systems and flexible/wearable devices. TENGs capture mechanical energy from the environment and transform it into electricity to power the integrated electronic devices directly via the triboelectric effect and electrostatic induction (356, 357). Mostly TENGs are made up of two electrodes that include two portions of triboelectric materials with differing triboelectric polarities for electric induction and establish a closed circuit for electron flow (182, 358). TENGs with such

sophisticated configurations necessitate a difficult operating mode and consumes more space, limiting their practical applicability. Single-electrode-based TENG approaches are becoming widely used in wearable electronics since they can be easily produced on flexible substrates using simple integration procedures that are inexpensive and highly efficient as far as portable objects are concerned. Because of its flexibility, simple one electrode construction, and ability to harvest mechanical energy from human motions opens the way for self-powered personal electronics.

A unique single-electrode TENG based on PDMS/LSCO composite was fabricated and its electrical characteristics were examined. This compact device was made up of simply one friction surface made of PDMS/LSCO composite and one induction electrode, copper electrode. When an active object makes contact with the PDMS/LSCO composite surface, the surface of the object becomes another triboelectric layer. By capturing mechanical energy from human movements, this PDMS/LSCO composite could create a significant amount of power.

The device developed in this study was single electrode based TENG (8 cm × 8 cm) which consists of copper as bottom electrode and PDMS/LSCO composites as negative tribo layer which was placed on the electrode. Bottom electrode was connected to ground. When touched by a human hand with a nitrile glove, the PDMS/LSCO composite based TENG produced electric energy.

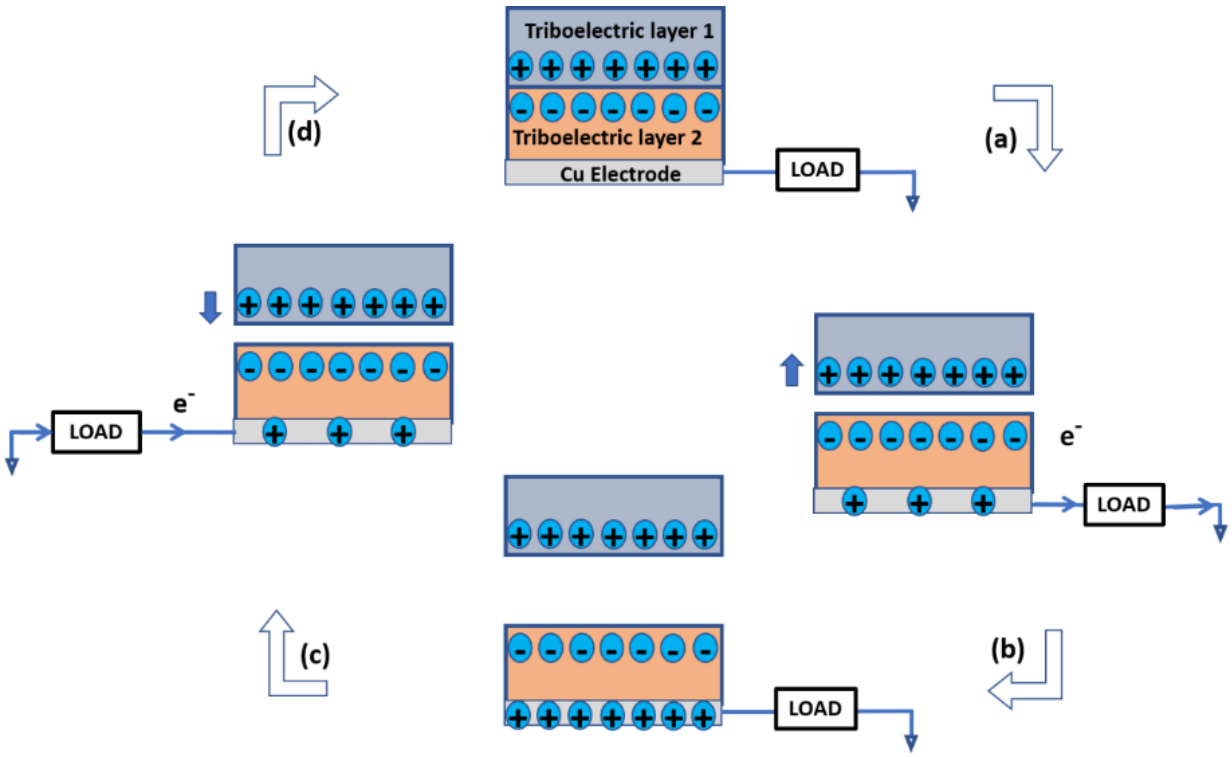

Figure 5. 10. Schematic diagram of mechanism of fabricated single electrode PDMS/LSCO composite based TENG.

Once the nitrile glove begins to detach from the PDMS/LSCO composite, it will be impossible to restore equilibrium due to the triboelectric charges. Positive charges on the copper electrode are induced as a result of the negative charges on the surface of the PDMS/LSCO composite, which creates an electrical equilibrium condition. Now, free electrons flow from the copper electrode to the ground as seen in figure 5.10 (b). When the nitrile glove moves away from the PDMS/LSCO composite, the negative charges on the surface of the PDMS/LSCO composite induces positive charges on the Cu electrode. No output signals are observed as the nitrile glove get completely separated from the PDMS/LSCO

composite (figure 5.10 c). The generated positive charges on the copper electrode will diminish when the nitrile glove returns to contact with PDMS/LSCO composite surface. Consequently, in figure 5.10 (d), free electrons flow from the ground electrode to the Cu electrode, producing a reversed output current signal. TENG system with single electrode PDMS/LSCO composite is restored to its original condition when the nitrile glove makes complete contact with the PDMS/LSCO composite for a second time after being removed. At this stage, TENG has completed a complete cycle of the power generating process.

Because of flexibility, simple one electrode structure, and ability to harvest mechanical energy from human motions, this PDMS/LSCO composite single electrode TENG could open up new opportunities for developing self-powered personal electronics. Tian et al. developed a flexible nanogenerator based on graphene oxide (GO) thin film, which worked in single electrode mode. Kim and his colleagues (359) have developed a flexible and transparent nanogenerator based on graphene 1-layer (L), 2-layer (L), 3-layer (L), and 4-layer (L).

Various topologies using a single electrode with contact separation mode have been developed by a number of different research groups (360). The rapidly developing TENG has been anticipated to be extremely competent, cost-effective, and the next generation device for harvesting of a wide range of mechanical energy sources. Figure 5.11 (a) shows the photograph of single electrode PDSM/LSCO composite based TENG prepared and (b) represent the schematic diagram of single electrode PDSM/LSCO composite based TENG.

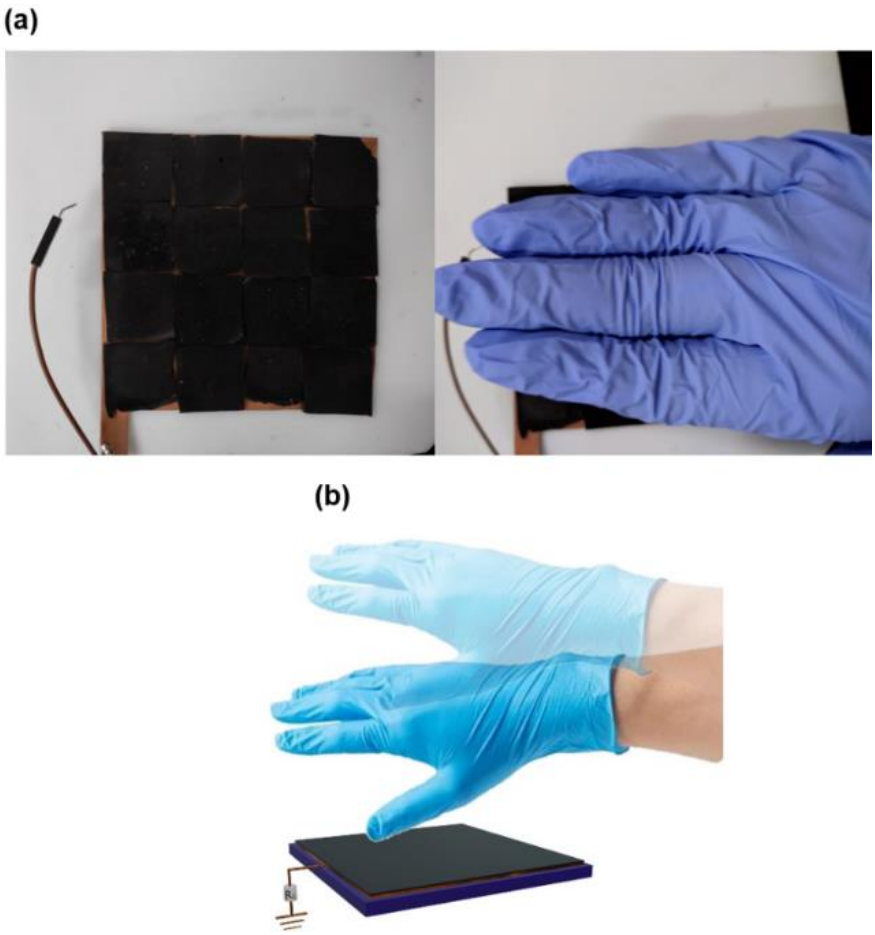

Figure 5. 11. Single electrode PDSM/LSCO composite based TENG. (a)Photograph of single electrode PDSM/LSCO composite based TENG. (b) Schematic representation of PDSM/LSCO composite based TENG.

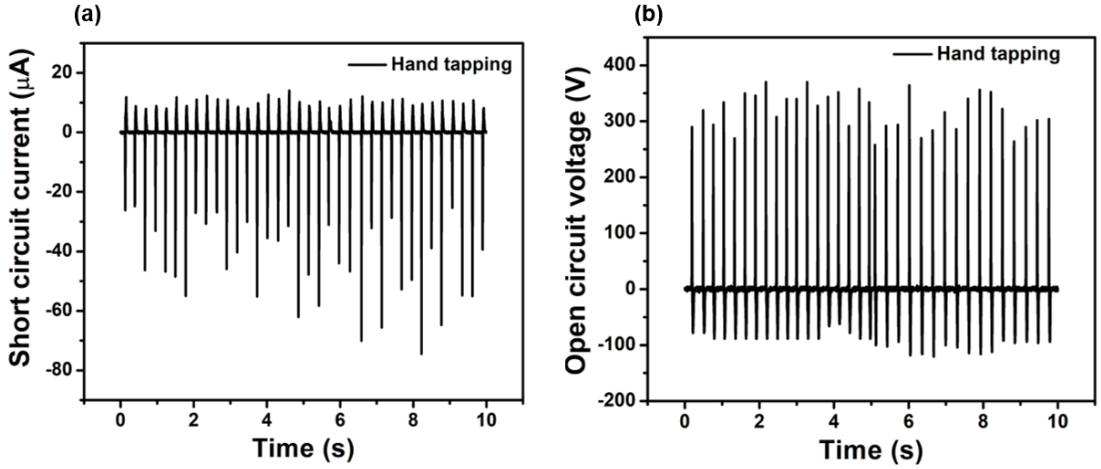

Figure 5. 12. Electrical characteristics of single electrode PDMS/LSCO composite based TENG (a)Short circuit current and (b) Open circuit voltage.

Figure 5.12 depicts the electrical characterization of single electrode PDMS/LSCO composite based TENG. An open circuit voltage (V_{oc}) of 352 V and short circuit current (I_{sc}) of 55 μA was achieved through hand tapping. This innovation opens up a lot of possibilities for constructing self-powered personal gadgets.

5.5 Conclusions

In this chapter, we have demonstrated a new structural design of 3D-TENG which was fabricated using vertically integrated PDMS/LSCO composite based TENG. This design improved the output of TENG by enhancing the frictional area and uses minimum space for energy production. In this integrated structure, all TENGs were connected in parallel so that enhanced output was extracted. Vertically stacked TENG should inspire further development of energy harvesting modules for self-powered mobile electronic systems such as wearable and implantable devices. Also, the output of PDMS/LSCO composite based TENG were used to power 25 LED lights implying the utilization of energy as a power source for electronic devices. Studies based on ball experiment opened the way for the usage of PDMS/LSCO based TENG as impact sensors which could be successfully incorporated to sense and measure impacts especially as a rain sensor. Such sensors could harness energies from these external impulses and generate electricity. Single electrode based TENG with PDMS/LSCO as tribolayer has been tried and as single electrode mode was very adaptive structure for portable devices. Developed TENG also could be a promising choice as a self-power unit for mobile gadgets. Advantages of single electrode based TENG could be efficiently utilized to trap human motions and generate electricity. Thus, these applications place TENG as an important new generation power source to pacify the energy demands of the electronic industry.

Chapter 6

Summary, Future Work and Recommendations

Abstract

This chapter briefs the summary of the work done so far and details about the work expected to be performed in future. Also, different possible applications of TENGs are explained. TENG has the potential to function as a very sensitive, self-powered sensor that can detect mechanical triggering and stimulations. The electric current and voltage signals that are produced by TENG reflect different types of information in relation to a mechanical action. The fact that such a sensor need not require a power supply to be driven will be a radical shift from the traditional sensors. Micromechanical systems, human-machine interfacing, touch-pad technology, security systems, and motion sensing are some of the sectors that find applications for this technology.

6.1 Introduction

Energy is one of the most essential resources, and there is a substantial demand for it from contemporary society because of the vital role it plays in determining the standard of living **(62)**. Issues related to the climate and diminishing fossil fuel supplies are driving society toward an energy transition, which may be one of the most difficult tasks civilizations has ever faced. As a result, there is a significant and growing need for alternative and renewable sources of energy that can be utilized on a big scale such as solar, wind, and hydropower. Recent technologies like wearable electronics, implantable medical devices, robotics, and artificial intelligence (AI), etc require new compact and efficient sources of energy (361). They are all expected to make substantial progress in the near future, which will likely result in a worldwide distribution of a large number of mobile electronics. This is prominently driven by the recent progress seen in the development of the internet of things (IoT), wireless sensor networks (WSN), microelectromechanical systems (MEMS), etc. Conventional external power sources, such as batteries, have a finite lifespan and need to be replaced on a regular basis. This is a challenge for a huge number of devices, and has to be addressed seriously.

During the course of the previous decade, there has, fortunately, been observed a steady reduction in both the size and the power requirements of integrated circuits to values that are lower than a few μW **(2)**. As a result, the idea of nano energy was conceived. This term refers to the application of nanomaterials and nanotechnology in the development of integrated power sources that are capable of harvesting many kinds of energy, such as light, thermal, and mechanical (362, 363). Because of this, several different kinds of nanogenerators (NG) have already been investigated, including those for self-powered industrial and health monitoring systems, smart housing and clothing, ambient intelligence, self-powered wearable electronics, intelligent traffic systems, vibration shock absorbers, wireless power transmitters, and so on **(7)**.

Compared to other types of electromagnetic generators, triboelectric nanogenerators have various benefits such as light weight, low density, low cost, greater adaptability, and the absence of heavy coils and magnets (364, 365). Triboelectric layers in flexible devices are usually made of soft substrates and polymers. For instance, PTFE (polytetrafluoroethylene), polyimide (PI), PET (poly ethylene terephthalate), and PDMS (poly-dimethyl siloxane) are commonly used tribo materials. In addition to its desirable qualities such as chemical inertness, conformability, and high flexibility, deposition process is very simple which could be carried out at room -temperature itself (366).

6.2 Advantages of TENGs

TENGs are known to be mechanically flexible, compact, economic, and readily scalable with low operation frequencies and huge bandwidths (367). Consequently, the TENG has a higher power density in terms of volume and weight ratios than its contemporaries. They make use of a wide variety of ordinary materials and requires a minimal number of materials because of the surface charging effect, which are ubiquitous and widely available. Self-powered portable/wearable electronics with regulated dimension and weight are beneficial for incorporating them into portable electronic equipments. For real world applications, production of TENGs is cost-effective due to its flexible and simple fabrication techniques.

Electromagnetic generators are well-known for their high frequency of operation, productivity, adaptability, durability, and efficiency even when applied to large scales. Additionally, their internal impedance can be controlled easily. Electrically, TENGs behave as low current sources with high parallel input impedance due to the electrostatic induction process as well as the nature of the dielectric-to-dielectric or dielectric-to-conductor interface. Nanogenerators often exhibit high output open-circuit voltages generally of 1–1000 V, low short-circuit currents (1–1000 μA), and internal impedance properties that are capacitive in nature. The practical uses of TENGs are currently restricted because of their high output

voltage and low current, as well as their vulnerability to wear, atmospheric humidity and temperature, and their small and fluctuating charge density on tribo-layers (368). Due to the electromagnetic induction process and the high conductivity of the coils, electromagnetic generators, on the other hand, act as low voltage sources with low series internal impedance. They usually have low output voltages (1–1000 mV), large currents (1–1000 mA), and internal impedance characteristics that are resistive and inductive in nature. Consequently, the two technologies are synergistic.

6.3 Objectives of present work

Main objective of the study was to improve the output performance of the TENGs fabricated by using polymer material as one of the tribo layer. As a result of the incorporation of fillers with the characteristics that are desired, the properties of the polymer can be tailored to accommodate the requirements. Dielectric engineering is the technique utilized to improve the output performance of the tribo layer. Poly dimethyl siloxane (PDMS) was the polymer matrix in which different conducting fillers as well as ceramic materials have been incorporated with an aim to improve the charge transfer ability of the polymer layer. The present study employs metal to dielectric mode in which copper electrode act as both electrode as well as positive tribo-layer while polydimethylsiloxane (PDMS) act as the negative-tribo layer. The metal/PDMS based TENGs as well as PDMS/LSCO based TENGs exhibited enhanced electrical characteristics as predicted by the theoretical studies.

In the case of metal/PDMS composite, different metals having different conductivity has been embedded into PDMS matrix which exhibited excellent results. The concentration of metals in the polymer matrix was varied from 0.5 wt% to 20 wt% in a systematic manner to examine the properties of the composite. The dielectric constant as well as the electrical conductivity increased monotonously as the weight percent of metals in the matrix was increased. This trend was reflected in the electrical performance of the TENG. It was found

advantageous to incorporate metals into the polymers as the flexibility of the composite can be preserved to some extent. Thus, with the inclusion of metals into the polymer matrix, the aim to improve the output of TENGs was successfully fulfilled.

Adding ceramics to the polymer matrix was yet another strategy that was utilised in an effort to increase the output performance of TENGs. This approach was employed as an alternate method to improve the dielectric constant of the composite. In the current study, $La_{0.8}Sr_{0.2}CoO_3$ (LSCO) was embedded with PDMS polymer matrix and as the weight percent of ceramic increased, the output performance of TENG was improved. The PDMS/LSCO composite based TENG demonstrated improvements in both its dielectric constant and its electrical characteristics as a result of the high ionic conductivity and dielectric constant of LSCO. PDMS/LSCO composites were made into 3D vertically integrated TENG which could act as self-powered units and was incorporated into a circuit of a smart watch. This illustrated the capability of the fabricated TENG to act as a power source to drive personal and smart electronic gadgets. Also output of TENG made out of PDMS/LSCO composite was used to lite light emitting diodes and also utilized to charge different capacitors. Apart from vertical-contact mode of TENG, single electrode mode was also tried using PDMS/LSCO composite as negative tribo layer and copper sheet as positive tribo layer. This attempt was done to examine the peculiarities of single electrode mode based TENG. The results suggest that different modes could be tried beside vertical-contact separation mode so as to explore the merits and demerits of concerned modes. The researcher would therefore be able to design TENGs of an acceptable mode that are suited for a variety of applications.

6.4 Summary of present work

Table 6. 1.Summary of the parameters investigated for 20 wt% of conducting fillers introduced in to the PDMS matrix

(20wt%)	Pure PDMS	Silver	Copper	Aluminium	Zinc	Tin	LSCO
Short circuit current (μA)	0.5	5.1	3.9	4.2	3.3	3.03	3.5
Open circuit voltage (V)	2.6	33.6	30.6	32.2	25.5	24.6	23. 8
Dielectric constant @1 kHz	5.3	16.9	14.9	14.8	13.0	12.2	17.7
Power (μW)		72.2	37.6	42.3	32.5	14.7	29.4
Stored Charge (μC)		28.4	18.6	14.2	10.2	11	8.76
Stored Energy (mJ)		1.8	1.6	1.0	0.7	0.6	0.94

Main parameters focused during this study were dielectric constant, short circuit current (I_{sc}), open circuit voltage (V_{oc}), maximum power (P) and stored energy (E). Pure PDMS has a dielectric constant of 5.3 when tested at 1 kHz, with a short circuit current (I_{sc}) of 0.5 μA and an open circuit voltage (V_{oc}) of 2.6 V. When fillers such as metal nanoparticles and LSCO ceramic were added to the polymer matrix, the composite exhibited proportional modifications in its characteristics. Table 6.1 summarizes the parameters examined when different fillers were added to the polymer matrix. Compared to the qualities of pure polymer, the polymer composites exhibited improved performance. Table 6.1 demonstrates that as fillers are introduced into the PDMS matrix, the characteristics of resultant polymer composites are modified to improve the properties of PDMS in order to meet the requirement of enhanced

output performance. The Silver/PDMS composite showed the highest values for all of the criteria when compared to the other fillers.

The primary purpose of this work was to develop and expand the applicability of triboelectric nanogenerators, which involves utilizing different fundamental working mode, functional material fabrication, and application-directed device design for mechanical energy harvesting. The concept and design elaborated in this thesis can significantly advance the development of TENG as sustainable power sources and self-powered active sensors.

6.5 Future scope and recommendations

Self-powered implantable and wearable electronic devices become an indispensable part of electronic industry, especially with the introduction of Internet of Things (IoT) technology. Triboelectric devices are a promising energy harvester for self-powered wearable devices associated with various sorts of applications, as the triboelectric effect is one of the most commonly seen phenomena in daily life. Despite the fact that triboelectric devices with excellent output performances have been constructed using device architectures with combined operating modes (369, 370), it is important to improve the output performance of multiple devices. Till now, studies have mostly concentrated on the production of triboelectric pair materials (mostly negative triboelectric materials), whereas dielectric tribo-materials have received less attention. As dielectric materials have the capacity to boost triboelectric performances based on the relationship between the surface charge density and dielectric constant, the advent of triboelectric materials based on various polarization strategies could facilitate the generation of high-powered portable devices.

Due to the fact that a plethora of high-k dielectric materials have been fostered by regulating the structural component (371) or chemical doping (372), there are a number of potential possibilities for boosting the dielectric constant of polymer composites. In addition,

the surface treatment of dielectric nanomaterials for proper dispersion into the polymer matrix (373) and the regulation of the dielectric framework such as preparation of heterostructure multilayer composite materials are tried (374). Studies have been reported where dielectric composites with oriented conductive materials embedded into polymer matrix with an aim to boost the dielectric properties of polymer matrix (375). However, in triboelectric devices, few methods have been employed to improve its output performance. The high adaptability or integration of additives in the polymer matrix will provide an increase in the interfacial area or a subsequent decrease in the leakage current, leading to an improvement in the dielectric constant as well as output performance.

As far as dielectric polarization is concerned, an electric poling method could promote dipole realignment in a high electric field. This method is yet another way that can be used to increase the dielectric constant, which therefore permits the improvements in triboelectric performances **(376)**. Currently, self-poling approaches have been implemented in piezoelectric generators to effectively enhance ferroelectric properties via the shear-induced process **(377)**, but the output performance is still lower than that of triboelectric generators. When paired with dielectric polarization and self-poling in dielectric composites, the process has the potential to have a beneficial effect that greatly improves the dielectric constant. This, in turn, can lead to a notable improvement in triboelectric performances.

The majority of research has concentrated on studying materials with a negative triboelectric in nature. Since triboelectric performance results from the contact electrification that occurs between positive and negative triboelectric layers, the triboelectric materials with positive polarity are also an essential component in the process of improving output performances. Polarization-induced triboelectric pair materials have the potential to accelerate the production of triboelectric devices with substantially improved output performances. This

opens the door for practical applications that requires a significant amount of output power, such as smart wearable devices and portable IoT devices.

Exploring TENGs in ways other than conventional solid contact pairs is an exciting area of research with many opportunities and challenges. Understanding the basic physics and chemistry of these TENGs could change the way devices are designed right now. Simultaneous sensible correlation with experimental data is essential and helps to navigate the most important factors that affect the performance of TENGs. Triboelectric nanogenerators (TENGs) feature four different modes of operation that may be utilized to collect triboelectricity from contact electrification. But, the primary focus of the research being done currently is on improving the output performance of TENGs that employ the contact-separation mode. Very few reports describe enhancements achieved to sliding mode, single electrode mode, and freestanding mode TENGs by employing various modification strategies. Different TENG operation modes may respond differently to a given modification approach. Modifying TENGs with additional operation modes may need extra factors. Sliding-mode TENGs need some more durable structures to withstand cyclic mechanical wear. It's vital to research TENG modification approaches based on various operating modes comprehensively. Due to different contact behaviors in TENGs with different operating modes, nanostructures and microstructures need to be altered to improve TENG performance.

The triboelectric nanogenerator's performance may be improved in numerous ways from a material perspective. In this approach, the chemist and the material scientist may come up with new ways to identify the most suitable material and its composites for a certain application (150). Surface functionalization and morphologies are introduced in recent TENGs to vary the chemical property of a triboelectric material, depending on which chemical property

get tailored. These modifications also represent an increase in charge transfer density. As a result, the output power of constructed TENG could be increased by several tens of mW (131).

6.6 Challenges faced by TENGs

Even though TENGs are being implemented as modern power sources, there are many challenges which have to be addressed in detail, in future studies.

a) Efficiency of energy conversion is the prominent parameter for TENGs are concerned. The energy harvesting abilities of TENGs are not yet adequate to constantly power the majority of traditional electronic devices. It is found that output power rises proportionally with the square of the triboelectric surface charge density and hence it is crucial that this quantity has to be increased. A viable technique is establishing control over ambient factors such as temperature and air pressure in order to raise the surface charge density and the dielectric breakdown voltage (152).

b) In order to power electronic devices, it is also necessary to convert pulsating electrical outputs into steady DC. Using traditional rectifiers and transformers results in considerable energy losses. Hence employment of sophisticated power management technologies are important (185).

c) Stability and durability of TENGs pose another challenge as real-life applications demand stable and efficient materials as well as gadgets. This issue is prominent for lateral-sliding mode where high-friction is important for efficient output of TENGs.

d) Packaging of TENGs is very important since their performance is extremely dependent on humidity and temperature. Thus, good wrapping techniques for devices with moving mechanical parts are essential to provide a complete isolation from water (378). Elevating the working temperature of the devices may also be beneficial for improving the performance.

e) Unstable electrical outputs necessitate the storage of energy. The problem of leakage in supercapacitors must be improved, and new Li-ion battery designs must be evaluated (379).

f) Broader bandwidths of input frequencies and amplitudes are advantageous. This may be accomplished, by periodic tuning of the resonant frequency, mechanical halting techniques, and nonlinear springs or bi-stable structures (380). Low frequencies and smaller displacements of excitations are related to lesser input powers.

g) A deeper knowledge about the mechanism of energy conversion and its relationship to environmental circumstances is important for optimizing the harvesters' performance. Experimental techniques such as atomic force microscopy and Kelvin probe microscopy (381) and theoretical quantum tools have to be developed in order to improve the knowledge behind the triboelectric effect and contact electrification phenomenon. New approaches to precisely quantify the surface charge density and its relationship to the dielectric characteristics as well as to surface morphology of the materials are much desired. A revised triboelectric series might be useful for guiding material selection. Development of new computer models to anticipate the electromechanical output for realistic irregular three-dimensional movements of combination hybrid harvesters are well appreciated.

h) Quantitative testing guidelines should be used for analyzing and evaluating the performance of manufactured TENG prototypes (382), as testing circumstances in the literature vary substantially. Information about the average value of output power or efficiency is more recommended than presenting the instantaneous peak values of electrical parameters. It is necessary to supply values for the amplitudes of the input displacement, acceleration, or force.

i) It is important to establish pragmatic designs in order to integrate systems with a variety of dynamic configurations. In addition to the device structures, evaluation is necessary

about the competitiveness of hybrid nanogenerators in the energy market. Economic studies need to be carried out to determine the cost of production and management of these devices.

j) It is important to investigate the possibility of miniaturizing TENGs for the purpose of incorporating them with wearable devices or into novel bioelectronic medical equipment (383). It is feasible to anticipate that individual small scale power generators will have low output powers; however, it is theoretically possible for many arrays of similar devices to provide good results.

The enumerated challenges could open up a wide variety of possibilities for the creation of novel triboelectric nanogenerators and could anticipate a substantial expansion of this sector during the coming decade.

6.7 Future Applications

A few applications of TENGs as an energy source and self-powered sensors are demonstrated in this thesis**.** By monitoring the change in the TENG's output signal, it is possible to quantify the different forms of vibrations caused by diverse surroundings for the self-powered sensors. In addition, because the output signal of TENG itself is a detecting signal, an additional power supply is unnecessary. In the case of TENGs used for gathering wind energy, different configurations have been developed based on the vast selection of materials that are now accessible. Since the tribolayer developed in this research work is flexible, it is a suitable application for future study.

Acoustic energy, which includes voice, music, and even noise, has been overlooked as a source of electricity. Scientists and technologists have long been fascinated by sound-to-electricity conversion. As a result, developing a realistic approach for collecting acoustic energy from the ambient environment and developing an acoustic sensor could be a future scope of work. Blue energy harvesting is yet another application where several models have been designed to capture water-based energy. In the current work, an attempt has been made

to fabricate prototype of rain sensor and hence other regimes of blue energy harvesting is a good opening for future work. In addition to harnessing ubiquitous energy from the environment and providing power to electronic devices, the TENG functions as a self-powered sensor unit. TENGs produce electrical impulses when stimulated by an external mechanical energy source, such as mechanical touching, pressing, or item movement. The induced mechanical energy can be identified based on the amplitude and profile of the TENG's electrical output signal.

As the output amplitude of the TENG has a strong correlation with the contact pressure, such that the contact pressure may be calculated from the output amplitude. In addition, the TENG is capable of identifying particular substances, as certain molecules can alter the output signals. Consequently, the TENG can serve as a sensor in the chemical and biological areas if properly calibrated. TENG-based sensor does not require an additional actuator capable of converting a non-electrical input signal to an electrical output signal because the TENG always provides an electrical signal. Fabrication of TENG-based sensor is simple and requires neither a complex production technique nor an expensive material. Moreover, TENGs can be made in an appropriate form for the intended application, allowing its easy implementation in a variety of disciplines.

TENGs creates electrical signals based on electrostatic induction in response to changes in the relative position of surfaces induced by external mechanical excitations, such as touch. By monitoring the TENG's electrical output, a touch on the TENG can be easily recognized.

Essential component of robot perception is displacement sensors which are utilized in a variety of situations. Displacement sensors are necessary for both the motion feedback and awareness of the robot's external surroundings. The displacement sensor primarily measures linear displacement, rotational displacement, and gathers information about dynamic

acceleration in the direction of the motion. By utilizing the sliding mode or single electrode mode of TENGs, a displacement sensor can be fabricated with good performance which is an essential component in many of the robotic gadgets. Additionally, TENG can be employed as a motion or trajectory sensor. A mechanical motion can be characterized by a combination of factors including displacement, velocity, and acceleration. Therefore, these factors must be monitored correctly for a moving body. TENGs are able to generate power via linear, sliding, rotational, and rolling motions. TENGs are self-powered motion sensors because the frequency and intensity of the electric signals are directly dependent on the strength of the input mechanical vibrations. Vibration is a unique sort of mechanical motion found nearly everywhere in engines, buildings, aircraft, and infrastructures, and it indicates the operational status of machineries. Using vibration-induced periodic contact and separation of two triboelectric surfaces, a contact-mode TENG may collect both vibration energy and detect the magnitude, frequency, and location of a vibration source.

The triboelectric charge density created on the material surface by contact electrification is a crucial factor in determining the output performance of a TENG. The surface modification of specific chemical groups and the modifications of atmospheric conditions will have a significant impact on the triboelectric charge density and, consequently, the output power. A well-built TENG can therefore function as a self-powered chemical and environmental sensor for sensing ion concentration, UV irradiation, humidity, etc. by monitoring the change in its output performance.

Since there are numerous applications possible for TENGs, future work can be focused on applications such as displacement sensor, velocity sensor, acoustic sensor, touch sensor etc. These sensors can be easily integrated with TENGs so that a self-powered system can be devised for all electronic equipments. In low-power electronic systems, self-powered sensors offer a number of benefits that are unmatched by other types of sensors. It is of the utmost

importance that low power electronic devices optimize their self-powered sensors in order to improve the energy conversion efficiency of their gadgets. It is a fact that TENG sensors will be utilized in real-world or even commercial applications, there have a great deal of applications in day today life.

6.8 Conclusions

TENGs are capable of successfully harvesting electrical energy from low-frequency of the order of 1 Hz and low-amplitude of around 5 mm mechanical vibrations resulting in high output voltages. Utilizing the contact electrification and electrostatic induction, a triboelectric nanogenerator generates electricity. It offers a viable method for harvesting mechanical energy in many forms, such as impact, vibration, sliding, and rotation, among others. It has the potential to become a sustainable power source for tiny electronics and perhaps a solution for large-scale energy production. TENG represents a significant step forward in the development of energy harvesting technologies, making it possible to build self-powered systems that are really sustainable and require minimum maintenance. It is reasonable to foresee that through the efforts of people all over the world working on TENGs as a sustainable power source, they will soon be made into commercialized products for use in a variety of applications, including the Internet of Things, mobile electronics, self-powered e-skins, fabric electronics, medical/health monitoring, and ecological sustainability.

REFERENCES

1. Wang ZL. Triboelectric Nanogenerators as New Energy Technology for Self-Powered Systems and as Active Mechanical and Chemical Sensors. ACS Nano. 2013;7(11):9533-57.
2. Otis B, Rabaey J. Wireless Sensor Networks. US: Springer; 2007.
3. Soares dos Santos MP, Coutinho J, Marote A, Sousa B, Ramos A, Ferreira JAF, et al. Capacitive technologies for highly controlled and personalized electrical stimulation by implantable biomedical systems. Scientific Reports. 2019;9(1):5001.
4. Priya S, Song H-C, Zhou Y, Varghese R, Chopra A, Kim S-G, et al. A Review on Piezoelectric Energy Harvesting: Materials, Methods, and Circuits Energy Harvesting and Systems. 2017;4(1):3-39.
5. Fernández-Caramés TM, Fraga-Lamas P. Towards the Internet of smart clothing: A review on IoT wearables and garments for creating intelligent connected e-textiles. Electronics. 2018;7(12):405.
6. Lim HR, Kim HS, Qazi R, Kwon YT, Jeong JW, Yeo WH. Advanced soft materials, sensor integrations, and applications of wearable flexible hybrid electronics in healthcare, energy, and environment. Advanced Materials. 2020;32(15):1901924.
7. Romero E, Warrington RO, Neuman MR. Energy scavenging sources for biomedical sensors. Physiological Measurement. 2009;30(9):R35-R62.
8. Matiko JW, Grabham NJ, Beeby SP, Tudor MJ. Review of the application of energy harvesting in buildings. Measurement Science and Technology. 2013;25(1):012002.
9. Pu X, Hu W, Wang ZL. Toward wearable self-charging power systems: the integration of energy-harvesting and storage devices. Small. 2018;14(1):1702817.
10. Beeby SP, Tudor MJ, White NM. Energy harvesting vibration sources for microsystems applications. Measurement Science and Technology. 2006;17(12):R175-R95.
11. Singh HH, Khare N. Improved performance of ferroelectric nanocomposite flexible film based triboelectric nanogenerator by controlling surface morphology, polarizability, and hydrophobicity. Energy. 2019;178:765-71.
12. Liu W, Song MS, Kong B, Cui Y. Flexible and stretchable energy storage: recent advances and future perspectives. Advanced materials. 2017;29(1):1603436.
13. Sharma K, Arora A, Tripathi SK. Review of supercapacitors: Materials and devices. Journal of Energy Storage. 2019;21:801-25.
14. Whittingham MS. Ultimate limits to intercalation reactions for lithium batteries. Chemical reviews. 2014;114(23):11414-43.
15. Lee TD, Ebong AU. A review of thin film solar cell technologies and challenges. Renewable and Sustainable Energy Reviews. 2017;70:1286-97.
16. Wang J, Liu S, Li L. Experiments and modeling on thermoelectric power generators used for waste heat recovery from hot water pipes. Energy Procedia. 2019;158:1052-8.
17. Zeng W, Shu L, Li Q, Chen S, Wang F, Tao XM. Fiber-based wearable electronics: a review of materials, fabrication, devices, and applications. Advanced materials. 2014;26(31):5310-36.
18. Pu X, Hu W, Wang ZL. Toward wearable self-charging power systems: the integration of energy-harvesting and storage devices. Small. 2018;14(1):1702817.
19. Cai F, Chen T, Peng H. All carbon nanotube fiber electrode-based dye-sensitized photovoltaic wire. Journal of Materials Chemistry. 2012;22(30):14856-60.
20. Sebald G, Guyomar D, Agbossou A, Structures. On thermoelectric and pyroelectric energy harvesting. Smart Materials. 2009;18(12):125006.
21. Lou Z, Li L, Wang L, Shen G. Recent progress of self-powered sensing systems for wearable electronics. Small. 2017;13(45):1701791.
22. Nozariasbmarz A, Collins H, Dsouza K, Polash MH, Hosseini M, Hyland M, et al. Review of wearable thermoelectric energy harvesting: From body temperature to electronic systems. Applied Energy. 2020;258:114069.
23. Bell LE. Cooling, heating, generating power, and recovering waste heat with thermoelectric systems. Science advances. 2008;321(5895):1457-61.
24. Vasel-Be-Hagh A, Archer CL. Wind farms with counter-rotating wind turbines. Sustainable Energy Technologies Assessments. 2017;24:19-30.

25. Al-Hamidi H, Al Asfar J. Hybrid renewable energy system with minimum noise wind turbine. Renewable Energy. 2017;114:581-7.
26. Selvan KV, Ali MSM. Micro-scale energy harvesting devices: Review of methodological performances in the last decade. Renewable Sustainable Energy Reviews. 2016;54:1035-47.
27. Bowen CR, Taylor J, LeBoulbar E, Zabek D, Chauhan A, Vaish R. Pyroelectric materials and devices for energy harvesting applications. Energy Environmental Science. 2014;7(12):3836-56.
28. Sampaio PGV, González MOA. Photovoltaic solar energy: Conceptual framework. Renewable Sustainable Energy Reviews. 2017;74:590-601.
29. Zi Y, Wang ZL. Nanogenerators: An emerging technology towards nanoenergy. Aplied Materials. 2017;5(7):074103.
30. Wang J, Li Y, Zhao C, Cai Y, Zhu L, Zhang C, et al. An optimization study of structural size of parameterized thermoelectric generator module on performance. Energy Conversion Management. 2018;160:176-81.
31. Hadas Z, Janak L, Smilek J. Virtual prototypes of energy harvesting systems for industrial applications. Mechanical Systems Signal Processing. 2018;110:152-64.
32. Sultana A, Alam MM, Middya TR, Mandal D. A pyroelectric generator as a self-powered temperature sensor for sustainable thermal energy harvesting from waste heat and human body heat. Applied Energy. 2018;221:299-307.
33. Hunter SR, Lavrik NV, Mostafa S, Rajic S, Datskos PG, editors. Review of pyroelectric thermal energy harvesting and new MEMs-based resonant energy conversion techniques. Energy Harvesting and Storage: Materials, Devices, and Applications III; 2012; United States: International Society for Optics and Photonics.
34. Truitt A, Mahmoodi SN. A review on active wind energy harvesting designs. International Journal of Precision Engineering. 2013;14(9):1667-75.
35. Wang ZL, Jiang T, Xu L. Toward the blue energy dream by triboelectric nanogenerator networks. Nano Energy. 2017;39:9-23.
36. Ylli K, Hoffmann D, Willmann A, Becker P, Folkmer B, Manoli Y, et al. Energy harvesting from human motion: exploiting swing and shock excitations. Smart Materials. 2015;24(2):025029.
37. Choi J, Jung I, Kang C-Y. A brief review of sound energy harvesting. Nano energy. 2019;56:169-83.
38. Beeby SP, Torah R, Tudor M, Glynne-Jones P, O'donnell T, Saha C, et al. A micro electromagnetic generator for vibration energy harvesting. Journal of Micromechanics microengineering. 2007;17(7):1257.
39. Wang X. Piezoelectric nanogenerators—Harvesting ambient mechanical energy at the nanometer scale. Nano Energy. 2012;1(1):13-24.
40. Wang ZL, Lin L, Chen J, Niu S, Zi Y. Triboelectric nanogenerator: single-electrode mode. Triboelectric Nanogenerators. NewYork City: Springer; 2016. p. 91-107.
41. Wang ZL. On Maxwell's displacement current for energy and sensors: the origin of nanogenerators. Materials Today. 2017;20(2):74-82.
42. Wang ZL. Self-Powered Nanosensors: Self-Powered Nanosensors and Nanosystems Advanced Materials. 2012;24(2):279-.
43. Shen D, Park J-H, Noh JH, Choe S-Y, Kim S-H, Wikle III HC, et al. Micromachined PZT cantilever based on SOI structure for low frequency vibration energy harvesting. Sensors and actuators A: physical. 2009;154(1):103-8.
44. Dong K, Peng X, Wang ZL. Fiber/fabric-based piezoelectric and triboelectric nanogenerators for flexible/stretchable and wearable electronics and artificial intelligence. Advanced Materials. 2020;32(5):1902549.
45. Wu C, Wang AC, Ding W, Guo H, Wang ZL. Triboelectric nanogenerator: a foundation of the energy for the new era. Advanced Energy Materials. 2019;9(1):1802906.
46. Suzuki Y, Miki D, Edamoto M, Honzumi M, Microengineering. A MEMS electret generator with electrostatic levitation for vibration-driven energy-harvesting applications. Journal of Micromechanics. 2010;20(10):104002.
47. Chen J, Wang ZL. Reviving vibration energy harvesting and self-powered sensing by a triboelectric nanogenerator. Joule. 2017;1(3):480-521.

48. Waterbury AC, Wright PK. Vibration energy harvesting to power condition monitoring sensors for industrial and manufacturing equipment. Proceedings of the Institution of Mechanical Engineers, Part C: Journal of Mechanical Engineering Science. 2013;227(6):1187-202.
49. Chung T-K, Yeh P-C, Lee H, Lin C-M, Tseng C-Y, Lo W-T, et al. An attachable electromagnetic energy harvester driven wireless sensing system demonstrating milling-processes and cutter-wear/breakage-condition monitoring. Sensors. 2016;16(3):269.
50. Fan F-R, Tang W, Yao Y, Luo J, Zhang C, Wang ZL. Complementary power output characteristics of electromagnetic generators and triboelectric generators. Nanotechnology. 2014;25(13):135402.
51. Petrini F, Gkoumas K. Piezoelectric energy harvesting from vortex shedding and galloping induced vibrations inside HVAC ducts. Energy Buildings. 2018;158:371-83.
52. Nesser H, Debeda H, Yuan J, Colin A, Poulin P, Dufour I, et al. All-organic microelectromechanical systems integrating electrostrictive nanocomposite for mechanical energy harvesting. Nano Energy. 2018;44:1-6.
53. Dhakar L. Triboelectric devices for power generation and self-powered sensing applications. NewYork City: Springer; 2017.
54. Zhang Y, Wang T, Luo A, Hu Y, Li X, Wang F. Micro electrostatic energy harvester with both broad bandwidth and high normalized power density. Applied energy. 2018;212:362-71.
55. Park K-I, Son JH, Hwang G-T, Jeong CK, Ryu J, Koo M, et al. Highly-Efficient, Flexible Piezoelectric PZT Thin Film Nanogenerator on Plastic Substrates. Advanced Materials. 2014;26(16):2514-20.
56. Valarmathi M, Ganesan J, Dharaneeswari J, Sindhu A. Studies on Energy Density Enhancement of Supercapacitors by using Nanostructure Materials. International Journal of Solid State Materials. 2020;6(1):8-16.
57. Kagan CR, Fernandez LE, Gogotsi Y, Hammond PT, Hersam MC, Nel AE, et al. Nano Day: Celebrating the Next Decade of Nanoscience and Nanotechnology. ACS Nano. 2016;10(10):9093-103.
58. Wang ZL, Song J. Piezoelectric Nanogenerators Based on Zinc Oxide Nanowire Arrays. Science. 2006;312(5771):242-6.
59. Fan F-R, Tian Z-Q, Lin Wang Z. Flexible triboelectric generator. Nano Energy. 2012;1(2):328-34.
60. Gordon DH. Triboelectric interference in the ECG. IEEE Transactions on Biomedical Engineering; NewYork City: IEEE; 1975. p. 252-5.
61. Weiss PS. A Conversation with Prof. Zhong Lin Wang, Energy Harvester. ACS Nano. 2015;9(3):2221-6.
62. Wang ZL, Chen J, Lin L. Progress in triboelectric nanogenerators as a new energy technology and self-powered sensors. Energy & Environmental Science. 2015;8(8):2250-82.
63. Zhu G, Pan C, Guo W, Chen C-Y, Zhou Y, Yu R, et al. Triboelectric-Generator-Driven Pulse Electrodeposition for Micropatterning. Nano Letters. 2012;12(9):4960-5.
64. Zhu G, Peng B, Chen J, Jing Q, Wang ZL. Triboelectric nanogenerators as a new energy technology: from fundamentals, devices, to applications. Nano Energy. 2015;14:126-38.
65. Williams MW. Triboelectric charging of insulating polymers–some new perspectives. AIP Advances. 2012;2(1):010701.
66. Lowell J. Contact electrification of metals. Journal of Physics D: Applied Physics. 1975;8(1):53.
67. Harper W. The Volta effect as a cause of static electrification. Proceedings of the Royal Society of London Series A Mathematical Physical Sciences. 1951;205(1080):83-103.
68. Matsusaka S, Maruyama H, Matsuyama T, Ghadiri M. Triboelectric charging of powders: A review. Chemical Engineering Science. 2010;65(22):5781-807.
69. Lowell J, Truscott W. Triboelectrification of identical insulators. II. Theory and further experiments. Journal of Physics D: Applied Physics. 1986;19(7):1281.
70. Fabish TJ, Duke CB. Molecular charge states and contact charge exchange in polymers. Journal of Applied Physics. 1977;48(10):4256-66.
71. McCarty LS, Whitesides GM. Electrostatic charging due to separation of ions at interfaces: contact electrification of ionic electrets. Angewandte Chemie International Edition. 2008;47(12):2188-207.
72. Diaz A. Contact electrification of materials: the chemistry of ions on polymer surfaces. The Journal of Adhesion. 1998;67(1-4):111-22.
73. Mizes H, Conwell E, Salamida D. Direct observation of ion transfer in contact charging between a metal and a polymer. Applied physics letters. 1990;56(16):1597-9.

74. McCarty LS, Winkleman A, Whitesides GM. Ionic electrets: electrostatic charging of surfaces by transferring mobile ions upon contact. Journal of the American Chemical Society. 2007;129(13):4075-88.
75. Zimmermann R, Dukhin S, Werner C. Electrokinetic measurements reveal interfacial charge at polymer films caused by simple electrolyte ions. The Journal of Physical Chemistry B. 2001;105(36):8544-9.
76. Baytekin HT, Baytekin B, Soh S, Grzybowski BA. Is water necessary for contact electrification? Angewandte Chemie. 2011;123(30):6898-902.
77. Salaneck W, Paton A, Clark D. Double mass transfer during polymer-polymer contacts. Journal of Applied Physics. 1976;47(1):144-7.
78. Lowell J. The role of material transfer in contact electrification. Journal of Physics D: Applied Physics. 1977;10(17):L233.
79. Baytekin H, Patashinski A, Branicki M, Baytekin B, Soh S, Grzybowski BA. The mosaic of surface charge in contact electrification. Science advances. 2011;333(6040):308-12.
80. Baytekin HT, Baytekin B, Incorvati JT, Grzybowski BA. Material transfer and polarity reversal in contact charging. Angewandte Chemie International Edition. 2012;51(20):4843-7.
81. Cross J. Electrostatics, principles, problems and applications. United Kingdom: Taylor & Francis; 1987.
82. Liu Y, Wang L, Zhao L, Yu X, Zi Y. Recent progress on flexible nanogenerators toward self-powered systems. InfoMat. 2020;2(2):318-40.
83. Lee JP, Lee JW, Baik JM. The progress of PVDF as a functional material for triboelectric nanogenerators and self-powered sensors. Micromachines. 2018;9(10):532.
84. Li S, Fan Y, Chen H, Nie J, Liang Y, Tao X, et al. Manipulating the triboelectric surface charge density of polymers by low-energy helium ion irradiation/implantation. Energy Environmental Science. 2020;13(3):896-907.
85. Wang S, Lin L, Wang ZL. Triboelectric nanogenerators as self-powered active sensors. Nano Energy. 2015;11:436-62.
86. Xu S, Ding W, Guo H, Wang X, Wang ZL. Boost the Performance of Triboelectric Nanogenerators through Circuit Oscillation. Adv Energy Mater. 2019;9(30):1900772.
87. Yang J, Chen J, Liu Y, Yang W, Su Y, Wang ZL. Triboelectrification-Based Organic Film Nanogenerator for Acoustic Energy Harvesting and Self-Powered Active Acoustic Sensing. ACS Nano. 2014;8(3):2649-57.
88. Yang Y, Zhang H, Chen J, Jing Q, Zhou YS, Wen X, et al. Single-Electrode-Based Sliding Triboelectric Nanogenerator for Self-Powered Displacement Vector Sensor System. ACS Nano. 2013;7(8):7342-51.
89. Wang S, Lin L, Wang ZL. Nanoscale triboelectric-effect-enabled energy conversion for sustainably powering portable electronics. Nano letters. 2012;12(12):6339-46.
90. Bai P, Zhu G, Lin Z-H, Jing Q, Chen J, Zhang G, et al. Integrated multilayered triboelectric nanogenerator for harvesting biomechanical energy from human motions. ACS nano. 2013;7(4):3713-9.
91. Chen J, Zhu G, Yang W, Jing Q, Bai P, Yang Y, et al. Harmonic-resonator-based triboelectric nanogenerator as a sustainable power source and a self-powered active vibration sensor. Advanced materials. 2013;25(42):6094-9.
92. Han J, Xu N, Liang Y, Ding M, Zhai J, Sun Q, et al. Paper-based triboelectric nanogenerators and their applications: a review. Beilstein Journal of Nanotechnology. 2021;12:151-71.
93. Wang S, Lin L, Xie Y, Jing Q, Niu S, Wang ZL. Sliding-triboelectric nanogenerators based on in-plane charge-separation mechanism. Nano letters. 2013;13(5):2226-33.
94. Lin L, Wang S, Xie Y, Jing Q, Niu S, Hu Y, et al. Segmentally structured disk triboelectric nanogenerator for harvesting rotational mechanical energy. Nano letters. 2013;13(6):2916-23.
95. Feng H, Zhao C, Tan P, Liu R, Chen X, Li Z. Nanogenerator for Biomedical Applications. Adv Healthc Mater. 2018;7(10):1701298.
96. Bai P, Zhu G, Liu Y, Chen J, Jing Q, Yang W, et al. Cylindrical Rotating Triboelectric Nanogenerator. ACS Nano. 2013;7(7):6361-6.
97. Han CB, Zhang C, Li XH, Zhang L, Zhou T, Hu W, et al. Self-powered velocity and trajectory tracking sensor array made of planar triboelectric nanogenerator pixels. Nano Energy. 2014;9:325-33.
98. Niu S, Zhou YS, Wang S, Liu Y, Lin L, Bando Y, et al. Simulation method for optimizing the performance of an integrated triboelectric nanogenerator energy harvesting system. Nano Energy. 2014;8:150-6.

99. Su Y, Wen X, Zhu G, Yang J, Chen J, Bai P, et al. Hybrid triboelectric nanogenerator for harvesting water wave energy and as a self-powered distress signal emitter. Nano Energy. 2014;9:186-95.
100. Niu S, Liu Y, Chen X, Wang S, Zhou YS, Lin L, et al. Theory of freestanding triboelectric-layer-based nanogenerators. Nano Energy. 2015;12:760-74.
101. Wang S, Xie Y, Niu S, Lin L, Wang ZL. Freestanding Triboelectric-Layer-Based Nanogenerators for Harvesting Energy from a Moving Object or Human Motion in Contact and Non-contact Modes. Adv Mater. 2014;26(18):2818-24.
102. Wang S, Niu S, Yang J, Lin L, Wang ZL. Quantitative Measurements of Vibration Amplitude Using a Contact-Mode Freestanding Triboelectric Nanogenerator. ACS Nano. 2014;8(12):12004-13.
103. Zhu G, Lin Z-H, Jing Q, Bai P, Pan C, Yang Y, et al. Toward Large-Scale Energy Harvesting by a Nanoparticle-Enhanced Triboelectric Nanogenerator. Nano Letters. 2013;13(2):847-53.
104. Yun BK, Kim JW, Kim HS, Jung KW, Yi Y, Jeong M-S, et al. Base-treated polydimethylsiloxane surfaces as enhanced triboelectric nanogenerators. Nano Energy. 2015;15:523-9.
105. Hu Y, Yang J, Jing Q, Niu S, Wu W, Wang ZL. Triboelectric Nanogenerator Built on Suspended 3D Spiral Structure as Vibration and Positioning Sensor and Wave Energy Harvester. ACS Nano. 2013;7(11):10424-32.
106. Cheng G, Lin Z-H, Lin L, Du Z-l, Wang ZL. Pulsed Nanogenerator with Huge Instantaneous Output Power Density. ACS Nano. 2013;7(8):7383-91.
107. Yang W, Chen J, Jing Q, Yang J, Wen X, Su Y, et al. 3D Stack Integrated Triboelectric Nanogenerator for Harvesting Vibration Energy. Adv Funct Mater. 2014;24(26):4090-6.
108. Lin Z-H, Cheng G, Lee S, Pradel KC, Wang ZL. Harvesting Water Drop Energy by a Sequential Contact-Electrification and Electrostatic-Induction Process. Adv Mater. 2014;26(27):4690-6.
109. Yong H, Chung J, Choi D, Jung D, Cho M, Lee S. Highly reliable wind-rolling triboelectric nanogenerator operating in a wide wind speed range. Scientific Reports. 2016;6(1):33977.
110. Chen B, Tang W, Jiang T, Zhu L, Chen X, He C, et al. Three-dimensional ultraflexible triboelectric nanogenerator made by 3D printing. Nano Energy. 2018;45:380-9.
111. Mallineni SSK, Dong Y, Behlow H, Rao AM, Podila R. A Wireless Triboelectric Nanogenerator. Adv Energy Mater. 2018;8(10):1702736.
112. Wang AC, Wu C, Pisignano D, Wang ZL, Persano L. Polymer nanogenerators: Opportunities and challenges for large-scale applications. Journal of Applied Polymer Science. 2018;135(24):45674.
113. Xu C, Wang AC, Zou H, Zhang B, Zhang C, Zi Y, et al. Raising the working temperature of a triboelectric nanogenerator by quenching down electron thermionic emission in contact-electrification. Advanced Materials. 2018;30(38):1803968.
114. Xiong J, Cui P, Chen X, Wang J, Parida K, Lin M-F, et al. Skin-touch-actuated textile-based triboelectric nanogenerator with black phosphorus for durable biomechanical energy harvesting. Nature communications. 2018;9(1):1-9.
115. Han Y, Han Y, Zhang X, Li L, Zhang C, Liu J, et al. Fish Gelatin Based Triboelectric Nanogenerator for Harvesting Biomechanical Energy and Self-Powered Sensing of Human Physiological Signals. ACS Applied Materials & Interfaces. 2020;12(14):16442-50.
116. Seung W, Gupta MK, Lee KY, Shin K-S, Lee J-H, Kim TY, et al. Nanopatterned Textile-Based Wearable Triboelectric Nanogenerator. ACS Nano. 2015;9(4):3501-9.
117. Yang Y, Sun N, Wen Z, Cheng P, Zheng H, Shao H, et al. Liquid-Metal-Based Super-Stretchable and Structure-Designable Triboelectric Nanogenerator for Wearable Electronics. ACS Nano. 2018;12(2):2027-34.
118. Chen X, Parida K, Wang J, Xiong J, Lin M-F, Shao J, et al. A Stretchable and Transparent Nanocomposite Nanogenerator for Self-Powered Physiological Monitoring. ACS Applied Materials & Interfaces. 2017;9(48):42200-9.
119. Kim J, Ryu H, Lee JH, Khan U, Kwak SS, Yoon H-J, et al. High Permittivity CaCu3Ti4O12 Particle-Induced Internal Polarization Amplification for High Performance Triboelectric Nanogenerators. Adv Energy Mater. 2020;10(9):1903524.
120. Ba Y-Y, Bao J-F, Deng H-T, Wang Z-Y, Li X-W, Gong T, et al. Single-Layer Triboelectric Nanogenerators Based on Ion-Doped Natural Nanofibrils. ACS Applied Materials & Interfaces. 2020;12(38):42859-67.

121. Parandeh S, Kharaziha M, Karimzadeh F, Hosseinabadi F. Triboelectric nanogenerators based on graphene oxide coated nanocomposite fibers for biomedical applications. Nanotechnology. 2020;31(38):385402.
122. Cheng X, Tang W, Song Y, Chen H, Zhang H, Wang ZL. Power management and effective energy storage of pulsed output from triboelectric nanogenerator. Nano Energy. 2019;61:517-32.
123. Pu X, An S, Tang Q, Guo H, Hu C. Wearable triboelectric sensors for biomedical monitoring and human-machine interface. Iscience. 2021;24(1):102027.
124. Qin K, Chen C, Pu X, Tang Q, He W, Liu Y, et al. Magnetic array assisted triboelectric nanogenerator sensor for real-time gesture interaction. Nano-micro letters. 2021;13(1):1-9.
125. He W, Fu X, Zhang D, Zhang Q, Zhuo K, Yuan Z, et al. Recent progress of flexible/wearable self-charging power units based on triboelectric nanogenerators. Nano Energy. 2021;84:105880.
126. Fan F-R, Lin L, Zhu G, Wu W, Zhang R, Wang ZL. Transparent triboelectric nanogenerators and self-powered pressure sensors based on micropatterned plastic films. Nano letters. 2012;12(6):3109-14.
127. Wang ZL, Wang AC. On the origin of contact-electrification. Materials Today. 2019;30:34-51.
128. Jackson JD. Classical electrodynamics. New York: John Wiley & Sons, Inc,; 1962.
129. Niu S, Wang S, Lin L, Liu Y, Zhou YS, Hu Y, et al. Theoretical study of contact-mode triboelectric nanogenerators as an effective power source. Energy and Environmental Science. 2013;6(12):3576-83.
130. Niu S, Liu Y, Wang S, Lin L, Zhou YS, Hu Y, et al. Theoretical investigation and structural optimization of single-electrode triboelectric nanogenerators. Advanced Functional Materials. 2014;24(22):3332-40.
131. Alluri NR, Chandrasekhar A, Vivekananthan V, Purusothaman Y, Selvarajan S, Jeong JH, et al. Scavenging biomechanical energy using high-performance, flexible BaTiO3 nanocube/PDMS composite films. ACS Sustainable Chemistry Engineering. 2017;5(6):4730-8.
132. Kim W-G, Kim D-W, Tcho I-W, Kim J-K, Kim M-S, Choi Y-K. Triboelectric Nanogenerator: Structure, Mechanism, and Applications. ACS Nano. 2021;15(1):258-87.
133. Kim D, Jeon S-B, Kim JY, Seol M-L, Kim SO, Choi Y-K. High-performance nanopattern triboelectric generator by block copolymer lithography. Nano Energy. 2015;12:331-8.
134. Shin S-H, Bae YE, Moon HK, Kim J, Choi S-H, Kim Y, et al. Formation of triboelectric series via atomic-level surface functionalization for triboelectric energy harvesting. ACS nano. 2017;11(6):6131-8.
135. Vivekananthan V, Chandrasekhar A, Alluri NR, Purusothaman Y, Kim S-J. A highly reliable, impervious and sustainable triboelectric nanogenerator as a zero-power consuming active pressure sensor. Nanoscale Advances. 2020;2(2):746-54.
136. Rasel MS, Maharjan P, Salauddin M, Rahman MT, Cho HO, Kim JW, et al. An impedance tunable and highly efficient triboelectric nanogenerator for large-scale, ultra-sensitive pressure sensing applications. Nano Energy. 2018;49:603-13.
137. Lee KY, Yoon HJ, Jiang T, Wen X, Seung W, Kim SW, et al. Fully packaged self-powered triboelectric pressure sensor using hemispheres-array. Advanced energy materials. 2016;6(11):1502566.
138. Cheng T, Gao Q, Wang ZL. The current development and future outlook of triboelectric nanogenerators: a survey of literature. Advanced Materials Technologies. 2019;4(3):1800588.
139. Rasel MSU, Park J-Y. A sandpaper assisted micro-structured polydimethylsiloxane fabrication for human skin based triboelectric energy harvesting application. Applied Energy. 2017;206:150-8.
140. Seol M-L, Han J-W, Moon D-I, Meyyappan M. Hysteretic behavior of contact force response in triboelectric nanogenerator. Nano Energy. 2017;32:408-13.
141. Sow M, Lacks DJ, Sankaran RM. Effects of material strain on triboelectric charging: Influence of material properties. Journal of electrostatics. 2013;71(3):396-9.
142. Pourrahimi AM, Olsson RT, Hedenqvist MS. The role of interfaces in polyethylene/metal-oxide nanocomposites for ultrahigh-voltage insulating materials. Advanced Materials. 2018;30(4):1703624.
143. Wang Z, Cheng L, Zheng Y, Qin Y, Wang ZL. Enhancing the performance of triboelectric nanogenerator through prior-charge injection and its application on self-powered anticorrosion. Nano Energy. 2014;10:37-43.

144. Feng Y, Zheng Y, Ma S, Wang D, Zhou F, Liu W. High output polypropylene nanowire array triboelectric nanogenerator through surface structural control and chemical modification. Nano Energy. 2016;19:48-57.
145. Cheon S, Kang H, Kim H, Son Y, Lee JY, Shin HJ, et al. High-performance triboelectric nanogenerators based on electrospun polyvinylidene fluoride–silver nanowire composite nanofibers. Advanced Functional Materials. 2018;28(2):1703778.
146. Yao C, Yin X, Yu Y, Cai Z, Wang X. Chemically functionalized natural cellulose materials for effective triboelectric nanogenerator development. Advanced Functional Materials. 2017;27(30):1700794.
147. Li Z, Wang ZL. Air/liquid-pressure and heartbeat-driven flexible fiber nanogenerators as a micro/nano-power source or diagnostic sensor. Advanced Materials. 2011;23(1):84-9.
148. Zhang J, Rogers FJ, Darwish N, Gonçales VR, Vogel YB, Wang F, et al. Electrochemistry on tribocharged polymers is governed by the stability of surface charges rather than charging magnitude. Journal of the American Chemical Society. 2019;141(14):5863-70.
149. Zhang J, Rogers FJ, Darwish N, Gonçales VR, Vogel YB, Wang F, et al. Electrochemistry on tribocharged polymers is governed by the stability of surface charges rather than charging magnitude. Journal of the American Chemical Society. 2019;141(14):5863-70.
150. Chandrasekhar A, Vivekananthan V, Khandelwal G, Kim SJ. A fully packed water-proof, humidity resistant triboelectric nanogenerator for transmitting Morse code. Nano Energy. 2019;60:850-6.
151. Khandelwal G, Chandrasekhar A, Alluri NR, Vivekananthan V, Raj NPMJ, Kim S-J. Trash to energy: A facile, robust and cheap approach for mitigating environment pollutant using household triboelectric nanogenerator. Applied Energy. 2018;219:338-49.
152. Wang S, Xie Y, Niu S, Lin L, Liu C, Zhou YS, et al. Maximum surface charge density for triboelectric nanogenerators achieved by ionized-air injection: methodology and theoretical understanding. Advanced Materials. 2014;26(39):6720-8.
153. Lai M, Du B, Guo H, Xi Y, Yang H, Hu C, et al. Enhancing the output charge density of TENG via building longitudinal paths of electrostatic charges in the contacting layers. ACS applied materials interfaces. 2018;10(2):2158-65.
154. Huang T, Lu M, Yu H, Zhang Q, Wang H, Zhu M. Enhanced power output of a triboelectric nanogenerator composed of electrospun nanofiber mats doped with graphene oxide. Scientific reports. 2015;5(1):1-8.
155. Uddin AI, Yaqoob U, Chung G-S. Improving the working efficiency of a triboelectric nanogenerator by the semimetallic PEDOT: PSS hole transport layer and its application in self-powered active acetylene gas sensing. ACS applied materials interfaces. 2016;8(44):30079-89.
156. Kim S, Gupta MK, Lee KY, Sohn A, Kim TY, Shin KS, et al. Transparent flexible graphene triboelectric nanogenerators. Advanced materials. 2014;26(23):3918-25.
157. Dong Y, Mallineni SSK, Maleski K, Behlow H, Mochalin VN, Rao AM, et al. Metallic MXenes: A new family of materials for flexible triboelectric nanogenerators. Nano Energy. 2018;44:103-10.
158. Wu C, Kim TW, Park JH, An H, Shao J, Chen X, et al. Enhanced triboelectric nanogenerators based on MoS2 monolayer nanocomposites acting as electron-acceptor layers. ACS nano. 2017;11(8):8356-63.
159. Wu C, Kim TW, Choi HY. Reduced graphene-oxide acting as electron-trapping sites in the friction layer for giant triboelectric enhancement. Nano Energy. 2017;32:542-50.
160. Seol M, Kim S, Cho Y, Byun KE, Kim H, Kim J, et al. Triboelectric series of 2D layered materials. Advanced Materials. 2018;30(39):1801210.
161. Fan FR, Luo J, Tang W, Li C, Zhang C, Tian Z, et al. Highly transparent and flexible triboelectric nanogenerators: performance improvements and fundamental mechanisms. Journal of Materials Chemistry A. 2014;2(33):13219-25.
162. Lee JS, Romero R, Han YM, Kim HC, Kim CJ, Hong J-S, et al. Placenta-on-a-chip: a novel platform to study the biology of the human placenta. The Journal of Maternal-Fetal Neonatal Medicine. 2016;29(7):1046-54.

163. Kang Y, Wang B, Dai S, Liu G, Pu Y, Hu C. Folded elastic strip-based triboelectric nanogenerator for harvesting human motion energy for multiple applications. ACS applied materials interfaces. 2015;7(36):20469-76.
164. Zhang X-S, Han M-D, Wang R-X, Meng B, Zhu F-Y, Sun X-M, et al. High-performance triboelectric nanogenerator with enhanced energy density based on single-step fluorocarbon plasma treatment. Nano Energy. 2014;4:123-31.
165. Kwon YH, Shin S-H, Kim Y-H, Jung J-Y, Lee MH, Nah J. Triboelectric contact surface charge modulation and piezoelectric charge inducement using polarized composite thin film for performance enhancement of triboelectric generators. Nano Energy. 2016;25:225-31.
166. Yue X, Xi Y, Hu C, He X, Dai S, Cheng L, et al. Enhanced output-power of nanogenerator by modifying PDMS film with lateral ZnO nanotubes and Ag nanowires. RSC Advances. 2015;5(41):32566-71.
167. Zhang X, Qiao J, Zhao J, Xu D, Wang F, Liu C, et al. High-efficiency electromagnetic wave absorption of cobalt-decorated NH2-UIO-66-derived porous ZrO2/C. ACS applied materials interfaces. 2019;11(39):35959-68.
168. Jeong CK, Lee J, Han S, Ryu J, Hwang GT, Park DY, et al. A hyper-stretchable elastic-composite energy harvester. Advanced materials. 2015;27(18):2866-75.
169. Inaguma Y, Sakurai D, Aimi A, Yoshida M, Katsumata T, Mori D, et al. Dielectric properties of a polar ZnSnO3 with LiNbO3-type structure. Journal of Solid State Chemistry. 2012;195:115-9.
170. Paria S, Karan SK, Bera R, Das AK, Maitra A, Khatua BB. A facile approach to develop a highly stretchable PVC/ZnSnO3 piezoelectric nanogenerator with high output power generation for powering portable electronic devices. Industrial Engineering Chemistry Research. 2016;55(40):10671-80.
171. He X, Guo H, Yue X, Gao J, Xi Y, Hu C. Improving energy conversion efficiency for triboelectric nanogenerator with capacitor structure by maximizing surface charge density. Nanoscale. 2015;7(5):1896-903.
172. Karumuthil SC, Rajeev SP, Varghese S. Piezo-tribo nanoenergy harvester using hybrid polydimethyl siloxane based nanocomposite. Nano Energy. 2017;40:487-94.
173. Park KI, Lee M, Liu Y, Moon S, Hwang GT, Zhu G, et al. Flexible nanocomposite generator made of BaTiO3 nanoparticles and graphitic carbons. Advanced materials. 2012;24(22):2999-3004.
174. Park D, Shin S-H, Yoon I-J, Nah J. Ferroelectric nanoparticle-embedded sponge structure triboelectric generators. Nanotechnology. 2018;29(18):185402.
175. Chen J, Guo H, He X, Liu G, Xi Y, Shi H, et al. Enhancing performance of triboelectric nanogenerator by filling high dielectric nanoparticles into sponge PDMS film. ACS applied materials interfaces. 2016;8(1):736-44.
176. Kang Y, Wang B, Dai S, Liu G, Pu Y, Hu C, et al. Folded elastic strip-based triboelectric nanogenerator for harvesting human motion energy for multiple applications. ACS applied materials. 2015;7(36):20469-76.
177. Alam MM, Ghosh SK, Sultana A, Mandal D. Lead-free ZnSnO3/MWCNTs-based self-poled flexible hybrid nanogenerator for piezoelectric power generation. Nanotechnology. 2015;26(16):165403.
178. Han P, Pang S, Fan J, Shen X, Pan T. Highly enhanced piezoelectric properties of PLZT/PVDF composite by tailoring the ceramic Curie temperature, particle size and volume fraction. Sensors Actuators A: Physical. 2013;204:74-8.
179. Ghaffarinejad A, Hasani JY, Hinchet R, Lu Y, Zhang H, Karami A, et al. A conditioning circuit with exponential enhancement of output energy for triboelectric nanogenerator. Nano Energy. 2018;51:173-84.
180. Cheng L, Xu Q, Zheng Y, Jia X, Qin Y. A self-improving triboelectric nanogenerator with improved charge density and increased charge accumulation speed. Nature communications. 2018;9(1):1-8.
181. Niu S, Wang ZL. Theoretical systems of triboelectric nanogenerators. Nano Energy. 2015;14:161-92.
182. Wang J, Li X, Zi Y, Wang S, Li Z, Zheng L, et al. A Flexible Fiber-Based Supercapacitor–Triboelectric-Nanogenerator Power System for Wearable Electronics. Adv Mater. 2015;27(33):4830-6.

183. Zhang K, Wang X, Yang Y, Wang ZL. Hybridized electromagnetic–triboelectric nanogenerator for scavenging biomechanical energy for sustainably powering wearable electronics. ACS nano. 2015;9(4):3521-9.
184. Tang W, Zhou T, Zhang C, Fan FR, Han CB, Wang ZL. A power-transformed-and-managed triboelectric nanogenerator and its applications in a self-powered wireless sensing node. Nanotechnology. 2014;25(22):225402.
185. Xi F, Pang Y, Li W, Jiang T, Zhang L, Guo T, et al. Universal power management strategy for triboelectric nanogenerator. Nano Energy. 2017;37:168-76.
186. Gonsalves KE, Merhari L, Wu H, Hu Y. Organic–inorganic nanocomposites: unique resists for nanolithography. Advanced Materials. 2001;13(10):703-14.
187. Lopera S, Mansano R. Plasma-based surface modification of polydimethylsiloxane for PDMS-PDMS molding. International Scholarly Research Notices. 2012;2012.
188. Sia SK, Whitesides GM. Microfluidic devices fabricated in poly (dimethylsiloxane) for biological studies. Electrophoresis. 2003;24(21):3563-76.
189. Nair B. Final report on the safety assessment of stearoxy dimethicone, dimethicone, methicone, amino bispropyl dimethicone, aminopropyl dimethicone, amodimethicone, amodimethicone hydroxystearate, behenoxy dimethicone, C24-28 alkyl methicone, C30-45 alkyl methicone, C30-45 alkyl dimethicone, cetearyl methicone, cetyl dimethicone, dimethoxysilyl ethylenediaminopropyl dimethicone, hexyl methicone, hydroxypropyldimethicone, stearamidopropyl dimethicone, stearyl dimethicone, stearyl methicone, and vinyldimethicone. International journal of toxicology. 2003;22:11-35.
190. Rogers JA, Nuzzo RG. Recent progress in soft lithography. Materials today. 2005;8(2):50-6.
191. Sia SK, Whitesides GM. Microfluidic devices fabricated in poly (dimethylsiloxane) for biological studies. Electrophoresis. 2003;24(21):3563-76.
192. Rogers JA, Nuzzo RG. Recent progress in soft lithography. Materials today. 2005;8(2):50-6.
193. Hoang MV, Chung H-J, Elias AL. Irreversible bonding of polyimide and polydimethylsiloxane (PDMS) based on a thiol-epoxy click reaction. Journal of Micromechanics Microengineering. 2016;26(10):105019.
194. Johnston I, McCluskey D, Tan C, Tracey M. Mechanical characterization of bulk Sylgard 184 for microfluidics and microengineering. Journal of Micromechanics Microengineering. 2014;24(3):035017.
195. Leinberg S, Kisand V, Šutka A, Saal K, Lõhmus R, Joost U, et al. Switchable optical transmittance of TiO2 submicron-diameter wire suspension-based “smart window” device. Optical Materials. 2015;46:418-22.
196. Bergeron V, Cooper P, Fischer C, Giermanska-Kahn J, Langevin D, Pouchelon A. Polydimethylsiloxane (PDMS)-based antifoams. Colloids Surfaces A: Physicochemical Engineering Aspects. 1997;122(1-3):103-20.
197. Lin C-H, Yeh Y-H, Lin W-C, Yang M-C. Novel silicone hydrogel based on PDMS and PEGMA for contact lens application. Colloids Surfaces B: Biointerfaces. 2014;123:986-94.
198. Bharathidasan T, Kumar SV, Bobji M, Chakradhar R, Basu BJ. Effect of wettability and surface roughness on ice-adhesion strength of hydrophilic, hydrophobic and superhydrophobic surfaces. Applied surface science. 2014;314:241-50.
199. Burgess IF. The mode of action of dimeticone 4% lotion against head lice, Pediculus capitis. BMC pharmacology. 2009;9(1):1-8.
200. Tottey LS, Coulson SA, Wevers GE, Fabian L, McClelland H, Dustin M. Persistence of polydimethylsiloxane condom lubricants. Journal of forensic sciences. 2019;64(1):207-17.
201. Landherr LJ, Cohen C, Agarwal P, Archer LA. Interfacial friction and adhesion of polymer brushes. Langmuir. 2011;27(15):9387-95.
202. Lu MY, Li Y, He QS, Dai ZD, editors. Study on Polarization and Adhesion Property of Gecko Inspired Mushroom-Shaped Pillars. Materials Science Forum; 2020: Trans Tech Publ.
203. Casanova-Moreno J, To J, Yang CWT, Turner RF, Bizzotto D, Cheung KC. Fabricating devices with improved adhesion between PDMS and gold-patterned glass. Sensors Actuators B: Chemical. 2017;246:904-9.
204. Yun BK, Kim JW, Kim HS, Jung KW, Yi Y, Jeong M-S, et al. Base-treated polydimethylsiloxane surfaces as enhanced triboelectric nanogenerators. Nano Energy. 2015;15:523-9.

205. Pandey RK, Kakehashi H, Nakanishi H, Soh S. Correlating material transfer and charge transfer in contact electrification. The Journal of Physical Chemistry C. 2018;122(28):16154-60.
206. Frisenda R, Navarro-Moratalla E, Gant P, De Lara DP, Jarillo-Herrero P, Gorbachev RV, et al. Recent progress in the assembly of nanodevices and van der Waals heterostructures by deterministic placement of 2D materials. Chemical Society Reviews. 2018;47(1):53-68.
207. Vlassov S, Oras S, Antsov M, Sosnin I, Polyakov B, Shutka A, et al. Adhesion and mechanical properties of PDMS-based materials probed with AFM: a review. Reviews on Advanced Materials Science. 2018;56(1):62-78.
208. Johnston I, McCluskey D, Tan C, Tracey M. Mechanical characterization of bulk Sylgard 184 for microfluidics and microengineering. Journal of Micromechanics Microengineering. 2014;24(3):035017.
209. Sollier E, Murray C, Maoddi P, Di Carlo D. Rapid prototyping polymers for microfluidic devices and high pressure injections. Lab on a Chip. 2011;11(22):3752-65.
210. Pandey RK, Kakehashi H, Nakanishi H, Soh S. Correlating Material Transfer and Charge Transfer in Contact Electrification. The Journal of Physical Chemistry C. 2018;122(28):16154-60.
211. Fang Y, Chen L, Sun Y, Yong WP, Soh S. Anomalous charging behavior of inorganic materials. Journal of Physical Chemistry C. 2018;122(21):11414-21.
212. Pandey RK, Sun Y, Nakanishi H, Soh S. Reversible and continuously tunable control of charge of close surfaces. Journal of Physical Chemistry Letters. 2017;8(24):6142-7.
213. Fortunati E, D'angelo F, Martino S, Orlacchio A, Kenny J, Armentano I. Carbon nanotubes and silver nanoparticles for multifunctional conductive biopolymer composites. Carbon. 2011;49(7):2370-9.
214. Gómez-Romero P, Sanchez C. Functional hybrid materials. Hoboken, New Jersey: John Wiley & Sons; 2006.
215. Faupel F, Zaporojtchenko V, Greve H, Schürmann U, Chakravadhanula V, Hanisch C, et al. Deposition of nanocomposites by plasmas. Contributions to Plasma Physics. 2007;47(7):537-44.
216. Hanemann T, Szabó DV. Polymer-nanoparticle composites: from synthesis to modern applications. Materials. 2010;3(6):3468-517.
217. Ramesh G, Porel S, Radhakrishnan T. Polymer thin films embedded with in situ grown metal nanoparticles. Chemical Society Reviews. 2009;38(9):2646-56.
218. Swain SK, Jena I. Polymer/carbon nanotube nanocomposites: a novel material. Asian Journal of Chemistry. 2010;22(1):1.
219. Panahi-Sarmad M, Zahiri B, Noroozi M. Graphene-based composite for dielectric elastomer actuator: A comprehensive review. Sensors Actuators A: Physical. 2019;293:222-41.
220. Tiwari D, Sen V, Sharma R. Temperature dependent studies of electric and dielectric properties of polythiophene based nano composite. Indian Journal of Pure and Applied Physics. 2012;50.
221. Rubrice K, Castel X, Himdi M, Parneix P. Dielectric characteristics and microwave absorption of graphene composite materials. Materials. 2016;9(10):825.
222. Shukla MK, Sharma K. Molecular modeling and experimental investigation of graphene/CNT hybrid epoxy composites for characterization of tensile properties. Materials Today: Proceedings. 2020;26:3234-7.
223. Barber P, Balasubramanian S, Anguchamy Y, Gong S, Wibowo A, Gao H, et al. Polymer composite and nanocomposite dielectric materials for pulse power energy storage. Materials. 2009;2(4):1697-733.
224. Mathpal MC, Kumar P, Kumar S, Tripathi AK, Singh MK, Prakash J, et al. Opacity and plasmonic properties of Ag embedded glass based metamaterials. RSC advances. 2015;5(17):12555-62.
225. Stepanov A. Synthesis of silver nanoparticles in dielectric matrix by ion implantation: A review. Rev Adv Mater Sci. 2010;26(1/2):1-29.
226. Kumar P, Mathpal MC, Tripathi AK, Prakash J, Agarwal A, Ahmad M, et al. Plasmonic resonance of Ag nanoclusters diffused in soda-lime glasses. Physical Chemistry Chemical Physics. 2015;17(14):8596-603.
227. Lee J-Y, Peumans P. The origin of enhanced optical absorption in solar cells with metal nanoparticles embedded in the active layer. Optics Express. 2010;18(10):10078-87.

228. Zaporojtchenko V, Strunskus T, Erichsen J, Faupel F. Embedding of noble metal nanoclusters into polymers as a potential probe of the surface glass transition. Macromolecules. 2001;34(5):1125-7.
229. Maier SA. Plasmonics: fundamentals and applications. NewYork: Springer; 2007.
230. Murray C, Sun S, Doyle H, Betley T. Monodisperse 3d transition-metal (Co, Ni, Fe) nanoparticles and their assembly intonanoparticle superlattices. Mrs Bulletin. 2001;26(12):985-91.
231. Okumura M, Kitagawa Y, Haruta M, Yamaguchi K. DFT studies of interaction between O2 and Au clusters. The role of anionic surface Au atoms on Au clusters for catalyzed oxygenation. Chemical physics letters. 2001;346(1-2):163-8.
232. Quinten M, Heilmann A, Kiesow A. Refined interpretation of optical extinction spectra of nanoparticles in plasma polymer films. Applied Physics B. 1999;68(4):707-12.
233. Stepanov A. Metal-Polymer Nanocomposites. Nicolais, G Garotenuto, Eds. 2004:241-63.
234. Avasthi D, Mishra Y, Kabiraj D, Lalla N, Pivin J. Synthesis of metal–polymer nanocomposite for optical applications. Nanotechnology. 2007;18(12):125604.
235. Takele H, Schürmann U, Greve H, Paretkar D, Zaporojtchenko V, Faupel F. Controlled growth of Au nanoparticles in co-evaporated metal/polymer composite films and their optical and electrical properties. The European Physical Journal-Applied Physics. 2006;33(2):83-9.
236. Takele H, Jebril S, Strunskus T, Zaporojchenko V, Adelung R, Faupel F. Tuning of electrical and structural properties of metal-polymer nanocomposite films prepared by co-evaporation technique. Applied Physics A. 2008;92(2):345-50.
237. Deshmukh RD, Composto RJ. Direct observation of nanoparticle embedding into the surface of a polymer melt. Langmuir. 2007;23(26):13169-73.
238. Skirtach AG, Kurth DG, Möhwald H. Laser-embossing nanoparticles into a polymeric film. Applied Physics Letters. 2009;94(9):093106.
239. RangaReddy P, MohanaRaju K, SubbaramiReddy N. A review on polymer nanocomposites: monometallic and bimetallic nanoparticles for biomedical, optical and engineering applications. Chem Sci Rev Lett. 2013;1(4):228-35.
240. Dang ZM, Lin YH, Nan CW. Novel ferroelectric polymer composites with high dielectric constants. Advanced Materials. 2003;15(19):1625-9.
241. Qi L, Lee BI, Chen S, Samuels WD, Exarhos GJ. High-dielectric-constant silver–epoxy composites as embedded dielectrics. Advanced Materials. 2005;17(14):1777-81.
242. Finishing IoM. Transactions of the Institute of Metal Finishing. US: Taylor & Francis; 1990.
243. Zwicky-Sobczyk C, Stern W. X-ray fluorescence and density measurements on surface-treated Roman silver coins. Archaeometry. 1997;39(2):393-405.
244. Minin V, Minin I, Minin O. Explosive Synthesis of Diamond-Like Boron-Nitride. Int J of Modern Applied Physics. 2013;2(3):167.
245. Zuhailawati H, Samayamutthirian P, CH MH. Fabrication of low cost of aluminium, matrix composite reinforced with silica sand. Journal of physical science. 2007;18(1):47-55.
246. Walsh F. Electrode Reactions in Metal Finishing. Transactions of the Institute of Metal Finishing. 1991;69:107-11.
247. Zuhailawati H, Samayamutthirian P, CH MH. Fabrication of low cost of aluminium, matrix composite reinforced with silica sand. Journal of physical science. 2007;18(1):47-55.
248. Deepa K, Shaiju P, Sebastian M, Gowd EB, James J. Poly (vinylidene fluoride)–La 0.5 Sr 0.5 CoO 3− δ composites: the influence of LSCO particle size on the structure and dielectric properties. Physical Chemistry Chemical Physics. 2014;16(32):17008-17.
249. Kong K, Mariatti M, Rashid A, Busfield J. Enhanced conductivity behavior of polydimethylsiloxane (PDMS) hybrid composites containing exfoliated graphite nanoplatelets and carbon nanotubes. Composites Part B: Engineering. 2014;58:457-62.
250. Tanaka T. Dielectric nanocomposites with insulating properties. IEEE Transactions on Dielectrics Electrical Insulation. 2005;12(5):914-28.
251. Lebedev S, Gefle O, Pokholkov YP. The barrier effect in dielectrics: the role of interfaces in the breakdown of inhomogeneous dielectrics. IEEE Transactions on Dielectrics Electrical Insulation. 2005;12(3):537-55.
252. Chan H, Chan W, Zhang Y, Choy C. Pyroelectric and piezoelectric properties of lead titanate/polyvinylidene fluoride-trifluoroethylene 0-3 composites. IEEE transactions on dielectrics electrical insulation. 1998;5(4):505-12.

253. Goodenough JB. Electronic and ionic transport properties and other physical aspects of perovskites. Reports on Progress in Physics. 2004;67(11):1915.
254. Goodenough J, Raccah P. Complex vs band formation in perovskite oxides. Journal of Applied Physics. 1965;36(3):1031-2.
255. Raccah P, Goodenough J. A Localized-Electron to Collective-Electron Transition in the System (La, Sr) CoO3. Journal of Applied Physics. 1968;39(2):1209-10.
256. Mineshige A, Kobune M, Fujii S, Ogumi Z, Inaba M, Yao T, et al. Metal–Insulator Transition and Crystal Structure of La1− xSrxCoO3as Functions of Sr-Content, Temperature, and Oxygen Partial Pressure. Journal of Solid State Chemistry. 1999;142(2):374-81.
257. Thornton G, Tofield B, Hewat A. A neutron diffraction study of LaCoO3 in the temperature range 4.2< T< 1248 K. Journal of Solid State Chemistry. 1986;61(3):301-7.
258. Iguchi E, Ueda K, Jung W. Conduction in LaCo O 3 by small-polaron hopping below room temperature. Physical Review B. 1996;54(24):17431.
259. Kozuka H, Yamada H, Hishida T, Yamagiwa K, Ohbayashi K, Koumoto K. Electronic transport properties of the perovskite-type oxides La1−xSrxCoO3±δ. Journal of Materials Chemistry. 2012;22(38):20217-22.
260. Cullity B, Stock S. Elements of X-ray diffraction third edition. Prenrice hall, New Jersey. 2001.
261. Kittel C, McEuen P. Kittel's Introduction to Solid State Physics. NewJersey: John Wiley & Sons; 2018.
262. Fleischmann M, Hendra PJ, McQuillan AJ. Raman spectra of pyridine adsorbed at a silver electrode. Chemical physics letters. 1974;26(2):163-6.
263. Kneipp K, Wang Y, Kneipp H, Perelman LT, Itzkan I, Dasari RR, et al. Single molecule detection using surface-enhanced Raman scattering (SERS). Physical review letters. 1997;78(9):1667.
264. Kim W, Yasmeen S, Nguyen CT, Lee H-B-R, Choi D. Toward Enhanced Humidity Stability of Triboelectric Mechanical Sensors via Atomic Layer Deposition. Nanomaterials. 2021;11(7):1795.
265. Ha M, Park J, Lee Y, Ko H. Triboelectric Generators and Sensors for Self-Powered Wearable Electronics. ACS Nano. 2015;9(4):3421-7.
266. Xie L, Huang X, Huang Y, Yang K, Jiang P. Core@ double-shell structured BaTiO3–polymer nanocomposites with high dielectric constant and low dielectric loss for energy storage application. Journal of Physical Chemistry C. 2013;117(44):22525-37.
267. Chen J, Guo H, He X, Liu G, Xi Y, Shi H, et al. Enhancing performance of triboelectric nanogenerator by filling high dielectric nanoparticles into sponge PDMS film. ACS Applied Materials and Interfaces. 2016;8(1):736-44.
268. Chi Q, Sun J, Zhang C, Liu G, Lin J, Wang Y, et al. Enhanced dielectric performance of amorphous calcium copper titanate/polyimide hybrid film. Journal of Materials Chemistry C. 2014;2(1):172-7.
269. Dong L, Xiong C, Quan H, Zhao G. Polyvinyl-butyral/lead zirconate titanates composites with high dielectric constant and low dielectric loss. Scripta materialia. 2006;55(9):835-7.
270. Wang W, Zhang J, Zhang Y, Chen F, Wang H, Wu M, et al. Remarkably enhanced hybrid piezo/triboelectric nanogenerator via rational modulation of piezoelectric and dielectric properties for self-powered electronics. Applied Physics Letters. 2020;116(2):023901.
271. Ye Q, Wu Y, Qi Y, Shi L, Huang S, Zhang L, et al. Effects of liquid metal particles on performance of triboelectric nanogenerator with electrospun polyacrylonitrile fiber films. Nano Energy. 2019;61:381-8.
272. Feng S, Zhang H, He D, Xu Y, Zhang A, Liu Y, et al. Synergistic Effects of BaTiO3/Multiwall Carbon Nanotube as Fillers on the Electrical Performance of Triboelectric Nanogenerator Based on Polydimethylsiloxane Composite Films. Energy Technology. 2019;7(6):1900101.
273. Ren L, Meng X, Zha J-W, Dang Z-M. Coulomb block effect inducing distinctive dielectric properties in electroless plated barium titanate@ silver/poly (vinylidene fluoride) nanocomposites. RSC Advances. 2015;5(80):65167-74.
274. Chi Q, Gao L, Wang X, Chen Y, Dong J, Cui Y, et al. Effects of magnetic field treatment on dielectric properties of CCTO@ Ni/PVDF composite with low concentration of ceramic fillers. AIP Advances. 2015;5(11):117103.
275. Kim MP, Um D-S, Shin Y-E, Ko H. High-Performance Triboelectric Devices via Dielectric Polarization: A Review. Nanoscale Research Letters. 2021;16(1):35.

276. Harnchana V, Ngoc HV, He W, Rasheed A, Park H, Amornkitbamrung V, et al. Enhanced power output of a triboelectric nanogenerator using poly (dimethylsiloxane) modified with graphene oxide and sodium dodecyl sulfate. ACS applied materials. 2018;10(30):25263-72.
277. Shetty HD, Maity KP, Prasad V. Adjustable radio-frequency negative permittivity in graphite-PDMS elastomer metacomposites. Surfaces and Interfaces. 2020;21:100670.
278. Tanabe K. Field enhancement around metal nanoparticles and nanoshells: a systematic investigation. The Journal of Physical Chemistry C. 2008;112(40):15721-8.
279. Stiles PL, Dieringer JA, Shah NC, Van Duyne RP. Surface-enhanced Raman spectroscopy. Annu Rev Anal Chem. 2008;1:601-26.
280. Bae SC, Lee H, Lin Z, Granick S. Chemical Imaging in a Surface Forces Apparatus: Confocal Raman Spectroscopy of Confined Poly(dimethylsiloxane). Langmuir. 2005;21(13):5685-8.
281. Liao F, Cheng L, Li J, Shao M, Wang Z, Lee S-T. An effective oxide shell-protected surface-enhanced Raman scattering (SERS) substrate: the easy route to Ag@ Ag x O-silicon nanowire films via surface doping. JJournal of Materials Chemistry C. 2013;1(8):1628-32.
282. Orozco S, Riascos H, Duque S. Raman spectroscopy of ZnMnO thin films grown by pulsed laser deposition. Journal of Physics: Conference Series. 2016;687:012036.
283. Du P, Lin X, Zhang X, editors. Dielectric constants of PDMS nanocomposites using conducting polymer nanowires. 2011 16th International Solid-State Sensors, Actuators and Microsystems Conference; 2011; NewYork City: IEEE.
284. MARK JE. Polymer Data Handbook. Oxford: Oxford University Press; 1999.
285. Dang Z-M, Yuan J-K, Zha J-W, Zhou T, Li S-T, Hu G-H. Fundamentals, processes and applications of high-permittivity polymer–matrix composites. Progress in Materials Science. 2012;57(4):660-723.
286. Dang Z-M, Shen Y, Nan C-W. Dielectric behavior of three-phase percolative Ni–BaTiO 3/polyvinylidene fluoride composites. Applied Physics Letters. 2002;81(25):4814-6.
287. Roldughin V, Vysotskii V. Percolation properties of metal-filled polymer films, structure and mechanisms of conductivity. Progress in organic coating. 2000;39(2-4):81-100.
288. Brosseau C, Quéffélec P, Talbot P. Microwave characterization of filled polymers. Journal of Applied Physics. 2001;89(8):4532-40.
289. Zhu G, Pan C, Guo W, Chen C-Y, Zhou Y, Yu R, et al. Triboelectric-generator-driven pulse electrodeposition for micropatterning. Nano letters. 2012;12(9):4960-5.
290. Lee JW, Cho HJ, Chun J, Kim KN, Kim S, Ahn CW, et al. Robust nanogenerators based on graft copolymers via control of dielectrics for remarkable output power enhancement. Science Advances. 2017;3(5):1602902.
291. Niu S, Liu Y, Wang S, Lin L, Zhou YS, Hu Y, et al. Theory of sliding-mode triboelectric nanogenerators. Advanced materials. 2013;25(43):6184-93.
292. Wang ZL. On the first principle theory of nanogenerators from Maxwell's equations. Nano Energy. 2020;68:104272.
293. Yang Y. High performance of polyimide/$CaCu_3Ti_4O_{12}$@Ag hybrid films with enhanced dielectric permittivity and low dielectric loss. Journal of Materials Chemistry A. 2015; 3(9):pp. 4916-21-2015.
294. Dang ZM, Wang L, Yin Y, Zhang Q, Lei QQ. Giant dielectric permittivities in functionalized carbon-nanotube/electroactive-polymer nanocomposites. Advanced Materials. 2007;19(6):852-7.
295. Bhunia R, Ghosh D, Ghosh B, Hussain S, Bhar R, Pal A. Free-standing flexible nanocrystalline-ZnO-impregnated polyvinylidene fluoride composite thin films. Journal of Composite Materials. 2015;49(25):3089-101.
296. Bhunia R, Ghosh D, Ghosh B, Hussain S, Bhar R, Pal AK. Some aspects of microstructural and dielectric properties of nanocrystalline CdS/poly (vinylidene fluoride) composite thin films. Polymer International. 2015;64(7):924-34.
297. Zhang Y, Wang Y, Deng Y, Li M, Bai J. Enhanced dielectric properties of ferroelectric polymer composites induced by metal-semiconductor Zn-ZnO core–shell structure. ACS Applied Materials and Interfaces. 2012;4(1):65-8.
298. Chen J, Guo H, He X, Liu G, Xi Y, Shi H, et al. Enhancing performance of triboelectric nanogenerator by filling high dielectric nanoparticles into sponge PDMS film. ACS Applied Materials & Interfaces. 2016;8(1):736-44.

299. Liu Y, Han R, Li L, Zhou Z, Chen G, Li Q. Tuning of highly dielectric calcium copper titanate nanowires to enhance the output performance of a triboelectric nanogenerator. ACS Applied Electronic Materials. 2020;2(6):1709-15.
300. Eglitis RI, Popov AI. Systematic trends in (001) surface ab initio calculations of ABO3 perovskites. Journal of Saudi Chemical Society. 2018;22(4):459-68.
301. Assirey EAR. Perovskite synthesis, properties and their related biochemical and industrial application. Saudi Pharmaceutical Journal. 2019;27(6):817-29.
302. Kharton VV, Figueiredo FM, Kovalevsky AV, Viskup AP, Naumovich EN, Yaremchenko AA, et al. Processing, microstructure and properties of LaCoO3−δ ceramics. Journal of the European Ceramic Society. 2001;21(13):2301-9.
303. Koehler W, Wollan E, Solids Co. Neutron-diffraction study of the magnetic properties of perovskite-like compounds LaBO3. Journal of Physics D: Applied Physics. 1957;2(2):100-6.
304. Iwasaki K, Ito T, Nagasaki T, Arita Y, Yoshino M, Matsui T. Thermoelectric properties of polycrystalline La1− xSrxCoO3. Journal of Solid State Chemistry. 2008;181(11):3145-50.
305. Wang ZL, Zhang J. Tetragonal domain structure and magnetoresistance of $La_{1-x}Sr_xCoO_3$. Physical Review B. 1996;54(2):1153-8.
306. Van Doorn R, Burggraaf A. Structural aspects of the ionic conductivity of La1− xSrxCoO3− δ. Solid State Ionics. 2000;128(1-4):65-78.
307. van Doorn RHE, Burggraaf AJ. Structural aspects of the ionic conductivity of La1−xSrxCoO3−δ. Solid State Ionics. 2000;128(1):65-78.
308. Sathe V, Pimpale A, Siruguri V, Paranjpe S. Neutron diffraction studies of perovskite-type compounds. Journal of Physics: Condensed Matter. 1996;8(21):3889.
309. Ohbayashi H, Kudo T, Gejo T. Crystallographic, Electric and Thermochemical Properties of the Perovskite-Type Ln1-xSrxCoO3 (Ln: Lanthanoid Element). Japanese Journal of Applied Physics. 1974;13(1):1.
310. Wang F, Leppävuori S. Properties of epitaxial ferroelectric PbZr 0.56 Ti 0.44 O 3 heterostructures with La 0.5 Sr 0.5 CoO 3 metallic oxide electrodes. Journal of Applied physics. 1997;82(3):1293-8.
311. Iwasaki K, Ito T, Nagasaki T, Arita Y, Yoshino M, Matsui T. Thermoelectric properties of polycrystalline La1− xSrxCoO3. Journal of Solid State Chemistry. 2008;181(11):3145-50.
312. Chen C, Bouwmeester H. RHE vanDoorn, H. Kruidhof, and AJ Burggraaf. Solid State Ionics. 1997;98(1-2):7.
313. Inagaki T, Miura K, Yoshida H, Maric R, Ohara S, Zhang X, et al. High-performance electrodes for reduced temperature solid oxide fuel cells with doped lanthanum gallate electrolyte: II. La (Sr) CoO3 cathode. Journal of Power Sources. 2000;86(1-2):347-51.
314. Itoh M, Natori I, Kubota S, Motoya K. Spin-glass behavior and magnetic phase diagram of La1-xSrxCoO3 ($0\leq x\leq 0.5$) studied by magnetization measurements. Journal of the Physical Society of Japan. 1994;63(4):1486-93.
315. Nakamura T, Misono M, Yoneda Y. Reduction-oxidation and catalytic properties of La1− xSrxCoO3. Journal of Catalysis. 1983;83(1):151-9.
316. Wang G, Hu Z, Huang Z, Wang X, Lin T, Chen J, et al., editors. Infrared optical properties of lanthanum strontium cobalt thin films. Twenty Seventh International Conference on Infrared and Millimeter Waves; 2002; San Diego, USA: IEEE.
317. Closset NM, van Doorn RH, Kruidhof H, Boeijsma J. About the crystal structure of La1− xSrxCoO3− δ ($0\leq x\leq 0.6$). Powder diffraction. 1996;11(1):31-4.
318. Orlovskaya N, Steinmetz D, Yarmolenko S, Pai D, Sankar J, Goodenough J. Detection of temperature-and stress-induced modifications of La Co O 3 by micro-Raman spectroscopy. Physical Review B. 2005;72(1):014122.
319. Qureshi A, Mergen A, Eroğlu MS, Singh NL, Güllüoğlu A. Dielectric Properties of Polymer Composites Filled with Different Metals. Journal of Macromolecular Science, Part A. 2008;45(6):462-9.
320. Singh V, Kulkarni A, Rama Mohan T. Dielectric properties of aluminum–epoxy composites. Journal of Applied Polymer Science. 2003;90(13):3602-8.
321. Dang Z, Zhou T, Yao S, Yuan JC, WT Yang, J. Bai:. JW-Zha, HT Song, JY Li, Q. Advanced Materials. 2009;21:2077.

322. Lewis T. Interfaces: nanometric dielectrics. Journal of Physics D: Applied Physics. 2005;38(2):202.
323. Zhang LM, Han CB, Jiang T, Zhou T, Li XH, Zhang C, et al. Multilayer wavy-structured robust triboelectric nanogenerator for harvesting water wave energy. J Nano Energy. 2016;22:87-94.
324. Chung J, Lee S, Yong H, Moon H, Choi D, Lee S. Self-packaging elastic bellows-type triboelectric nanogenerator. Nano Energy. 2016;20:84-93.
325. Jing Q, Zhu G, Bai P, Xie Y, Chen J, Han RPS, et al. Case-Encapsulated Triboelectric Nanogenerator for Harvesting Energy from Reciprocating Sliding Motion. ACS Nano. 2014;8(4):3836-42.
326. Wu C, Wang X, Lin L, Guo H, Wang ZL. Paper-Based Triboelectric Nanogenerators Made of Stretchable Interlocking Kirigami Patterns. ACS Nano. 2016;10(4):4652-9.
327. Yang P-K, Lin Z-H, Pradel KC, Lin L, Li X, Wen X, et al. Paper-Based Origami Triboelectric Nanogenerators and Self-Powered Pressure Sensors. ACS Nano. 2015;9(1):901-7.
328. Wang ZL. Triboelectric nanogenerators as new energy technology for self-powered systems and as active mechanical and chemical sensors. J ACS nano. 2013;7(11):9533-57.
329. Phan H, Shin D-M, Heon Jeon S, Young Kang T, Han P, Han Kim G, et al. Aerodynamic and aeroelastic flutters driven triboelectric nanogenerators for harvesting broadband airflow energy. Nano Energy. 2017;33:476-84.
330. Wang J, Wang H, Thakor NV, Lee C. Self-Powered Direct Muscle Stimulation Using a Triboelectric Nanogenerator (TENG) Integrated with a Flexible Multiple-Channel Intramuscular Electrode. ACS Nano. 2019;13(3):3589-99.
331. Tang W, Meng B, Zhang HX. Investigation of power generation based on stacked triboelectric nanogenerator. Nano Energy. 2013;2(6):1164-71.
332. Seol M-L, Woo J-H, Jeon S-B, Kim D, Park S-J, Hur J, et al. Vertically stacked thin triboelectric nanogenerator for wind energy harvesting. Nano Energy. 2015;14:201-8.
333. Kwon J-H, Jeong J, Lee Y, Biswas S, Park J-K, Lee S, et al. Importance of Architectural Asymmetry for Improved Triboelectric Nanogenerators with 3D Spacer Fabrics. Macromolecular Research. 2021;29:443-7.
334. Pang Y, Yang Z, Han X, Jian J, Li Y, Wang X, et al. Multifunctional Mechanical Sensors for Versatile Physiological Signal Detection. ACS Applied Materials & Interfaces. 2018;10(50):44173-82.
335. Jing Q, Choi YS, Smith M, Ćatić N, Ou C, Kar-Narayan S. Aerosol-Jet Printed Fine-Featured Triboelectric Sensors for Motion Sensing. Advanced Material Technologies. 2019;4(1):1800328.
336. Zhou YS, Zhu G, Niu S, Liu Y, Bai P, Jing Q, et al. Nanometer Resolution Self-Powered Static and Dynamic Motion Sensor Based on Micro-Grated Triboelectrification. Advanced Materials. 2014;26(11):1719-24.
337. Bao Han C, Zhang C, Li XH, Zhang L, Zhou T, Hu W, et al. Self-powered velocity and trajectory tracking sensor array made of planar triboelectric nanogenerator pixels. Nano Energy. 2014;9:325-33.
338. Jing Q, Zhu G, Wu W, Bai P, Xie Y, Han RPS, et al. Self-powered triboelectric velocity sensor for dual-mode sensing of rectified linear and rotary motions. Nano Energy. 2014;10:305-12.
339. Yi F, Lin L, Niu S, Yang J, Wu W, Wang S, et al. Self-Powered Trajectory, Velocity, and Acceleration Tracking of a Moving Object/Body using a Triboelectric Sensor. Advanced Functional Materials. 2014;24(47):7488-94.
340. Wu Z, Ding W, Dai Y, Dong K, Wu C, Zhang L, et al. Self-Powered Multifunctional Motion Sensor Enabled by Magnetic-Regulated Triboelectric Nanogenerator. ACS Nano. 2018;12(6):5726-33.
341. Garcia C, Trendafilova I. Real-time diagnosis of small energy impacts using a triboelectric nanosensor. Sensors and Actuators A: Physical. 2019;291:196-203.
342. Vijoy K, John H, Saji K. Self-powered ultra-sensitive millijoule impact sensor using room temperature cured PDMS based triboelectric nanogenerator. Microelectronic Engineering. 2021;251:111664.
343. He C, Zhu W, Gu GQ, Jiang T, Xu L, Chen BD, et al. Integrative square-grid triboelectric nanogenerator as a vibrational energy harvester and impulsive force sensor. Nano Research. 2018;11(2):1157-64.
344. Heo D, Kim T, Yong H, Yoo KT, Lee S. Sustainable oscillating triboelectric nanogenerator as omnidirectional self-powered impact sensor. Nano Energy. 2018;50:1-8.

345. Zhang J, Cao Y, Qiao M, Ai L, Sun K, Mi Q, et al. Human motion monitoring in sports using wearable graphene-coated fiber sensors. Sensors and Actuators A: Physical. 2018;274:132-40.
346. King K, Yoon SW, Perkins NC, Najafi K. Wireless MEMS inertial sensor system for golf swing dynamics. Sensors and Actuators A: Physical. 2008;141(2):619-30.
347. Troiano RP, McClain JJ, Brychta RJ, Chen KY. Evolution of accelerometer methods for physical activity research. British journal of sports medicine. 2014;48(13):1019-23.
348. Chandra B, Chandra V, Mahobia S, Jha P, Tiwari R, Haldar B. Real-time mechanoluminescence sensing of the amplitude and duration of impact stress. Sensors Actuators A: Physical. 2012;173(1):9-16.
349. Aminullah, Kasi AK, Kasi JK, Uddin M, Bokhari M. Triboelectric nanogenerator as self-powered impact force sensor for falling object. Current Applied Physics. 2020;20(1):137-44.
350. Xu C, Zi Y, Wang AC, Zou H, Dai Y, He X, et al. On the Electron-Transfer Mechanism in the Contact-Electrification Effect. Advanced Materials. 2018;30(15):1706790.
351. Ravelo B, Duval F, Kane S, Nsom B. Demonstration of the triboelectricity effect by the flow of liquid water in the insulating pipe. Journal of Electrostatics. 2011;69(6):473-8.
352. Lin ZH, Cheng G, Lee S, Pradel KC, Wang ZL. Harvesting water drop energy by a sequential contact-electrification and electrostatic-induction process. Advanced Materials. 2014;26(27):4690-6.
353. Van Boxel JH, editor Numerical model for the fall speed of rain drops in a rain fall simulator. Workshop on wind and water erosion; 1997; Amsterdam: Faculteit der Ruimtelijke Wetenschappen.
354. Wang X, Lu X, Liu B, Chen D, Tong Y, Shen G. Flexible Energy-Storage Devices: Design Consideration and Recent Progress. Advanced Materials. 2014;26(28):4763-82.
355. Gu T, Wei B. High-performance all-solid-state asymmetric stretchable supercapacitors based on wrinkled MnO 2/CNT and Fe 2 O 3/CNT macrofilms. Journal of Materials Chemistry A. 2016;4(31):12289-95.
356. Zhu G, Zhou YS, Bai P, Meng XS, Jing Q, Chen J, et al. A shape-adaptive thin-film-based approach for 50% high-efficiency energy generation through micro-grating sliding electrification. Advanced materials. 2014;26(23):3788-96.
357. Wang S, Lin L, Wang ZL. Nanoscale triboelectric-effect-enabled energy conversion for sustainably powering portable electronics. Nano Letters. 2012;12(12):6339-46.
358. Yang B, Zeng W, Peng ZH, Liu SR, Chen K, Tao XM. A fully verified theoretical analysis of contact-mode triboelectric nanogenerators as a wearable power source. Advanced Energy Materials. 2016;6(16):1600505.
359. Tian H, Ma S, Zhao H-M, Wu C, Ge J, Xie D, et al. Flexible electrostatic nanogenerator using graphene oxide film. Nanoscale. 2013;5(19):8951-7.
360. Yang Y, Zhou YS, Zhang H, Liu Y, Lee S, Wang ZL. A single-electrode based triboelectric nanogenerator as self-powered tracking system. Advanced Materials. 2013;25(45):6594-601.
361. Soares dos Santos MP, Bernardo R, Henriques L, Ramos A, Ferreira JAF, Furlani EP, et al. Towards an effective sensing technology to monitor micro-scale interface loosening of bioelectronic implants. Scientific Reports. 2021;11(1):3449.
362. Priya S. Advances in energy harvesting using low profile piezoelectric transducers. Journal of Electroceramics. 2007;19(1):167-84.
363. 363. Priya S, Inman DJ. Energy harvesting technologies. NewYork city: Springer; 2009.
364. Gao W, Brennan R, Hu Y, Wuttig M, Yuan G, Quandt E, et al. Energy transduction ferroic materials. Materials Today. 2018;21(7):771-84.
365. Vidal JV, Turutin AV, Kubasov IV, Kislyuk AM, Kiselev DA, Malinkovich MD, et al. Dual vibration and magnetic energy harvesting with bidomain LiNbO 3-based composite. IEEE Transactions on Ultrasonics, Ferroelectrics Frequency Control. 2020;67(6):1219-29.
366. Shao J, Jiang T, Tang W, Xu L, Kim TW, Wu C, et al. Studying about applied force and the output performance of sliding-mode triboelectric nanogenerators. Nano Energy. 2018;48:292-300.
367. Beeby SP, O'Donnell T. Electromagnetic energy harvesting. Energy Harvesting Technologies. 2009:129-61.
368. Liu W, Wang Z, Wang G, Liu G, Chen J, Pu X, et al. Integrated charge excitation triboelectric nanogenerator. Nature communications. 2019;10(1):1-9.
369. Li Z, Zheng Q, Wang ZL, Li Z. Nanogenerator-based self-powered sensors for wearable and implantable electronics. Research. 2020;2020.

370. Lee JW, Jung S, Lee TW, Jo J, Chae HY, Choi K, et al. High-output triboelectric nanogenerator based on dual inductive and resonance effects-controlled highly transparent polyimide for self-powered sensor network systems. Advanced Energy Materials. 2019;9(36):1901987.
371. Jiang B, Iocozzia J, Zhao L, Zhang H, Harn Y-W, Chen Y, et al. Barium titanate at the nanoscale: controlled synthesis and dielectric and ferroelectric properties. Chemical Society Reviews. 2019;48(4):1194-228.
372. Jana A, Kundu T, Pradhan S, Chakravorty D. Dielectric behavior of Fe-ion-doped BaTi O 3 nanoparticles. Journal of applied physics. 2005;97(4):044311.
373. Niu Y, Wang H. Dielectric nanomaterials for power energy storage: surface modification and characterization. ACS Applied Nano Materials. 2019;2(2):627-42.
374. Sharma S, Tomar M, Puri NK, Gupta V, editors. Enhanced dielectric properties of multilayered BiFeO3/BaTiO3 capacitors deposited by pulsed laser deposition. AIP Conference Proceedings; 2016; Baroda (India): AIP Publishing LLC.
375. Ning N, Bai X, Yang D, Zhang L, Lu Y, Nishi T, et al. Dramatically improved dielectric properties of polymer composites by controlling the alignment of carbon nanotubes in matrix. RSC Advances. 2014;4(9):4543-51.
376. Lee KY, Kim SK, Lee JH, Seol D, Gupta MK, Kim Y, et al. Controllable charge transfer by ferroelectric polarization mediated triboelectricity. Advanced Functional Materials. 2016;26(18):3067-73.
377. Shepelin NA, Sherrell PC, Goudeli E, Skountzos EN, Lussini VC, Dicinoski GW, et al. Printed recyclable and self-poled polymer piezoelectric generators through single-walled carbon nanotube templating. Energy Environmental Science. 2020;13(3):868-83.
378. Guo H, Wen Z, Zi Y, Yeh MH, Wang J, Zhu L, et al. A water-proof triboelectric–electromagnetic hybrid generator for energy harvesting in harsh environments. Advanced Energy Materials. 2016;6(6):1501593.
379. Li S, Zhang D, Meng X, Huang Q-A, Sun C, Wang ZL. A flexible lithium-ion battery with quasi-solid gel electrolyte for storing pulsed energy generated by triboelectric nanogenerator. Energy Storage Materials. 2018;12:17-22.
380. Zhu D, Tudor MJ, Beeby SP. Strategies for increasing the operating frequency range of vibration energy harvesters: a review. Measurement Science Technology. 2009;21(2):022001.
381. Zhou YS, Liu Y, Zhu G, Lin Z-H, Pan C, Jing Q, et al. In situ quantitative study of nanoscale triboelectrification and patterning. Nano letters. 2013;13(6):2771-6.
382. Xia X, Fu J, Zi Y. A universal standardized method for output capability assessment of nanogenerators. Nature communications. 2019;10(1):1-9.
383. Zheng Q, Shi B, Fan F, Wang X, Yan L, Yuan W, et al. In vivo powering of pacemaker by breathing-driven implanted triboelectric nanogenerator. Advanced materials. 2014;26(33):5851-6.